The role of *CBL* genes in the salt stress response of *Nicotiana tabacum*

Jingjing Mao

Propositions

1. H^+ homeostasis is as important as Na^+ homeostasis for the salt tolerance of plants.

(this thesis)

2. Our current knowledge about ion distribution over different cell organelles is inadequate in understanding plant response to salinity stress.

(this thesis)

3. Statistical significance is often misused to describe physiological significance.

4. ChatGPT is harmful to researchers who lack independent thinking.

5. Caring too much about other people's opinions makes people lose themselves.

6. Moderate stress makes both plants and humans stronger.

Propositions belonging to the thesis entitled

The role of *CBL* genes in the salt stress response of *Nicotiana tabacum*

Jingjing Mao

Wageningen, 13 June 2023

The role of *CBL* genes in the salt stress response of *Nicotiana tabacum*

Jingjing Mao

Thesis committee

Promotors

Prof. Dr Richard G.F. Visser

Professor of Plant Breeding

Wageningen University & Research

Prof. Dr Yuling Bai

Personal Chair, Plant Breeding

Wageningen University & Research

Co-promotors

Dr C. G. Gerard van der Linden

Senior Scientist, Plant Breeding

Wageningen University & Research

Prof. Dr Haobao Liu

Professor of Tobacco Research Institute

Chinese Academy of Agricultural Sciences, Beijing, China

Other members

Prof. Dr Christa Testerink, Wageningen University & Research

Dr Teun Munnik, University of Amsterdam

Dr Elias Kaiser, Wageningen University & Research

Dr Ivo Rieu, Radboud University, Nijmegen

This research was conducted under the auspices of the Graduate School Experimental Plant Sciences

The role of *CBL* genes in the salt stress response of *Nicotiana tabacum*

Jingjing Mao

Thesis

Submitted in fulfilment of the requirements for the degree of doctor

at Wageningen University

by the authority of the Rector Magnificus,

Prof. Dr A.P.J.Mol,

in the presence of the

Thesis Committee appointed by the Academic Board

to be defended in public

on Tuesday 13 June 2023

at 11 a.m. in the Omnia Auditorium.

Jingjing Mao

The role of *CBL* genes in the salt stress response of *Nicotiana tabacum*,

233 pages.

PhD thesis, Wageningen University, Wageningen, the Netherlands (2023)

With references, with summary in English

ISBN: 978-94-6447-682-8

DOI: https://doi.org/10.18174/629736

Table of Contents

Chapter 1……....1
General Introduction
Chapter 2……19
The CBL-CIPK network is involved in the physiological crosstalk between plant growth and stress adaptation
Chapter 3……....51
Genome-wide identification of *CBL* family genes in *Nicotiana tabacum* and the functional analysis of *NtCBL4A-1* under salt stress
Chapter 4……101
Overexpression of *NtCBL5A* leads to necrotic lesions by enhancing Na^+ sensitivity of tobacco leaves under salt stress
Chapter 5……..153
NtCBL10A and *NtCBL10B* are essential for the salt tolerance of tobacco
Chapter 6……..197
General Discussion

Summary……....219

Acknowledgments……....223

About the Author……...229

Education Statement……....231

Acknowledgments of Financial Support……....233

Chapter 1

General Introduction

Climate change leads to increasing stresses and reduction of crop yield

Anthropogenically driven climate change is increasing the frequency of weather extremes (Cook et al., 2016), which directly and indirectly affects agricultural production. The changes in exposure of crops to abiotic environmental factors not only directly affect crop production, but climate change also affects other species such as pollinators, pests, disease vectors, and invasive species, indirectly impeding crop production (Liliane and Charles, 2020). Moreover, crops are usually not subject to a single stress, but to a combination of different stresses in the field (Mittler, 2006). These stresses lead to yield losses that threaten the increasing food needs of a growing world population (Ferguson, 2019). It is therefore of the utmost importance for plants and crops to be able to adapt to these changing conditions, and have high yields even when the growing conditions are not optimal. Knowledge about the adaptive strategies and mechanisms to changing environmental conditions is essential for breeders to develop varieties that are resilient to the changing climate.

Stress and the second messenger Ca^{2+}

Plants perceive stresses and respond appropriately through signaling pathways, which include signaling molecules such as Ca^{2+} (Bartels and Sunkar, 2005). Many years ago, researchers already showed that different environmental stimuli induced specific cytosolic Ca^{2+} concentration spikes ($[Ca^{2+}]_{cyt}$ transients) (Price et al., 1994; Haley et al., 1995; Bush, 1996; Okazaki et al., 1996; Gong et al., 1998; McAinsh and Hetherington, 1998). When triggered, the $[Ca^{2+}]_{cyt}$ increases from ~10^{-7} M to 10^{-6} M depending on the kind of external stimulus (Costa et al., 2018), generating unique $[Ca^{2+}]_{cyt}$ signatures that initiate specific molecular and physiological responses to diverse developmental cues and environmental stimuli (Lee and Seo, 2021).

Increased $[Ca^{2+}]_{cyt}$ is caused by the release of Ca^{2+} from storage compartments such as the vacuole and the apoplast (Stael et al., 2012). The central vacuole is the main intracellular Ca^{2+} store and contributes to changes in $[Ca^{2+}]_{cyt}$ (Stael et al., 2012). Vacuolar Ca^{2+} release in the cytosol leads to the propagation of systemic Ca^{2+} waves

throughout the whole plant (Choi et al., 2014; Evans et al., 2016; Lee and Seo, 2021). The apoplast is another important Ca^{2+} storage location and Ca^{2+} can be quickly transported through the plant by means of the water transpiration stream (Stael et al., 2012). The endoplasmic reticulum (ER) is well known for its important calcium storage role in humans and animals, while relatively little is known about the Ca^{2+} storage properties of the plant ER. The plant ER was reported to act as a Ca^{2+} source for the generation of a cytosolic Ca^{2+} transient (Shkolnik et al., 2018; Luo et al., 2020) as well as a Ca^{2+} sink that contributes to the dampening of Ca^{2+} transient (Bonza et al., 2013; Corso et al., 2018; Resentini et al., 2021).

The $[Ca^{2+}]_{cyt}$ increase requires specific signals and Ca^{2+} transport routes from the apoplastic fluid or intracellular compartments into the cytosol (Navazio et al., 2000; Vincent et al., 2017). With advanced bioimaging techniques, stress-sensing machinery components have been identified, such as lipid-binding proteins, membrane-anchored kinases, and Ca^{2+} channels (Lee and Seo, 2021). These molecular sensors recognize external cues such as osmotic stress, ionic stress, pathogens, extracellular ATP, and reactive oxygen species (ROS), initiating a corresponding Ca^{2+} influx in the cytosol (Lee and Seo, 2021).

CBL-CIPK network decodes Ca^{2+} signals

The transduction of Ca^{2+} signals triggered by environmental stimuli to downstream adaptive responses depends on Ca^{2+}-sensor proteins (Trewavas and Malhó, 1998). To date, five major classes of Ca^{2+} sensor proteins have been characterized in plants: calmodulins (CaMs), CaM-like proteins (CMLs), calcium-dependent protein kinases (CDPKs), calcium- and calmodulin-dependent protein kinases (CCaMKs), and calcineurin B-like proteins (CBLs) (Yip Delormel and Boudsocq, 2019). All of these Ca^{2+}-sensor families are known to transmit stress signals (Zhu, 2000; Snedden and Fromm, 2001; Luan et al., 2002; Singh and Parniske, 2012). In *Arabidopsis thaliana*, 7 CaMs (McCormack et al., 2005), 50 CMLs (McCormack et al., 2005), 34 CDPKs (Hrabak et al., 2003), and 10 CBLs (Kolukisaoglu et al., 2004) have been identified.

CCaMKs are absent in *Arabidopsis* and are required for both root nodule and arbuscular mycorrhiza symbioses in legumes (Singh and Parniske, 2012). CBLs act together with CIPKs (CBL-interacting protein kinases) by activating CIPK phosphorylation, and each CBL-CIPK module triggers specific downstream responses. CBLs and CIPKs thus are interwoven in a complex but flexible Ca^{2+}-signal-decoding hub in plants (Figure 1). Therefore, the CBL family plays an essential role in regulating physiological development and the response to external stress stimuli in plants (Luan, 2009; Weinl and Kudla, 2009).

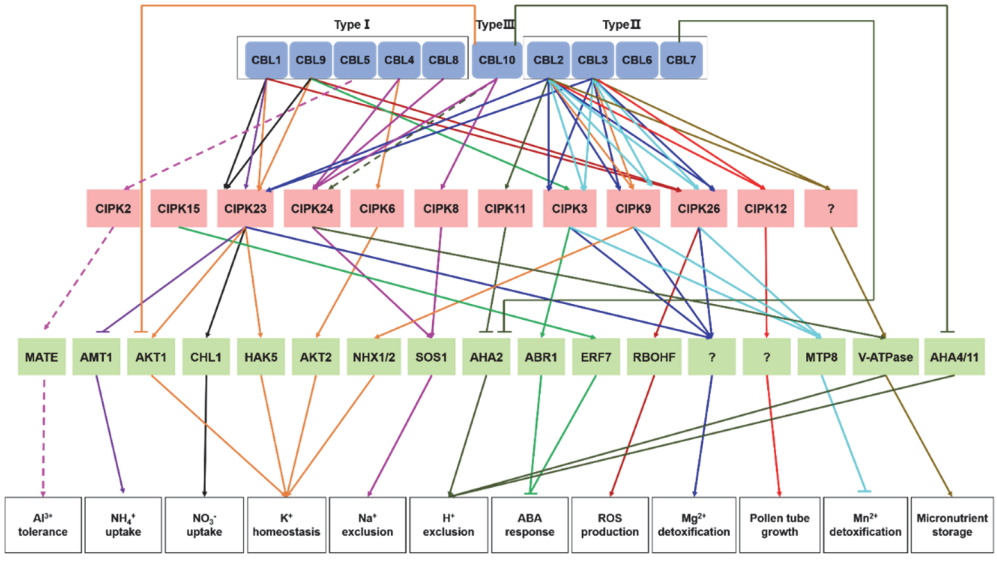

Figure 1 The CBL-CIPK regulatory network in *Arabidopsis thaliana*. The figure is modified based on (Ma et al., 2020; Mao et al., 2022). AtCBLs can be divided into three types (type Ⅰ, Ⅱ, and Ⅲ) (Kleist et al., 2014). Pointed and blunt arrowheads indicate activating and inhibitory connections, respectively. The dotted lines indicate proposed connections that still require validation.

For Ca^{2+}-binding, CBL proteins feature four EF-hands that are formed by conserved α-helix-loop-α-helix structures (Sánchez-Barrena et al., 2013). The Ca^{2+} binding affinity of EF-hands can vary within and between CBLs, which is assumed to enable specific and appropriate responses to the specific $[Ca^{2+}]_{cyt}$ signatures of different stimuli. When bound with Ca^{2+}, the molecular surface properties of CBL change. This

change contributes to the interaction of the CBL protein with the NAF domain (named after the highly conserved amino acids Asn (N), Ala (A), Phe (F)) of the CIPK, (Sánchez-Barrena et al., 2013). Once combined with its CBL counterpart, the phosphorylation site located in the CIPK activation loop is uncovered, turning its auto-inhibited state into an active state and thereby authorizing it to phosphorylate downstream substrates (Guo et al., 2001; Nunez-Ramirez et al., 2012; Sánchez-Barrena et al., 2013). This phosphorylation is reversible, which is important for organisms to modulate cellular processes in response to environmental cues. One of the better established roles of CBL-CIPK in stress tolerance is its regulation of ion homeostasis under salt stress (Figure 2).

Plant adaptation to salt stress

Salinity stress is characterized by a high concentration of soluble salts (often NaCl) in the soil with a soil electrical conductivity (EC) measured in the saturated extract (ECe) of 4 dS/m or more at 25℃, which is equivalent to approximately 40 mM NaCl (Richards, 1954). Glycophytes including the most important food crops often have growth and yield penalties already at 5 dS/m, while halophytes can withstand much higher salinity levels and may have optimal growth at soil salinity ranging from 20-40 dS/m (Flowers and Colmer, 2015; Joshi et al., 2015).

Salt stress imposes both osmotic stress and ionic stress on plants (Munns, 2005). The osmotic effect triggered by salt stress is similar to that triggered by drought stress. The osmotic effect makes it harder for roots to take up water because of the difference in osmotic potential between the saline soil and roots. At the cellular level, both stresses cause cellular dehydration, leading to a decrease in the cytosolic and vacuolar volumes (Bartels and Sunkar, 2005; Munns and Tester, 2008). The stress from water deficiency also affects the electron-transport chains of mitochondria and chloroplasts, which results in excessive ROS production and oxidative stress. This secondary oxidative stress modifies cellular structures and metabolism, leading to a decrease in photosynthesis and/or an increase in plant hormones such as ABA and

ultimately cell and tissue damage (Bartels and Sunkar, 2005).

In addition to osmotic stress, salinity leads to ion accumulation in plants (Munns, 2005; Munns and Tester, 2008). Na^+ appears to reach a toxic concentration before Cl^- does for most species (Munns and Tester, 2008), so most studies focus on Na^+ accumulation in different plant tissues when it comes to salt stress. Under continuous salt stress, Na^+ is transported to the leaf blades with the transpiration stream and is deposited there, because only a small proportion of the Na^+ can be recirculated to roots through phloem for most plants (Tester, 2003). Na^+ and Cl^- accumulate over time, and become toxic when they reach a threshold (Munns and Tester, 2008). The threshold of cytosolic Na^+ and Cl^- concentration varies between plant species. Some reports claim that the threshold of cytosolic Na^+ concentration is ~30 mmol/L while others suggest a range between 50 and 200 mmol/L (Wu, 2018). The toxic threshold of the cytosolic Cl^- concentration is reported to be 4-7 mg/g DW (~11-19 mmol/L) for Cl^- sensitive species and 15-50 mg/g DW (~42-141 mmol/L) for Cl^--tolerant species (Tavakkoli et al., 2010).

Adaptation to salinity requires many complex physiological changes, including reduced photosynthesis and transpiration, attenuated growth, accumulation of compatible solutes and protective proteins, and increased levels of antioxidants (Bartels and Sunkar, 2005). Plants have developed many strategies to minimize damage from salt stress, such as enhancing tolerance to osmotic stress, promoting Na^+ exclusion from leaf blades, and enhancing tissue tolerance to Na^+ accumulation (Munns and Tester, 2008). Minimizing the net delivery of Na^+ into the root xylem and minimizing the concentration of salt in the cytoplasm are particularly important for plants to survive (Munns, 2005). The inhibition of Na^+ accumulation in the cytoplasm entails salt excretion and salt compartmentalization.

Using Ca^{2+}-imaging techniques, plants were shown to be able to distinguish osmotic and ionic stress by different sensing modules and induce corresponding specific Ca^{2+} signals (Lee and Seo, 2021). Ionic stress and osmotic stress stimulate different

primary Ca^{2+} signals through different pathways of the stress-sensing machinery. The osmotic stress-sensing machinery includes the hyperosmolality-gated Ca^{2+}-permeable channel OSCA1 localized at the plasma membrane (Yuan et al., 2014). OSCA1 is anchored to the lipid bilayer and can perceive membrane tension changes induced by turgor pressure (Jojoa-Cruz et al., 2018; Liu et al., 2018; Maity et al., 2019). The sphingolipid GIPCs (glycosylinositol phosphorylceramide) are the major constituents of the outer layer of the lipid bilayer in the plasma membranes of plants and are important components of the ionic stress-sensing machinery under salt stress. GIPCs can directly bind with Na^+ and other ions that have a single positive charge, such as K^+ and Li^+ (Cacas et al., 2016; Jiang et al., 2019; Mamode Cassim et al., 2021). Direct binding of Na^+ by GIPCs and directly/indirectly interacting between GIPC and Ca^{2+} channels are essential in plant Na^+ sensing and the increase of $[Ca^{2+}]_{cyt}$ that lead to salt-tolerance responses (Jiang et al., 2019; Steinhorst and Kudla, 2019).

CBL-CIPK pathways and salt stress response

For different Ca^{2+} signals triggered by different degrees of stress, plants employ different Ca^{2+} sensors (Mehra and Bennett, 2022; Steinhorst et al., 2022). Steinhorst et al. (2022) found that the amplitude of the Ca^{2+} signal as well as the speed of the resulting Ca^{2+} wave is proportional to the intensity of salt stress, and different intensities of Ca^{2+} waves may be decoded by different CBL members (Mehra and Bennett, 2022; Steinhorst et al., 2022).

AtCBL4 is well known to work with AtCIPK24 to phosphorylate and activate the Na^+/H^+ antiporter SOS1 (the SOS (Salt Overly Sensitive) pathway), resulting in Na^+ extrusion from the roots into the root environment and Na^+ loading into the xylem for long-distance transport driven by the transpiration stream from root to shoot (Figure 2) (Shi et al., 2002). The SOS pathway has also been identified in many other plant species (Martinez-Atienza et al., 2007; Tang et al., 2010; Hu et al., 2012). Recently, AtCBL8 was suggested to be a Ca^{2+}-sensor switch for enhanced efficiency of the

SOS pathway based on the following experimental evidence (Mehra and Bennett, 2022; Steinhorst et al., 2022): *At-cbl8* mutants only exhibit salt sensitivity under high degrees of salt stress (75 mM or 100 mM NaCl), while *At-cbl4* mutants are sensitive to a very low degree of salt stress (25 mM NaCl). In addition, AtCBL8-AtCIPK24 was evidenced to activate SOS1 in yeast and human HEK293T cells (Mehra and Bennett, 2022; Steinhorst et al., 2022). Furthermore, different from AtCBL4, the structural conformation, interaction with AtCIPK24, and AtCIPK24-mediated phosphorylation of AtCBL8 are all Ca^{2+} dependent. These factors together all indicate that the AtCBL8-AtCIPK24 pathway activates SOS1 when a higher $[Ca^{2+}]_{cyt}$ level is reached under high salt stress (Figure 2).

AtCBL10 also functions in the SOS pathway. AtCBL10-AtCIPK8/24 complexes phosphorylate SOS1 and enhance Na^+ efflux from cells (Figure 2) (Quan et al., 2007; Lin et al., 2009; Yin et al., 2019). Moreover, the AtCBL10-AtCIPK24 complex was suggested to activate a Na^+/H^+ antiporter to sequester Na^+ into the vacuole for salt storage and detoxification of the cytosol (Kim et al., 2007), but the antiporter is not identified yet. Other research suggested that AtCBL10-AtCIPK24 may drive Na^+ compartmentalization by activating the vacuolar H^+ pump H^+-pyrophosphatase (AVP1) and vacuolar H^+-ATPase (VHA-A1) to generate an electrochemical gradient of H^+ (Figure 2) (Plasencia et al., 2021).

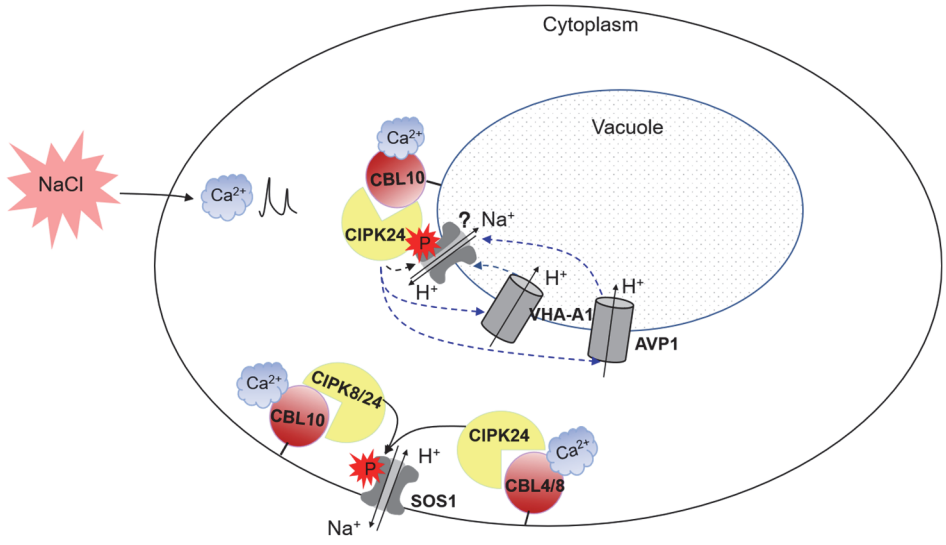

Figure 2 Schematic picture to show the important CBL-CIPK pathways in salt stress response. Pointed arrowheads indicate activating processes. The dotted lines indicate proposed connections that still require validation. The question mark (?) means the Na^+/H^+ antiporter has not been identified yet. The red lighting sign with a "P" inside means phosphorylation.

The salt tolerance and tobacco *CBL* genes

The role of the CBL-CIPK pathway is studied well in *Arabidopsis* but much less in other crops including representatives of the *Solanaceae*. Cultivated tobacco (*Nicotiana tabacum*) is a member of the *Solanaceae* family including important crops like tomato, potato, and pepper. Identification and characterization of salt stress-related tobacco genes can unlock their potential to improve the salt stress tolerance of tobacco, and the results are potentially translatable to other *Solanaceae* crops thus benefiting the sustainable production of these important vegetable crops. *N. tabacum* is a natural allotetraploid derived from the maternal genome donor *N. sylvestris* and the paternal genome donor *N. tomentosiformis* (Murad et al., 2002; Yukawa et al., 2006). Tobacco can generate up to 170 tons/ha of green tissue and 600 kg/acre of seeds that can be used for producing biomass, biofuel, seed oil, and antibodies (Schillberg et al., 2003; Andrianov et al., 2010; Grisan et al., 2016). In

addition, tobacco is widely considered to be a model plant for fundamental research, because of its available high-quality genome sequence, easily-operated genetic transformation, and short reproduction cycle. This makes tobacco an interesting model plant to study the role of *CBL* genes as decoding hubs of salt stress stimuli.

Objectives and scope of this thesis

The research described in this thesis was initiated to enhance our understanding of the roles of tobacco *NtCBL* genes in the response to salt stress, and their possible contribution to salt tolerance. The present thesis consists of six chapters including this general introduction (**Chapter 1**).

In **Chapter 2,** we reviewed the role of the CBL-CIPK network in the physiological crosstalk between plant growth and stress adaption.

In **Chapter 3**, a genome-wide analysis of the *NtCBL* gene family in tobacco was performed to identify *CBL* family members in tobacco. Their genic and protein structural features were discussed, and expression profiles in different tissues at different developmental stages and under salt stress were analyzed. The *NtCBL4A-1* gene from the ancestral *N. sylvestris* genome was characterized in more detail because of its potential role in the salt stress response.

In **Chapter 4,** we focused on another member of the CBL family that was suggested to play a role in salt tolerance: CBL5. Tobacco plants overexpressing *NtCBL5A* were evaluated under saline conditions and were shown to be hypersensitive to salinity (expressed as highly necrotic leaves). This hypersensitive phenotype was shown to be potentially linked to abnormal Na^+ compartmentalization, plant photosynthesis, and plant immune response triggered by the constitutive overexpression of *NtCBL5A*.

The results described in Chapter 3 and Chapter 4 suggest that the (ectopic) overexpression of *NtCBL4A-1* and *NtCBL5A* may interfere with the function of other CBL-CIPK modules. In **Chapter 5**, we assessed the salt tolerance of *NtCBL4A-1::NtCBL5A* co-overexpressing lines and *NtCBL10A::NtCBL5A* co-overexpressing lines. Results showed that co-overexpression of *NtCBL4A-1* and *NtCBL5A* has an

additive effect on the salt sensitivity of transgenic tobacco, while *NtCBL10A* overexpression greatly relieved the salt sensitivity of *NtCBL5A*-OE lines. This indicates that the salt sensitivity caused by *NtCBL4A-1* overexpression and *NtCBL5A* overexpression may be linked to the function of *NtCBL10A*. This was corroborated by the fact that NtCBL4A-1, NtCBL5A, and NtCBL10A interact with the same NtCIPK24 in the yeast two-hybrid system. Increased salt sensitivity of *Nt-cbl10a* single mutants and *Nt-cbl10b* single mutants, and the hypersensitivity of the *Nt-cbl10acbl10b* double mutants further demonstrate that *NtCBL10A* and *NtCBL10B* are key components for salt tolerance of tobacco.

In **Chapter 6**, I summarized all findings and discussed our hypothesis on the salt-sensitive phenotypes induced by the overexpression of *NtCBL4A-1*, *NtCBL5A*, and the knock-out of *NtCBL10*. In addition, I discussed some findings in our research, which are useful to understand the salt stress response of plants.

REFERENCES

Andrianov, V., Borisjuk, N., Pogrebnyak, N., Brinker, A., Dixon, J., Spitsin, S., Flynn, J., Matyszczuk, P., Andryszak, K., Laurelli, M., Golovkin, M., and Koprowski, H. Tobacco as a production platform for biofuel: overexpression of *Arabidopsis* DGAT and LEC2 genes increases accumulation and shifts the composition of lipids in green biomass. *Plant Biotechnol J*. **2010**, *8*, 277-287.

Bartels, D., and Sunkar, R. Drought and salt tolerance in plants. *CRC Crit Rev Plant Sci*. **2005**, *24*, 23-58.

Bonza, M. C., Loro, G., Behera, S., Wong, A., Kudla, J., and Costa, A. Analyses of Ca^{2+} accumulation and dynamics in the endoplasmic reticulum of *Arabidopsis* root cells using a genetically encoded Cameleon sensor. *Plant Physiol*. **2013**, *163*, 1230-1241.

Bush, D. S. Effects of gibberellic acid and environmental factors on cytosolic calcium in wheat aleurone cells. *Planta*. **1996**, *199*, 89-99.

Cacas, J. L., Bure, C., Grosjean, K., Gerbeau-Pissot, P., Lherminier, J., Rombouts, Y., Maes, E., Bossard, C., Gronnier, J., Furt, F., Fouillen, L., Germain, V., Bayer, E., Cluzet, S., Robert, F., Schmitter, J. M., Deleu, M., Lins, L., Simon-Plas, F., and Mongrand, S. Revisiting plant plasma membrane lipids in tobacco: a focus on sphingolipids. *Plant Physiol*. **2016**, *170*, 367-384.

Choi, W. G., Toyota, M., Kim, S. H., Hilleary, R., and Gilroy, S. Salt stress-induced Ca^{2+} waves are associated with rapid, long-distance root-to-shoot signaling in plants. *Proc Natl Acad Sci U S A*. **2014**, *111*, 6497-6502.

Cook, J., Oreskes, N., Doran, P. T., Anderegg, W. R. L., Verheggen, B., Maibach, E. W., Carlton, J. S., Lewandowsky, S., Skuce, A. G., Green, S. A., Nuccitelli, D., Jacobs, P., Richardson, M., Winkler, B., Painting, R., and Rice, K. Consensus on consensus: a synthesis of consensus estimates on human-caused global warming. *Environ Res Lett*. **2016**, *11*, 048002.

Corso, M., Doccula, F. G., de Melo, J. R. F., Costa, A., and Verbruggen, N. Endoplasmic reticulum-localized CCX2 is required for osmotolerance by regulating ER and cytosolic Ca^{2+} dynamics in *Arabidopsis*. *Proc Natl Acad Sci U S A*. **2018**, *115*, 3966-3971.

Costa, A., Navazio, L., and Szabo, I. The contribution of organelles to plant intracellular calcium signalling. *J Exp Bot*. **2018**, *69*, 4175-4193.

Evans, M. J., Choi, W. G., Gilroy, S., and Morris, R. J. A ROS-assisted calcium wave dependent on the AtRBOHD NADPH oxidase and TPC1 cation channel propagates the systemic response to salt stress.

Plant Physiol. **2016**, *171*, 1771-1784.

Ferguson, J. N. Climate change and abiotic stress mechanisms in plants. *Emerg Top Life Sci*. **2019**, *3*, 165-181.

Flowers, T. J., and Colmer, T. D. Plant salt tolerance: adaptations in halophytes. *Ann Bot*. **2015**, *115*, 327-331.

Gong, M., Luit, A. H. v. d., Knight, M. R., and Trewavas, A. J. Heat-shock-induced changes in intracellular Ca^{2+} level in tobacco seedlings in relation to thermotolerance. *Plant Physiol*. **1998**, *116*, 429-437.

Grisan, S., Polizzotto, R., Raiola, P., Cristiani, S., Ventura, F., di Lucia, F., Zuin, M., Tommasini, S., Morbidelli, R., Damiani, F., Pupilli, F., and Bellucci, M. Alternative use of tobacco as a sustainable crop for seed oil, biofuel, and biomass. *Agron Sustain Dev*. **2016**, *36*, 1-8.

Guo, Y., Halfter, U., Ishitani, M., and Zhu, J. K. Molecular characterization of functional domains in the protein kinase SOS2 that is required for plant salt tolerance. *Plant Cell*. **2001**, *13*, 1383–1399.

Haley, A., Russell, A. J., Wood, N., Allan, A. C., Knight, M., Campbell, A. K., and Trewavas, A. J. Effects of mechanical signaling on plant cell cytosolic calcium. *Proc. Natl. Acad. Sci. USA*. **1995**, *92*, 4124-4128.

Hrabak, E. M., Chan, C. W., Gribskov, M., Harper, J. F., Choi, J. H., Halford, N., Kudla, J., Luan, S., Nimmo, H. G., Sussman, M. R., Thomas, M., Walker-Simmons, K., Zhu, J. K., and Harmon, A. C. The Arabidopsis CDPK-SnRK superfamily of protein kinases. *Plant Physiol*. **2003**, *132*, 666-680.

Hu, D. G., Li, M., Luo, H., Dong, Q. L., Yao, Y. X., You, C. X., and Hao, Y. J. Molecular cloning and functional characterization of MdSOS2 reveals its involvement in salt tolerance in apple callus and *Arabidopsis*. *Plant Cell Rep*. **2012**, *31*, 713-722.

Jiang, Z., Zhou, X., Tao, M., Yuan, F., Liu, L., Wu, F., Wu, X., Xiang, Y., Niu, Y., Liu, F., Li, C., Ye, R., Byeon, B., Xue, Y., Zhao, H., Wang, H.-N., Crawford, B. M., Johnson, D. M., Hu, C., Pei, C., Zhou, W., Swift, G. B., Zhang, H., Vo-Dinh, T., Hu, Z., Siedow, J. N., and Pei, Z.-M. Plant cell-surface GIPC sphingolipids sense salt to trigger Ca^{2+} influx. *Nature*. **2019**, *572*, 341-346.

Jojoa-Cruz, S., Saotome, K., Murthy, S. E., Tsui, C. C. A., Sansom, M. S., Patapoutian, A., and Ward, A. B. Cryo-EM structure of the mechanically activated ion channel OSCA1.2. *Elife*. **2018**, *7*, e41845.

Joshi, R., Mangu, V. R., Bedre, R., Sanchez, L., Pilcher, W., Zandkarimi, H., and Baisakh, N. Salt adaptation mechanisms of halophytes: improvement of salt tolerance in crop plants. In: Pandey GK.

Elucidation of abiotic stress signaling in plants: functional genomics perspectives. **2015**, *2*, 243-279.

Kim, B. G., Waadt, R., Cheong, Y. H., Pandey, G. K., Dominguez-Solis, J. R., Schultke, S., Lee, S. C., Kudla, J., and Luan, S. The calcium sensor CBL10 mediates salt tolerance by regulating ion homeostasis in *Arabidopsis*. *Plant J*. **2007**, *52*, 473-484.

Kleist, T. J., Spencley, A. L., and Luan, S. Comparative phylogenomics of the CBL-CIPK calcium-decoding network in the moss *Physcomitrella*, *Arabidopsis*, and other green lineages. *Front Plant Sci*. **2014**, *5*, 187.

Kolukisaoglu, U., Weinl, S., Blazevic, D., Batistic, O., and Kudla, J. Calcium sensors and their interacting protein kinases: genomics of the *Arabidopsis* and rice CBL-CIPK signaling networks. *Plant Physiol*. **2004**, *134*, 43-58.

Lee, H.-J., and Seo, P. J. Ca^{2+} talyzing initial responses to environmental stresses. *Trends Plant Sci*. **2021**, *26*, 849-870.

Liliane, T. N., and Charles, M. S. Factors affecting yield of crops. *Agronomy-climate change & food security*. **2020**, 9.

Lin, H. X., Yang, Y. Q., Quan, R. D., Mendoza, I., Wu, Y. S., Du, W. M., Zhao, S. S., Schumaker, K. S., Pardo, J. M., and Guo, Y. Phosphorylation of SOS3-LIKE CALCIUM BINDING PROTEIN8 by SOS2 protein kinase stabilizes their protein complex and regulates salt tolerance in *Arabidopsis*. *Plant Cell*. **2009**, *21*, 1607-1619.

Liu, X., Wang, J., and Sun, L. Structure of the hyperosmolality-gated calcium-permeable channel OSCA1.2. *Nat Commun*. **2018**, *9*, 5060.

Luan, S. The CBL-CIPK network in plant calcium signaling. *Trends Plant Sci*. **2009**, *14*, 37-42.

Luan, S., Kudla, J., Rodriguez-Concepcion, M., Yalovsky, S., and Gruissem, W. Calmodulins and calcineurin B-like proteins: calcium sensors for specific signal response coupling in plants. *Plant Cell*. **2002**, *14 Suppl*, S389-400.

Luo, J., Chen, L., Huang, F., Gao, P., Zhao, H., Wang, Y., and Han, S. Intraorganellar calcium imaging in Arabidopsis seedling roots using the GCaMP variants GCaMP6m and R-CEPIA1er. *J Plant Physiol*. **2020**, *246-247*, 153127.

Ma, X., Li, Q. H., Yu, Y. N., Qiao, Y. M., Haq, S. U., and Gong, Z. H. The CBL-CIPK pathway in plant response to stress signals. *Int J Mol Sci*. **2020**, *21*, 5668.

Maity, K., Heumann, J. M., McGrath, A. P., Kopcho, N. J., Hsu, P. K., Lee, C. W., Mapes, J. H., Garza, D., Krishnan, S., Morgan, G. P., Hendargo, K. J., Klose, T., Rees, S. D., Medrano-Soto, A., Saier, M. H., Jr., Pineros, M., Komives, E. A., Schroeder, J. I., Chang, G., and Stowell, M. H. B. Cryo-EM structure of OSCA1.2 from *Oryza sativa* elucidates the mechanical basis of potential membrane hyperosmolality gating. *Proc Natl Acad Sci U S A*. **2019**, *116*, 14309-14318.

Mamode Cassim, A., Navon, Y., Gao, Y., Decossas, M., Fouillen, L., Grélard, A., Nagano, M., Lambert, O., Bahammou, D., Van Delft, P., Maneta-Peyret, L., Simon-Plas, F., Heux, L., Jean, B., Fragneto, G., Mortimer, J. C., Deleu, M., Lins, L., and Mongrand, S. Biophysical analysis of the plant-specific GIPC sphingolipids reveals multiple modes of membrane regulation. *J Biol Chem*. **2021**, 296.

Mao, J., Mo, Z., Yuan, G., Xiang, H., Visser, R. G. F., Bai, Y., Liu, H., Wang, Q., and Linden, C. G. v. d. The CBL-CIPK network is involved in the physiological crosstalk between plant growth and stress adaptation. *Plant Cell Environ*. **2022**.

Martinez-Atienza, J., Jiang, X., Garciadeblas, B., Mendoza, I., Zhu, J. K., Pardo, J. M., and Quintero, F. J. Conservation of the salt overly sensitive pathway in rice. *Plant Physiol*. **2007**, *143*, 1001-1012.

McAinsh, M. R., and Hetherington, A. M. Encoding specificity in Ca^{2+} signalling systems. *Trends Plant Sci*. **1998**, *3*, 32-36.

McCormack, E., Tsai, Y. C., and Braam, J. Handling calcium signaling: *Arabidopsis* CaMs and CMLs. *Trends Plant Sci*. **2005**, *10*, 383-389.

Mehra, P., and Bennett, M. J. A novel Ca^{2+} sensor switch for elevated salt tolerance in plants. *Dev Cell*. **2022**, *57*, 2045-2047.

Mittler, R. Abiotic stress, the field environment and stress combination. *Trends Plant Sci*. **2006**, *11*, 15-19.

Munns, R. Genes and salt tolerance: bringing them together. *New Phytol*. **2005**, *167*, 645-663.

Munns, R., and Tester, M. Mechanisms of salinity tolerance. *Annu Rev Plant Biol*. **2008**, *59*, 651-681.

Murad, L., Lim, K. Y., Christopodulou, V., Matyasek, R., Lichtenstein, C. P., Kovarik, A., and Leitch, A. R. The origin of tobacco's T genome is traced to a particular lineage within *Nicotiana tomentosiformis* (Solanaceae). *Am J Bot*. **2002**, *89*, 921-928.

Navazio, L., Bewell, M. A., Siddiqua, A., Dickinson, G. D., Galione, A., and Sanders, D. Calcium release from the endoplasmic reticulum of higher plants elicited by the NADP metabolite nicotinic acid adenine dinucleotide phosphate. *Proc. Natl. Acad. Sci. USA*. **2000**, *97*, 8693-8698.

Nunez-Ramirez, R., Sanchez-Barrena, M. J., Villalta, I., Vega, J. F., Pardo, J. M., Quintero, F. J., Martinez-Salazar, J., and Albert, A. Structural insights on the plant salt-overly-sensitive 1 (SOS1) Na^+/H^+ antiporter. *J Mol Biol*. **2012**, *424*, 283-294.

Okazaki, Y., Kikuyama, M., Hiramoto, Y., and Iwasaki, N. Short-term regulation of cytosolic Ca^{2+}, cytosolic pH and vacuolar pH under NaCl stress in the charophyte alga *Nitellopsis obtusa*. *Plant Cell Environ*. **1996**, *19*, 569-557.

Plasencia, F. A., Estrada, Y., Flores, F. B., Ortiz-Atienza, A., Lozano, R., and Egea, I. The Ca^{2+} sensor calcineurin B-Like protein 10 in plants: emerging new crucial roles for plant abiotic stress tolerance. *Front Plant Sci*. **2021**, *11*, 599944.

Price, A. H., Taylor, A., Ripley, S. J., Griffiths, A., Ttewavas, A. J., and Knigh, M. R. Oxidative signals in tobacco increase cytosolic calcium. *Plant Cell*. **1994**, *6*, 1301-1310.

Quan, R., Lin, H., Mendoza, I., Zhang, Y., Cao, W., Yang, Y., Shang, M., Chen, S., Pardo, J. M., and Guo, Y. SCABP8/CBL10, a putative calcium sensor, interacts with the protein kinase SOS2 to protect *Arabidopsis* shoots from salt stress. *Plant Cell*. **2007**, *19*, 1415-1431.

Resentini, F., Grenzi, M., Ancora, D., Cademartori, M., Luoni, L., Franco, M., Bassi, A., Bonza, M. C., and Costa, A. Simultaneous imaging of ER and cytosolic Ca^{2+} dynamics reveals long-distance ER Ca^{2+} waves in plants. *Plant Physiol*. **2021**, *187*, 603-617.

Richards, L. A. Diagnosis and improvement of saline and alkali soils. *Soil Sci*. **1954**, *78*, 154.

Sánchez-Barrena, M. J., Martínez-Ripoll, M., and Albert, A. Structural biology of a major signaling network that regulates plant abiotic stress: The CBL-CIPK mediated pathway. *Int J Mol Sci*. **2013**, *14*, 5734-5749.

Schillberg, S., Fischer, R., and Emans, N. 'Molecular farming' of antibodies in plants. *Naturwissenschaften*. **2003**, *90*, 145-155.

Shi, H., Quintero, F. J., Pardo, J. M., and Zhu, J. K. The putative plasma membrane Na^+/H^+ antiporter SOS1 controls long-distance Na^+ transport in plants. *Plant Cell*. **2002**, *14*, 465-477.

Shkolnik, D., Nuriel, R., Bonza, M. C., Costa, A., and Fromm, H. MIZ1 regulates ECA1 to generate a slow, long-distance phloem-transmitted Ca^{2+} signal essential for root water tracking in *Arabidopsis*. *Proc Natl Acad Sci U S A*. **2018**, *115*, 8031-8036.

Singh, S., and Parniske, M. Activation of calcium- and calmodulin-dependent protein kinase (CCaMK),

the central regulator of plant root endosymbiosis. *Curr Opin Plant Biol*. **2012**, *15*, 444-453.

Snedden, W. A., and Fromm, H. Calmodulin as a versatile calcium signal transducer in plants. *New Phytol*. **2001**, *151*, 35-66.

Stael, S., Wurzinger, B., Mair, A., Mehlmer, N., Vothknecht, U. C., and Teige, M. Plant organellar calcium signalling: an emerging field. *J Exp Bot*. **2012**, *63*, 1525-1542.

Steinhorst, L., He, G., Moore, L. K., Schultke, S., Schmitz-Thom, I., Cao, Y., Hashimoto, K., Andres, Z., Piepenburg, K., Ragel, P., Behera, S., Almutairi, B. O., Batistic, O., Wyganowski, T., Koster, P., Edel, K. H., Zhang, C., Krebs, M., Jiang, C., Guo, Y., Quintero, F. J., Bock, R., and Kudla, J. A Ca^{2+}-sensor switch for tolerance to elevated salt stress in *Arabidopsis*. *Dev Cell*. **2022**, *57*, 2081-2094.

Steinhorst, L., and Kudla, J. How plants perceive salt. *Nature*. **2019**, *572*, 318-319.

Tang, R. J., Liu, H., Bao, Y., Lv, Q. D., Yang, L., and Zhang, H. X. The woody plant poplar has a functionally conserved salt overly sensitive pathway in response to salinity stress. *Plant Mol Biol*. **2010**, *74*, 367-380.

Tavakkoli, E., Rengasamy, P., and McDonald, G. K. High concentrations of Na^+ and Cl^- ions in soil solution have simultaneous detrimental effects on growth of faba bean under salinity stress. *J Exp Bot*. **2010**, *61*, 4449-4459.

Tester, M. Na^+ tolerance and Na^+ transport in higher plants. *Ann Bot*. **2003**, *91*, 503-527.

Trewavas, A. J., and Malhó, R. Ca^{2+} signalling in plant cells: the big network! *Curr Opin Plant Biol*. **1998**, *1*, 428-433.

Vincent, T. R., Avramova, M., Canham, J., Higgins, P., Bilkey, N., Mugford, S. T., Pitino, M., Toyota, M., Gilroy, S., Miller, A. J., Hogenhout, S. A., and Sanders, D. Interplay of plasma membrane and vacuolar ion channels, together with BAK1, elicits rapid cytosolic calcium elevations in *Arabidopsis* during aphid feeding. *Plant Cell*. **2017**, *29*, 1460-1479.

Weinl, S., and Kudla, J. The CBL-CIPK Ca^{2+}-decoding signaling network: function and perspectives. *New Phytol*. **2009**, *184*, 517-528.

Wu, H. Plant salt tolerance and Na^+ sensing and transport. *Crop J*. **2018**, *6*, 215-225.

Yin, X., Xia, Y., Xie, Q., Cao, Y., Wang, Z., Hao, G., Song, J., Zhou, Y., and Jiang, X. The protein kinase complex CBL10-CIPK8-SOS1 functions in *Arabidopsis* to regulate salt tolerance. *J Exp Bot*. **2019**, *71*, 1801-1814.

Yip Delormel, T., and Boudsocq, M. Properties and functions of calcium-dependent protein kinases and their relatives in *Arabidopsis thaliana*. *New Phytol*. **2019**, *224*, 585-604.

Yuan, F., Yang, H., Xue, Y., Kong, D., Ye, R., Li, C., Zhang, J., Theprungsirikul, L., Shrift, T., Krichilsky, B., Johnson, D. M., Swift, G. B., He, Y., Siedow, J. N., and Pei, Z. M. OSCA1 mediates osmotic-stress-evoked Ca^{2+} increases vital for osmosensing in *Arabidopsis*. *Nature*. **2014**, *514*, 367-371.

Yukawa, M., Tsudzuki, T., and Sugiura, M. The chloroplast genome of *Nicotiana sylvestris* and *Nicotiana tomentosiformis*: complete sequencing confirms that the *Nicotiana sylvestris* progenitor is the maternal genome donor of *Nicotiana tabacum*. *Mol Genet Genomics*. **2006**, *275*, 367-373.

Zhu, J. K. Genetic analysis of plant salt tolerance using *Arabidopsis*. *Plant Physiol*. **2000**, *124*, 941-948.

Chapter 2

The CBL-CIPK network is involved in the physiological crosstalk between plant growth and stress adaptation

Jingjing Mao, Zhijie Mo, Guang Yuan, Haiying Xiang, Richard G.F. Visser, Yuling Bai, Haobao Liu, Qian Wang, C. Gerard van der Linden

Published in Plant, Cell, & Environment (2022)

ABSTRACT

Plants have evolved to deal with different stresses during plant growth, relying on complex interactions or crosstalk between multiple signaling pathways in plant cells. In this sophisticated regulatory network, Ca^{2+} transients in the cytosol ($[Ca^{2+}]_{cyt}$) act as major physiological signals to initiate appropriate responses. The CALCINEURIN B-LIKE PROTEIN (CBL)-CBL-INTERACTING PROTEIN KINASE (CIPK) network relays physiological signals characterized by $[Ca^{2+}]_{cyt}$ transients during plant development and in response to environmental changes. Many studies are aimed at elucidating the role of the CBL-CIPK network in plant growth and stress responses. This review discusses the involvement of the CBL-CIPK pathways in two levels of crosstalk between plant development and stress adaptation: direct crosstalk through interaction with regulatory proteins, and indirect crosstalk through adaptation of correlated physiological processes that affect both plant development and stress responses. This review thus provides novel insights into the physiological roles of the CBL-CIPK network in plant growth and stress adaptation.

Keywords: CBL, CIPK, crosstalk, plant development, abiotic stress, biotic stress, stress adaptation

1 INTRODUCTION

During their lifecycle, plants are continuously exposed to a plethora of abiotic and biotic stresses. Being sessile, plants need to develop defense mechanisms to adapt to these stresses and not only survive but also grow and reproduce (Shanker and Venkateswarlu, 2011). Stress responses typically come at the cost of growth and yield in crops (Huot et al., 2014; Karasov et al., 2017). More and more studies show that the negative correlations between growth and defense are partially caused by crosstalk between sophisticated molecular regulatory pathways (Karasov et al., 2017). These regulatory networks connect plant growth and stress tolerance, enabling a rapid adaptation of plant metabolism to mitigate the effects of the constantly changing environmental conditions. Campos et al. (2016) have shown

that it is in principle possible to uncouple pathways involved in the crosstalk between plant growth and defense, thus considerably reducing the trade-off of growth for defense. Knowledge of the integration of the molecular regulatory networks related to stress response and plant development may therefore be crucial for yield improvement of crops in a changing environment.

Ca^{2+} is a vital secondary messenger for both plant development and early stress responses (Hepler, 2005; Kudla et al., 2010; Reddy et al., 2011; Steinhorst and Kudla, 2014). Specific $[Ca^{2+}]_{cyt}$ transients are triggered in the cytoplasm when plants are exposed to environmental stimuli (Price et al., 1994; Haley et al., 1995; Okazaki et al., 1996; Gong et al., 1998). The $[Ca^{2+}]_{cyt}$ transients are recognized by calcium sensors that relay the Ca^{2+} signals to downstream response pathways. These sensors include CALCINEURIN B-LIKE PROTEINs (CBLs) that bind Ca^{2+} through EF-hand motifs (Sánchez-Barrena et al., 2013). The naming "EF-hand" describes its helix-loop-helix structure that resembles a right hand with the thumb (F-helix) and the forefinger (E-helix) extended at 90° (Kretsinger and Nockolds, 1973). Upon binding Ca^{2+}, the molecular surface properties of the CBL proteins are modified (Sánchez-Barrena et al., 2013). This facilitates the interaction of CBL with the NAF domain of a CBL-INTERACTING PROTEIN KINASE (CIPK) (Sánchez-Barrena et al., 2013). The Ca^{2+}-induced interaction of CBL with CIPK uncovers a phosphorylation site located in the activation loop of the CIPK protein (Sánchez-Barrena et al., 2013). The exposed activation loop of the CIPK protein is assumed to be phosphorylated and activated by as yet unknown upstream kinases (Sanyal et al., 2015). The activated CIPK protein typically phosphorylates and thus regulates multiple downstream targets (Sánchez-Barrena et al., 2013), including ion channels and enzymes (Nunez-Ramirez et al., 2012; Drerup et al., 2013). An exception for this general activation mechanism of CBL-CIPK was reported for potassium channel AKT2, which was shown to be activated by the interaction with but not the phosphorylation by the CBL-CIPK complex (Held et al., 2011).

The CBL-CIPK modules, as part of environmental signaling pathways, are well-

conserved across the plant kingdom. With the availability of the whole-genome sequence data of many plant species, the evolution of the CBL-CIPK network (from green algae to flowering plants) can be studied (Weinl and Kudla, 2009; Kleist et al., 2014; Edel and Kudla, 2015). A single CBL-CIPK pair is present in green algae *Chlorella spec.*, suggesting that the prototype of this signaling module may date back to single-cell plant ancestors (Weinl et al., 2009; Edel and Kudla, 2015; Tang et al., 2020a). The number of CBL and CIPK members expanded from lower plants to higher plants by gene duplication and whole-genome duplication events, indicating that the CBL-CIPK network plays an essential role in plant adaptation to a changing environment (Kleist et al., 2014).

Numerous expression and functional studies have demonstrated the broad involvement of the CBL-CIPK network in plant development and stress response. Recently, more and more studies indicate that the CBL-CIPK network connects plant development and stress adaptation at two levels. At the first level, the CBL-CIPK complexes directly interact with regulatory components involved in plant development and stress response. At the second level, the physiological adaptations regulated by CBL-CIPK pathways in response to stress affect plant growth and development, and vice versa.

2 LEVEL 1: The CBL-CIPK MODULES CONNECT PLANT DEVELOPMENT AND STRESS ADAPTATION BY INTERACTING WITH REGULATORY PROTEINS

The SALT OVERLY SENSITIVE (SOS) pathway is the first CBL-CIPK pathway that was uncovered in *Arabidopsis thaliana* and it is a well-studied example of crosstalk through direct interaction of components involved in plant development and stress adaptation. Under saline conditions, the induced Ca^{2+} transient promotes the phosphorylation activity of the AtCBL4-AtCIPK24 complex which activates the plasma membrane (PM)-localized Na^+/H^+ antiporter AtSOS1, leading to Na^+ extrusion from the roots into the root environment and Na^+ loading into the xylem for long-distance transport (Qiu et al., 2002; Shi et al., 2002; Nunez-Ramirez et al.,

2012). The SOS pathway is conserved in other plant species such as rice, poplar, and apple (Mao et al., 2021). Of all AtCIPKs, AtCIPK8 resembles AtCIPK24 the most (60.9% AA pairwise identity) (Kleist et al., 2014), and it has been shown that the AtCBL10-AtCIPK8 complex also functions in the SOS pathway, positively regulating AtSOS1 activity to extrude excess Na^+ from cells in the shoot under saline conditions (Yin et al., 2019).

Under normal conditions, the SOS pathway is suppressed by several proteins including 14-3-3, BRASSINOSTEROID INSENSITIVE 2 (BIN2), and GIGANTEA (GI). These proteins interact with AtCIPK24 and repress its kinase activity (Kim et al., 2013; Zhou et al., 2014; Yang et al., 2019; Li et al., 2020), thus working as molecular switches of the SOS pathway during dynamic growth and floral transition under varying soil salinity (Figure 1) (Kim et al., 2013; Park et al., 2013).

Plant 14-3-3 proteins, like their highly conserved homologs in mammals, function by binding to phosphorylated target proteins and thus modulating their function (Denison et al., 2011). Under normal conditions, AtCIPK11 phosphorylates Ser^{294} of AtCIPK24 and this promotes the interaction of AtCIPK24 with 14-3-3 proteins, which blocks AtCIPK24 activity and shuts down the SOS pathway. Under saline conditions, the interaction between 14-3-3 and AtCIPK11 is stimulated, releasing AtCIPK24 (Yang et al., 2019). The released AtCIPK24 then interacts with Ca^{2+}-binding AtCBL4, thus activating downstream AtSOS1 to regulate cellular Na^+ homeostasis (Qiu et al., 2002; Shi et al., 2002; Nunez-Ramirez et al., 2012).

The SOS pathway is also linked to plant growth through BIN2, a GLYCOGEN SYNTHASE KINASE 3 (GSK3)-like kinase. BIN2 phosphorylates and represses the transcription factors BRASSINAZOLE RESISTANT 1 (BZR1) and BRI1-EMS-SUPPRESSOR (BES1) and thus retards plant growth under salt stress (Li et al., 2020). In the rapid recovery phase after salt stress, however, AtCBL4 and AtCBL10 interact with BIN2 and recruit it to the PM. BIN2 then phosphorylates AtCIPK24 and inhibits the kinase activity of AtCIPK24, effectively switching off the AtSOS1-induced

Na^+ efflux. At the same time, the repression of the transcriptional activity of BZR1/BES1 by BIN2 is released, and growth is restored (Li et al., 2020).

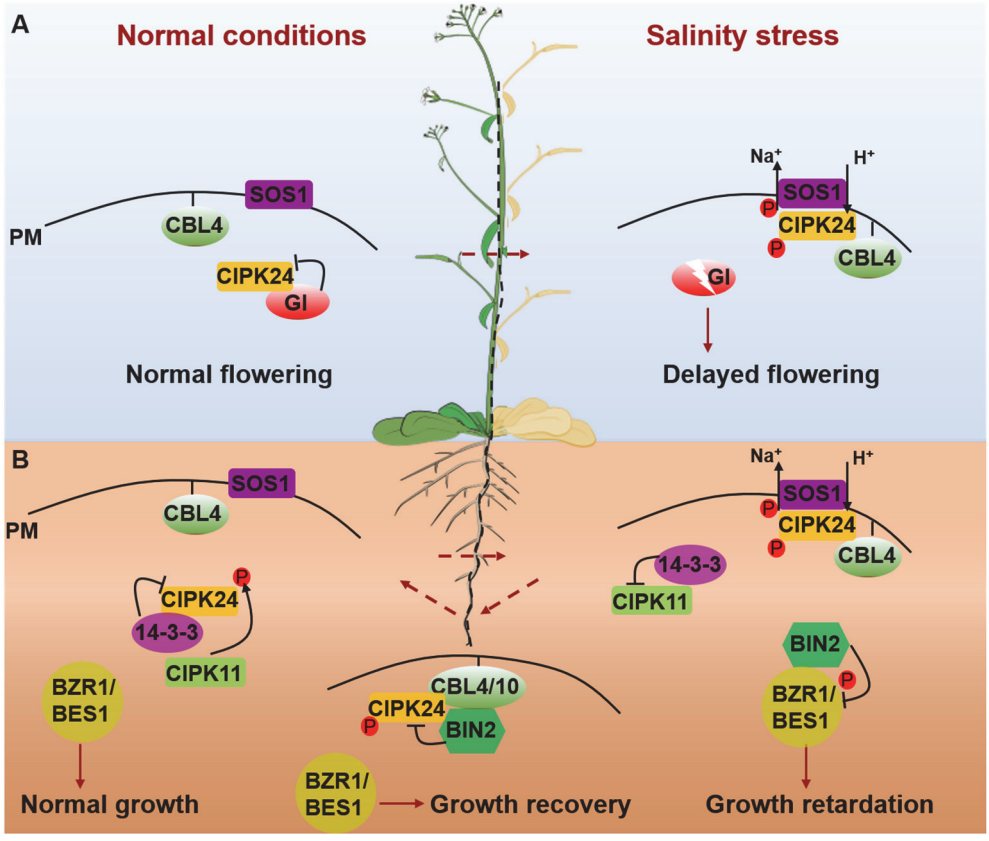

Figure 1 | SOS pathway is involved in the crosstalk between plant growth and salt stress response. **(A)** The interaction between GI and SOS pathway (Kim et al., 2013; Park et al., 2013). Under normal conditions (left side of the figure), GI interacts with AtCIPK24 and inhibits its activity, therefore AtCIPK24 does not interact with AtCBL4 and cannot phosphorylate AtSOS1. Salt stress (right side of the figure) induces the degradation of GI, releasing AtCIPK24. AtCIPK24 then interacts with PM-localized Ca^{2+}-binding AtCBL4 and activates AtSOS1. At the same time, salt-dependent degradation of GI retards or abolishes the initiation of flowering. **(B)** A proposed working model of the role of the SOS pathway in the dynamic growth of plants when switching between normal and salinity conditions (Li et al., 2020). Under normal conditions, AtCIPK11 phosphorylates AtCIPK24 and promotes its interaction with 14-3-3, inhibiting AtCIPK24 activity. BZR1/BES1 stimulates plant growth. Under salt stress, AtCBL4/AtCBL10 recruits

AtCIPK24 to the PM to activate AtSOS1. BIN2 is disassociated from the PM to phosphorylate and inhibit BZR1/BES1, thus retarding plant growth. In the recovery phase, AtCBL4/AtCBL10 recruits BIN2 to the PM to inhibit the activity of phosphorylated AtCIPK24. This reduces Na^+ efflux and releases BZR1/BES1 to stimulate plant growth. Black pointed and blunt arrowheads indicate activating and inhibiting interactions, respectively.

AtCIPK24 also interacts with GI, a nuclear protein that functions to promote the elicitation of photoperiod-dependent flowering (Park et al., 1999; Oliverio et al., 2007; Kim et al., 2013). Under normal conditions, GI interacts with AtCIPK24 and prevents AtCIPK24 from phosphorylating AtSOS1. Under saline conditions, however, the AtCIPK24-GI complex disintegrates and GI is then degraded, leading to delayed flowering (Figure 1). At the same time, the SOS pathway is activated to regulate Na^+ homeostasis and Na^+ extrusion (Kim et al., 2013; Park et al., 2013). This is consistent with the finding that *GI*-overexpressing *Arabidopsis* plants exhibited a salt-sensitive phenotype and *gi* mutants had increased salt tolerance (Kim et al., 2013).

One CIPK can be regulated by different proteins (AtCIPK24 by AtCIPK11, GI, 14-3-3, and BIN2). These interactions of CIPKs with other proteins provide the molecular basis for the first level of direct crosstalk between plant growth and stress response.

3 LEVEL 2: THE CBL-CIPK MODULES CONNECT PLANT DEVELOPMENT AND STRESS ADAPTATION BY MODULATING CORRELATED PHYSIOLOGICAL PROCESSES

To adapt to stress conditions, new biochemical pathways are activated and others that are characteristic of the non-stressed state are repressed in plants (Bohnert and Sheveleva, 1998). Protective metabolic adaptation of plants includes changes in phytohormones, ion homeostasis, and the concentration of metabolites such as sugars, sugar alcohols, low-complexity carbohydrates, tertiary amines, sulfonium compounds, and amino acids (Bohnert et al., 1998; Wolters and Jurgens, 2009). These metabolic adaptations of plants to stress alter their physiology (Bohnert et al., 1998), and affect plant development at the same time. Therefore, the CBL-CIPK

network connects plant growth and stress adaptations by modulating correlated physiological processes, including mediating phytohormone signals (Guo et al., 2002; Pandey, 2005; Song et al., 2005; Pandey et al., 2008) and regulating the homeostasis of sugar and various ions (Ma et al., 2019a; Ma et al., 2019b; Dong et al., 2021).

3.1 Phytohormone-related plant development and stress adaptation connected by CBL-CIPK network

Phytohormones are central regulators of plant growth and stress response. ABSCISIC ACID (ABA) stimulates dormancy during seed maturation (Sano and Marion-Poll, 2021), and also accumulates under osmotic stress to promote stomatal closure and reduce water loss (Luan, 2002). It has been reported that the CBL-CIPK network affects ABA-regulated plant development and abiotic stress response.

ABSCISIC ACID REPRESSOR 1 (ABR1) is a repressor of the ABA response because disruption of *ABR1* leads to a hypersensitive response to ABA in seed germination (Pandey, 2005). The AtCBL9-AtCIPK3 complex was found to activate ABR1 in the nucleus, suppressing ABA-dependent dormancy and stimulating seed germination (Figure 2A) (Pandey, 2005; Pandey et al., 2008; Sanyal et al., 2017b). When treated with ABA or under osmotic stress, *At-cbl9*, *At-cipk3*, *At-cbl9cipk3*, and *At-abr1* mutants all showed reduced germination frequency but also impaired early seedling development (Pandey, 2005; Pandey et al., 2008). The germination impairment of these mutants under osmotic stress could be caused by the osmotic stress-induced increase in ABA levels. In addition, *At-abr1* adult seedlings exhibited smaller stomatal aperture after ABA treatment, which could be the reason why they had less water loss and showed a tolerant phenotype under drought stress (Sanyal et al., 2017b).

ETHYLENE RESPONSE FACTOR 7 (AtERF7) also represses the ABA response of plants. The RNAi-mediated suppression of *AtERF7* led to increased ABA sensitivity during seed germination, while the *AtERF7*-overexpressing lines had less stomatal

closure and higher sensitivity to drought stress than wild-type seedlings (Song et al., 2005). AtCIPK15 has been shown to phosphorylate AtERF7 and this may further repress the ABA response (Figure 2A) (Song et al., 2005). *At-cipk15* RNAi lines exhibited a series of ABA hypersensitivity phenotypes, including delayed seed germination, arrested early seedling development, and dramatically reduced stomatal pores and leaf transpiration (Guo et al., 2002; Song et al., 2005). The reduced water loss of the *At-cipk15* RNAi lines may also enhance its drought tolerance.

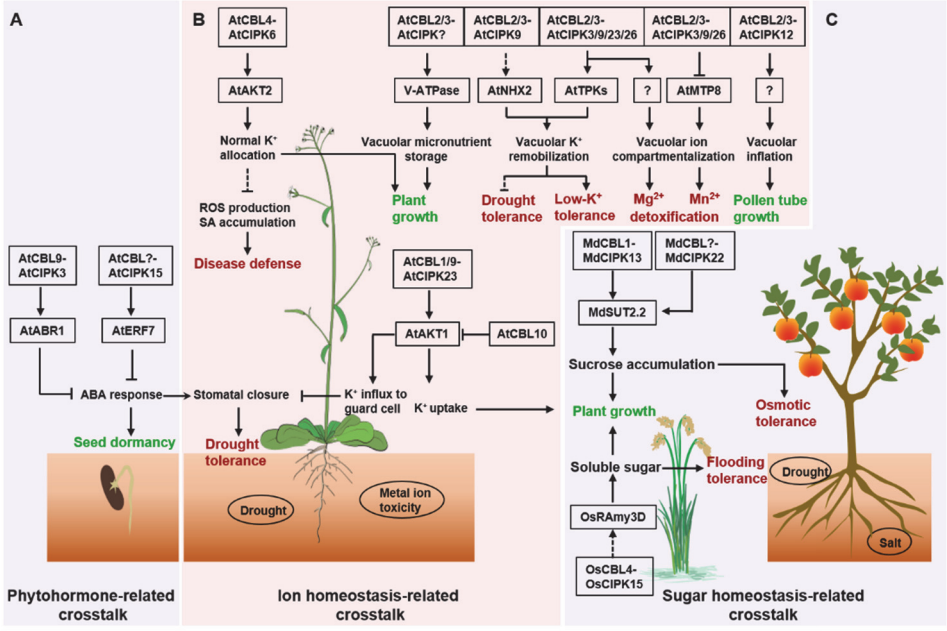

Figure 2 | Representative CBL-CIPK pathways involved in the crosstalk between plant development and stress adaptation. (A-C) CBL-CIPK pathways involved in phytohormone-related (A), ion homeostasis-related (B), and sucrose homeostasis-related (C) crosstalk between plant development and stress adaptation. Black pointed and blunt arrowheads indicate activating and inhibitory processes, respectively. The dotted lines indicate proposed processes. The green color in the text indicates plant development processes, while the red color in the text indicates plant stress responses.

3.2 Ion homeostasis-related plant development and stress adaptation connected by CBL-CIPK network

Bioinformatic analysis showed that the algal CIPKs are likely to be the closest orthologs of AtCIPK24, a key regulator of Na^+ homeostasis when interacting with AtCBL4 (Kleist et al., 2014; Edel and Kudla, 2015). All CIPKs from *Physcomitrium patens* and *Selaginella moellendorffii* are orthologs of AtCIPK24 and AtCIPK23 (Weinl et al., 2009). AtCIPK23 is a key regulator of K^+ homeostasis when interacting with AtCBL1 and AtCBL9 (Xu et al., 2006). In addition, algal CBLs feature the dual-lipid modification motif (or relicts of this motif) MGCXXS/T that presents in *Arabidopsis* AtCBL1/AtCBL9/AtCBL4 for PM localization (Kleist et al., 2014). This indicates that the ancestral role of the CBL-CIPK network is linked to the regulation of ion transport across the PM (Weinl et al., 2009; Kleist et al., 2014; Edel and Kudla, 2015).

From lower to higher plants, the number and complexity of CBLs and CIPKs increase (Weinl et al., 2009; Kleist et al., 2014), but the physiological functions of most CBL-CIPK pathways are still linked to ion homeostasis regulation (Dong et al., 2021). As the regulation of ion transport and homeostasis is essential in growth, development, as well as adaptation to stress conditions, it is not unexpected that the adaptation of ion transport regulated by CBL-CIPK pathways in stress response affects plant growth and development, and vice versa.

Ion homeostasis regulated by the CBL1/CBL9-CIPK23 pathway

Potassium (K^+) is a vital nutrient that affects many biochemical and physiological processes in plants. K^+ not only regulates plant growth and metabolism, but also contributes greatly to plant defense against various stresses (Wang et al., 2013).

The CBL1/CBL9-CIPK23-AKT1 pathway connects K^+ homeostasis to plant growth, which is conserved in several plant species. CBL1 and CBL9 are two CBL proteins that have strong sequence similarity and have functional redundancy in ion uptake and transport. In *Arabidopsis*, AtCBL1/AtCBL9-AtCIPK23 complexes are important

positive regulators of root K^+ uptake through phosphorylation of K^+ transport systems HAK5 or AKT1 under different external K^+ concentrations (Xu et al., 2006; Aleman et al., 2011; Ragel et al., 2015). Leaf development and growth of *At-cbl1cbl9* double mutant, *At-cipk23* mutant, and *At-akt1* mutant were extremely impaired under K^+ deficiency (Figure 2B) (Xu et al., 2006). Rice (*Oryza sativa*) *OsCIPK23* RNAi lines and *Os-akt1* mutant showed similar K^+-deficient symptoms under low K^+ conditions, including reduced K^+ content, leaf brown spots, and growth inhibition (Li et al., 2014). In addition, *OsCIPK23* RNAi lines had irregularly shaped pollen grains without any starch granules, which is typical for rice sterile pollen and may be related to impaired K^+ loading ability into the pollen (Yang et al., 2008). In grapevine (*Vitis vinifera*), the VvCBL1-VvCIPK4 complex (homologs of AtCBL1-AtCIPK23 complex) can activate the AKT1 ortholog VvK1.2, potentially mediating whole plant K^+ transport and translocation in fleshy fruit development (Cuellar et al., 2010; Cuellar et al., 2013). A dysfunctional SlCBL1/SlCBL9-SlCIPK23-LKT1 (AKT1 ortholog) pathway in tomato (*Solanum lycopersicum*) did not affect growth, but the tomato *lkt1* mutant displayed sensitivity to excessive Mg^{2+} with chlorosis at leaf margins (Amo et al., 2021). This may be linked to impaired K^+ accumulation in the cytosol (Amo et al., 2021): Mg^{2+} is preferentially stored in vacuoles (Shaul, 2002), and impaired K^+ loading may affect the osmotic adjustment that compensates for the increased osmotic pressure in the vacuole caused by the accumulation of metal ions (Wang et al., 2013).

The K^+ nutritional status of plants affects their drought tolerance by regulating stomatal aperture, osmotic adjustment, and REACTIVE OXYGEN SPECIES (ROS) scavenging (Wang et al., 2013). AtCBL1/AtCBL9-AtCIPK23 complexes activate AKT1 and increase K^+ influx from leaf apoplast to guard cells, leading to stomatal opening and increased leaf transpiration (Figure 2B) (Cheong et al., 2007; Nieves-Cordones et al., 2012). Mutants with a disabled AtCBL1/AtCBL9-AtCIPK23-AKT1 pathway had decreased stomatal opening, which contributes to drought tolerance (Cheong et al., 2007; Nieves-Cordones et al., 2012). In addition, the NO_3^- transporter CHLORATE RESISTANT 1 (CHL1) is also activated by the AtCBL1/AtCBL9-

AtCIPK23 complexes, switching on high-affinity nitrate transport under low external NO_3^- concentrations (Liu and Tsay, 2003; Ho et al., 2009; Leran et al., 2015). The decreased nitrate accumulation in the guard cells may also contribute to stomatal closure and reduced transpiration rates in the mutants with a disabled AtCBL1/AtCBL9-AtCIPK23-AKT1 pathway. Indeed, there is evidence for enhanced drought tolerance in *At-chl1* mutants, with reduced stomatal opening and transpiration rates (Guo et al., 2003). It should be noted that the behavior of mutants with an impaired CBL1/CBL9-CIPK23 pathway under drought stress may vary between plant species. For instance, the *OsCIPK23* RNAi lines with reduced *OsCIPK23* expression were more sensitive to drought stress compared to wild-type plants rather than more tolerant, which is different from the phenotype of *At-cipk23* (Cheong et al., 2007; Yang et al., 2008). Possibly, the K^+ deficiency of *OsCIPK23* RNAi lines negatively affected their ability for osmotic adjustment or ROS detoxification.

Ion homeostasis regulated by the CBL4-CIPK6 pathway

Regulation of K^+ homeostasis also affects disease infection by inducing the synthesis of molecules like ROS and phytohormones (Ashley et al., 2006; Amtmann et al., 2008). AKT2 is a phloem-expressed weakly rectifying K^+ channel that is active in a wide membrane potential range and can mediate both influx and efflux of K^+ (Lacombe et al., 2000). The AtCBL4-AtCIPK6 complex regulates K^+ allocation by modulating the activity of AKT2 for both K^+ loading in the source and unloading in the sink (Figure 2B) (Lacombe et al., 2000; Held et al., 2011). *At-cipk6* mutants had enhanced disease resistance with increased ROS production and SA accumulation compared to wild-type plants after the infection of the bacterial pathogen *Pseudomonas syringae* pv. *tomato* DC3000 (Sardar et al., 2017). Increased ROS production and SA accumulation in *At-cipk6* mutants may be caused by disruption of the AtCBL4-AtCIPK6 regulated K^+ transport and allocation.

Different from the general activation mechanism of CBL-CIPK, the activation of AKT2 is dependent on the interaction but not the phosphorylation by the AtCBL4-AtCIPK6

complex. AKT2 is activated when it is translocated from the endoplasmic reticulum to PM and this translocation depends on AtCBL4 (Held et al., 2011). Aberrant K^+ transport and allocation in the *At-cbl4*, *At-cipk6*, and *At-akt2* mutants were accompanied by reduced rosette size and delayed flowering phenotypes (Held et al., 2011). The *At-cipk6* mutants also had a remarkably decreased shoot-to-root and root basipetal auxin transport, resulting in fused cotyledons, swollen hypocotyls, and compromised lateral root growth (Tripathi et al., 2009).

Ion homeostasis regulated by CBL2/CBL3-CIPK3/CIPK9/CIPK23/CIPK26 pathway

Vacuolar ion homeostasis affects ion compartmentalization, vacuole inflation, and polar growth, which are required for multiple physiological processes in plant development and stress adaptation, including metal ionic tolerance, stomatal movement, pollen germination, and polarized pollen tube growth.

Tonoplast-localized AtCBL2 and AtCBL3, another two partly functionally redundant CBLs, work as crucial regulators of vacuolar ion homeostasis. Ion compartmentalization of *At-cbl2cbl3* double mutant was affected, thus its abilities of ionic tolerance (to excessive Ca^{2+}, Fe^{3+}, Cu^{2+}, K^+, and Zn^{3+}) and micronutrient storage (of Ca^{2+}, Mg^{2+}, Mn^{2+}, Fe^{3+}) were compromised (Tang et al., 2012). It was suggested that AtCBL2 and AtCBL3 positively regulate the activity of vacuolar H^+-ATPase (V-ATPase) (Figure 2B) (Tang et al., 2012), which is the major proton pump in establishing and maintaining an electrochemical proton gradient across the tonoplast to drive ion transport (Lüttge et al., 2001). However, a more recent study showed that AtCBL2 and AtCBL3 regulate Mg^{2+} compartmentalization together with multiple AtCIPKs (AtCIPK3/AtCIPK9/AtCIPK23/AtCIPK26) through a V-ATPase-independent pathway (Figure 2B) (Tang et al., 2015), indicating that AtCBL2 and AtCBL3 regulate ion homeostasis through several different downstream pathways. Recently, more pathways under the control of AtCBL2 and AtCBL3 were discovered: AtCBL2/AtCBL3-AtCIPK3/AtCIPK9/AtCIPK26 negatively regulates the transport activity of vacuolar Mn^{2+} transporter AtMTP8, inhibiting Mn^{2+} transport from the cytoplasm to the vacuole (Ju et al., 2022).

In addition, AtCBL2/AtCBL3-AtCIPK3/AtCIPK9/AtCIPK23/AtCIPK26 complexes were found to activate the vacuolar two-pore K^+ channels AtTPKs for K^+ remobilization to the cytoplasm under low-K^+ stress (Tang et al., 2020b), explaining why the *At-cbl2cbl3* double mutants retain more K^+ even though they showed more sensitive to K^+ deficiency than wild-type (Tang et al., 2012; Tang et al., 2020b). The mutation of *AtCIPK9* alone leads to a discernible vacuolar K^+ conductance reduction and sensitivity to K^+ deficiency, suggesting that *AtCIPK9* might be a dominating *AtCIPK* in the regulation of vacuolar K^+ homeostasis (Tang et al., 2020b). The importance of *AtCIPK9* for vacuolar K^+ homeostasis is exemplified by the study of Song et al. (2018), in which the *At-cipk9* mutant had reduced vacuolar K^+ influx through K^+/H^+ antiporter AtNHX1 and AtNHX2 but not defective vacuolar K^+ release through AtTPK1, resulting in ABA-hypersensitive stomatal closure and thus enhanced drought tolerance (Song et al., 2018).

Interestingly, Tang et al. (2012; 2020b) reported on contrasting phenotypes of the *At-cbl2cbl3* double mutant under low-K^+ stress. In their earlier study, they reported *At-cbl2cbl3* double mutant was more tolerant than WT under low-K^+ (50 μM, 100 μM, 200 μM) conditions (Tang et al., 2012), while they recently observed the *At-cbl2cbl3* double mutant was more sensitive than WT under low-K^+ (10μM, 100 μM) conditions (Tang et al., 2020b). The different NH_4^+ concentrations used in root media (20 mM in the previous study and 1 mM in the recent study) were suggested as the cause for the contradicting phenotypes (Tang et al., 2020b), as NH_4^+ toxicity might mask the true phenotype of mutants under low-K^+ stress (Shi et al., 2020). It is well known that NH_4^+ toxicity enhances the plant sensitivity to low-K^+ stress while K^+ relieves plant sensitivity to NH_4^+ toxicity (Shi et al., 2020), while the *At-cbl2cbl3* double mutant exhibited a more tolerant phenotype than the wild-type under the more severe combined stress conditions (low-K^+ and high NH_4^+), suggesting that AtCBL2 and AtCBL3 might also be involved in the regulation of NH_4^+ homeostasis. For another study, however, *At-cbl3* and *At-cipk9* mutant were reported to be more tolerant than wild-type under K^+ deficiency even when NH_4^+ concentration in root media was as

low as 1.25 mM (Liu et al., 2013), indicating the possible role of CBL-CIPK network in regulating K^+ and NH_4^+ homeostasis is worth exploring in more detail.

Both *At-cbl2cbl3* double mutants and *At-cipk3/9/23/26* quadruple mutants were severely inhibited in growth (Tang et al., 2012; Tang et al., 2020b), and the *At-cbl2cbl3* double mutant also displayed leaf tip necrosis, underdeveloped roots, shorter siliques, fewer seeds, and defective embryonic development (Tang et al., 2012; Eckert et al., 2014), which are symptoms that may be related to micronutrient deficiency (e.g. Ca^{2+}, Mg^{2+}, Mn^{2+}, Fe^{3+}) or abnormal vacuolar K^+ homeostasis (Song et al., 2018; Tang et al., 2020b). In addition, *At-cbl2*, *At-cbl3*, *At-cbl2cbl3*, and *At-cipk12* mutant lines all showed dramatically reduced pollen germination rates and altered tonoplast morphologies in pollen tubes. This suggests that AtCBL2, AtCBL3, and AtCIPK12 play a role in maintaining vacuole inflation and polar growth, which is required for essential processes for reproduction like pollen germination, polarized tube growth, and vacuolar morphology (Steinhorst et al., 2015). This reproduction barrier in *At-cbl2*, *At-cbl3*, *At-cbl2cbl3*, and *At-cipk12* mutants therefore may also be resulting from abnormal vacuolar ion homeostasis in pollen.

3.3 Sugar homeostasis-related plant development and stress adaptation connected by CBL-CIPK network

Sugars are the main carbon- and energy-containing molecules needed for plant growth and development, and they are substrates for cell wall construction as well as cellular solutes for osmotic balance (Griffiths et al., 2016). Several CBL-CIPK complexes were shown to play roles in the phosphorylation of sugar transporters and regulation of sugar homeostasis. For example, cotton (*Gossypium hirsutum*) GhCBL2-GhCIPK6 was reported to promote sugar (glucose) accumulation via interaction with the tonoplast sugar transporter TONOPLAST SUGAR TRANSPORTER 2 (TST2) (Deng et al., 2020). The *GhCIPK6*-overexpressing lines had more energy for growth under starvation treatment (a 10-day dark treatment followed by a 3-day recovery period) compared to the wild-type that had a withering

phenotype (Deng et al., 2020).

In apple (*Malus domestica*), the overexpression of *SUCROSE TRANSPORTER 2.2* (*MdSUT2.2*) improves sucrose accumulation and tolerance to salt stress and drought stress (Ma et al., 2019a; Ma et al., 2019b). The enhanced salt and drought tolerance of *MdSUT2.2*-overexpressing apple seedlings were shown to be dependent on the phosphorylation of MdSUT2.2 by MdCIPK13 and MdCIPK22, respectively (Figure 2C) (Ma et al., 2019a; Ma et al., 2019b). In addition, the overexpression of *MdCIPK13* and *MdCIPK22* improved sugar accumulation, as well as the salt stress and drought stress tolerance of transgenic apple seedlings, respectively (Ma et al., 2019a; Ma et al., 2019b). This may be related to osmotic adjustment through increased sucrose accumulation in these *MdCIPK13*- and *MdCIPK22*- overexpressing apple seedlings in response to osmotic stress (Figure 2C) (Ma et al., 2019a; Ma et al., 2019b). Sugar content also influences fruit flavor, color, and other quality traits in apple. Transient overexpression of *MdCBL1* and *MdCIPK13* increased the sugar content of apple fruit, whereas transient suppression of these genes decreased the sugar content of apple fruit (Jiang et al., 2021). These are clear examples of the CBL-CIPK pathway regulating the response to salt and drought stress (through osmotic adjustment) while also affecting apple growth and fruit quality.

Sugar accumulation during cold acclimation may contribute to the stabilization of membranes, protecting plants from cold-induced cellular damage (Thomashow, 1999). In *Arabidopsis*, AtCBL1 was predicted to regulate sugar metabolism by interacting with AtCIPK7 to target sucrose synthase (Chikano et al., 2001; Huang et al., 2011). The *At-cbl1* mutant was sensitive to low temperature and exhibited much more severe wilting symptoms than the wild-type (Huang et al., 2011). The wilting symptoms of *At-cbl1* under cold stress may be related to cold-induced cellular damage caused by deficient sugar accumulation (Huang et al., 2011). More research needs to be done to confirm the involvement of AtCBL1-AtCIPK7 in sugar metabolism during cold stress.

Soluble sugars are substrates for glycolysis, producing pyruvate that enables alcohol dehydrogenase (Adh) to reoxidize NADH to produce ATP under hypoxia conditions like flooding stress (Zabalza et al., 2009). Rice *OsCIPK15* is necessary for the expression of α-amylase genes (*αAmy3*, *αAmy7*, and *αAmy8*) and *Adh2* and the production of α-amylase and Adh under flooding stress, which are required for sugar production and fermentation (Lee et al., 2009). Energy deficiency of the *Os-cipk15* mutant leads to sensitivity to flooding stress at both the germination stage and seedling growth stage (Lee et al., 2009). Another further study showed that OsCBL4 is the partner of OsCIPK15 in regulating the expression of *αAmy3* (also named *RAmy3D*) (Ho et al., 2017) (Figure 2C). Knowledge about the role of the CBL-CIPK network in sugar homeostasis is as yet limited, but it deserves more attention considering the important physiological roles of sugars in plant development and stress adaptation.

4 PROSPECTS: BREEDING STRATEGIES TARGETING COMPONENTS OF THE CBL-CIPK NETWORK

Developing crops with improved stress tolerance is a highly sustainable strategy to meet the food demand of an increasing human population. Genome-editing based on the CRISPR-Cas9 technique is regarded as a new plant breeding technology that can help achieve this goal. However, few genes have been successfully used for improving stress tolerance without yield penalties under normal conditions in field trials. One of the reasons is that the molecular regulatory networks of plant growth and stress tolerance are complicated and their crosstalk is poorly understood. The CBL-CIPK network is involved in both stress response and plant development, and components of this network can be a target for plant breeding. More detailed knowledge about how the CBL-CIPK network connects with other pathways can help us to better target and modulate the components in the CBL-CIPK network for breeding varieties with optimized stress tolerance and a minimal yield penalty.

The information presented in this review indicates that constitutive overexpression

or complete knockout of *CBL* and *CIPK* genes is likely to interrupt other signaling pathways and thus may lead to unwanted side effects. For example, the *At-cipk6* mutant exhibits enhanced disease resistance (Sardar et al., 2017), but the growth and development of the *At-cipk6* mutant are disrupted, showing reduced rosette size and later flowering (Held et al., 2011). In this case, an alternative approach would be to modify the gene expression or protein function rather than knocking out or constitutively overexpressing the gene.

4.1 Modify gene expression through promoter-editing

Gene promoter provides a rich source of targets for genome-editing, contributing to dissecting tradeoff effects in crop breeding (Song et al., 2022). The DNA double-strand break in the target locus generated through CRISPR-Cas9 genome editing can be repaired through the high-fidelity homology-directed repair, stimulating precise sequence alteration. Based on this, promoter fragment insertion and swap can be generated when a DNA repair template is exogenously supplied (Shi et al., 2017). This would enable fine-tuning the gene expression to a specific tissue, under a specific stress condition, or at a specific developmental stage to reduce the trade-off between disease defense and growth.

The promoter of a gene can be replaced with a tissue-specific driving promoter. For instance, with a phloem-specific expression, *AtCIPK6* is still able to regulate the activity of phloem-expressed AKT2 to ensure the K^+ nutrition for plant growth, and the loss of *AtCIPK6* in leaves will increase resistance to the pathogen infection. This effectively uncouples the tradeoff between plant growth and disease response connected by AtCIPK6. In some cases, *cis*-regulatory elements in a promoter can be deleted through CRISPR-Cas9 to alter the tissue-specific gene expression by avoiding the inhibition of tissue-specific expressed transcription factors, thus uncoupling linkage traits (Song et al., 2022).

In addition, stress-inducible promoters can also be used so that the gene is highly expressed only under specific stress without yield loss under normal conditions (Pino

et al., 2007). For example, AtCBL2 and AtCBL3 positively regulate plant tolerance to Mg^{2+} toxicity (Tang et al., 2015), but their overexpression interferes with pollen germination and tube growth (Steinhorst et al., 2015). In this case, an Mg^{2+} toxicity-inducible promoter with a higher driving activity under Mg^{2+} toxicity stress will help to resolve this tradeoff. Another alternative approach would be to insert Mg^{2+} toxicity-responsive *cis*-regulatory elements in the native promoter of *AtCBL2* and *AtCBL3*.

4.2 Fine-tune protein function through gene-editing

Generating single-nucleotide polymorphism (SNP) is able to modify a protein function, which could be another way to reduce the growth-defense tradeoff. A reference case is about RESISTANCE OF RICE TO DISEASES1 (ROD1), which is a Ca^{2+} sensor that can scavenge ROS by stimulating catalase activity and thus suppress rice immunity (Gao et al., 2021). ROD1 inhibits ROS production under normal conditions to avoid the growth penalty, while it was degraded upon pathogen infection to ensure proper plant defense. Therefore, constitutively activated immunity in *rod1* mutants increased the pathogen resistance but compromised plant growth, leading to reduced grain yield (Gao et al., 2021). The researchers found that a natural SNP mutation of *ROD1* attenuated its ROS scavenging ability, contributing to improved basal defense without yield penalty (Gao et al., 2021). In this theory, inducing targeted mutations can potentially attenuate the protein kinase activity of AtCIPK6, retaining basal defense and plant growth at the same time.

4.3 Modify the expression of splice variants

Alternative splicing (AS) of genes is a key regulatory mechanism for plants to adapt to the environment (Rigo et al., 2019). The analysis of genome sequencing results has shown that AS-induced splice variants widely exist in *CBL* and *CIPK* families (Kolukisaoglu et al., 2004; Kanwar et al., 2014; Hu et al., 2015). It was reported that splice variants of *AtCIPK3* showed transcript and interaction preference (Sanyal et al., 2017a), which may lead to different expression patterns, protein kinase activity, and downstream targets. The splice variants of some *CBL*s (eg. *AtCBL4*) may have

different protein localization and interactors because of the difference in the N-terminus and EF domain of their encoded proteins (Figure S1). AS of CBL-CIPK components could play roles in the crosstalk between growth and defense, thus overexpressing or knocking out a specific splice variant could be another possibility to tune the gene function and relieve the growth-defense tradeoff.

In summary, to take optimal advantage of these powerful strategies to target the CBL-CIPK network, advanced knowledge about the roles of the CBL-CIPK network and its crosstalk with other pathways is essential. With more research and deeper insight into the physiological roles of splice variants of these genes, the potential for the moderation of CBL-CIPK gene functions may be exploited in the future for breeding climate-proof crop varieties.

CONFLICT OF INTEREST STATEMENT

The authors declare that the research was conducted in the absence of any commercial or financial relationships that could be construed as a potential conflict of interest.

AUTHOR CONTRIBUTIONS

J.M. conceived the original writing plans; J.M., C.G.V.L., and Q.W. completed the writing; H.L., Q.W., and C.G.V.L. co-supervised the writing; Z.M., Y.G., and H.X. provided ideas and joined discussion; R.G.F.V. and Y.B. helped with manuscript revision. H.L. and Q.W. agree to serve as the authors responsible for contact and ensure communication. All authors contributed to the article and approved the submitted version.

FUNDING

This work was supported by the National Natural Science Foundation of China (32170387), International Foundation of Tobacco Research Institute of CAAS (IFT202102), Key Funding of CNTC (No. 110202101035(JY-12)) and YNTI (No. 2020JC03, 2022JY03), China Scholarships Council (CSC No. 201803250083), and

International Exchange Scholarship of the GSCAAS.

ACKNOWLEDGMENTS

We would like to acknowledge the support of the PhD Education Programs between the GSCAAS and WUR. We would like to thank Dr. Clemens van de Wiel from Plant Breeding, WUR for the discussion.

REFERENCES

Aleman, F., Nieves-Cordones, M., Martinez, V., and Rubio, F. (2011) Root K^+ acquisition in plants: the *Arabidopsis thaliana* model. *Plant and Cell Physiology*, 52 (9), 1603-1612.

Amo, J., Lara, A., Martinez-Martinez, A., Martinez, V., Rubio, F., and Nieves-Cordones, M. (2021) The protein kinase SlCIPK23 boosts K^+ and Na^+ uptake in tomato plants. *Plant, Cell & Environment*, 44 (12), 3589-3605.

Amtmann, A., Troufflard, S., and Armengaud, P. (2008) The effect of potassium nutrition on pest and disease resistance in plants. *Physiologia Plantarum*, 133 (4), 682-691.

Ashley, M. K., Grant, M., and Grabov, A. (2006) Plant responses to potassium deficiencies: a role for potassium transport proteins. *Journal of Experimental Botany*, 57 (2), 425-436.

Bohnert, H. J., and Sheveleva, E. (1998) Plant stress adaptations— making metabolism move. *Current Opinion in Plant Biology*, 1 (3), 267–274.

Campos, M. L., Yoshida, Y., Major, I. T., de Oliveira Ferreira, D., Weraduwage, S. M., Froehlich, J. E., Johnson, B. F., Kramer, D. M., Jander, G., Sharkey, T. D., and Howe, G. A. (2016) Rewiring of jasmonate and phytochrome B signalling uncouples plant growth-defense tradeoffs. *Nature Communications*, 7 (1), 1-10.

Cheong, Y. H., Pandey, G. K., Grant, J. J., Batistic, O., Li, L., Kim, B. G., Lee, S. C., Kudla, J., and Luan, S. (2007) Two calcineurin B-like calcium sensors, interacting with protein kinase CIPK23, regulate leaf transpiration and root potassium uptake in Arabidopsis. *The Plant Journal*, 52 (2), 223-239.

Chikano, H., Ogawa, M., Ikeda, Y., Koizumi, N., Kusano, T., and Sano, H. (2001) Two novel genes encoding SNF-1 related protein kinases from *Arabidopsis thaliana*: differential accumulation of AtSR1 and AtSR2 transcripts in response to cytokinins and sugars, and phosphorylation of sucrose synthase by AtSR2. *Molecular and General Genetics*, 264 (5), 674-681.

Cuellar, T., Azeem, F., Andrianteranagna, M., Pascaud, F., Verdeil, J. L., Sentenac, H., Zimmermann, S., and Gaillard, I. (2013) Potassium transport in developing fleshy fruits: the grapevine inward K^+ channel VvK1.2 is activated by CIPK-CBL complexes and induced in ripening berry flesh cells. *The Plant Journal*, 73 (6), 1006-1018.

Cuellar, T., Pascaud, F., Verdeil, J. L., Torregrosa, L., Adam-Blondon, A. F., Thibaud, J. B., Sentenac, H., and Gaillard, I. (2010) A grapevine Shaker inward K^+ channel activated by the calcineurin B-like calcium sensor 1-protein kinase CIPK23 network is expressed in grape berries under drought stress conditions. *The Plant Journal*, 61 (1), 58-69.

Deng, J., Yang, X., Sun, W., Miao, Y., He, L., and Zhang, X. (2020) The calcium sensor CBL2 and its interacting kinase CIPK6 are involved in plant sugar homeostasis via interacting with tonoplast sugar transporter TST2. *Plant Physiology*, 183 (1), 236-249.

Denison, F. C., Paul, A. L., Zupanska, A. K., and Ferl, R. J. (2011) 14-3-3 proteins in plant physiology. *Seminars in Cell & Developmental Biology*, 22 (7), 720-727.

Dong, Q., Bai, B., Almutairi, B. O., and Kudla, J. (2021) Emerging roles of the CBL-CIPK calcium signaling network as key regulatory hub in plant nutrition. *Journal of Plant Physiology*, 257, 153335.

Drerup, M. M., Schlucking, K., Hashimoto, K., Manishankar, P., Steinhorst, L., Kuchitsu, K., and Kudla, J. (2013) The calcineurin B-like calcium sensors CBL1 and CBL9 together with their interacting protein kinase CIPK26 regulate the *Arabidopsis* NADPH oxidase RBOHF. *Molecular Plant*, 6 (2), 559-569.

Eckert, C., Offenborn, J. N., Heinz, T., Armarego-Marriott, T., Schultke, S., Zhang, C., Hillmer, S., Heilmann, M., Schumacher, K., Bock, R., Heilmann, I., and Kudla, J. (2014) The vacuolar calcium sensors CBL2 and CBL3 affect seed size and embryonic development in *Arabidopsis thaliana*. *The Plant Journal*, 78 (1), 146-156.

Edel, K. H., and Kudla, J. (2015) Increasing complexity and versatility: how the calcium signaling toolkit was shaped during plant land colonization. *Cell Calcium*, 57 (3), 231-246.

Gao, M., He, Y., Yin, X., Zhong, X., Yan, B., Wu, Y., Chen, J., Li, X., Zhai, K., Huang, Y., Gong, X., Chang, H., Xie, S., Liu, J., Yue, J., Xu, J., Zhang, G., Deng, Y., Wang, E., Tharreau, D., Wang, G. L., Yang, W., and He, Z. (2021) Ca^{2+} sensor-mediated ROS scavenging suppresses rice immunity and is exploited by a fungal effector. *Cell*, 184 (21), 5391-5404.

Gong, M., Luit, A. H. v. d., Knight, M. R., and Trewavas, A. J. (1998) Heat-shock-induced changes in intracellular Ca^{2+} level in tobacco seedlings in relation to thermotolerance. *Plant Physiology*, 116 (1), 429-437.

Griffiths, C. A., Paul, M. J., and Foyer, C. H. (2016) Metabolite transport and associated sugar signalling systems underpinning source/sink interactions. *Biochimica et Biophysica Acta*, 1857 (10), 1715-1725.

Guo, F.-Q., Young, J., and Crawford, N. M. (2003) The nitrate transporter AtNRT1.1 (CHL1) functions in stomatal opening and contributes to drought susceptibility in *Arabidopsis*. *The Plant Cell*, 15 (1), 107-117.

Guo, Y., Xiong, L., Song, C.-P., Gong, D., Halfter, U., and Zhu, J.-K. (2002) A calcium sensor and its interacting protein kinase are global regulators of abscisic acid signaling in *Arabidopsis*. *Developmental Cell*, 3 (2), 233-244.

Haley, A., Russell, A. J., Wood, N., Allan, A. C., Knight, M., Campbell, A. K., and Trewavas, A. J. (1995) Effects of mechanical signaling on plant cell cytosolic calcium. *Proceedings of the National Academy of Sciences of the United States of America*, 92 (10), 4124-4128.

Held, K., Pascaud, F., Eckert, C., Gajdanowicz, P., Hashimoto, K., Corratgé-Faillie, C., Offenborn, J. N., Lacombe, B., Dreyer, I., and Thibaud, J.-B. (2011) Calcium-dependent modulation and plasma membrane targeting of the AKT2 potassium channel by the CBL4/CIPK6 calcium sensor/protein kinase complex. *Cell Research*, 21 (7), 1116-1130.

Hepler, P. K. (2005) Calcium: A central regulator of plant growth and development. *The Plant Cell*, 17 (8), 2142-2155.

Ho, C. H., Lin, S. H., Hu, H. C., and Tsay, Y. F. (2009) CHL1 functions as a nitrate sensor in plants. *Cell*, 138 (6), 1184-1194.

Ho, V. T., Tran, A. N., Cardarelli, F., Perata, P., and Pucciariello, C. (2017) A calcineurin B-like protein participates in low oxygen signalling in rice. *Functional Plant Biology*, 44 (9), 917-928.

Hu, W., Xia, Z., Yan, Y., Ding, Z., Tie, W., Wang, L., Zou, M., Wei, Y., Lu, C., Hou, X., Wang, W., and Peng, M. (2015) Genome-wide gene phylogeny of CIPK family in cassava and expression analysis of partial drought-induced genes. *Frontiers in Plant Science*, 6, 914.

Huang, C., Ding, S., Zhang, H., Du, H., and An, L. (2011) CIPK7 is involved in cold response by interacting with CBL1 in *Arabidopsis thaliana*. *Plant Science*, 181 (1), 57-64.

Huot, B., Yao, J., Montgomery, B. L., and He, S. Y. (2014) Growth-defense tradeoffs in plants: a balancing

act to optimize fitness. *Molecular Plant*, 7 (8), 1267-1287.

Jiang, H., Ma, Q. J., Zhong, M. S., Gao, H. N., Li, Y. Y., and Hao, Y. J. (2021) The apple palmitoyltransferase MdPAT16 influences sugar content and salt tolerance via an MdCBL1-MdCIPK13-MdSUT2.2 pathway. *The Plant Journal*, 106 (3), 689-705.

Ju, C., Zhang, Z., Deng, J., Miao, C., Wang, Z., Wallrad, L., Javed, L., Fu, D., Zhang, T., Kudla, J., Gong, Z., and Wang, C. (2022) Ca^{2+}-dependent successive phosphorylation of vacuolar transporter MTP8 by CBL2/3-CIPK3/9/26 and CPK5 is critical for manganese homeostasis in Arabidopsis. *Molecular Plant*, 15 (3), 419-437.

Kanwar, P., Sanyal, S. K., Tokas, I., Yadav, A. K., Pandey, A., Kapoor, S., and Pandey, G. K. (2014) Comprehensive structural, interaction and expression analysis of CBL and CIPK complement during abiotic stresses and development in rice. *Cell Calcium*, 56 (2), 81-95.

Karasov, T. L., Chae, E., Herman, J. J., and Bergelson, J. (2017) Mechanisms to mitigate the trade-off between growth and defense. *The Plant Cell*, 29 (4), 666-680.

Kim, W. Y., Ali, Z., Park, H. J., Park, S. J., Cha, J. Y., Perez-Hormaeche, J., Quintero, F. J., Shin, G., Kim, M. R., Qiang, Z., Ning, L., Park, H. C., Lee, S. Y., Bressan, R. A., Pardo, J. M., Bohnert, H. J., and Yun, D. J. (2013) Release of SOS2 kinase from sequestration with GIGANTEA determines salt tolerance in *Arabidopsis*. *Nature Communications*, 4 (1), 1-13.

Kleist, T. J., Spencley, A. L., and Luan, S. (2014) Comparative phylogenomics of the CBL-CIPK calcium-decoding network in the moss *Physcomitrella*, *Arabidopsis*, and other green lineages. *Frontiers in Plant Science*, 5, 187.

Kolukisaoglu, U., Weinl, S., Blazevic, D., Batistic, O., and Kudla, J. (2004) Calcium sensors and their interacting protein kinases: genomics of the Arabidopsis and rice CBL-CIPK signaling networks. *Plant Physiology*, 134 (1), 43-58.

Kretsinger, R. H., and Nockolds, C. E. (1973) Carp muscle calcium-binding protein. *Journal of Biological Chemistry*, 248 (9), 3313-3326.

Kudla, J., Batistic, O., and Hashimoto, K. (2010) Calcium signals: the lead currency of plant information processing. *The Plant Cell*, 22 (3), 541-563.

Lacombe, B., Pilot, G., Michard, E., Gaymard, F., Sentenac, H., and Thibaud, J. B. (2000) A Shaker-like K^+ channel with weak rectification is expressed in both source and sink phloem tissues of *Arabidopsis*. *The Plant Cell*, 12 (6), 837-851.

Lee, K.-W., Chen, P.-W., Chung-An Lu, Chen, S., Ho, T.-H. D., and Yu, S.-M. (2009) Coordinated responses to oxygen and sugar deficiency allow rice seedlings to tolerate flooding. *Science Signaling*, 2 (91), ra61-ra61.

Leran, S., Edel, K. H., Pervent, M., Hashimoto, K., Corratge-Faillie, C., Offenborn, J. N., Tillard, P., Gojon, A., Kudla, J., and Lacombe, B. (2015) Nitrate sensing and uptake in *Arabidopsis* are enhanced by ABI2, a phosphatase inactivated by the stress hormone abscisic acid. *Science Signaling*, 8 (375), ra43.

Li, J., Long, Y., Qi, G. N., Li, J., Xu, Z. J., Wu, W. H., and Wang, Y. (2014) The Os-AKT1 channel is critical for K^+ uptake in rice roots and is modulated by the rice CBL1-CIPK23 complex. *The Plant Cell*, 26 (8), 3387-3402.

Li, J., Zhou, H., Zhang, Y., Li, Z., Yang, Y., and Guo, Y. (2020) The GSK3-like kinase BIN2 is a molecular switch between the salt stress response and growth recovery in *Arabidopsis thaliana*. *Developmental Cell*, 55 (3), 367-380.

Liu, K. H., and Tsay, Y., F. (2003) Switching between the two action modes of the dual-affinity nitrate transporter CHL1 by phosphorylation. *The EMBO Journal*, 22 (5), 1005-1013.

Liu, L. L., Ren, H. M., Chen, L. Q., Wang, Y., and Wu, W. H. (2013) A protein kinase, calcineurin B-like protein-interacting protein kinase9, interacts with calcium sensor calcineurin B-like protein3 and regulates potassium homeostasis under low-potassium stress in *Arabidopsis*. *Plant Physiology*, 161 (1), 266-277.

Luan, S. (2002) Signalling drought in guard cells. *Plant, Cell & Environment*, 25 (2), 229–237.

Lüttge, U., Fischer-Schliebs, E., and Ratajczak, R. (2001) The H^+-pumping V-ATPase of higher plants: a versatile. *Cellular & Molecular Biology Letters*, 6 (2A), 356-361.

Ma, Q. J., Sun, M. H., Kang, H., Lu, J., You, C. X., and Hao, Y. J. (2019a) A CIPK protein kinase targets sucrose transporter MdSUT2.2 at Ser(254) for phosphorylation to enhance salt tolerance. *Plant, Cell*

& Environment, 42 (3), 918-930.

Ma, Q. J., Sun, M. H., Lu, J., Kang, H., You, C. X., and Hao, Y. J. (2019b) An apple sucrose transporter MdSUT2.2 is a phosphorylation target for protein kinase MdCIPK22 in response to drought. *Plant Biotechnology Journal*, 17 (3), 625-637.

Mao, J., Yuan, J., Mo, Z., An, L., Shi, S., Visser, R. G., Bai, Y., Sun, Y., Liu, G., and Wang, Q. (2021) Overexpression of *NtCBL5A* leads to necrotic lesions by enhancing Na^+ sensitivity of tobacco leaves under salt stress. *Frontiers in Plant Science*, 12.

Nieves-Cordones, M., Caballero, F., Martinez, V., and Rubio, F. (2012) Disruption of the *Arabidopsis thaliana* inward-rectifier K^+ channel AKT1 improves plant responses to water stress. *Plant and Cell Physiology*, 53 (2), 423-432.

Nunez-Ramirez, R., Sanchez-Barrena, M. J., Villalta, I., Vega, J. F., Pardo, J. M., Quintero, F. J., Martinez-Salazar, J., and Albert, A. (2012) Structural insights on the plant salt-overly-sensitive 1 (SOS1) Na^+/H^+ antiporter. *Journal of Molecular Biology*, 424 (5), 283-294.

Okazaki, Y., Kikuyama, M., Hiramoto, Y., and Iwasaki, N. (1996) Short-term regulation of cytosolic Ca^{2+}, cytosolic pH and vacuolar pH under NaCl stress in the charophyte alga *Nitellopsis obtusa*. *Plant, Cell & Environment*, 19 (5), 569-576.

Oliverio, K. A., Crepy, M., Martin-Tryon, E. L., Milich, R., Harmer, S. L., Putterill, J., Yanovsky, M. J., and Casal, J. J. (2007) GIGANTEA regulates phytochrome A-mediated photomorphogenesis independently of its role in the circadian clock. *Plant Physiology*, 144 (1), 495-502.

Pandey, G. K. (2005) ABR1, an APETALA2-Domain transcription factor that functions as a repressor of ABA response in *Arabidopsis*. *Plant Physiology*, 139 (3), 1185-1193.

Pandey, G. K., Grant, J. J., Cheong, Y. H., Kim, B. G., Li le, G., and Luan, S. (2008) Calcineurin-B-like protein CBL9 interacts with target kinase CIPK3 in the regulation of ABA response in seed germination. *Molecular Plant*, 1 (2), 238-248.

Park, D. H., Somers, D. E., Kim, Y. S., Choy, Y. H., Lim, H. K., Soh, M. S., Kim, H. J., Kay, S. A., and Nam, H. G. (1999) Control of circadian rhythms and photoperiodic flowering by the *Arabidopsis GIGANTEA* gene. *Science*, 285 (5433), 1579-1582.

Park, H. J., Kim, W. Y., and Yun, D. J. (2013) A role for GIGANTEA: keeping the balance between flowering and salinity stress tolerance. *Plant Signaling & Behavior*, 8 (7), e24820.

Pino, M. T., Skinner, J. S., Park, E. J., Jeknic, Z., Hayes, P. M., Thomashow, M. F., and Chen, T. H. (2007) Use of a stress inducible promoter to drive ectopic *AtCBF* expression improves potato freezing tolerance while minimizing negative effects on tuber yield. *Plant Biotechnology Journal*, 5 (5), 591-604.

Price, A. H., Taylor, A., Ripley, S. J., Griffiths, A., Ttewavas, A. J., and Knigh, M. R. (1994) Oxidative signals in tobacco increase cytosolic calcium. *The Plant Cell*, 6 (9), 1301-1310.

Qiu, Q.-S., Guo, Y., Dietrich, M. A., Schumaker, K. S., and Zhu, J.-K. (2002) Regulation of SOS1, a plasma membrane Na^+/H^+ exchanger in *Arabidopsis thaliana*, by SOS2 and SOS3. *Proceedings of the National Academy of Sciences of the United States of America*, 99 (12), 8436-8441.

Ragel, P., Ródenas, R., García-Martín, E., Andrés, Z., Villalta, I., Nieves-Cordones, M., Rivero, R. M., Martínez, V., Pardo, J. M., and Quintero, F. J. (2015) CIPK23 regulates HAK5-mediated high-affinity K^+ uptake in *Arabidopsis* roots. *Plant Physiology*, 169, 2863-2873.

Reddy, A. S., Ali, G. S., Celesnik, H., and Day, I. S. (2011) Coping with stresses: roles of calcium- and calcium/calmodulin-regulated gene expression. *The Plant Cell*, 23 (6), 2010-2032.

Rigo, R., Bazin, J. R. M., Crespi, M., and Charon, C. L. (2019) Alternative splicing in the regulation of plant-microbe interactions. *Plant and Cell Physiology*, 60 (9), 1906-1916.

Sánchez-Barrena, M. J., Martínez-Ripoll, M., and Albert, A. (2013) Structural biology of a major signaling network that regulates plant abiotic stress: The CBL-CIPK mediated pathway. *International Journal of Molecular Sciences*, 14 (3), 5734-5749.

Sano, N., and Marion-Poll, A. (2021) ABA metabolism and homeostasis in seed dormancy and germination. *International Journal of Molecular Sciences*, 22 (10), 5069.

Sanyal, S. K., Kanwar, P., Samtani, H., Kaur, K., Jha, S. K., and Pandey, G. K. (2017a) Alternative splicing of CIPK3 results in distinct target selection to propagate ABA signaling in *Arabidopsis*. *Frontiers in Plant Science*, 8, 1924.

Sanyal, S. K., Kanwar, P., Yadav, A. K., Sharma, C., Kumar, A., and Pandey, G. K. (2017b) *Arabidopsis*

CBL interacting protein kinase 3 interacts with ABR1, an APETALA2 domain transcription factor, to regulate ABA responses. *Plant Science*, 254, 48-59.

Sanyal, S. K., Pandey, A., and Pandey, G. K. (2015) The CBL-CIPK signaling module in plants: a mechanistic perspective. *Physiologia Plantarum*, 155 (2), 89-108.

Sardar, A., Nandi, A. K., and Chattopadhyay, D. (2017) CBL-interacting protein kinase 6 negatively regulates immune response to *Pseudomonas syringae* in *Arabidopsis*. *Journal of Experimental Botany*, 68 (13), 3573-3584.

Shanker, A. K., and Venkateswarlu, B. 2011. Abiotic stress response in plants - physiological, biochemical and genetic perspectives. Janeza Trdine 9, 51000 Rijeka, Croatia.

Shaul, O. (2002) Magnesium transport and function in plants: the tip of the iceberg. *Biometals*, 15 (3), 307-321.

Shi, H., Quintero, F. J., Pardo, J. M., and Zhu, J.-K. (2002) The putative plasma membrane Na^+/H^+ antiporter SOS1 controls long-distance Na^+ transport in plants. *The Plant Cell*, 14 (2), 465-477.

Shi, J., Gao, H., Wang, H., Lafitte, H. R., Archibald, R. L., Yang, M., Hakimi, S. M., Mo, H., and Habben, J. E. (2017) ARGOS8 variants generated by CRISPR-Cas9 improve maize grain yield under field. *Plant Biotechnology Journal*, 2017 (15), 207–216.

Shi, S., Xu, F., Ge, Y., Mao, J., An, L., Deng, S., Ullah, Z., Yuan, X., Liu, G., Liu, H., and Wang, Q. (2020) NH_4^+ toxicity, which is mainly determined by the high NH_4^+ /K^+ ratio, is alleviated by CIPK23 in *Arabidopsis*. *Plants (Basel)*, 9 (4), 501.

Song, C. P., Agarwal, M., Ohta, M., Guo, Y., Halfter, U., Wang, P., and Zhu, J. K. (2005) Role of an *Arabidopsis* AP2/EREBP-type transcriptional repressor in abscisic acid and drought stress responses. *The Plant Cell*, 17 (8), 2384-2396.

Song, S. J., Feng, Q. N., Li, C. L., Li, E., Liu, Q., Kang, H., Zhang, W., Zhang, Y., and Li, S. (2018) A tonoplast-associated calcium-signaling module dampens ABA signaling during stomatal movement. *Plant Physiology*, 177 (4), 1666-1678.

Song, X., Meng, X., Guo, H., Cheng, Q., Jing, Y., Chen, M., Liu, G., Wang, B., Wang, Y., Li, J., and Yu, H. (2022) Targeting a gene regulatory element enhances rice grain yield by decoupling panicle number

and size. *Nature Biotechnology*, 1-9.

Steinhorst, L., and Kudla, J. (2014) Signaling in cells and organisms — calcium holds the line. *Current Opinion in Plant Biology*, 22, 14-21.

Steinhorst, L., Mähs, A., Ischebeck, T., Zhang, C., Zhang, X., Arendt, S., Schültke, S., Heilmann, I., and Kudla, J. (2015) Vacuolar CBL-CIPK12 Ca^{2+}-sensor-kinase complexes are required for polarized pollen tube growth. *Current Biology*, 25 (11), 1475-1482.

Tang, R.-J., Wang, C., Li, K., and Luan, S. (2020a) The CBL–CIPK calcium signaling network: unified paradigm from 20 years of discoveries. *Trends in Plant Science*, 25 (6), 604-617.

Tang, R.-J., Zhao, F.-G., Garcia, V. J., Kleist, T. J., Yang, L., Zhang, H.-X., and Luan, S. (2015) Tonoplast CBL-CIPK calcium signaling network regulates magnesium homeostasis in *Arabidopsis*. *Proceedings of the National Academy of Sciences of the United States of America*, 112 (10), 3134-3139.

Tang, R. J., Liu, H., Yang, Y., Yang, L., Gao, X. S., Garcia, V. J., Luan, S., and Zhang, H. X. (2012) Tonoplast calcium sensors CBL2 and CBL3 control plant growth and ion homeostasis through regulating V-ATPase activity in *Arabidopsis*. *Cell Research*, 22 (12), 1650-1665.

Tang, R. J., Zhao, F. G., Yang, Y., Wang, C., Li, K., Kleist, T. J., Lemaux, P. G., and Luan, S. (2020b) A calcium signalling network activates vacuolar K^+ remobilization to enable plant adaptation to low-K environments. *Nature Plants*, 6 (4), 384-393.

Thomashow, M. F. (1999) Plant cold acclimation: freezing tolerance genes and regulatory mechanisms. *Annual Review of Plant Physiology and Plant Molecular Biology*, 50 (1), 571-599.

Tripathi, V., Parasuraman, B., Laxmi, A., and Chattopadhyay, D. (2009) CIPK6, a CBL-interacting protein kinase is required for development and salt tolerance in plants. *The Plant Journal*, 58 (5), 778-790.

Wang, M., Zheng, Q., Shen, Q., and Guo, S. (2013) The critical role of potassium in plant stress response. *International Journal of Molecular Sciences*, 14 (4), 7370-7390.

Weinl, S., and Kudla, J. (2009) The CBL-CIPK Ca^{2+}-decoding signaling network: function and perspectives. *New Phytologist*, 184 (3), 517-528.

Wolters, H., and Jurgens, G. (2009) Survival of the flexible: hormonal growth control and adaptation in plant development. *Nature Reviews Genetics*, 10 (5), 305-317.

Xu, J., Li, H. D., Chen, L. Q., Wang, Y., Liu, L. L., He, L., and Wu, W. H. (2006) A protein kinase, interacting with two calcineurin B-like proteins, regulates K^+ transporter AKT1 in *Arabidopsis*. *Cell*, 125 (7), 1347-1360.

Yang, W., Kong, Z., Omo-Ikerodah, E., Xu, W., Li, Q., and Xue, Y. (2008) Calcineurin B-like interacting protein kinase OsCIPK23 functions in pollination and drought stress responses in rice (*Oryza sativa* L.). *Journal of Genetics and Genomics*, 35 (2008), 531-543.

Yang, Z., Wang, C., Xue, Y., Liu, X., Chen, S., Song, C., Yang, Y., and Guo, Y. (2019) Calcium-activated 14-3-3 proteins as a molecular switch in salt stress tolerance. *Nature Communications*, 10 (1), 1199.

Yin, X., Xia, Y., Xie, Q., Cao, Y., Wang, Z., Hao, G., Song, J., Zhou, Y., and Jiang, X. (2019) The protein kinase complex CBL10-CIPK8-SOS1 functions in *Arabidopsis* to regulate salt tolerance. *Journal of Experimental Botany*, 71 (6), 1801-1814.

Zabalza, A., van Dongen, J. T., Froehlich, A., Oliver, S. N., Faix, B., Gupta, K. J., Schmalzlin, E., Igal, M., Orcaray, L., Royuela, M., and Geigenberger, P. (2009) Regulation of respiration and fermentation to control the plant internal oxygen concentration. *Plant Physiology*, 149 (2), 1087-1098.

Zhou, H., Lin, H., Chen, S., Becker, K., Yang, Y., Zhao, J., Kudla, J., Schumaker, K. S., and Guo, Y. (2014) Inhibition of the *Arabidopsis* salt overly sensitive pathway by 14-3-3 proteins. *The Plant Cell*, 26 (3), 1166-1182.

Supplementary Material

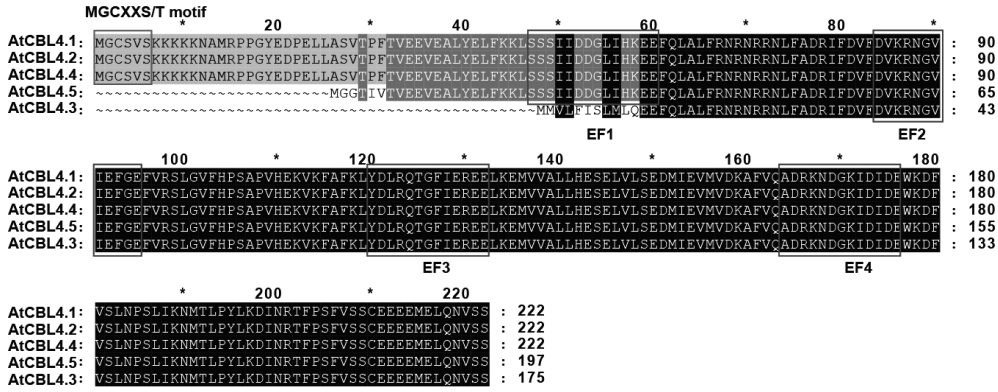

Figure S1 | Splicing variants of *AtCBL4* (*AtSOS3*).

Chapter 3

Genome-wide identification of *CBL* family genes in *Nicotiana tabacum* and the functional analysis of *NtCBL4A-1* under salt stress

Jingjing Mao, Guang Yuan, Kaiyan Han, Haiying Xiang, Wanli Zeng, Richard G.F. Visser, Yuling Bai, C. Gerard van der Linden, Haobao Liu, Qian Wang

Published in Environmental and Experimental Botany (2023)

ABSTRACT

The *CALCINEURIN B-LIKE PROTEIN* family genes (*CBLs*) encode a group of plant-specific calcium sensor proteins that play critical roles in plant development and stress response. Although genome-wide analysis of *CBL* family genes has been conducted in several diploid plant species, less is known about their functions in allopolyploid plant species. This study conducted a detailed analysis of tobacco *CBL* family genes. Of the 24 *NtCBL* genes identified, 14 were derived from the maternal genome donor *N. sylvestris*, and 10 were from the paternal genome donor *N. tomentosiformis*. Phylogenetic analysis revealed that NtCBLs could be clustered into three different groups with distinct N-terminal characteristics. All NtCBLs contain EF-hand motifs, but amino acid substitutions and configuration changes may be responsible for variations in their Ca^{2+}-binding abilities. Alternative splicing is common for *NtCBL* gene transcripts, which may contribute to variations in translation efficiency or protein interaction preferences. Several *NtCBL* genes exhibited shoot- or root-predominant expression patterns, and some were responsive to salt and/or drought stress. *NtCBL4A-1*, an ortholog of *Arabidopsis thaliana AtCBL4* (SOS3), was predominantly expressed in roots and exhibited a lower gene expression level under salt stress. Further functional analysis showed that overexpression of *NtCBL4A-1* increased the sensitivity of transgenic tobacco to Na^+-induced salt stress, which is inconsistent with the role of *AtCBL4* in contributing to salt tolerance. This study provides data for identifying *CBL* gene functions and selecting candidate stress-tolerant genes in *N. tabacum*. Additionally, the results may aid gene function studies in other allopolyploid plant species.

Keywords: tobacco; CBL; EF-hand; splicing variants; gene expression; salt stress; drought stress

INTRODUCTION

Climate change directly impedes crop production by affecting water availability and weather extremes (Kang et al., 2009; Reynolds, 2010), and indirectly impedes crop production by affecting other species such as pollinators, pests, disease vectors, and invasive species (Liliane and Charles, 2020). Moreover, crops are often subjected to a combination of different stresses in the field (Mittler, 2006). It is therefore of the utmost importance that crops are able to adapt to these changing conditions, and maintain high yields even under adverse growing conditions. Dissection of abiotic stress sensing and signaling networks and the downstream adjustments in metabolism and development continues to provide knowledge that contributes to solutions for crop improvement (Vanderschuren et al., 2013; Brozynska et al., 2016).

The CALCINEURIN B-LIKE PROTEIN (*CBL*) family genes encode plant-specific Ca^{2+} sensor proteins that interpret and relay intracellular Ca^{2+} signals triggered by external stimuli. CBL proteins transmit various Ca^{2+} signals during plant development and in response to stress by interacting with different CBL-INTERACTING PROTEIN KINASE PROTEINs (CIPKs) to evoke downstream responses (Luan, 2009). CBL proteins detect and recognize the Ca^{2+} signals using the Ca^{2+}-binding EF-hand (Shanker and Venkateswarlu, 2011; Sánchez-Barrena et al., 2013). When CBLs bind Ca^{2+}, their molecular surface properties are modified, enabling interaction with the NAF domain (named for its highly conserved amino acids Asn (N), Ala (A), and Phe (F)) of CIPK proteins (Sánchez-Barrena et al., 2013). CIPK proteins are subsequently activated to phosphorylate downstream targets such as ion transporters and enzymes involved in plant development and the stress response (Guo et al., 2001; Nunez-Ramirez et al., 2012; Sánchez-Barrena et al., 2013).

The typical structure of CBL proteins includes four EF-hands composed of two α-helixes and an intervening loop that resembles a right hand with the thumb (F-helix) and the forefinger (E-helix) extended at 90° (Kretsinger and Nockolds, 1973; Batistic and Kudla, 2009; Sánchez-Barrena et al., 2013). The subcellular location of the CBLs partially depends on motifs in their N-terminus (Kleist et al., 2014). CBL

proteins whose N-termini harbor a dual lipid modification motif can be anchored to the plasma membrane (PM) (Batistic et al., 2008; Held et al., 2011; Saito et al., 2018). CBL proteins harboring a conserved tonoplast targeting sequence (TTS) are generally tonoplast-targeted (Batistic et al., 2012). CBL10 is a special CBL protein that contains a transmembrane helix in its N-terminus, so that it can be localized to both PM and tonoplast (Kleist et al., 2014). The FPSF domain in the C-termini of CBL proteins is another conserved motif containing a Ser (S) residue, which is the phosphorylation target of CIPKs (Hashimoto et al., 2012). The phosphorylation status of CBLs affects the stability of some CBL-CIPK complexes, such as AtCBL10-AtCIPK24 and AtCBL1/9-AtCIPK23, but not AtCBL4-AtCIPK24 (Hashimoto et al., 2012).

One CBL may interact with different CIPKs, and vice versa. Thus, CBLs and CIPKs form an intricate CBL-CIPK signaling network. The prototype of the CBL-CIPK signaling modules dates back to single-cell green algae, in which only one single CBL-CIPK signaling module exists (Weinl and Kudla, 2009; Kleist et al., 2014). The ancestral function of CBL-CIPK signaling module is likely to regulate ion homeostasis (Kleist et al., 2014). The number of CBL and CIPK members expanded from lower plants to higher plants (Kleist et al., 2014). CBL and CIPK members have been widely identified in many plant species and most extensively studied in *Arabidopsis thaliana*. The key roles of identified *CBL*s in plant development and stress response indicate that *CBL* family genes may have great potential as targets for crop stress tolerance improvement (Mao et al., 2022).

The genome-wide analysis of *CBL* family genes has been conducted in several plant species, including *Arabidopsis*, rice, pineapple, tea, apple, turnip, and grapevine (Kolukisaoglu et al., 2004; Xi et al., 2017; Yin et al., 2017; Aslam et al., 2019; Liu et al., 2019; Chen et al., 2021). However, this analysis has been rarely done for allopolyploid species. In allopolyploid plants, the expression of genes from the homoeologous chromosomes needs to be orchestrated to enable the parental genomes to coexist harmoniously and contribute to growth vigor and broader

phenotypic diversity (Feldman and Levy, 2009; Akhunova et al., 2010). Homoeologs, the 'corresponding' genes derived from different species in an allopolyploid (Glover et al., 2016), may have redundant or different functions depending on their sequence similarity and expression profile. This makes the functional characterization of a specific gene in allopolyploidy more complicated. Researchers must consider the functional relevance and dominance of homoeologs when deciding whether to knock out all the homoeologs together when constructing mutants. In most cases, it is more efficient to construct both the single mutant and the double/multiple mutant. Without considering these factors, it is very likely that the single mutant appears relatively normal or exhibits only a mild phenotype because of redundancy/compensation (Peng, 2019), with no evidence that the gene is non-functional or less functional. Therefore, a detailed overview of family genes at the level of individual homoeologs in allopolyploidy is helpful, particularly in the design and interpretation of forward and reverse genetic functional studies.

Cultivated tobacco (*Nicotiana tabacum*) is a typical allotetraploid species that is derived from the maternal genome donor *N. sylvestris* and the paternal genome donor *N. tomentosiformis* (Murad et al., 2002; Yukawa et al., 2006). The functional identification and characterization of *CBL* genes in *N. tabacum* are scarce. The only report shows that overexpression of *NtCBL5A* increases the salt sensitivity of transgenic tobacco (Mao et al., 2021). This study provides a detailed analysis of individual *NtCBL* homoeologs. It includes identification and structural analysis of NtCBL family members, prediction of subcellular localization and Ca^{2+}-binding ability of NtCBL proteins, identification of key amino acid sites for the functions of NtCBL proteins, examination of gene structure and splicing variants (contributing to variation in translation efficiency or preference of protein interaction) of *NtCBL* genes at the level of individual homoeologs. In addition, this study investigates the expression profiles of *NtCBL* genes in different tissues, at different developmental stages, as well as under salt and drought stresses. *NtCBL4A-1*, an ortholog of AtCBL4 (SOS3) that was identified as a key component in plant salt stress response, was identified as responsive to salt stress and studied in more detail. This study

provides insight into *the NtCBL* family genes and the *NtCBL* gene homoeologs from the two parental genomes, serving as a guide for further detailed functional characterization of individual *NtCBL* family genes.

MATERIALS AND METHODS

Identification of NtCBL genes

The amino acid sequences of ten *Arabidopsis CBL* genes were obtained from the TAIR database (https://www.arabidopsis.org/). Using these sequences as queries, the NtCBL protein sequences from the *N. tabacum* genome were identified in the NCBI database (https://www.ncbi.nlm.nih.gov/) with the BLASTP method (E-value cutoff was $1e^{-5}$). Redundant entries resulting from alternative splicing were manually removed, and the remaining sequences were used as new queries for a second BLASTP search. After sequence alignment and SMART analysis (http://smart.embl-heidelberg.de/), sequences lacking CBL-specific motifs were removed. The ExPASy tool (https://web.expasy.org/protparam/) was used to calculate the molecular weight, isoelectric point, and amino acid number of the identified proteins.

Classification of NtCBL genes

To classify the NtCBLs, AtCBL and NtCBL protein sequences were used in the phylogenetic analysis. The phylogenetic tree was constructed using the Neighbor-Joining method with default parameters in MEGA6 (bootstrap replicates=1000). Multi-sequence alignment was conducted using Clustal Omega (https://www.ebi.ac.uk/Tools/msa/clustalo/) and the result was presented by GeneDoc (Nicholas, 1997).

Prediction of conserved motifs and analysis of 3D protein structure

The conserved motifs of NtCBLs were predicted using SMART (http://smart.embl-heidelberg.de/) (Letunic et al., 2021). The 3D protein structures of NtCBLs were predicted with SWISS-MODEL (https://swissmodel.expasy.org/) (Waterhouse et al., 2018). The EF-hand backbones and potential Ca^{2+}-binding sites were visualized using Swiss-Pdb Viewer (Guex and Peitsch, 1997).

Analysis of cis-acting elements in the promoter of NtCBL genes

To find *cis*-acting elements localized in the promoter region of *NtCBL* genes, 3000 bp of promoter regions upstream of the 5'-UTR of *NtCBL* genes were queried. The *cis*-acting elements were predicted by PlantCARE (http://bioinformatics.psb.ugent.be/webtools/plantcare/html/) (Rombauts et al., 1999) and presented with a heatmap by Tbtools (Chen et al., 2020).

Plant materials, growth conditions, and application of salt and drought treatment

N. tabacum L. cv. Zhongyan 100 cultivar was used as plant material in this study. For determining the expression profiles of *NtCBL* genes in different tobacco tissues at a young stage, tobacco plants were grown in 2019 at Unifarm, Wageningen University & Research in the Netherlands. The conditions of the greenhouse were 16 h light / 8 h dark at 25/23^{o}C and 70% relative humidity. The shortwave radiation level was maintained in the greenhouse compartment using artificial PAR (photosynthetically active radiation) when the incoming shortwave radiation was below 200 Wm^{-2} (Mao et al., 2021). Tobacco seeds were first sown in the soil. At 20 days after germination (DAG), the young tobacco plants were transplanted in rock-wool plugs within float trays for hydroponic cultivation (1/2 Hoagland's nutrient solution). After 6 days of acclimatization (at ~30 DAG), different tissues (leaf blades: all leaves with main veins removed; main veins: main veins from all leaves; stems; roots) of young tobacco plants were sampled at 35 DAG and frozen in liquid nitrogen.

For determining the expression profiles of *NtCBL* genes under salt and drought stresses, tobacco plants were grown in 2022 at the Tobacco Research Institute of the Chinese Academy of Agricultural Sciences in China. The climate chamber was set to maintain 24 h lighting (with an intensity of 7500 lux) at a temperature of 25^{o}C and 70% relative humidity. Tobacco seeds were initially sown in the soil, and for the salt treatment, young tobacco plants were transplanted into rock-wool plugs within float trays for hydroponic cultivation (1/2 Hoagland's nutrient solution) at 20 DAG. After a period of 6 days of acclimatization (at ~30 DAG), the nutrient solution was supplemented with NaCl to a concentration of 50 mM on the first day to avoid salt

shock, with the final NaCl concentration of 100 mM being achieved on the following day.

At 1 day after the start of 100 mM NaCl treatment, leaves from both the control and salt-stressed plants were sampled and immediately frozen in liquid nitrogen. For the drought treatment, young tobacco plants were transplanted into pots at 24 DAG. After 6 days of acclimatization (at ~30 DAG), watering was stopped until the leaves began to show slight wilting. At 5 days after the start of the treatment, leaves from both the control and drought-stressed plants were sampled and immediately frozen in liquid nitrogen.

Real-time quantitative PCR

Total RNA was extracted from tissues of young tobacco plant tissues using the RNeasy Plus Mini Kit (Qiagen, Cat No./ID: 74134) and purified according to the manufacturer's protocol. The RT-qPCR protocol used was described by Mao et al. (2021). RNA was reverse transcribed into cDNA using Evo M-MLV Mix Kit with gDNA Clean for qPCR (Accurate Biotechnology (Hunan) Co., Ltd, Cat No./ID: AG11728, Changsha, China), and the cDNA was amplified using SYBR Green *Pro Taq* HS qPCR Premix (Accurate Biotechnology (Hunan) Co., Ltd, Cat No./ID: AG11701, Changsha, China) on the LightCycler® 96 Instrument (F. Hoffmann-La Roche Ltd, Switzerland). All the primers used for RT-qPCR are listed in Table S1. Amplification reactions were carried out in a total volume of 10 µl, containing 5 µl 2×SYBR Green *Pro Taq* HS qPCR Premix, 0.6 µl forward and reverse primers (10 µM), 1 µl cDNA (10 times diluted), and 3.4 µl ddH_2O. The RT-qPCR amplification program was as follows: 95°C for 10 min, followed by 40 cycles of amplification at 95°C for 10 s, 60°C for 30 s. Relative gene expression data were analyzed using the $2^{-\Delta C't}$ method (Livak and Schmittgen, 2001).

Generation of NtCBL4A-1-OE plants

The coding sequence of *NtCBL4A-1* (NCBI reference sequence: XM_016613931.1) was first amplified from cDNA synthesized from RNA extracted from roots of *N. tabacum* L. cv. Zhongyan 100 with the primer pair NtCBL4A-1F/NtCBL4A-1R (Table

S1). The *NtCBL4A-1* cDNA was firstly cloned into the pMD19-T vector for sequencing and then was amplified with primer pair NtCBL4A-1F-*Kpn* Ⅰ/NtCBL4A-1R-*Xba* Ⅰ (Table S1). The gel-purified amplicon was digested with *Kpn* Ⅰ and *Xba* Ⅰ and cloned into the binary recombinant vector pCHF3 to generate the vector pCHF3-NtCBL4A-1. To generate the *NtCBL4A-1*-overexpressing lines, pCHF3-NtCBL4A-1 plasmid was transformed into *Agrobacterium tumefaciens* EHA105 and then was introduced into Zhongyan 100 by the *Agrobacterium*-mediated leaf disc transformation method (Horsch et al., 1985).

Nine positive transgenic plants of the T0 generation were identified by PCR with the primers pCHF3-62F and NtCBL4A-1R (Table S1). The expression of endogenous *NtCBL4A-1* was determined by RT-qPCR with the primer pair NtCBL4-qF/NtCBL4A-1qR, and the expression of exogenous *NtCBL4A-1* was determined by using the primers NtCBL4A-1-qF and pCHF3-Allcheck-2 (Shi et al., 2021). Six lines with high *NtCBL4A-1* overexpression were selected for propagation. The screening strategy of homozygous plants was mentioned in our previous publication (Mao et al., 2021). Two independent homozygous lines (OE-2 and OE-9) were selected for the evaluation of stress tolerance. The ion and osmotic stress evaluation of different tobacco lines were conducted as previously described (Mao et al., 2021).

RNAseq data expression analysis

Expression profiles of *NtCBL* genes in leaves (SRA accession ID: SRX2655430, SRX2655478, SRX2655480, SRX2655632, SRX2655633, SRX2655634) and roots (SRA accession ID: SRX4407884, SRX4407877, SRX4407878) of tobacco at the adult stage were analyzed from published RNA-seq data (Li et al., 2017; Qin et al., 2020).

Statistical analysis

Statistical analysis was done using IBM SPSS Statistics 23 software. Significant differences were examined by Student's *t* test or one-way ANOVA with LSD test at $p<0.05$ and $p<0.01$. The figures were drawn by GraphPad Prism 6.0.

RESULTS AND DISCUSSION

Identification and designation of *NtCBL*s

The protein sequences of ten *A*. *thaliana* AtCBLs were used as queries to identify *NtCBL* genes in the *N*. *tabacum* genome in the NCBI database (https://www.ncbi.nlm.nih.gov/). Twenty-four *NtCBL* gene loci were found in total. Generally, these *NtCBLs* were numbered based on the names of the most similar *AtCBL* genes (Figure 1A, Table 1). *NtCBL6* is an exception because it does not have close homologs in *Arabidopsis* (a detailed explanation is provided in section 3.4). It was numbered as "6" because that was the only unoccupied number from "1" to "10". Of the 24 NtCBLs analyzed, 15 showed the greatest sequence similarity to the CBLs of the maternal tobacco progenitor *N*. *sylvestris*, and were therefore labeled as "A". The remaining 9 NtCBLs were more similar to CBLs of the paternal tobacco progenitor *N*. *tomentosiformis*, and were labeled as "B" (Mao et al., 2021). *NtCBL*s with the highest similarity to the same *AtCBL* protein were numerically ordered. For example, the three *NtCBL* genes that were found to be most similar to *AtCBL1* were named *NtCBL1A-1*, *NtCBL1A-2*, and *NtCBL1A-3*. (Figure 1A, Table 1). For brevity, we refer in this paper to all the homoeologous genes of one specific NtCBL when "A" or "B" is not specially indicated.

The number of amino acids (AA), theoretical isoelectric point (p*I*), and molecular weight (MW) of the NtCBLs are listed in Table 1. Some *NtCBL* genes (NtCBL2/4A-1/4A-2/5/9B) encode splicing variants that are translated into proteins of different lengths. For these, one encoded protein was selected as a representative. More information about other variants is provided in section 3.4. The amino acid number of the 24 NtCBLs ranged from 210 to 260, with MW ranging from 23.79 kDa to 30.00 kDa, and p*I* ranging from 4.57 to 5.20. The sequence alignment shows that all the NtCBLs have four EF-hands and an FPSF domain (named by its highly conserved amino acids Phe (F), Pro (P), Ser (S), and Phe (F)), but vary in length at their N-terminal sides (Figure S1).

Table 1 Properties of NtCBLs

Name	Diploid Progenitors	Gene Symbol in NCBI	Representative Protein Accession	AA	p*I*	MW (kDa)	Classification
NtCBL1A-1	*N. sylvestris*	LOC107784127	XP_016460683.1	213	4.81	24311.67	Type Ⅰ
NtCBL1A-2	*N. sylvestris*	LOC107780982	XP_016457091.1	213	5.03	24461.01	Type Ⅰ
NtCBL1A-3	*N. sylvestris*	LOC107823299	XP_006505411.1	213	5.04	24394.89	Type Ⅰ
NtCBL1B	*N. tomentosiformis*	LOC107776182	XP_016451516.1	213	4.80	24403.77	Type Ⅰ
NtCBL2A	*N. sylvestris*	LOC107790626	XP_016468067.1	224	4.76	25640.15	Type Ⅱ
NtCBL2B	*N. tomentosiformis*	LOC107781368	XP_016457544.1	224	4.74	25484.95	Type Ⅱ
NtCBL3A	*N. sylvestris*	LOC107788654	XP_016465836.1	222	4.97	25347.87	Type Ⅱ
NtCBL3B	*N. tomentosiformis*	LOC107764963	XP_016439026.1	222	4.91	25338.86	Type Ⅱ
NtCBL4A-1	*N. sylvestris*	LOC107791794	XP_016469417.1	213	4.70	24464.87	Type Ⅰ
NtCBL4A-2	*N. sylvestris*	LOC107785211	XP_016461942.1	215	4.63	24758.25	Type Ⅰ
NtCBL4B	*N. tomentosiformis*	LOC107761260	XP_016434954.1	213	4.68	24382.83	Type Ⅰ
NtCBL5A	*N. sylvestris*	LOC107816392	XP_016497590.1	213	4.72	24581.04	Type Ⅰ
NtCBL5B	*N. tomentosiformis*	LOC107798355	XP_016476817.1	213	4.57	24435.79	Type Ⅰ
NtCBL6A	*N. sylvestris*	LOC107819027	XP_016500590.1	211	5.20	24750.37	Type Ⅱ
NtCBL7A	*N. sylvestris*	LOC107813595	NP_001312839.1	219	4.70	25222.61	Type Ⅱ
NtCBL7B	*N. tomentosiformis*	LOC107770660	XP_016445479.1	219	4.75	25221.62	Type Ⅱ
NtCBL8A-1	*N. sylvestris*	LOC107828726	XP_016511574.1	210	4.74	23769.00	Type Ⅰ
NtCBL8A-2	*N. sylvestris*	LOC107829633	XP_016512569.1	219	4.82	25463.25	Type Ⅰ
NtCBL8B-1	*N. tomentosiformis*	LOC107784734	XP_016461394.1	210	4.80	23792.04	Type Ⅰ
NtCBL8B-2	*N. tomentosiformis*	LOC107769778	XP_016444517.1	219	4.72	25360.12	Type Ⅰ
NtCBL9A	*N. sylvestris*	LOC107810670	XP_016490957.1	213	4.58	24593.84	Type Ⅰ
NtCBL9B	*N. tomentosiformis*	LOC107769000	XP_016443661.1	213	4.59	24591.86	Type Ⅰ
NtCBL10A	*N. sylvestris*	LOC107817068	XP_016498333.1	260	4.70	30004.21	Type Ⅲ
NtCBL10B	*N. tomentosiformis*	LOC107831597	XP_016514866.1	260	4.68	29919.10	Type Ⅲ

AA, the number of amino acids; p*I*, theoretical isoelectric point; MW, molecular weights. The AA, p*I*, and MW were calculated with the ExPASy tool (https://web.expasy.org/protparam/).

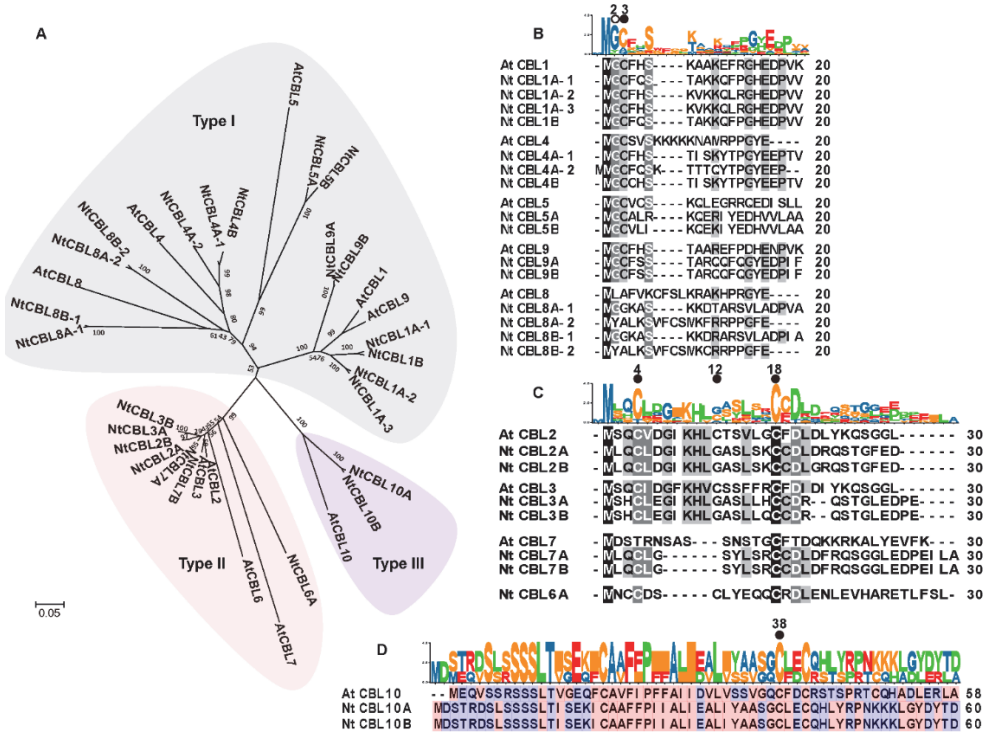

Figure 1. Phylogenetic tree and N-terminal sequence alignments of the NtCBLs and AtCBLs. (A) Phylogenetic analysis of NtCBLs and AtCBLs. The amino acid sequences of AtCBLs were downloaded from TAIR (https://www.arabidopsis.org/). The phylogenetic tree was constructed by MEGA6 using the Neighbor-Joining method. **(B-D)** N-terminal sequence alignments of the NtCBLs and AtCBLs. The key Cys (C) residues in CBLs for *S*-acylation and the key Gly (G) residue in CBLs for *N*-myristoylation were marked with hollow dots and full dots, respectively. The numbers above these dots mean the positions of these residues in the amino acid sequences of the first CBLs. The hydrophilic and hydrophobic amino acids in panel D were shaded with blue and pink, respectively.

Classification and subcellular localization analysis of NtCBLs

Similar to AtCBLs (Kleist et al., 2014), NtCBLs are classified into three types based on the phylogenetic analysis and the characteristics of their N-terminal sequences (Figure 1). The N-terminal motif is critical for the subcellular localization of CBLs (Kleist et al., 2014), and CBLs often affect the function of CIPKs by recruiting CIPKs

to specific subcellular locations (Luan, 2009).

Type Ⅰ includes 15 NtCBL members (Figure 1A, Table 1) that are the orthologs of AtCBL1/4/5/8/9. Most of them contain the dual lipid modification motif (MGCXXS/T) for *N*-myristoylation at the Gly residue (G at position 2) and *S*-acylation of the Cys residue (C at position 3) in their N-terminal regions (Figure 1B). NtCBL1/4/5/9 have the same G and C residues for dual lipid modification that ensures the plasma membrane (PM) localization of AtCBL1/4/5/9 (Batistic et al., 2008; Held et al., 2011; Saito et al., 2018), suggesting that these NtCBLs might be associated to the PM as well. It needs to be noted that the N-terminal dual lipid modification of CBLs is not a PM-specific localization signal, because AtCBL4 and AtCBL5 are also distributed in the cytoplasm and nucleus (Batistic et al., 2010). The subcellular localization of NtCBL8A-1, NtCBL8A-2, NtCBL8B-1, and NtCBL8B-2 might have different subcellular localization from those of other NtCBLs in type Ⅰ, because none of them has the C residue (position 3) and NtCBL8A-2 and NtCBL8B-2 do not have the G residue (position 2) (Figure 1B). Their ortholog AtCBL8 was shown to be mainly distributed in the cytoplasm and nucleus, and it also has a PM association (Batistic et al., 2010), indicating that CBL8 might have a unique mechanism for PM localization.

Type Ⅱ includes 7 NtCBL members (Figure 1A, Table 1) that are the orthologs of AtCBL2/3/6/7. NtCBL2/3 contain the consensus tonoplast targeting sequence (TTS, MSQCXDGXKHXCXSXXXCF) (Figure 1C) that is also present in AtCBL2 and AtCBL3 (Tang et al., 2012). In *Arabidopsis*, AtCBL2, AtCBL3, and AtCBL6 have been reported to localize to the tonoplast (Batistic et al., 2010). The *S*-acylation of the C residues at position 4 and position 18 is necessary for effective tonoplast targeting, while the substitution of C residue at position 12 of AtCBL2 resulted in the presence of a fraction of this protein in the cytoplasm and nucleus (Batistic et al., 2012). NtCBL2/3 have C residues at positions 4 and 18 but not at position 12, indicating they may be primarily but not exclusively localized to the tonoplast. AtCBL7 diverges from other type Ⅱ-AtCBLs in the phylogenetic tree because it contains a deletion in

its N-terminus (Figure 1A-B) (Kleist et al., 2014). The key C residue at position 4 is not present in AtCBL7, which might be the reason for its diffused nuclear and cytosolic localization (Batistic et al., 2010). NtCBL7A/7B also have deletions in their N-termini, but they still have both key conserved C residues for tonoplast localization, therefore they might still be tonoplast-localized. NtCBL6A also has a short deletion in its N-terminus between the C residues at positions 4 and 18 (Figure 1C). Whether this deletion affects NtCBL6A localization to the tonoplast remains to be clarified.

NtCBL10A/10B belong to type Ⅲ (Figure 1A, Table 1). Both NtCBL10A and NtCBL10B are predicted to contain a transmembrane (TM) helix for membrane association, similar to AtCBL10 (Figure 1D). AtCBL10 was found to be localized to the PM, as well as endosomal and tonoplast compartments (Kim et al., 2007; Quan et al., 2007; Batistic et al., 2010). The tonoplast association of AtCBL10 also requires *S*-acylation of the C residue at position 38 (Figure 1D) and appears to be essential in response to salt stress (Chai et al., 2020). The substitution of this C residue to Ser (S) in AtCBL10 leads to cytoplasmic and nuclear localization and dysfunction under salt stress (Chai et al., 2020). Both NtCBL10A and NtCBL10B contain the key C residue (at position 38 in AtCBL10). In addition, NsylCBL10, an *N. sylvestris* CBL protein with the same amino acid sequence as NtCBL10A and three amino acids difference from NtCBL10B, was verified to associate with the PM (Dong et al., 2015). Therefore, it is highly possible that NtCBL10A and NtCBL10B are also localized to the PM, as well as to the endosomes and tonoplast.

Prediction of tertiary structure and Ca^{2+}-binding affinity of NtCBLs

The presence of EF-hands in the CBL proteins confers the ability to bind Ca^{2+} and respond to Ca^{2+}-mediated environmental cues. Whether they bind Ca^{2+} also depends on the spatial location of the EF-hands in the folded CBL protein. However, little is known about the tertiary structure of CBL proteins. Until now, only the crystallographic structures of AtCBL2 and its binary complex with the C-terminus of AtCIPK14, as well as AtCBL4 and its binary complex with the C-terminus of

AtCIPK24 have been determined (Nagae et al., 2003; Sanchez-Barrena et al., 2005; Sanchez-Barrena et al., 2007; Akaboshi et al., 2008). We predicted the tertiary structures of NtCBLs using the SWISS-MODEL (Waterhouse et al., 2018) to further assess the diversity of the EF-hand functionality in the NtCBL family. The tertiary structures of several NtCBLs fit together, which are NtCBL4/5/8A-2/8B-2, NtCBL2/3/6A, NtCBL1/7/9/10, and NtCBL8A-1/8B-1. The backbones of their EF-hands are displayed in Figure 2.

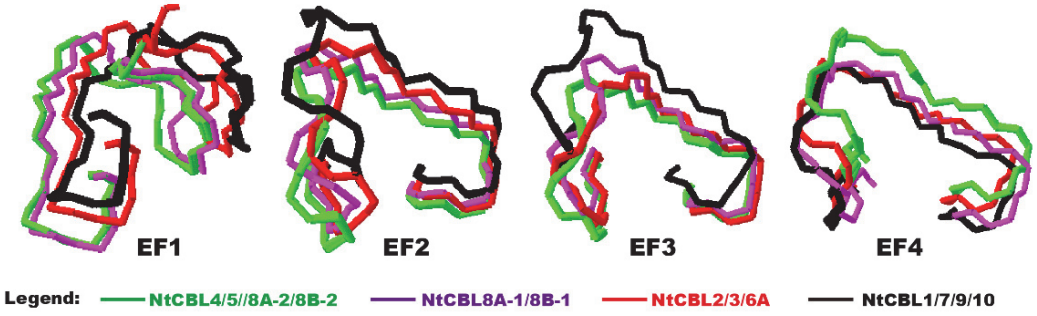

Figure 2. The tertiary structure of EF-hands of NtCBLs. The tertiary structures were built based on the whole protein backbones, and only the backbones of EF-hands were displayed.

EF-hands are composed of two α-helixes and an intervening loop, and several key amino acids in the intervening loop are important for Ca^{2+}-binding affinity (Batistic and Kudla, 2004). In *Arabidopsis* CBLs, the loop regions of EF2/3/4 consist of 12 amino acids while that of EF1 is extended to 14 amino acids. Positions 1, 5, 7, 9, 11, and 14 of the EF1 loop as well as positions 1, 3, 5, 7, 9, and 12 of EF2/3/4 loop are coordinates X, Y, Z, -Y, -X, -Z for Ca^{2+}-binding (Nagae et al., 2003; Batistic et al., 2009). Among them, coordinate -X of the EF-hand is a hydrophilic amino acid that binds Ca^{2+} via a water molecule, while other coordinates bind Ca^{2+} via side-chain donor oxygen or main-chain carbonyl oxygen (Nagae et al., 2003; Batistic et al., 2009; Sánchez-Barrena et al., 2013). The positions of the key amino acids for Ca^{2+}-binding in the loop region of EF-hands in NtCBLs (14 amino acids for the EF1 loop and 12 amino acids for the loops of EF2, EF3, and EF4) are predicted and listed in Table 2. The conserved amino acid sequences of EF-hands are presented in Figure

3. Based on the analysis, EF1/2/4 of NtCBLs were predicted to have two types of Ca^{2+}-oxygen (Ca-O) binding ways (marked with red or green squares in Figure 3), while EF3 of NtCBLs has one. The representative Ca-O binding structures are displayed correspondingly on the right of the panels (Figure 3).

Table 2 The positions of Ca^{2+}-binding amino acids in the loop region of EF-hands and their Ca^{2+}-binding ways

Name	Ca^{2+}-binding amino acids of EF1	Ca^{2+}-binding amino acids of EF2	Ca^{2+}-binding amino acids of EF3	Ca^{2+}-binding amino acids of EF4
NtCBL1A-1	—	—	—	—
NtCBL1A-2	1, 5, 7, 9, 14	—	—	—
NtCBL1A-3	1, 5, 7, 9, 14	—	—	—
NtCBL1B	1, 5, 7, 9, 14	—	—	—
NtCBL2A	—	1, 3, 7, 12, 12	1, 6, 7, 12, 12	1, 3, 7, 12, 12
NtCBL2B	—	1, 3, 7, 12, 12	1, 6, 7, 12, 12	1, 3, 7, 12, 12
NtCBL3A	1, 5, 7, 9, 14	1, 3, 7, 12, 12	1, 6, 7, 12, 12	1, 3, 7, 12, 12
NtCBL3B	1, 5, 7, 9, 14	1, 3, 7, 12, 12	1, 6, 7, 12, 12	1, 3, 7, 12, 12
NtCBL4A-1	1, 5, 9, 14	1, 7, 12, 12	—	—
NtCBL4A-2	1, 5, 9, 14	1, 7, 12, 12	—	—
NtCBL4B	1, 5, 9, 14	1, 7, 12, 12	—	—
NtCBL5A	—	—	—	—
NtCBL5B	—	—	—	—
NtCBL6A	—	—	—	—
NtCBL7A	1, 5, 7, 9, 14	—	—	1, 3, 5, 7, 12
NtCBL7B	1, 5, 7, 9, 14	—	—	1, 3, 5, 7, 12
NtCBL8A-1	—	—	—	—
NtCBL8A-2	1, 5, 9, 14	1, 7, 12, 12	—	—
NtCBL8B-1	—	—	—	—
NtCBL8B-2	1, 5, 9, 14	1, 7, 12, 12	—	—
NtCBL9A	1, 5, 7, 9, 14	—	—	—
NtCBL9B	1, 5, 7, 9, 14	—	—	—
NtCBL10A	1, 5, 7, 9, 14	—	—	—
NtCBL10B	1, 5, 7, 9, 14	—	—	—

Numbers in the table indicate the positions of Ca^{2+}-binding amino acids in the loop region of EF1, 2, 3, and 4. Twice the same number (12, 12) in one EF-hand means the amino acid at position 12 in the loop region binds Ca^{2+} with two oxygens. "—" means that no Ca^{2+}-binding amino acid was detected. Red or green squares displayed on the right of the numbers represent different Ca^{2+}-oxygen binding ways displayed in Figure 3. The amino acids for Ca^{2+}-binding were predicted by the SWISS-MODEl online tool (https://swissmodel.expasy.org/).

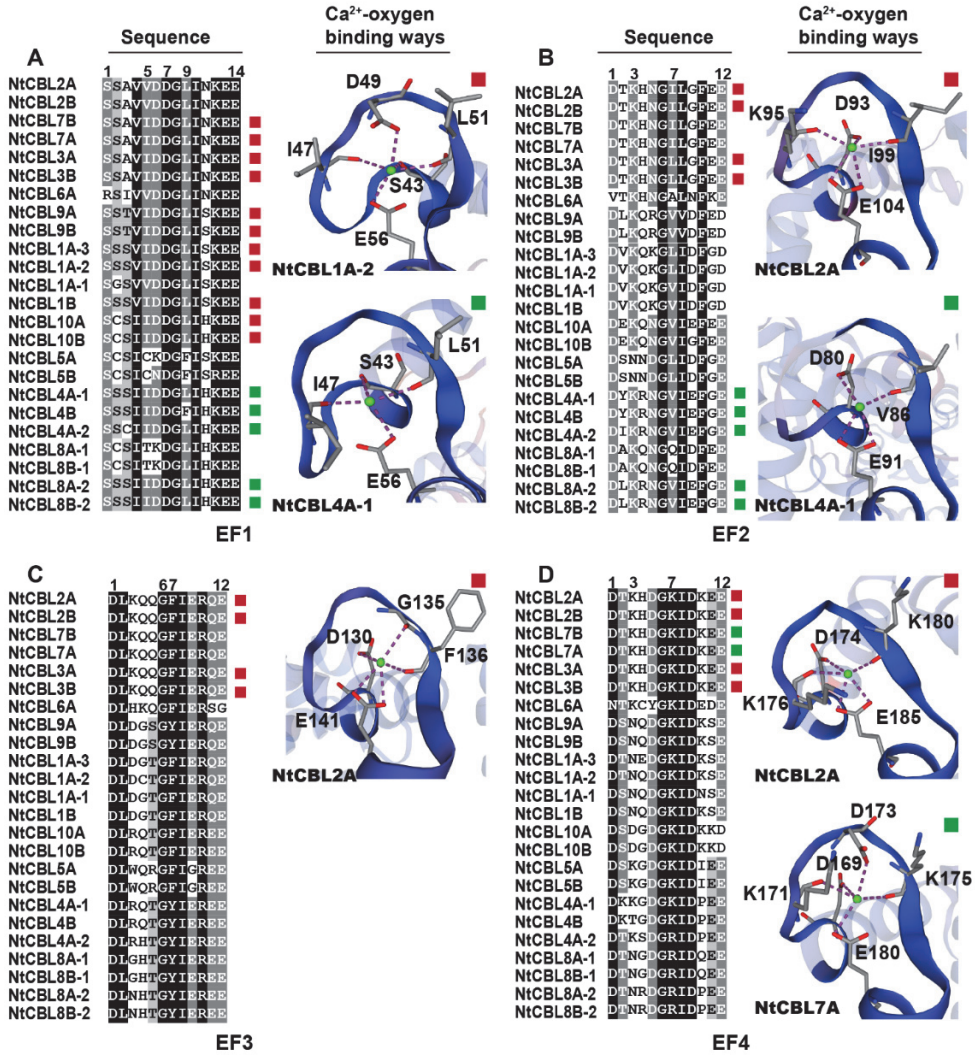

Figure 3. The Ca^{2+}-binding sites in the loop region of EF-hands. (A-D) The amino acid sequence alignments and tertiary structures of the loop region with predicted Ca^{2+}-binding sites of EF-hands EF1 **(A)**, EF2 **(B)**, EF3 **(C)**, and EF4 **(D)**. Numbers above the aligned sequences indicate the position of predicted Ca^{2+}-binding sites in EF-hand loops. Squares at the right side of the aligned sequences indicate different Ca^{2+}-oxygen binding ways (red or green), with an example of each Ca^{2+}-binding structure for this EF-hand displayed on the right of the panels. The tertiary structures were predicted by SWISS-MODEL (https://swissmodel.expasy.org/) (Waterhouse et al., 2018) and visualized via Swiss-Pdb Viewer (Guex et al., 1997).

The amino acid sequence of the EF-hand is not the only factor to influence Ca^{2+}-binding ability. For example, the EF3 of NtCBL2 is predicted to bind Ca^{2+} through positions 1, 6, 7, and 12. However, the EF3 of NtCBL7, with the same amino acid sequence as that of NtCBL2, is predicted to lack Ca^{2+}-binding ability (Figure 3C). To better understand the requirements for Ca^{2+}-binding affinity, the tertiary structures of NtCBL EF3 hands were examined in more detail. NtCBLs with similar EF3 tertiary structures (Figure 2) and the same Ca^{2+}-binding amino acids (Figure 3) are represented by one of them for analysis. To be specific, NtCBL2A is selected for NtCBL2/3, NtCBL1A-1 for NtCBL1/7/10, NtCBL4A-1 for NtCBL4/8A-2/8B-2, NtCBL5A for NtCBL5, and NtCBL8A-1 for NtCBL8A-1/8B-1. It was predicted that the EF3 of NtCBL2A binds Ca^{2+} with the oxygen atoms of amino acids D130, G135, F136, and E141 (providing 2 oxygen atoms) (Figure 4A). But the EF3 hand of NtCBL6A might possess an impaired Ca^{2+}-binding ability, because it has a G129 spatially positioned in the place of E141 (Figure 4B). G122 and F123 in NtCBL1A-1 spatially replace G135 and F136 of NtCBL2A (Figure 4C), which induce the spatial change of donor oxygen, thereby might strongly affect the Ca^{2+}-binding abilities. Similar changes were also predicted in the EF3 of NtCBL4/5/8/9 (Figure 4D-F). In summary, the spatial position of donor oxygens in the loop region of EF-hands might also be important for Ca^{2+}-binding.

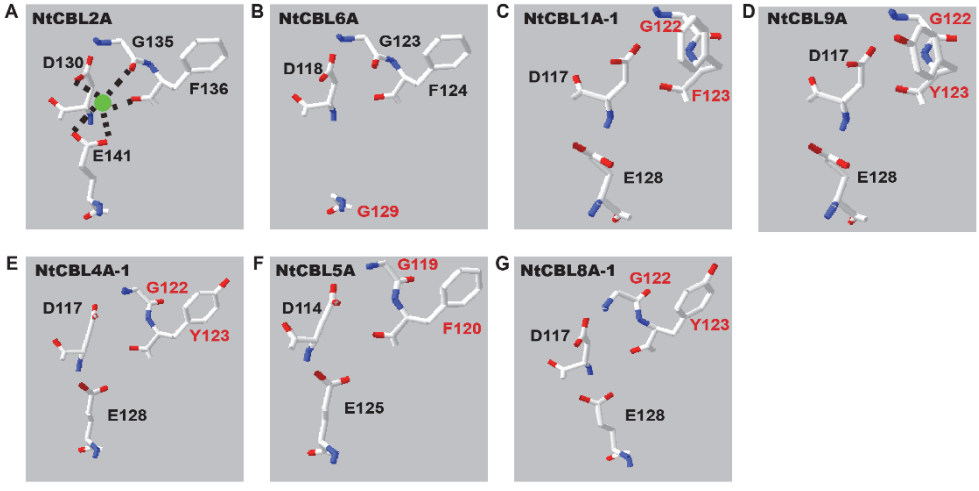

Figure 4. Predicted Ca^{2+}-binding sites in loop regions of EF3 of NtCBLs. The tertiary structures of EF3 were predicted by SWISS-MODEL (https://swissmodel.expasy.org/) (Waterhouse et al., 2018), and the potential Ca^{2+}-binding sites were visualized via Swiss-Pdb Viewer (Guex et al., 1997).

In addition, the interaction with CIPKs may also affect the Ca^{2+}-binding affinity of CBL by modifying the tertiary structure of an EF-hand (Sánchez-Barrena et al., 2013). The analysis of the crystal structure showed that AtCBL2 in free form (without binding AtCIPK) binds two Ca^{2+} ions while the AtCBL2-AtCIPK14 C-terminus complex binds four; EF2 and EF3 of AtCBL2 in free form do not bind Ca^{2+} but they are occupied by Ca^{2+} in the AtCBL2-AtCIPK14 complex (Nagae et al., 2003; Akaboshi et al., 2008). Another example is about AtCBL4. Free AtCBL4 binds four Ca^{2+} ions while the AtCBL4-AtCIPK24 C-terminus complex only binds two; EF2 and EF3 of AtCBL4 in free form bind Ca^{2+} but lose the Ca^{2+}-binding ability when AtCBL4 is bound to AtCIPK24 (Sanchez-Barrena et al., 2005; Sanchez-Barrena et al., 2007). Those findings indicate that the interaction of CBLs with CIPKs might in turn affect the Ca^{2+}-binding properties of CBLs. Hereby, it is important to note that the Ca^{2+}-binding ability of NtCBLs in this study is predicted for the free form, and that this binding ability may change when the CBL is part of a protein-protein complex. The EF-hands without Ca^{2+}-binding ability in free form may regain Ca^{2+}-binding ability when the tertiary structures of NtCBLs are modified by interacting proteins.

Analysis of gene structure and splicing variants of *NtCBL*s

The presence of differentially spliced isoforms of *CBL* and *CIPK* genes introduces additional complexity to the CBL-CIPK signaling system. A previous study showed that the splicing variants of *AtCIPK3* were differentially regulated, and their encoded proteins displayed distinct interaction preferences. Specifically, *AtCIPK3.1* and *AtCIPK3.4* variants were found to be relatively more induced by ABA and drought treatment, and AtCIPK3.1 and AtCIPK3.2 showed an interaction preference for ABSCISIC ACID-RESPONSIVE 1 (ABR1) (Sanyal et al., 2017). Nevertheless, information on alternative splicing of CBL and CIPK families is still limited, and the

biological significance of the resulting diversity in protein isoforms is not yet fully understood (Kolukisaoglu et al., 2004).

In this study, the gene structures of *NtCBL*s were predicted with the gene structure annotation pipeline in the NCBI database (https://www.ncbi.nlm.nih.gov/). The predicted introns, exons, and splicing variants are depicted in Figure 5. Eighteen *NtCBL*s were predicted to have splicing variants, except *NtCBL3A*, *NtCBL6A*, *NtCBL7A*, *NtCBL7B*, *NtCBL10A*, and *NtCBL10B*. Remarkably, only *NtCBL2/4A-1/4A-2/5/9B* (5 of the 18 *NtCBL*s) encode splicing variants that are translated into proteins of different lengths. Most of the *NtCBL* genes were predicted to have introns in their 5'-untranslated region (UTR): a single intron in most type Ⅰ members (NtCBL1/4B/8A-1/8B-1/8B-2/9), and two introns in most type Ⅱ members (NtCBL2/3/7). In addition, homoeologous genes from parental genomes have 5'-UTRs that differ in length and intron presence.

Alternative splicing in 5'-UTRs can regulate translation efficiency by producing mRNA variants that differ in terms of upstream open reading frames (uORFs) or riboswitches (the metabolite-sensing gene-control elements that are typically located in the noncoding portion of mRNAs) (Roy and Arnim, 2013; Srivastava et al., 2018). Whether the alternative splicing in 5'-UTRs of *NtCBL*s affects gene expression and translation efficiency at the post-transcriptional level remains to be established. This is worth exploring because posttranscriptional regulation may be useful in the activation of stress tolerance mechanisms and developmental transitions (Srivastava et al., 2018).

Figure 5. Gene structure of *NtCBL* genes. The information on exon-intron organizations was obtained from NCBI (https://www.ncbi.nlm.nih.gov/) and visualized with the Gene Structure Display Server (GSDS, http://gsds.cbi.pku.edu.cn/) of *NtCBL* family genes. The coding sequences (CDSs) and genomic sequences were obtained from NCBI.

Most identified *NtCBL* genes have seven introns in their coding regions (Figure 5),

while the gene structure of *NtCBL6A* differs from the others. *NtCBL6A* was predicted to be intronless, which was confirmed by PCR using genomic DNA as a template. This lack of introns is highly unusual for plant *CBL* genes. No intronless *CBL* member has been identified in *Arabidopsis* or rice genomes (Kolukisaoglu et al., 2004). These findings suggest that *NtCBL6A* may have lost its introns after the evolutionary divergence of *N. tabacum* from *Arabidopsis* and rice (Kolukisaoglu et al., 2004). Further analysis showed that *NtCBL6A* does not have an ortholog in the paternal progenitor *N. tomentosiformis* (Table 1), nor does it have close homologs in *N. attenuata* and other *Solanaceae* crops (*Solanum tuberosum*, *S. lycopersicum*, *S. pennellii*, and *Capsicum annuum*) (Figure S2). These results indicate that *NtCBL6A* may be a unique gene in *solanaceae* plants. However, more information is required to determine whether *NtCBL6A* has any function in tobacco.

Analysis of *cis*-acting elements in the promoter regions of *NtCBL*s

*CBL*s play important roles in plant development and stress responses, and their expression is regulated by plant hormones and stress-related transcription factors (Albrecht et al., 2003; Guo et al., 2010). Therefore, the promoter sequences of *NtCBL*s were analyzed, and the predicted hormone- and stress-responsive *cis*-acting elements in the 3 kb upstream sequences of *NtCBL* coding sequences were displayed in Figure 6. Many hormone-responsive and stress-responsive elements were found in the promoter regions of *NtCBL*s. Among these, ABRE, STRE, and MYC elements are widespread and abundant in most promoters of NtCBLs (Figure 6A). The promoters of *NtCBL1A-2*/*1A-3* and *NtCBL4A-1*/*4B* are rich in ABRE elements, the *NtCBL8B-1* promoter is rich in TGACG-motifs, and the *NtCBL10B* promoter has multiple ERE elements (Figure 6A), indicating the expression of these genes may be greatly regulated by ABA, MeJA, and ethylene, respectively. The promoters of *NtCBL8B-2* and *NtCBL4B* are enriched in Myb and W-box elements, respectively (Figure 6A), suggesting their expression level might be regulated by Myb and WRKY transcription factors.

To explore the *NtCBL*s with potentially similar expression profiles, the *NtCBL*s were clustered based on the presence of the *cis*-acting elements in their promoters (Figure 6B). It was found that some genes are clustered together (e.g. *NtCBL7A*/*8A-1*, *NtCBL5*/*7B*/*8A-2*, *NtCBL2A*/*3A*/*6A*/*9A*, *NtCBL1A-2*/*4A-2*, *NtCBL4B*/*4A-1*, *NtCBL1A-3*/*3B*/*8B-2*, and *NtCBL1A-1*/*1B*/*2B*/*9B*/*10*) (Figure 6B), suggesting these genes might be responsive to the same hormones and stress factors. For instance, there are many STREs (stress response elements) present in the promoter region of the clustered *NtCBL5/7B/8A-2*, and ABRE (*cis*-acting element involved in the abscisic acid responsiveness) in the promoter region of the clustered *NtCBL4B/4A-1*. Interestingly, most homoeologous *NtCBL* genes promoters from the two ancestral genomes do not have a highly similar *cis*-acting element presence (except *NtCBL10A/10B* and *NtCBL5A/5B*) (Figure 6B), suggesting that they may have differential expression responses to hormones and stress. This is consistent with the previous reports that the expression of genes from parental genomes needs to be orchestrated for their harmonious co-existence in allopolyploidy (Feldman and Levy, 2009; Akhunova et al., 2010).

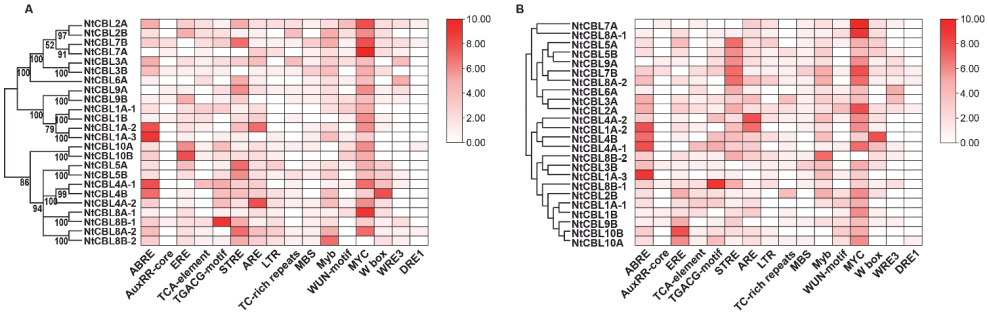

Figure 6. Analysis of *cis*-acting elements in the promoters of *NtCBL* genes. (A) Heatmap of *cis*-acting elements in *NtCBL* promoter regions ordered based on the phylogenetic relationship of the genes. **(B)** Heatmap of *cis*-acting elements in *NtCBL* promoter regions ordered based on similarity of *cis*-acting element presence. The intensity of the color represents the number of *cis*-acting elements in the *NtCBL* gene promoters. ABRE (*cis*-acting element involved in the abscisic acid responsiveness), AuxRR-core (the core of the auxin response region), ERE (ethylene-responsive *cis*-acting), TCA-element (*cis*-acting

element involved in salicylic acid responsiveness), TGACG-motif (*cis*-acting regulatory element involved in the methyl jasmonate (MeJA)-responsiveness), STRE (stress response element), ARE (anaerobic induction element), LTR (low-temperature-responsive element), TC-rich repeats (involved in defense and stress responsiveness), MBS (MYB binding site involved in drought-inducibility) (Sugimoto et al., 2000), Wun-motif (wound-responsive element), Myb (MYB-binding site) (Sugimoto et al., 2000), MYC (MYC recognition element), W-box (WRKY binding site) (Liu et al., 2016), WRE3 (wound-responsive element) (Yu et al., 2021), DRE1 (dehydration-responsive element).

Expression profiles of *NtCBL* genes in different tobacco tissues at the young stage and adult stage

The ancestral function of *CBL* genes is the regulation of ion homeostasis, and this has diversified during evolution (Kleist et al., 2014; Edel and Kudla, 2015). Functional diversification of *CBL* genes is reflected not only in the structural differences of proteins but also in the expression differences of genes. For example, *Arabidopsis* AtCBL4 and AtCBL10 mediate two independent salt tolerance pathways in different tissues because of their tissue-predominant expression patterns (Yang et al., 2019). *AtCBL4* is expressed and exerts its function in roots while *AtCBL10* is mainly expressed and functional in shoot green tissues (Kim et al., 2007; Quan et al., 2007). *AtCBL2* and *AtCBL3* on the other hand have largely overlapping expression patterns (Eckert et al., 2014) and their encoded proteins are structurally similar, so they were shown to be functionally redundant in both plant development and stress response (Tang et al., 2012; Steinhorst et al., 2015; Tang et al., 2015; Song et al., 2018; Tang et al., 2020b; Ju et al., 2022).

To get insight into the potential functions of *NtCBL* genes, we monitored their expression profiles in different tissues (leaf blade, main vein, stem, and root) of young tobacco plants (35 days after germination) by RT-qPCR (Figure 7A-D, primers are listed in Table S1). In young plants, *NtCBL2/3/7/10/1A-3/4A-1* had higher expression levels (Figure 7A), *NtCBL8/9/4A-2/4B* had medium expression levels (Figure 7B), and *NtCBL1A-1/1A-2/1B/4A-2/4B/5/8A-1/8A-2/8B-2* had very low

expression levels (Figure 7C). The expression of *NtCBL6A* was not detected in any sampled tissues in this study, but *NtCBL6A* may be expressed in some other tissues or at some specific developmental stages. In addition, several *NtCBL* genes exhibited a shoot- or root-predominant expression pattern: *NtCBL10* was predominantly expressed in shoot tissues while *NtCBL4A-1*/*8B-1*/*9* were mainly expressed in roots. The tissue-predominant expression patterns of *NtCBL4A-1* and *NtCBL10* are similar to that of their orthologs in *Arabidopsis* (Kim et al., 2007; Quan et al., 2007; Eckert et al., 2014), which suggests that they might have similar roles.

The expression profiles of *24 NtCBL* genes in different tissues (leaf, root) of adult plants were also analyzed using published RNA-seq data (Figure S3). Results showed that the expression profile of most *NtCBL*s at the adult stage is similar to that at the young plant stage, but *NtCBL4B* appeared to have a much higher expression level in both leaf and root at the adult stage (Figure S3), indicating that *NtCBL4B* may function at later developmental stages of the tobacco plant.

The interaction between homoeologous genomes in allopolyploidy orchestrates gene expression genome-wide, contributing to growth vigor and the broader phenotypic diversity of allopolyploid species (Feldman and Levy, 2009; Akhunova et al., 2010). We found that *NtCBL1A-3/4A-1/7A/9A/10A* from the maternal genome (*N. sylvestris)* and *NtCBL3B/5B/8B-1* from the paternal genome (*N. tomentosiformis)* are the dominant homoeologs in young plants (Figure 7). However, *NtCBL4B* and *NtCBL9B* are dominant in adult leaves and roots, respectively (Figure S3). These results indicate that the homoeologs of some *NtCBL* genes are differentially expressed at the mRNA level (Hovav et al., 2007).

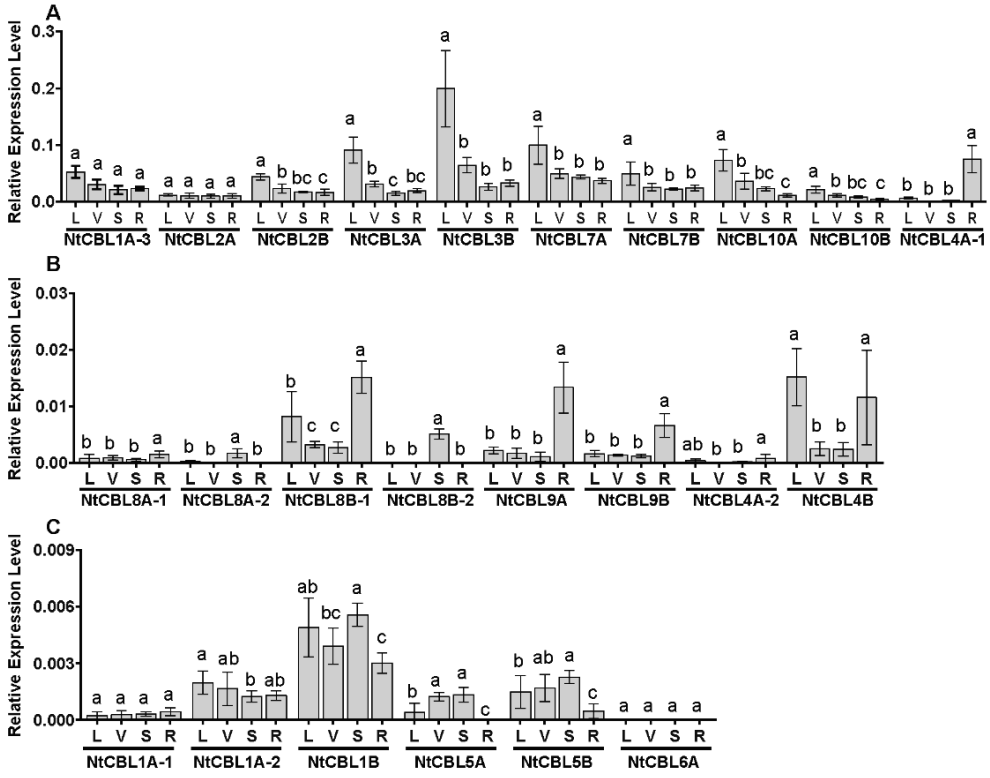

Figure 7. Expression profiles of *NtCBL* genes in different tissues of tobacco at the young stage. **(A-C)** Relative expression analysis of *NtCBL* genes in leaf blade (L), main vein (V), stem (S), and root (R) of young tobacco plants determined by RT-qPCR, which were grouped in three panels according to their expression levels (highest in panel A, lowest in panel C). The expression of these genes is relative to that of the reference gene *NtL25* (Schmidt and Delaney, 2010). The tobacco plants used for sampling were cultivated in a hydroponic system. Different tissues (leaf blade: leaf with main veins removed; main vein; stem; root) were sampled at 35 days after germination. Error bars indicate ±SD (n=6 for gene expression detection), and different letters above bars (a, b, and c) indicate significant statistical differences of a *NtCBL* gene expression in different tissues (one-way ANOVA with the LSD test, $p<0.05$).

Expression profiles of *NtCBL* genes in leaves from young tobacco plants under salt and drought stress

CBL proteins are reported to be involved in multiple stress responses (Tang et al., 2020a), and many hormone- and stress-responsive *cis*-acting elements were

identified in the promoter regions of *NtCBL* genes. Therefore, we analyzed the expression of *NtCBL* genes in young tobacco leaves under salt stress and drought stress using RT-qPCR (Figure S4). Under salt stress, the expression levels of *NtCBL3A/3B/7A/7B/8B-1/10A/10B* in leaves were increased, and the expression levels of *NtCBL1A-2/2A/4A-1/7A/7B/8B-2* in roots were reduced (Figure 8A). Under drought stress, the expression levels of *NtCBL2A/2B/3A/3B/4B/7A/7B* were reduced, while the expression of *NtCBL10B* was upregulated (Figure 8B).

Arabidopsis *AtCBL10* and *N. sylvestris NsylCBL10* (GeneBank accession number: KF667488.1), the orthologs of *NtCBL10*, were reported to be positive regulators of salt tolerance (Kim et al., 2007; Dong et al., 2015). The loss-of-function mutant of *AtCBL10* exhibited growth defects under saline conditions (Kim et al., 2007), and overexpression of *NsylCBL10* improved the salt tolerance of transgenic *Arabidopsis* (Dong et al., 2015). In this study, the expression levels of *NtCBL10A* and *NtCBL10B* are upregulated under salt stress. These results strongly suggest that *NtCBL10A* and *NtCBL10B* may play a role in the salt tolerance of tobacco as well. Under drought stress, the loss-of-function mutant of *AtCBL10* had increased drought tolerance in *Arabidopsis* (Kang and Nam, 2016), which is inconsistent with the up-regulation of *NtCBL10B* expression reported here. Further functional analysis is needed to understand the role of *NtCBL10B* in response to drought stress.

AtCBL4 (also known as SOS3), interacts with AtCIPK24 (also known as SOS2) to activate the PM-localized Na^+/H^+ exchanger AtSOS1, transporting Na^+ out of the root cell and enhancing the salt tolerance of *Arabidopsis* (Qiu et al., 2002; Shi et al., 2002; Nunez-Ramirez et al., 2012). *CBL4* has been reported to contribute to salt stress tolerance in many other plant species including *Oryza sativa* (Martinez-Atienza et al., 2007), *Setaria italica* (Zhang et al., 2017), *Brassica napus* (Liu et al., 2015), *Solanum lycopersicum* (Cho et al., 2021), and *Tamarix hispida* (Liu et al., 2020). In our study, the expression of *NtCBL4A-1* in roots was inhibited by salt stress, which does not seem consistent with the conserved role of *CBL4* in other plant species. This may point to a different function for *NtCBL4A-1* under salt stress compared to *AtCBL4*.

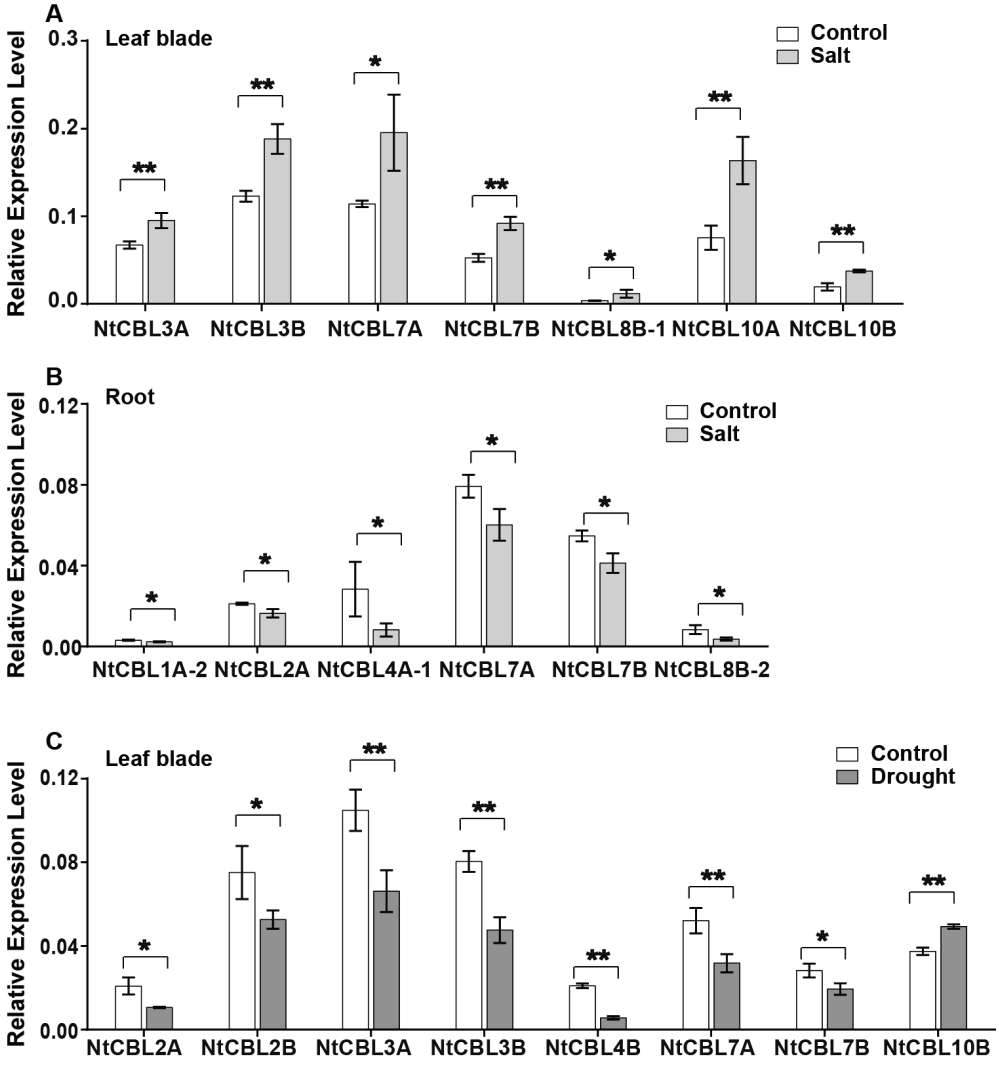

Figure 8. Expression profiles of *NtCBL* genes in tobacco leaves under salt stress and drought stress were determined by RT-qPCR. (A and B) Relative expression analysis of significantly regulated *NtCBL* genes in leaf blades and roots under salt stress (1 day after the start of 100 mM NaCl treatment), respectively. **(C)** Relative expression analysis of significantly regulated *NtCBL* genes in leaf blades under drought stress (5 days after stopping water). The expression of these genes is relative to that of the reference gene *NtL25* (Schmidt et al., 2010). Error bars indicate ±SD (n=3), every biological replicate is a mixed pool of 3 plants. Asterisks indicate statistically significant differences (Student's *t* test, **p*<0.05 and ***p*<0.01).

Overexpression of *NtCBL4A-1* leads to Na^+-induced salt sensitivity of transgenic tobacco plants

To better understand the role of *NtCBL4A-1* in the salt stress response of tobacco, two independent *NtCBL4A-1*-overexpressing (*NtCBL4A-1*-OE) lines (OE-2, OE-9) (Figure 9A, B) were selected and evaluated for salt tolerance. Under control conditions, wild-type (WT) and two *NtCBL4A-1*-OE lines exhibited similar growth vigor (Figure 9C-F). Under 100 mM NaCl treatment, however, *NtCBL4A-1*-OE lines exhibited salt-sensitive phenotypes with severe necrotic lesions on their leaves (Figure 9C). In addition, the plant height and shoot fresh/dry weight of *NtCBL4A-1*-OE lines were slightly lower than that of WT plants under salt stress (Figure 9D-F). Ion content analysis (Na^+, K^+, and Ca^{2+} in the 5th leaf blades) revealed that K^+ and Ca^{2+} contents of all three lines were significantly reduced under salt stress, but there is no significant ion content difference between WT and *NtCBL4A-1*-OE lines (Figure 9H, I). The Na^+ content of *NtCBL4A-1*-OE lines is only slightly higher than that of WT (Figure 9G).

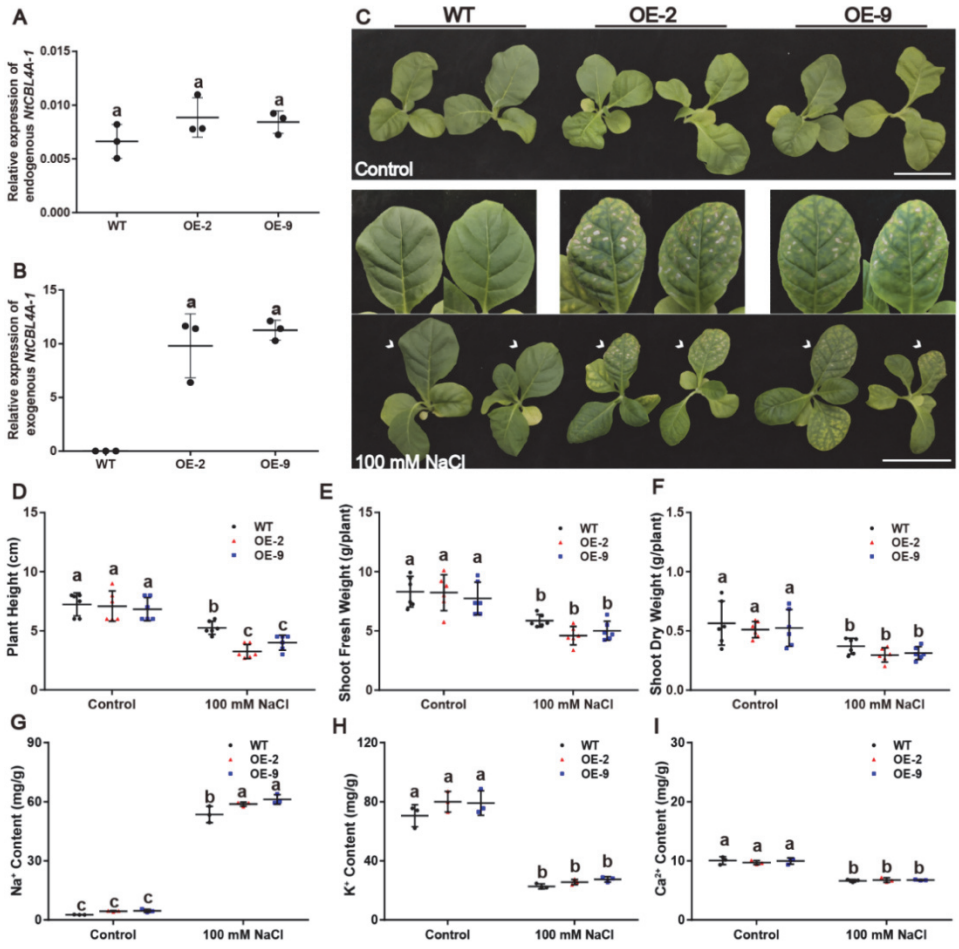

Figure 9. The detection of *NtCBL4A-1* expression and above-ground phenotype of wild-type (WT) and *NtCBL4A-1*-overexpressing (OE) lines (OE-2 and OE-9) under control conditions and salt stress (100 mM NaCl). Scale bars=10 cm. **(A and B)** Relative expression analysis of endogenous and exogenous *NtCBL4A-1* determined by RT-qPCR in leaves. The expression of *NtCBL4A-1* is relative to the reference gene *NtL25*. The reverse primer pCHF3-Allcheck-2 (Shi et al., 2021) used for amplifying exogenous *NtCBL4A-1* was designed according to the sequence of the overexpression vector pCHF3. **(C)** The shoot phenotype of WT and *NtCBL4A-1*-OE lines at 9 DAT. **(D-F)** The plant height, shoot fresh weight, and shoot dry weight of WT and *NtCBL4A-1*-OE lines at 9 DAT Error bars indicate ±SD (n=3 for gene expression detection, n=6 for plant height and shoot fresh/dry weight determination). **(G-I)** The Na^+, K^+, and Ca^{2+} contents of the 5th leaves of WT and *NtCBL4A-1*-OE lines. Error bars indicate ±SD (n=3), every biological replicate is a mixed pool of 3 plants. Different letters above bars (a, b, and c) indicate significant statistical difference based on one-way ANOVA with LSD test ($P<0.05$).

Salt stress imposes both osmotic stress and ionic stress on plants (Munns, 2005). To identify which stress component (osmotic or ionic) is responsible for the necrotic phenotype of *NtCBL4A-1*-OE lines under 100 mM NaCl conditions, a 15% PEG6000-mimic osmotic treatment (osmotic pressure is similar to 100 mM NaCl) and ionic treatments (100 mM NaCl, 100 mM $NaNO_3$, 100 mM KNO_3, and 100 mM KCl) were conducted. Compared with WT, *NtCBL4A-1*-OE lines exhibited necrotic lesions and growth penalties only under treatments of 100 mM NaCl and $NaNO_3$, but not under osmotic stress or 100 mM KNO_3 and KCl (Figure 10). These results indicate that the increased salt sensitivity of *NtCBL4A-1*-OE lines is Na^+ dependent.

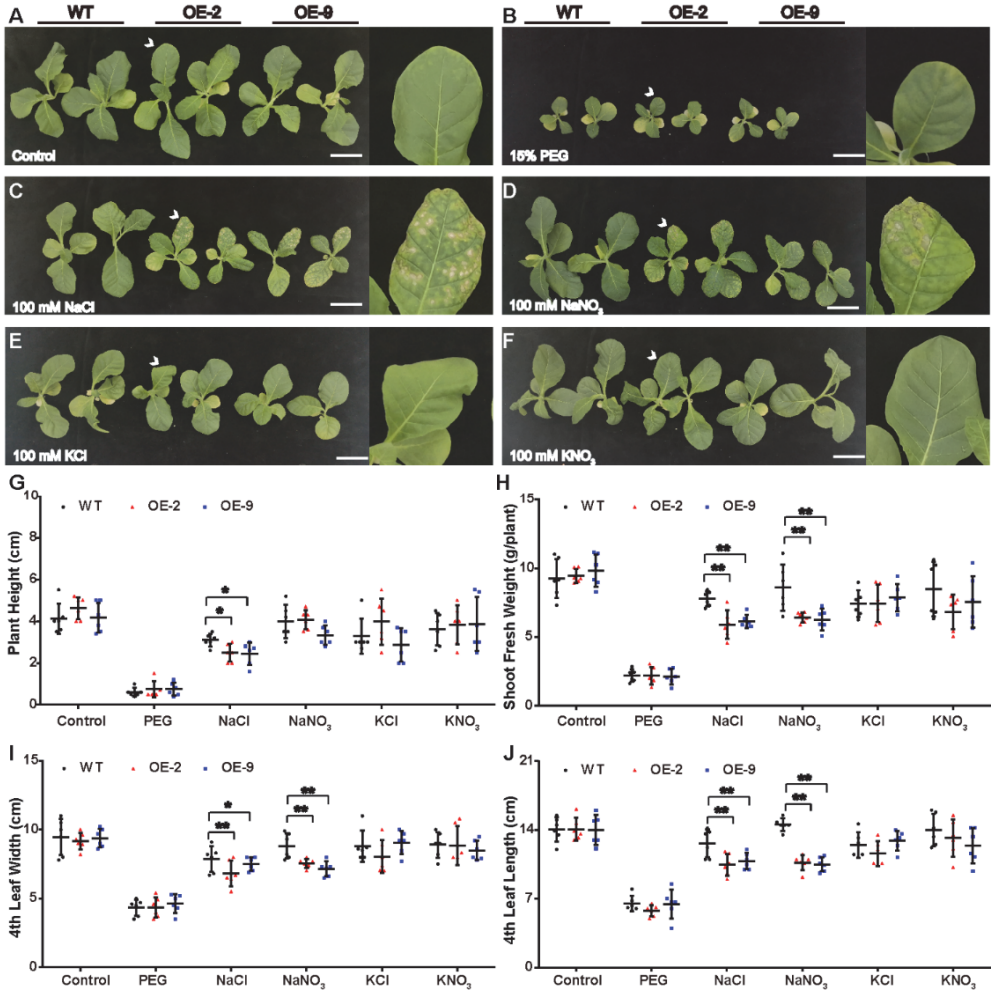

Figure 10. Ion and osmotic stress evaluation on wild-type (WT) and *NtCBL4A-1*-overexpressing lines (OE-2 and OE-9) at 9 days after the start of treatment. Scale bars=10 cm. **(A-F)** The phenotype of WT and *NtCBL4A-1*-OE lines under control condition (1/2 Hoagland's nutrient solution), osmotic stress (1/2 Hoagland's nutrient solution added 15% PEG6000, ion stresses (1/2 Hoagland's nutrient solutions added 100mM NaCl, 100mM NaNO3, 100mM KCl, and 100mM KNO3, respectively). Scale bars=10cm. **(G-J)** The plant height, shoot fresh weight, 5th leaf width, and 5th leaf length of WT and *NtCBL4A-1*-OE lines at 9 DAT Error bars indicate ±SD (n=6). Asterisks indicate statistically significant differences (Student's *t* test, **p*<0.05 and ***p*<0.01).

CBL4 and CBL5 share high sequence similarity and they belong to the type I CBLs (Figure 1A). In *Arabidopsis* and *S*. *italica*, both *CBL4* and *CBL5* were reported to be responsible for the salt tolerance of plants (Zhu, 2000; Cheong et al., 2010; Zhang et al., 2017; Yan et al., 2022). However, our results showed that the overexpression of *NtCBL4A-1* and *NtCBL5A* enhanced the salt sensitivity of transgenic tobacco plants based on this study and our previous report (Mao et al., 2021). Both *NtCBL4A-1*- and *NtCBL5A*-OE lines exhibited necrotic lesions on leaves under salt stress. In addition, the Na^+ content increases in both *NtCBL4A-1*- and *NtCBL5A*-OE lines were only slightly higher than that in WT under salt stress, indicating that the overexpressing lines exhibit higher Na^+ sensitivity than WT. Therefore, we speculate that the Na^+-sensitive mechanisms underlying the salt sensitivity of *NtCBL4A-1*-OE lines might be similar to that of *NtCBL5A*-OE lines, which is still unclear until now. A possible hypothesis is that the ectopic (over)expression of *NtCBL5A* might compete with other components of the CBL-CIPK network for Na^+ vacuolar compartmentalization, leading to abnormal Na^+ distribution (Mao et al., 2021). Considering many photosynthetic machinery-related genes were strongly inhibited and plant defense-related genes were induced under salt stress, the Na^+ sensitivity of *NtCBL5A*-OE lines may also be related to defective photosystems or induced plant immune response. The next step would be to identify the common interacting proteins of NtCBL4A-1 and NtCBL5A, some of which could be key components in the salt tolerance system of tobacco (Mao et al., 2021). The elucidation of these

questions will broaden our knowledge of the CBL-CIPK network and the salt stress response of plants.

CONCLUSIONS

In this study, a detailed analysis of *NtCBL* family genes was conducted by bioinformatic analysis and expression profile analysis. The homoeologous genes from the two parental genomes were predicted to encode proteins with key amino acids and similar tertiary structures for subcellular localization and Ca^{2+}-binding ability. Some *NtCBL* homoeologs from the two parental genomes are differentially regulated at the transcriptional level. The bioinformatics-supported information will serve as a basis for further research, including the characterization of family genes by using gene overexpressing or knock-out plants, elucidating their roles in stress response and growth trade-off, and accessing allelic variation to improve crop performance through breeding. In addition, the genetic experiment of *NtCBL4A-1* indicates the potential role of *CBL* genes in salt stress response. In summary, this study lays a good foundation for the functional characterization of *NtCBL* genes, and knowledge about these genes in tobacco will therefore likely support breeding efforts for improved *Solanaceae* crops under suboptimal conditions.

FUNDING INFORMATION

This work was supported by the National Natural Science Foundation of China (32170387); International Foundation of Tobacco Research Institute of CAAS (IFT202102); Key Funding of CNTC (No. 110202101035(JY-12)); Key Funding of YNTI (No. 2020JC03, 2022JY03); and International Exchange Scholarship of the GSCAAS.

CREDIT AUTHORSHIP CONTRIBUTION STATEMENT

J.M. designed the research plan, carried out the experiments, and analyzed the data; J.M., C.G.V.L., and Q.W. completed the writing; H.L., Q.W., and C.G.V.L. co-supervised the writing; Y.G., K.H., H.X., and W.Z. provided ideas and joined discussion; R.G.F.V. and Y.B. helped with manuscript revision. H.L. and Q.W. agree

to serve as the authors responsible for contact and ensure communication. All authors contributed to the article and approved the submitted version.

DECLARATION OF INTERESTS

The authors declare that they have no known competing financial interests or personal relationships that could have appeared to influence the work reported in this paper.

DATA AVAILABILITY

The datasets presented in this study can be found in online repositories. The names of the repository/repositories and accession number(s) can be found in the article/supplementary material.

ACKNOWLEDGMENTS

We would like to acknowledge the support of the PhD Education Programs between The GSCAAS and WUR. We would like to thank Jiangtao Chao from Tobacco Research Institute, Chinese Academy of Agricultural Sciences (CAAS) for helping to analyze the RNAseq data.

REFERENCES

Akaboshi, M., Hashimoto, H., Ishida, H., Saijo, S., Koizumi, N., Sato, M., and Shimizu, T. The crystal structure of plant-specific calcium-binding protein AtCBL2 in complex with the regulatory domain of AtCIPK14. *J Mol Biol*. **2008**, *377*, 246-257.

Akhunova, A. R., Matniyazov, R. T., Liang, H., and Akhunov, E. D. Homoeolog-specific transcriptional bias in allopolyploid wheat. *BMC Genomics*. **2010**, *11*, 505.

Albrecht, V., Weinl, S., Blazevic, D., D'Angelo, C., Batistic, O., Kolukisaoglu, U., Bock, R., Schulz, B., Harter, K., and Kudla, J. The calcium sensor CBL1 integrates plant responses to abiotic stresses. *Plant J*. **2003**, *36*, 457-470.

Aslam, M., Fakher, B., Jakada, B. H., Zhao, L., Cao, S., Cheng, Y., and Qin, Y. Genome-wide identification and expression profiling of CBL-CIPK gene family in pineapple (*Ananas comosus*) and the role of AcCBL1 in abiotic and biotic stress response. *Biomolecules*. **2019**, *9*, 293.

Batistic, O., and Kudla, J. Integration and channeling of calcium signaling through the CBL calcium sensor/CIPK protein kinase network. *Planta*. **2004**, *219*, 915-924.

Batistic, O., and Kudla, J. Plant calcineurin B-like proteins and their interacting protein kinases. *Biochim Biophys Acta*. **2009**, *1793*, 985-992.

Batistic, O., Rehers, M., Akerman, A., Schlucking, K., Steinhorst, L., Yalovsky, S., and Kudla, J. S-acylation-dependent association of the calcium sensor CBL2 with the vacuolar membrane is essential for proper abscisic acid responses. *Cell Res*. **2012**, *22*, 1155-1168.

Batistic, O., Sorek, N., Schultke, S., Yalovsky, S., and Kudla, J. Dual fatty acyl modification determines the localization and plasma membrane targeting of CBL/CIPK Ca^{2+} signaling complexes in *Arabidopsis*. *Plant Cell*. **2008**, *20*, 1346-1362.

Batistic, O., Waadt, R., Steinhorst, L., Held, K., and Kudla, J. CBL-mediated targeting of CIPKs facilitates the decoding of calcium signals emanating from distinct cellular stores. *Plant J*. **2010**, *61*, 211-222.

Brozynska, M., Furtado, A., and Henry, R. J. Genomics of crop wild relatives: expanding the gene pool for crop improvement. *Plant Biotechnol J*. **2016**, *14*, 1070-1085.

Chai, S., Ge, F. R., Zhang, Y., and Li, S. S-acylation of CBL10/SCaBP8 by PAT10 is crucial for its tonoplast association and function in salt tolerance. *J Integr Plant Biol*. **2020**, *62*, 718-722.

Chen, C., Chen, H., Zhang, Y., Thomas, H. R., Frank, M. H., He, Y., and Xia, R. TBtools: An integrative

toolkit developed for interactive analyses of big biological data. *Mol Plant*. **2020**, *13*, 1194-1202.

Chen, P., Yang, J., Mei, Q., Liu, H., Cheng, Y., Ma, F., and Mao, K. Genome-wide analysis of the apple CBL family reveals that Mdcbl10.1 functions positively in modulating apple salt tolerance. *Int J Mol Sci*. **2021**, *22*, 12430.

Cheong, Y. H., Sung, S. J., Kim, B. G., Pandey, G. K., Cho, J. S., Kim, K. N., and Luan, S. Constitutive overexpression of the calcium sensor *CBL5* confers osmotic or drought stress tolerance in Arabidopsis. *Mol Cells*. **2010**, *29*, 159-165.

Cho, J. H., Sim, S. C., and Kim, K. N. Calcium sensor SlCBL4 associates with SlCIPK24 protein kinase and mediates salt tolerance in *Solanum lycopersicum*. *Plants*. **2021**, *10*, 2173.

Dong, L. H., Wang, Q., Manik, S. M. N., Song, Y. F., Shi, S. J., Su, Y. L., Liu, G. S., and Liu, H. B. *Nicotiana sylvestris* calcineurin B-like protein NsylCBL10 enhances salt tolerance in transgenic *Arabidopsis*. *Plant Cell Rep*. **2015**, *34*, 2053-2063.

Eckert, C., Offenborn, J. N., Heinz, T., Armarego-Marriott, T., Schultke, S., Zhang, C., Hillmer, S., Heilmann, M., Schumacher, K., Bock, R., Heilmann, I., and Kudla, J. The vacuolar calcium sensors CBL2 and CBL3 affect seed size and embryonic development in *Arabidopsis thaliana*. *Plant J*. **2014**, *78*, 146-156.

Edel, K. H., and Kudla, J. Increasing complexity and versatility: how the calcium signaling toolkit was shaped during plant land colonization. *Cell Calcium*. **2015**, *57*, 231-246.

Feldman, M., and Levy, A. A. Genome evolution in allopolyploid wheat—a revolutionary reprogramming followed by gradual changes. *J Genet Genomics*. **2009**, *36*, 511-518.

Glover N M, Redestig H, Dessimoz C. Homoeologs: what are they and how do we infer them? *Trends Plant Sci*. **2016**, 21(7): 609-621.

Guex, N., and Peitsch, M. C. SWISS-MODEL and the Swiss-PdbViewer: an environment for comparative protein modeling. *Electrophoresis*. **1997**, *18*, 2714-2723.

Guo, L., Yu, Y., Xia, X., and Yin, W. Identification and functional characterization of the promoter of the calcium sensor gene *CBL1* from the xerophyte *Ammopiptanthus mongolicus*. *BMC Plant Biology* **2010**, *10*, 1-16.

Guo, Y., Halfter, U., Ishitani, M., and Zhu, J.-K. Molecular characterization of functional domains in the protein kinase SOS2 that is required for plant salt tolerance. *Plant Cell*. **2001**, *13*, 1383–1399.

Hashimoto, K., Eckert, C., Anschutz, U., Scholz, M., Held, K., Waadt, R., Reyer, A., Hippler, M., Becker, D., and Kudla, J. Phosphorylation of calcineurin B-like (CBL) calcium sensor proteins by their CBL-interacting protein kinases (CIPKs) is required for full activity of CBL-CIPK complexes toward their target proteins. *J Biol Chem*. **2012**, *287*, 7956-7968.

Held, K., Pascaud, F., Eckert, C., Gajdanowicz, P., Hashimoto, K., Corratge-Faillie, C., Offenborn, J. N., Lacombe, B., Dreyer, I., Thibaud, J. B., and Kudla, J. Calcium-dependent modulation and plasma membrane targeting of the AKT2 potassium channel by the CBL4/CIPK6 calcium sensor/protein kinase complex. *Cell Res*. **2011**, *21*, 1116-1130.

Horsch, R. B., Fry, J. E., Hoffmann, N. L., Eichholtz, D., Rogers, S. G., and Fraley, R. T. A simple and general method for transferring genes into plants. *Science*. **1985**, *227*, 1229-1231.

Hovav, R., Udall, J. A., Chaudhary, B., Rapp, R., Flagel, L., and Wendel, J. F. Partitioned expression of duplicated genes during development and evolution of a single cell in a polyploid plant. *Proc Natl Acad Sci USA*. **2007**, *105*, 6191–6195.

Ju, C., Zhang, Z., Deng, J., Miao, C., Wang, Z., Wallrad, L., Javed, L., Fu, D., Zhang, T., Kudla, J., Gong, Z., and Wang, C. Ca^{2+}-dependent successive phosphorylation of vacuolar transporter MTP8 by CBL2/3-CIPK3/9/26 and CPK5 is critical for manganese homeostasis in *Arabidopsis*. *Mol Plant*. **2022**, *15*, 419-437.

Kang, H. K., and Nam, K. H. Reverse function of ROS-induced CBL10 during salt and drought stress responses. *Plant Sci*. **2016**, *243*, 49-55.

Kang, Y., Khan, S., and Ma, X. Climate change impacts on crop yield, crop water productivity and food security – A review. *Prog Mater Sci*. **2009**, *19*, 1665-1674.

Kim, B.-G., Waadt, R., Cheong, Y. H., Pandey, G. K., Dominguez-Solis, J. R., Schültke, S., Lee, S. C., Kudla, J., and Luan, S. The calcium sensor CBL10 mediates salt tolerance by regulating ion homeostasis in *Arabidopsis*. *Plant J*. **2007**, *52*, 473-484.

Kleist, T. J., Spencley, A. L., and Luan, S. Comparative phylogenomics of the CBL-CIPK calcium-decoding network in the moss *Physcomitrella*, *Arabidopsis*, and other green lineages. *Front Plant Sci*. **2014**, *5*, 187.

Kolukisaoglu, U., Weinl, S., Blazevic, D., Batistic, O., and Kudla, J. Calcium sensors and their interacting protein kinases: genomics of the *Arabidopsis* and rice CBL-CIPK signaling networks. *Plant Physiol*.

2004, *134*, 43-58.

Kretsinger, R. H., and Nockolds, C. E. Carp muscle calcium-binding protein. *J Biol Chem*. **1973**, *248*, 3313-3326.

Letunic, I., Khedkar, S., and Bork, P. SMART: recent updates, new developments and status in 2020. *Nucleic Acids Res*. **2021**, *49*, D458-D460.

Li, W., Zhang, H., Li, X., Zhang, F., Liu, C., Du, Y., Gao, X., Zhang, Z., Zhang, X., Hou, Z., Zhou, H., Sheng, X., Wang, G., and Guo, Y. Intergrative metabolomic and transcriptomic analyses unveil nutrient remobilization events in leaf senescence of tobacco. *Sci Rep*. **2017**, *7*, 12126.

Liliane, T. N., and Charles, M. S. Factors affecting yield of crops. *Agronomy-climate change & food security*. **2020**, 9.

Liu, H., Wang, Y. X., Li, H., Teng, R. M., Wang, Y., and Zhuang, J. Genome-wide identification and expression analysis of calcineurin B-like protein and calcineurin B-like protein-interacting protein kinase family genes in tea plant. *DNA Cell Biol*. **2019**, *38*, 824-839.

Liu, L., Xu, W., Hu, X., Liu, H., and Lin, Y. W-box and G-box elements play important roles in early senescence of rice flag leaf. *Sci Rep*. **2016**, *6*, 20881.

Liu, W. Z., Deng, M., Li, L., Yang, B., Li, H., Deng, H., and Jiang, Y. Q. Rapeseed calcineurin B-like protein CBL4, interacting with CBL-interacting protein kinase CIPK24, modulates salt tolerance in plants. *Biochem Biophys Res Commun*. **2015**, *467*, 467-471.

Liu, Z., Xie, Q., Tang, F., Wu, J., Dong, W., Wang, C., and Gao, C. The *ThSOS3* gene improves the salt tolerance of transgenic *Tamarix hispida* and *Arabidopsis thaliana*. *Front Plant Sci*. **2020**, *11*, 597480.

Livak, K. J., and Schmittgen, T. D. Analysis of relative gene expression data using real-time quantitative PCR and the $2^{-\Delta\Delta CT}$ method. *Methods*. **2001**, *25*, 402-408.

Luan, S. The CBL-CIPK network in plant calcium signaling. *Trends Plant Sci*. **2009**, *14*, 37-42.

Mao, J., Mo, Z., Yuan, G., Xiang, H., Visser, R. G. F., Bai, Y., Liu, H., Wang, Q., and Linden, C. G. v. d. The CBL-CIPK network is involved in the physiological crosstalk between plant growth and stress adaptation. *Plant Cell Environ*. **2022**.

Mao, J., Yuan, J., Mo, Z., An, L., Shi, S., Visser, R. G. F., Bai, Y., Sun, Y., Liu, G., Liu, H., Wang, Q., and van der Linden, C. G. Overexpression of *NtCBL5A* leads to necrotic lesions by enhancing Na^+ sensitivity of tobacco leaves under salt stress. *Front Plant Sci*. **2021**, *12*, 740976.

Martinez-Atienza, J., Jiang, X., Garciadeblas, B., Mendoza, I., Zhu, J. K., Pardo, J. M., and Quintero, F. J. Conservation of the salt overly sensitive pathway in rice. *Plant Physiol*. **2007**, *143*, 1001-1012.

Mittler, R. Abiotic stress, the field environment and stress combination. *Trends Plant Sci*. **2006**, *11*, 15-19.

Munns, R. Genes and salt tolerance: bringing them together. *New Phytol*. **2005**, *167*, 645-663.

Nagae, M., Nozawa, A., Koizumi, N., Sano, H., Hashimoto, H., Sato, M., and Shimizu, T. The crystal structure of the novel calcium-binding protein AtCBL2 from *Arabidopsis thaliana*. *J Biol Chem*. **2003**, *278*, 42240-42246.

Nicholas, K. B. Genedoc: a tool for editing and annoting multiple sequence alignments. *http://wwwpscedu/biomed/genedoc*. **1997**.

Nunez-Ramirez, R., Sanchez-Barrena, M. J., Villalta, I., Vega, J. F., Pardo, J. M., Quintero, F. J., Martinez-Salazar, J., and Albert, A. Structural insights on the plant salt-overly-sensitive 1 (SOS1) Na^+/H^+ antiporter. *J Mol Biol*. **2012**, *424*, 283-294.

Peng, J. Gene redundancy and gene compensation: An updated view. *J Genet Genomics*. **2019**, *46*, 329-333.

Qin, Y., Bai, S., Li, W., Sun, T., Galbraith, D. W., Yang, Z., Zhou, Y., Sun, G., and Wang, B. Transcriptome analysis reveals key genes involved in the regulation of nicotine biosynthesis at early time points after topping in tobacco (*Nicotiana tabacum* L.). *BMC Plant Biol*. **2020**, *20*, 1-15.

Qiu, Q.-S., Guo, Y., Dietrich, M. A., Schumaker, K. S., and Zhu, J.-K. Regulation of SOS1, a plasma membrane Na^+/H^+ exchanger in *Arabidopsis thaliana*, by SOS2 and SOS3. *Proc Natl Acad Sci USA*. **2002**, *99*, 8436-8441.

Quan, R., Lin, H., Mendoza, I., Zhang, Y., Cao, W., Yang, Y., Shang, M., Chen, S., Pardo, J. M., and Guo, Y. SCABP8/CBL10, a putative calcium sensor, interacts with the protein kinase SOS2 to protect *Arabidopsis* shoots from salt stress. *Plant Cell*. **2007**, *19*, 1415-1431.

Reynolds, M. P. Climate change and crop production. CAB International. **2010**.

Rombauts, S., Déhais, P., Montagu, M. V., and Rouzé, P. PlantCARE, a plant cis-acting regulatory element database. *Nucleic Acids Res*. **1999**, *27*, 295-296.

Roy, B., and Arnim, A. G. v. Translational Regulation of Cytoplasmic mRNAs. In. The Arabidopsis Book: American Society of Plant Biologists. 11. **2013**.

Saito, S., Hamamoto, S., Moriya, K., Matsuura, A., Sato, Y., Muto, J., Noguchi, H., Yamauchi, S., Tozawa,

Y., Ueda, M., Hashimoto, K., Koster, P., Dong, Q., Held, K., Kudla, J., Utsumi, T., and Uozumi, N. *N*-myristoylation and *S*-acylation are common modifications of Ca^{2+}-regulated *Arabidopsis* kinases and are required for activation of the SLAC1 anion channel. *New Phytol*. **2018**, *218*, 1504-1521.

Sanchez-Barrena, M. J., Fujii, H., Angulo, I., Martinez-Ripoll, M., Zhu, J. K., and Albert, A. The structure of the C-terminal domain of the protein kinase AtSOS2 bound to the calcium sensor AtSOS3. *Mol Cell*. **2007**, *26*, 427-435.

Sánchez-Barrena, M. J., Martínez-Ripoll, M., and Albert, A. Structural biology of a major signaling network that regulates plant abiotic stress: The CBL-CIPK mediated pathway. *Int J Mol Sci*. **2013**, *14*, 5734-5749.

Sanchez-Barrena, M. J., Martinez-Ripoll, M., Zhu, J. K., and Albert, A. The structure of the *Arabidopsis thaliana* SOS3: molecular mechanism of sensing calcium for salt stress response. *J Mol Biol*. **2005**, *345*, 1253-1264.

Sanyal, S. K., Kanwar, P., Samtani, H., Kaur, K., Jha, S. K., and Pandey, G. K. Alternative splicing of CIPK3 results in distinct target selection to propagate ABA signaling in *Arabidopsis*. *Front Plant Sci*. **2017**, *8*, 1924.

Schmidt, G. W., and Delaney, S. K. Stable internal reference genes for normalization of real-time RT-PCR in tobacco (*Nicotiana tabacum*) during development and abiotic stress. *Mol Genet Genomics*. **2010**, *283*, 233-241.

Shanker, A. K., and Venkateswarlu, B. Abiotic stress response in plants - physiological, biochemical and genetic perspectives. Croatia: InTech. **2011**.

Shi, H., Quintero, F. J., Pardo, J. M., and Zhu, J.-K. The putative plasma membrane Na^+/H^+ antiporter SOS1 controls long-distance Na^+ transport in plants. *Plant Cell*. **2002**, *14*, 465-477.

Shi, S. J., An, L. L., Mao, J. J., Aluko, O. O., Ullah, Z., Xu, F. Z., Liu, G. S., Liu, H. B., and Wang, Q. The CBL-interacting protein kinase NtCIPK23 positively regulates seed germination and early seedling development in tobacco (*Nicotiana tabacum* L.). *Plants*. **2021**, *10*, 323.

Song, S. J., Feng, Q. N., Li, C. L., Li, E., Liu, Q., Kang, H., Zhang, W., Zhang, Y., and Li, S. A tonoplast-associated calcium-signaling module dampens ABA signaling during stomatal movement. *Plant Physiol*. **2018**, *177*, 1666-1678.

Srivastava, A. K., Lu, Y., Zinta, G., Lang, Z., and Zhu, J. K. UTR-dependent control of gene expression in

plants. *Trends Plant Sci*. **2018**, *23*, 248-259.

Steinhorst, L., Mähs, A., Ischebeck, T., Zhang, C., Zhang, X., Arendt, S., Schültke, S., Heilmann, I., and Kudla, J. Vacuolar CBL-CIPK12 Ca^{2+}-sensor-kinase complexes are required for polarized pollen tube growth. *Curr Biol*. **2015**, *25*, 1475-1482.

Sugimoto, K., Shin Takeda, and Hirochika, H. MYB-related transcription factor NtMYB2 induced by wounding and elicitors is a regulator of the tobacco retrotransposon *Tto1* and defense-related genes. *Plant Cell*. **2000**, *12*, 2511–2527.

Tang, R.-J., Wang, C., Li, K., and Luan, S. The CBL–CIPK calcium signaling network: unified paradigm from 20 years of discoveries. *Trends Plant Sci*. **2020a**, *25*, 604-617.

Tang, R.-J., Zhao, F.-G., Garcia, V. J., Kleist, T. J., Yang, L., Zhang, H.-X., and Luan, S. Tonoplast CBL-CIPK calcium signaling network regulates magnesium homeostasis in *Arabidopsis*. *Proc Natl Acad Sci U S A*. **2015**, *112*, 3134-3139.

Tang, R. J., Liu, H., Yang, Y., Yang, L., Gao, X. S., Garcia, V. J., Luan, S., and Zhang, H. X. Tonoplast calcium sensors CBL2 and CBL3 control plant growth and ion homeostasis through regulating V-ATPase activity in *Arabidopsis*. *Cell Res*. **2012**, *22*, 1650-1665.

Tang, R. J., Zhao, F. G., Yang, Y., Wang, C., Li, K., Kleist, T. J., Lemaux, P. G., and Luan, S. A calcium signalling network activates vacuolar K^+ remobilization to enable plant adaptation to low-K environments. *Nat Plants*. **2020b**, *6*, 384-393.

Vanderschuren, H., Lentz, E., Zainuddin, I., and Gruissem, W. Proteomics of model and crop plant species: status, current limitations and strategic advances for crop improvement. *J Proteomics*. **2013**, *93*, 5-19.

Waterhouse, A., Bertoni, M., Bienert, S., Studer, G., Tauriello, G., Gumienny, R., Heer, F. T., de Beer, T. A. P., Rempfer, C., Bordoli, L., Lepore, R., and Schwede, T. SWISS-MODEL: homology modelling of protein structures and complexes. *Nucleic Acids Res*. **2018**, *46*, W296-W303.

Weinl, S., and Kudla, J. The CBL-CIPK Ca^{2+}-decoding signaling network: function and perspectives. *New Phytologist*. **2009**, *184*, 517-528.

Xi, Y., Liu, J., Dong, C., and Cheng, Z. M. The CBL and CIPK gene family in grapevine (*Vitis vinifera*): genome-wide analysis and expression profiles in response to various abiotic stresses. *Front Plant Sci*. **2017**, *8*, 978.

Yan, J., Yang, L., Liu, Y., Zhao, Y., Han, T., Miao, X., and Zhang, A. Calcineurin B-like protein 5 (SiCBL5) in *Setaria italica* enhances salt tolerance by regulating Na^+ homeostasis. *Crop J*. **2022**, *10*, 234-242.

Yang, Y., Zhang, C., Tang, R. J., Xu, H. X., Lan, W. Z., Zhao, F., and Luan, S. Calcineurin B-like proteins CBL4 and CBL10 mediate two independent salt tolerance pathways in *Arabidopsis*. *Int J Mol Sci*. **2019**, *20*, 2421.

Yin, X., Wang, Q., Chen, Q., Xiang, N., Yang, Y., and Yang, Y. Genome-wide identification and functional analysis of the calcineurin B-like protein and calcineurin B-like protein-interacting protein kinase gene families in turnip (*Brassica rapa* var. *rapa*). *Front Plant Sci*. **2017**, *8*, 1191.

Yu, S., Sun, Q., Wu, J., Zhao, P., Sun, Y., and Guo, Z. Genome-wide identification and characterization of short-chain dehydrogenase/reductase (SDR) gene family in *Medicago truncatula*. *Int J Mol Sci*. **2021**, *22*, 9498.

Zhang, Y., Linghu, J., Wang, D., Liu, X., Yu, A., Li, F., Zhao, J., and Zhao, T. *Foxtail Millet* CBL4 (SiCBL4) interacts with SiCIPK24, modulates plant salt stress tolerance. *Plant Mol Biol Rep*. **2017**, *35*, 634-646.

Zhu, J. K. Genetic analysis of plant salt tolerance using Arabidopsis. *Plant Physiol*. **2000**, *124*, 941-948.

Supplementary Material

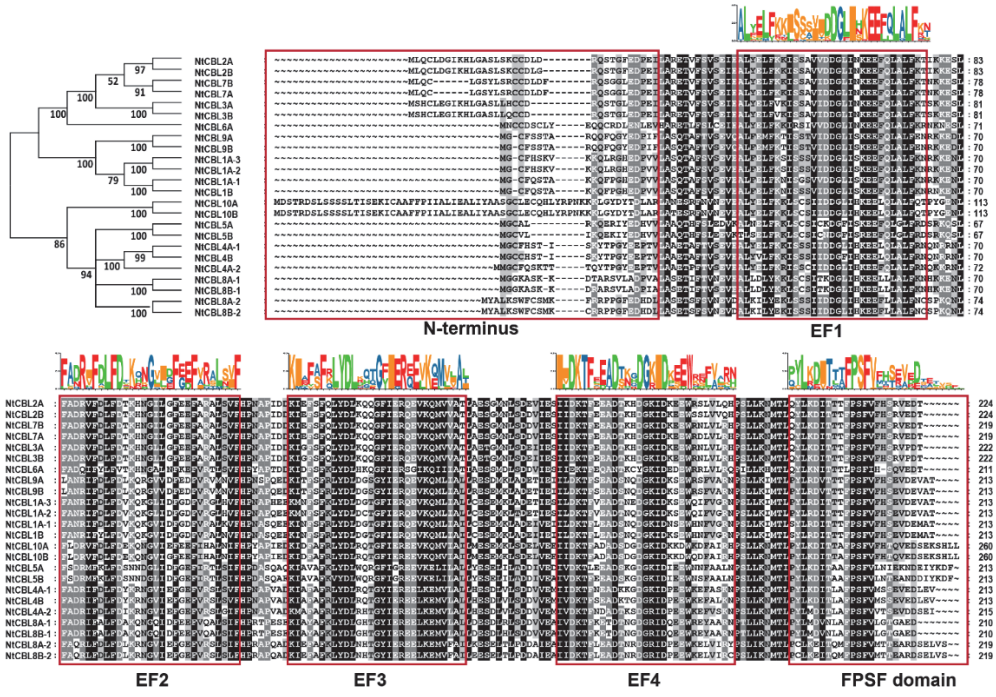

Figure S1. The domain analysis of NtCBLs. Amino acid sequence alignment of NtCBLs. The amino acid sequences alignment of NtCBLs were performed using Clustal Omega (https://www.ebi.ac.uk/Tools/msa/clustalo/) and displayed by GeneDoc (Nicholas, 1997). The domains of NtCBLs were predicted by the SMART online tool (http://smart.embl-heidelberg.de/).

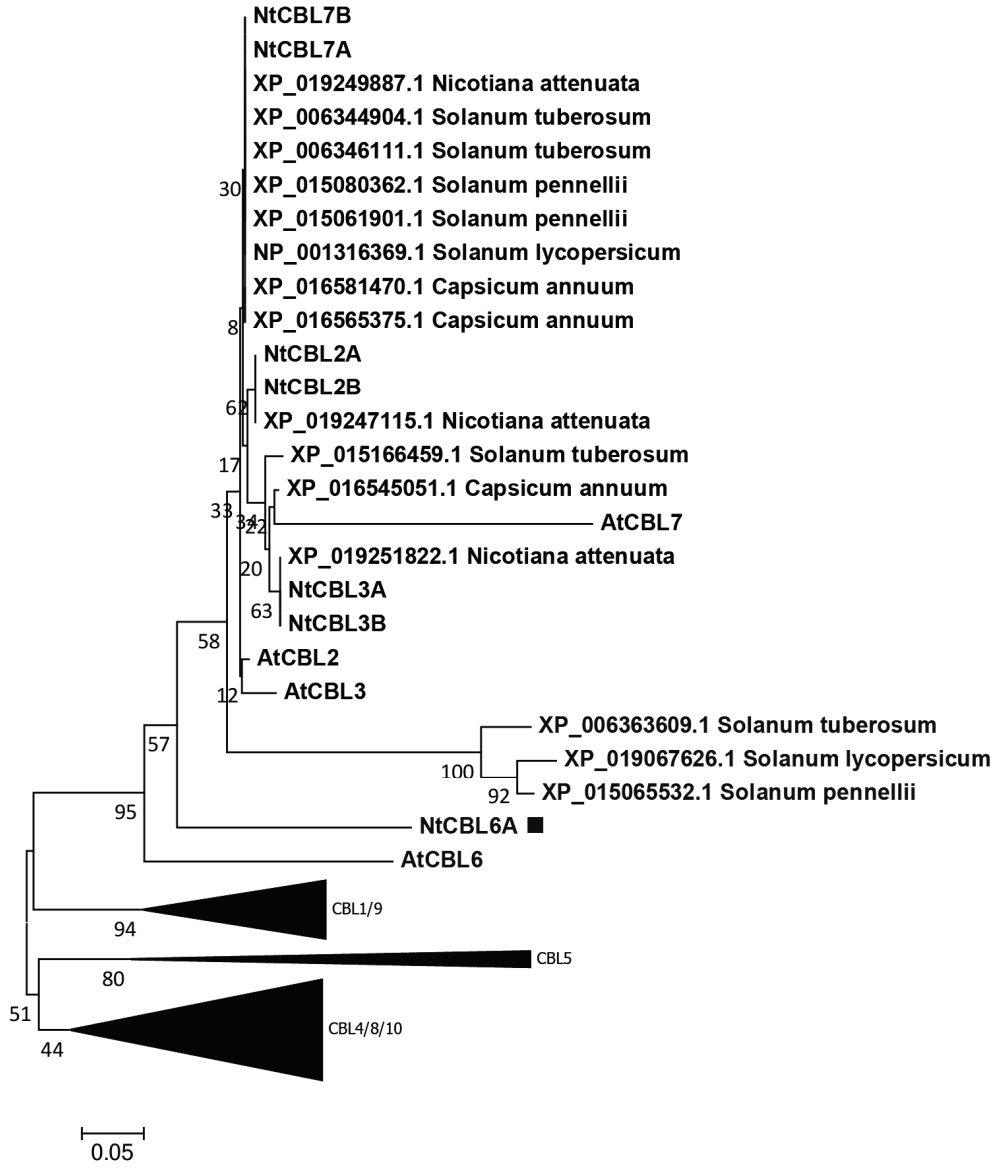

Figure S2. Phylogenetic analysis of the CBL families in *N. tabacum*, *A. thaliana*, *S. tuberosum*, *S. lycopersicum*, *S. pennellii*, and *C. annuum*. The amino acid sequences were downloaded from NCBI (https://www.ncbi.nlm.nih.gov/). The phylogenetic tree was constructed by MEGA6 using the Neighbor-Joining method.

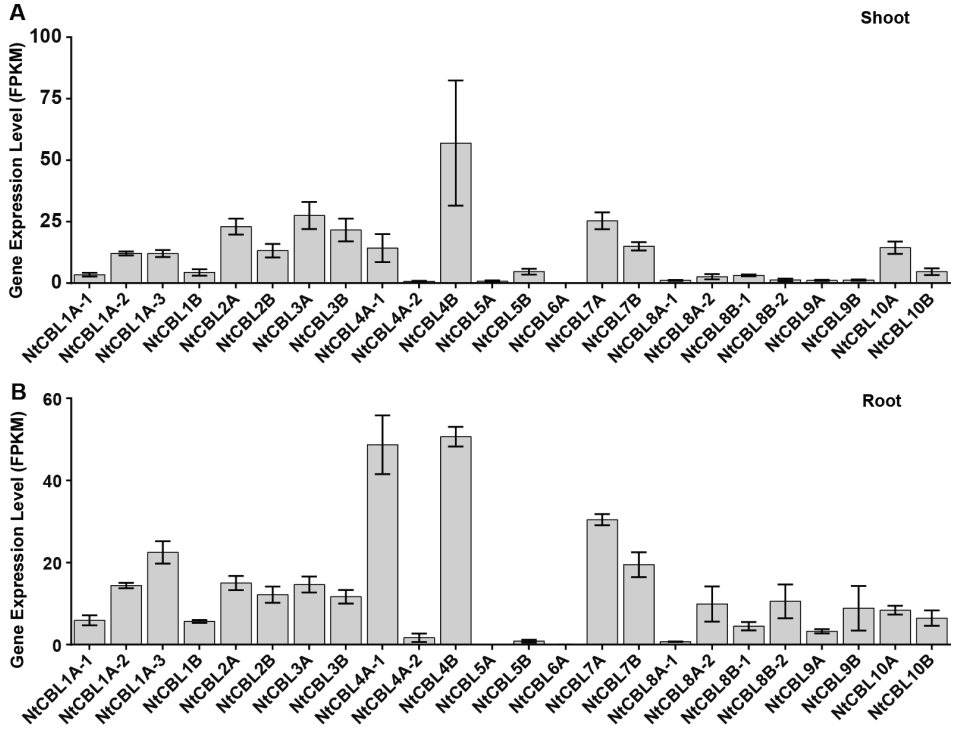

Figure S3. Expression profiles of *NtCBL* genes in different tissues of tobacco plants at the adult stage. Gene expression level of *NtCBL* genes in leaves **(A)** (SRA accession ID: SRX2655430, SRX2655478, SRX2655480, SRX2655632, SRX2655633, SRX2655634) and roots **(B)** (SRA accession ID: SRX4407884, SRX4407877, SRX4407878) of tobacco at the adult stage that determined by published RNA-seq data (Li et al., 2017; Qin et al., 2020). The six biological replicates (every two replicates for upper, middle, and lower leaves) of leaves are sampled at 15 days after topping (75 days after transplanting) (Li et al., 2017), while the three biological replicates of roots are sampled at 0 h after topping (56 days after transplanting) (Qin et al., 2020).

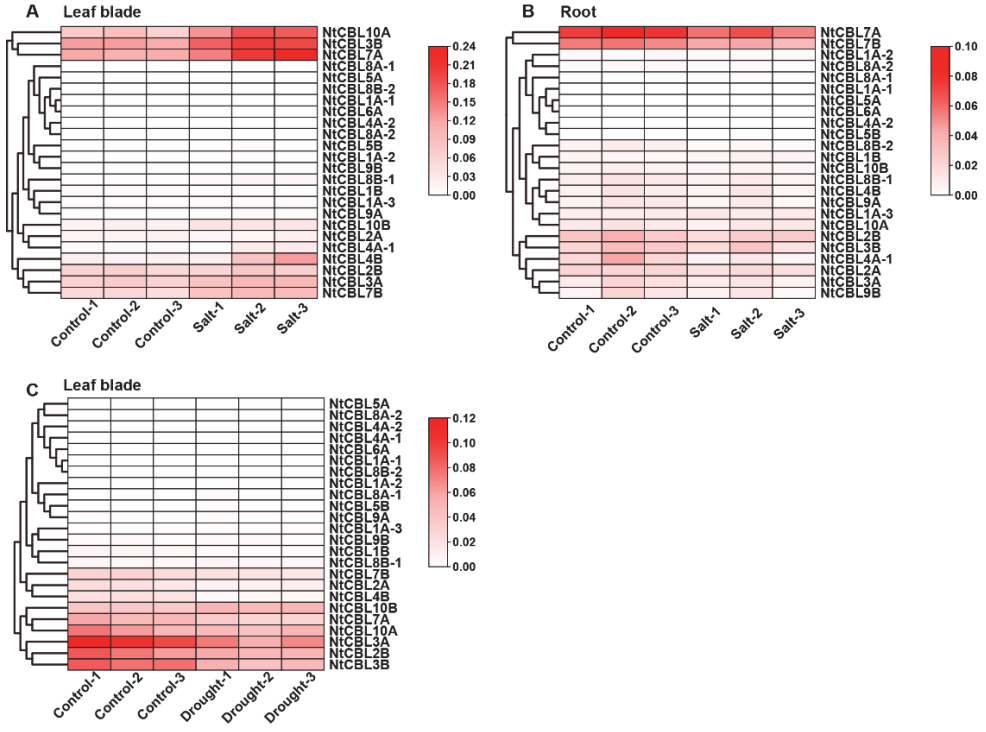

Figure S4. Expression profiles of *NtCBL* genes in tobacco leaves under salt stress and drought stress were determined by RT-qPCR. (A and B) Heatmap pictures display the expression profiles of *NtCBL*s in leaf blades and roots under salt stress (1 day after the start of 100 mM NaCl treatment), respectively. **(C)** Heatmap pictures display the expression profiles of *NtCBL*s in leaf blades under drought stress (5 days after stopping water). The genes were ordered based on the similar expression response to stresses. The expression of these genes under salt and drought stress is relative to that of the reference gene *NtL25* (Schmidt et al., 2010).

Table S1 | Primers used for RT-qPCR

Primer name	Sequence (5' to 3')	Description
NtCBL1A-1qF	GTTCTTCCTCGTTTGTCGTCCT	Forward primer for *NtCBL1A-1*, this primer was designed based on the 5'-UTR sequence of *NtCBL1A-1*
NtCBL1A-1qR	ACAGCTCAAACAATGCCTCAAC	Reverse primer for *NtCBL1A-1*
NtCBL1A-2qF	CCCTTTTATTGCTGGTTACTAG	Forward primer for *NtCBL1A-2*, this primer was designed based on the 5'-UTR sequence of *NtCBL1A-2*
NtCBL1B-qF	CTGTTCAGTGGACGGTCT	Forward primer for *NtCBL1B*, this primer was designed based on the 5'-UTR sequence of *NtCBL1B*
NtCBL1-qR	GAACAGCTCAAACAATGC	Common reverse primer for *NtCBL1A-2* and *NtCBL1B*
NtCBL1A-3qF	ATTGGGTGGGGAGGATGCTA	Forward primer for *NtCBL1A-3*, this primer was designed based on the 3'-UTR sequence of *NtCBL1A-3*
NtCBL1A-3qR	ACAGCATGCGTATCGTTCCA	Reverse primer for *NtCBL1A-3*, this primer was designed based on the 3'-UTR sequence of *NtCBL1A-3*
NtCBL2A-qF	CAGATTCATCTTATTTAGTCGTTT	Forward primer for *NtCBL2A*, this primer was designed based on the 5'-UTR sequence of *NtCBL2A*
NtCBL2B-qF	CATATTAGCATCCGTCTCC	Forward primer for *NtCBL2B*, this primer was designed based on the 5'-UTR sequence of *NtCBL2B*
NtCBL2-qR	CTCCGGATCTTCAAAGC	Common reverse primer for *NtCBL2A* and *NtCBL2B*
NtCBL3-qF	GACCCTTCAGTATCTTAAGGAC	Common forward primer for *NtCBL3A* and *NtCBL3B*
NtCBL3A-qR	AACTCAGAATAGATGAGCAAGAC	Reverse primer for *NtCBL3A*, this primer was designed based on the 3'-UTR sequence of *NtCBL3B*
NtCBL3B-qR	GAACTCAAAAATATATGAGCAAAA	Reverse primer for *NtCBL3B*, this primer was designed based on the 3'-UTR sequence of *NtCBL3B*
NtCBL4-qF	GCACTGCTGCATGAATC	Common forward primer for *NtCBL4A-1*, *NtCBL4A-2*, and *NtCBL4B*, even though this primer has a SNP with the CDS sequence of *NtCBL4A-2*

Primer name	Sequence (5' to 3')	Description
NtCBL4A-1qR	GCATCATCACTGTGGAATAT	Reverse primer for *NtCBL4A-1*, this primer was designed based on the 3'-UTR sequence of *NtCBL4A-1*
NtCBL4A-2qR	AACTCCTTTGCACTCCATAG	Reverse primer for *NtCBL4A-2*, this primer was designed based on the 3'-UTR sequence of *NtCBL4A-2*
NtCBL4B-qR	CTAATGTCTTTTTTGATTCTTGA	Reverse primer for *NtCBL4B*, this primer was designed based on the 3'-UTR sequence of *NtCBL4B*
NtCBL5A-UTR-31F	TTTGCTAATAAACCCATCTTTG	For the identification of endogenous *NtCBL5A*, NtCBL5A-UTR-31F was designed based on the 5'-UTR sequence of *NtCBL5A* (Mao et al., 2021)
NtCBL5A-81R	TCCAAAGAAAAATGTGTCTGAG	
NtCBL5B-595F	TTGTGCTGAATACAGAAGCG	Forward primer for *NtCBL5B*
NtCBL5BUTR-82R	TTCCTTTGATATTCGTGCAG	Reverse primer for *NtCBL5B*, this primer was designed based on the 3'-UTR sequence of *NtCBL5B*
NtCBL6A-qF	ATGAGCAACAATGCAGGGAC	Forward primer for *NtCBL6A*
NtCBL6A-qR	CCCGTTGTGCTTTGTGACG	Reverse primer for *NtCBL6A*
NtCBL7A-qF	AATCTCCGTTTACATATATAGCTC	Forward primer for *NtCBL7A*, this primer was designed based on the 5'-UTR sequence of *NtCBL7A*
NtCBL7B-qF	GAATCTCCGTATACTCATAAAACA	Forward primer for *NtCBL7B*, this primer was designed based on the 5'-UTR sequence of *NtCBL7B*
NtCBL7-qR	GCCTAAAATCAAGATCACAAC	Common reverse primer for *NtCBL7A* and *NtCBL7B*
NtCBL8A-1qF	TCCGAGCTTTGTCCTG	Forward primer for *NtCBL8A-1*
NtCBL8A-1qR	AAACAGATTTTCCACTACGAC	Reverse primer for *NtCBL8A-1*, this primer was designed based on the 3'-UTR sequence of *NtCBL8A-1*
NtCBL8A-2qF	GCCAAATTCTATCCTGCTACTGC	Forward primer for *NtCBL8A-2*, this primer was designed based on the 3'-UTR sequence of *NtCBL8A-2*

Primer name	Sequence (5' to 3')	Description
NtCBL8A-2qR	ACCAGAAATGAAGAA AAAGGGAAA	Reverse primer for *NtCBL8A-2*, this primer was designed based on the 3'-UTR sequence of *NtCBL8A-2*
NtCBL8B-1qF	TCCGAGCTTTGTCCTA	Forward primer for *NtCBL8B-1*
NtCBL8B-1qR	AGATGTTTCCGATACG CT	Reverse primer for *NtCBL8B-1*, this primer was designed based on the 3'-UTR sequence of *NtCBL8B-1*
NtCBL8B-2qF	TTGATCCAGAAGAGT GGAAGG	Forward primer for *NtCBL8B-2*
NtCBL8B-2qR	AGAATTTGGCAGTTG GCACC	Reverse primer for *NtCBL8B-2*, this primer was designed based on the 3'-UTR sequence of *NtCBL8B-2*
NtCBL9-qF	CAAATCTGAATGGCG AAG	Common forward primer for *NtCBL9A* and *NtCBL9B*
NtCBL9A-qR	TTTTGAACTAGCATTT CCTATTA	Reverse primer for *NtCBL9A*, this primer was designed based on the 3'-UTR sequence of *NtCBL9A*
NtCBL9B-qR	CTAATTCTGAACTACA TTTTCTACTC	Reverse primer for *NtCBL9B*, this primer was designed based on the 3'-UTR sequence of *NtCBL9B*
NtCBL10A-qF	CTTTCTCTCTCTCTCT CTGAATT	Forward primer for *NtCBL10A*, this primer was designed based on the 5'-UTR sequence of *NtCBL10A*
NtCBL10B-qF	ACCACATAAAAACACA CACCTTT	Forward primer for *NtCBL10B*, this primer was designed based on the 5'-UTR sequence of *NtCBL10B*
NtCBL10-qR	GCTATTATTGGGAAAA ATGC	Common reverse primer for *NtCBL10A* and *NtCBL10B*
NtCBL4A-1F	ATGGGCTGCTTTCACT CC	Used for the clone of *NtCBL4A-1* CDS
NtCBL4A-1R	TTAGACTTCCAAATCT TCAACC	
NtCBL4A-1F-Kpn Ⅰ	GGGTACCATGGGCTG CTTTCACTCC	Used for the construction of plasmid pCHF3-NtCBL4A-1
NtCBL4A-1R-Xba Ⅰ	CTCTAGATTAGACTTC CAAATCTTCAACC	

Primer name	Sequence (5' to 3')	Description
pCHF3-62F	GCACAATCCCACTATCCTTCG	For the identification of NtCBL4A-1-OE transgenic tobacco with NtCBL4A-1R
NtCBL4A-1-qF	AGTTCTTTCAGATGATGTTGTCG	For the identification of exogenous *NtCBL4A-1*, pCHF3-Allcheck-2 (Shi et al., 2021) was designed based on the sequence of 3'-UTR of exogenous gene
pCHF3-Allcheck-2	GATGATACGAACGAAAGCTCTGC	

For the gene with splicing variants, the primer pair was designed from the common sequence of splicing variants of a gene.

Chapter 4

Overexpression of *NtCBL5A* leads to necrotic lesions by enhancing Na^+ sensitivity of tobacco leaves under salt stress

Jingjing Mao, Jiaping Yuan, Zhijie Mo, Lulu An, Sujuan Shi, Richard G.F. Visser, Yuling Bai, Yuhe Sun, Guanshan Liu, Haobao Liu, Qian Wang, C. Gerard van der Linden

Published in Frontiers in Plant Science (2021)

ABSTRACT

Many tobacco (*Nicotiana tabacum*) cultivars are salt-tolerant and thus are potential model plants to study the mechanisms of salt stress tolerance. The CALCINEURIN B-LIKE PROTEIN (CBL) is a vital family of plant calcium sensor proteins that can transmit Ca^{2+} signals triggered by environmental stimuli including salt stress. Therefore, assessing the potential of *NtCBL* for genetic improvement of salt stress is valuable. In our studies on *NtCBL* members, constitutive overexpression of *NtCBL5A* was found to cause salt supersensitivity with necrotic lesions on leaves. *NtCBL5A*-overexpressing (OE) leaves tended to curl and accumulated high levels of reactive oxygen species (ROS) under salt stress. The supersensitivity of *NtCBL5A*-OE leaves was specifically induced by Na^+, but not by Cl^-, osmotic stress, or drought stress. Ion content measurements indicated that *NtCBL5A*-OE leaves showed sensitivity to the Na^+ accumulation levels that wild-type leaves could tolerate. Furthermore, transcriptome profiling showed that many immune response-related genes are significantly upregulated and photosynthetic machinery-related genes are significantly downregulated in salt-stressed *NtCBL5A*-OE leaves. In addition, the expression of several cation homeostasis-related genes were also affected in salt-stressed *NtCBL5A*-OE leaves. In conclusion, the constitutive overexpression of *NtCBL5A* interferes with the normal salt stress response of tobacco plants and leads to Na^+-dependent leaf necrosis by enhancing the sensitivity of transgenic leaves to Na^+. This Na^+ sensitivity of *NtCBL5A*-OE leaves might result from the abnormal Na^+ compartmentalization, plant photosynthesis, and plant immune response triggered by the constitutive overexpression of *NtCBL5A*. Identifying genes and pathways involved in this unusual salt stress response can provide new insights into the salt stress response of tobacco plants.

Keywords: CALCINEURIN B-LIKE PROTEIN (CBL), Na^+, immune response, necrotic lesions, photosystem, reactive oxygen species (ROS), salt stress, tobacco

INTRODUCTION

Soil salinity causes serious yield losses because of its widespread occurrence and severe effects on crop physiology and metabolism (Munns and Tester, 2008). The potential crop yield losses induced by moderate salinity (8~10 dS/m) are about 55%, 28%, and 15% in corn, wheat, and cotton, respectively (Satir and Berberoglu, 2016). It is estimated that about 30% of irrigated lands are salt-affected and thus commercially unproductive (Zaman and Heng, 2018). There are several strategies for the utilization of salt-affected lands, one of which is to breed or genetically engineer new varieties suitable for saline soils (Gong et al., 2020). Therefore, understanding the mechanisms underlying the plant salt stress response is of fundamental importance to mitigating the negative impact of soil degradation.

Salt stress can be divided into two phases, the first of which is the osmotic or water-deficit stress (Munns, 2005; Van Zelm et al., 2020). When exposed to salinity stress, plants experience an immediate osmotic effect around root cells that impairs water uptake and disturbs associated cell growth and metabolism, similar to the effects of drought stress. The second phase is a salt-specific ion toxicity effect (Munns, 2005; Van Zelm et al., 2020). At prolonged exposure to salinity, Na^+ and Cl^- are transported to leaf blades by the transpiration stream. When the ions accumulate to high levels, they become toxic and cause damage (Munns et al., 2008). The osmotic stress can be measured as a rapid inhibition of the rate of expansion of young leaves, while ion toxicity causes stress-induced senescence of older leaves due to either high leaf Na^+ concentrations or low tolerance of the accumulated Na^+ (Munns et al., 2008).

Plants respond to the two phases of salinity stress via different signaling pathways (Bartels and Sunkar, 2005). Ca^{2+} functions as a secondary messenger to couple a wide range of extracellular stimuli to intracellular responses (Snedden and Fromm, 1998; Snedden and Fromm, 2001). Osmotic and salt stresses induce rapid $[Ca^{2+}]_{cyt}$ transients in the cytosol that trigger downstream pathways, allowing plants to adapt to these environmental changes by regulating enzymatic activity, ion channel activity,

and gene expression (Knight and Knight, 2001; Snedden and Fromm, 2001). The transduction of Ca^{2+} signals depends on Ca^{2+}-sensor proteins (Trewavas and Malhó, 1998). To date, four major classes of Ca^{2+} sensor proteins have been characterized in plants: CALMODULIN (CaM), CALMODULIN-LIKE PROTEIN (CML), CALCIUM-DEPENDENT PROTEIN KINASE (CDPK), and CALCINEURIN B-LIKE PROTEIN (CBL) (Perochon et al., 2011).

As vital Ca^{2+}-sensors, CBLs mainly function by regulating the kinase activity of their partners CBL-INTERACTING PROTEIN KINASEs (CIPKs) in response to various abiotic stresses including salt stress (Luan, 2009). So far, several CBLs from various plant species have been reported to participate in the salt stress response by facilitating Na^+ exudation and vacuolar sequestration. In the root, *Arabidopsis thaliana* AtCBL4 interacts with AtCIPK24 to unlock its kinase activity, and the activated AtCIPK24 can phosphorylate and activate the plasma membrane-localized Na^+/H^+ antiporter SALT OVERLY SENSITIVE 1 (SOS1), leading to Na^+ extrusion from root cells (Qiu et al., 2002; Shi et al., 2002; Gong et al., 2020). This so-called SOS pathway was found to be conserved in many other plant species including rice (*Oryza sativa*), poplar (*Populus trichocarpa* and *Populus euphratica*), mustard (*Brassica juncea*), and apple (*Malus domestica*) (Martinez-Atienza et al., 2007; Tang et al., 2010; Chakraborty et al., 2012; Hu et al., 2012; Lv et al., 2014). In the shoot, AtCBL10 is capable of interacting with both AtCIPK24 and AtCIPK8 to phosphorylate SOS1, and thus enhancing Na^+ efflux from cells (Quan et al., 2007; Lin et al., 2009; Yin et al., 2019). Moreover, the AtCBL10-AtCIPK24 complex was suggested to activate the tonoplast-localized Na^+/H^+ EXCHANGER (AtNHX) to sequester Na^+ into vacuole for salt storage and detoxification of the cytosol (Qiu et al., 2004; Kim et al., 2007). Orthologs of AtCBL10 in other species including wild tobacco (*Nicotiana sylvestris*), tomato (*Solanum lycopersicum*), and poplar (*P. trichocarpa* and *P. euphratica*) were also reported to be involved in the Na^+ tissue tolerance mechanism (Li et al., 2012a; Tang et al., 2014; Dong et al., 2015; Egea et al., 2018). There are other CBLs that may participate in the salt stress response, although their roles and

mechanisms remain to be elucidated. For instance, both *AtCBL5*- and *AtCBL1*-overexpressing (OE) plants showed enhanced tolerance to salt stress (Cheong, 2003; Cheong et al., 2010). Ectopic and constitutive expression of *CBL1* orthologs from the epiphytic orchid (*Sedirea japonica*), rape (*Brassica napus*), and soybean (*Glycine max*) in Arabidopsis also enhanced salt tolerance (Chen et al., 2012; Li et al., 2012b; Cho et al., 2018). However, the ectopic expression of *PeCBL1* in Arabidopsis led to salt sensitivity, with the transgenic lines not being able to exclude Na^+ under saline conditions (Zhang et al., 2013).

Tobacco (*Nicotiana tabacum*) has been investigated as a potential model crop to adapt to salt stress via various strategies (Sun et al., 2020). *N. tabacum* L. cv. Zhongyan 100 is of good salt tolerance which can survive under 300 mM NaCl in a hydroponic growth system (data not shown). In our studies on *NtCBL* members in Zhongyan 100, *NtCBL5A* attracted our attention because its overexpression broke the salt tolerance of Zhongyan 100 and led to salt supersensitivity with severe necrotic lesions on leaves. Studies on *CBL5* orthologs were only reported in Arabidopsis: overexpression of *AtCBL5* enhanced the salt tolerance of transgenic Arabidopsis (Cheong et al., 2010; Wang et al., 2013). In this study, we explored the mechanisms underlying the salt sensitivity of *NtCBL5A*-OE leaves at the physiological, biochemical, and molecular levels. Our results indicate that constitutive overexpression of *NtCBL5A* leads to Na^+-dependent leaf necrosis by enhancing the sensitivity of transgenic tobacco leaves to Na^+. This Na^+ sensitivity may be related to Na^+ compartmentalization, plant photosynthesis, and plant immune response.

MATERIALS AND METHODS

Plant material

N. tabacum L. cv. Zhongyan 100 was obtained from the Tobacco Research Institute of CAAS.

Plasmids construction

The coding sequence of *NtCBL5A* was first amplified from cDNA synthesized from RNA extracted from veins of tobacco cultivar Zhongyan 100 with primers NtCBL5A-1F and NtCBL5A-1R (Table S1) and cloned into the pMD19-T vector for sequencing. The *NtCBL5A* CDS was amplified from pMD19-T-NtCBL5A with primers NtCBL5A-3F-*Sac* Ⅰ and NtCBL5A-3R-*Kpn* Ⅰ (Table S1). The gel-purified amplicon was digested with *Sac* Ⅰ and *Kpn* Ⅰ and cloned into the pCHF3 vector, resulting in the binary recombinant vector pCHF3-NtCBL5A. To construct the promoter plasmid pBI101-ProNtCBL5A::GUS, the upstream sequence of the *NtCBL5A* gene was identified from scaffold Nsyl_scaffold38441 of the tobacco genome. The 2780 bp upstream regulatory region of *NtCBL5A* including promoter sequence (ProNtCBL5A; Figure S1B) was amplified from Zhongyan100 DNA using the primer pair NtCBL5Apro-1F-*Sal* Ⅰ and NtCBL5Apro-1R-*Sma* Ⅰ (Table S1) and cloned into a pMD19-T vector for sequencing. The promoter segment was subcloned from the pMD19-T-ProNtCBL5A construct using *Sal* Ⅰ and *Sma* Ⅰ into pBI101. All the constructs were confirmed by DNA sequencing by the BGI company. Confirmed constructs were transformed into *Agrobacterium tumefaciens* EHA105 for tobacco transformation.

Generation of transgenic plants

To generate the *NtCBL5A*-OE lines and *ProNtCBL5A::GUS* transgenic plants, *Agrobacterium* carrying pCHF3-NtCBL5A plasmid and pBI101-ProNtCBL5A::GUS plasmid were introduced into Zhongyan 100 respectively, by the *Agrobacterium*-mediated leaf disc transformation method (Horsch et al., 1985). To screen for *NtCBL5A*-OE lines, positive transgenic plants of the T0 generation were identified by PCR with the primers NtCBL5A-1F and pCHF3-R (Table S1). The overexpression levels of all positive plants were checked by Real-Time quantitative PCR (RT-qPCR), the RNA samples for RT-qPCR were isolated from mixed whole plants at 12 days after germination (DAG) under control conditions. Eight lines with high *NtCBL5A* overexpression of the original 17 transgenic lines (T0 generation) were selected for propagation. More than 200 T1 seeds from T0 plants with high gene overexpression

levels were harvested and subsequently screened on the selection medium (1/2 MS medium with 50 μg/ml kanamycin). All these lines show sensitivity to salt stress. Two T1 lines (OE-2 and OE-15) with a segregation of around 3:1 (tolerance: sensitivity) were selected for harvesting T2 seeds. More than 200 T2 seeds were screened on the selection medium. The T2 generation with 100% kanamycin resistance was considered as homozygous plants and used for the evaluation of stress tolerance. Positive *ProNtCBL5A::GUS* transgenic lines of the T0 generation were identified by PCR with the primers pBI101-F and NtCBL5Apro-1R-*Sma* Ⅰ (Table S1). More than 200 seeds from T0 seedlings were harvested and subsequently screened on selection medium as described above and positive T1 plants from three independent lines were selected for GUS staining assay.

Application and phenotyping of salt and drought treatment

Salt and drought stress experiments were conducted in 2019 at Unifarm, Wageningen University & Research in the Netherlands. Conditions of the greenhouse were 16 h light / 8 h dark at 25/23℃ and 70% relative humidity. The shortwave radiation level was maintained in the greenhouse compartment using artificial PAR (photosynthetically active radiation) when the incoming shortwave radiation was below 200 Wm^{-2}.

For the salt tolerance evaluations, tobacco seeds were sown in soil, and they germinated after about 8 days. About at 12 DAG, the young seedlings were transplanted in rock-wool plugs within float trays for 8 days, then they were transplanted to a circular flow hydroponic system filled with 1/2 Hoagland's nutrient solution (500 L). The water used to prepare 1/2 Hoagland's nutrient solution contained trace amounts of Na^+ and Cl^- (5.04 μg/ml and 6.72 μg/ml, respectively). After 6 days of acclimatization (at ~ 30 DAG), NaCl was added to the nutrient solution to a concentration of 50 mM on the first day to avoid salt shock, and the final NaCl concentration of 100 mM NaCl was reached the next day. From 4 days after the start of the treatment (DAT), photographs of the plants were taken every day until harvest. For assessing salt tolerance, indicative traits such as growth traits (leaf width and

length, root length, fresh/dry biomass) and ion content were measured.

For the drought stress evaluation, a pilot experiment was conducted first to determine the wilting point of tobacco under the greenhouse conditions. Tobacco seeds were sown in soil. Young seedlings were transplanted to trays and pots at 12 DAG and 22 DAG. Sixteen days after transplantation to pots (38 DAG), watering was stopped until the leaves started to exhibit slight wilting, at a recorded Soil Water Content (SWC) of 28% Full Field Capacity (FFC) (~43 DAG). For the drought tolerance evaluation experiment, SWC was kept around 60% FFC (control conditions) and 28% FFC (drought conditions) by supplying a limited amount of water every day for 3 weeks (~64 DAG). The SWC was monitored and recorded with a Grodan Water Content Meter and a gravimetrical method, where SWC=(W_{wet}-W_{dry})/FFC*100% (W_{wet} is the weight of wet soil and W_{dry} is the weight of dry soil). For assessing salt tolerance, shoot biomass and chlorophyll content were measured. Chlorophyll content was measured with the Minolta SPAD 502 Chlorophyll Meter (Ling et al., 2011). For chlorophyll content values, the average was taken of the measurements of 5 different areas of the 8th leaf (the first new leaf that appeared after the drought treatment started).

Ion and osmotic stress evaluation

For the ion and osmotic stress evaluation experiments, the plants were prepared as described for the salt evaluation experiments. The experiments were conducted in a hydroponic system filled with 1/2 Hoagland's nutrient solution in 3 L containers. The solution was refreshed every two days to keep enough nutrition and a stable stress treatment. After 6 days of acclimatization, the stress was built up in two steps: ion concentrations were raised to 50 mM NaCl/$NaNO_3$/KNO_3/KCl, and for the osmotic stress treatment to 8% PEG6000, and the final stress conditions were reached 100 mM NaCl/$NaNO_3$/KNO_3/KCl, 15% PEG6000 at the next day. Photographs of the plants were taken at 9 DAT.

Ion content measurement

Ion content measurement contained 3 biological replications and every biological replication is a pool of 3 plants. Root samples were rinsed in ddH_2O first, then were dried with absorbent paper to get rid of ions on the outside of the roots. Fresh samples were dried at 105℃ until stable weights, then the dry tissue was crushed to powder with a grinder. 30~50 mg of dry sample was placed into a test tube. The powdered samples were ashed at 650℃ for 6 hours. One milliliter of 3 M formic acid was added into the test tube and was shaken for 20 min at 5000 rpm at 99.9℃. Then 9 mL Milli-Q® was added into the test tube and mixed. Then 0.2 mL sample was taken out and added into 9.8 mL Milli-Q® for 50 times dilution. The ion contents of dilution samples were measured using the Ion Chromatography (IC) system 850 Professional (Metrohm Switzerland).

GUS and DAB staining

GUS staining was conducted using *β*-Galactosidase Reporter Gene Staining Kit (Beijing Leagene Biotech. Co., Ltd, Cat No./ID: DP0013, Beijing, China). Samples were placed into GUS staining solution and incubated at 37℃ overnight. The tissues then were placed in 95% ethanol until chlorophyll was washed out, and samples were photographed. The tissues were stored in FAA (Formaldehyde-Acetic Acid-Ethanol) Fix Solution (Wuhan Servicebio Technology Co., Ltd, Cat No./ID: G1103-500 ML, Wuhan, China). For H_2O_2 visualization with DAB staining, leaves were put in 1 mg/ml DAB (3, 3'-Diaminobenzidine tetrahydrochloride hydrate) (Sigma-Aldrich, Cat No./ID: D5637-1G, Darmstadt, Germany) and vacuum infiltrated until DAB solution was taken up, after which the leaves were incubated in DAB staining solution for 16 h in the dark. The leaves were subsequently transferred to 95% ethanol for 24 h to remove chlorophyll. Afterwards, leaves were photographed (Kissoudis, 2016).

RNA isolation and RNA-seq analyses

At 4 DAT, the 5th leaf blades (with main veins removed) of four individual plants under control conditions and saline conditions in the daytime were sampled and frozen immediately in liquid nitrogen. Leaf blades from four individual plants were mixed

and ground to powder. RNA was isolated and purified with the RNeasy Plus Mini Kit (Qiagen, Cat No./ID: 74134, the Netherlands) following the manufacturer's protocol. RNA samples of WT and OE-2 overexpression lines from two independent salt treatment experiments were used for transcriptome sequencing. RNA integrity was assessed using the RNA Nano 6000 Assay Kit of the Bioanalyzer 2100 system (Agilent Technologies, CA, USA). RNA-seq was performed by the Novogene using Illumina Polymerase-based sequencing-by-synthesis, obtaining a read length of 150 bp and coverage of 48 to 81 million reads per sample. Raw reads of fastq format were firstly processed through in-house perl scripts so that all the downstream analyses were based on the clean data with high quality. Reference genome and gene model annotation files (ftp://ftp.solgenomics.net/genomes/Nicotiana_tabacum/edwards_et_al_2017/assembly/Nitab-v4.5_genome_Chr_Edwards2017.fasta.gz) were downloaded from NCBI. Index of the reference genome was built using Hisat2 v2.0.5 and paired-end clean reads were aligned to the reference genome using Hisat2 v2.05. The mapped reads of each sample were assembled by StringTie (v1.3.3b) (Pertea et al., 2015) in a reference-based approach. FeatureCounts v1.5.0-p3 was used to count the reads numbers mapped to each gene and then FPKM of each gene was calculated based on the length of the gene and read counts mapped to this gene. DEGs of two groups were performed using the DESeq2 R package (1.20.0) and resulting P-values were adjusted using the Benjamini and Hochberg's approach for controlling the false discovery rate. Genes with an adjusted P-value <0.05 found by DESeq2 were assigned as differentially expressed. ClusterProfiler R package was used to test the statistical enrichment of DEGs in KEGG pathways.

Real-time PCR and semi-quantitative RT-PCR

For RT-qPCR, RNA was reverse transcribed into cDNA using HiScript Ⅲ RT SuperMix for qPCR (+g DNA wiper) (Vazyme Biotech. Co., Ltd, Cat No./ID: R323-01, Nanjing, China) and the cDNA was amplified using ChamQ Universal SYBR qPCR Master Mix (Vazyme Biotech. Co., Ltd, Cat No./ID: Q711, Nanjing, China) on the

LightCycler® 96 Instrument (F. Hoffmann-La Roche Ltd, Switzerland). All the primers used for RT-qPCR can be found in **Table S1**. The amplification reactions were performed in a total volume of 10 µl, containing 5 µl 2×ChamQ SYBR qPCR mix, 0.6 µl forward and reverse primers (10 µM), 1 µl cDNA (10 times diluted), and 3.4 µl ddH_2O. The RT-qPCR amplification program was as follows: 95℃ for 10 min; 95℃ for 10 s, 60℃ for 30 s and amplification for 40 cycles. Each sample comprised 3 technical replications. Analysis of the relative gene expression data was conducted using the $2^{-\Delta C't}$ (Livak and Schmittgen, 2001). For semi-quantitative RT-PCR, RNA was reverse transcribed into cDNA using iScript™ Reverse Transcription Supermix for RT-qPCR (BIO-RAD, Cat No./ID: 6031, California, USA) and cDNA was amplified using DreamTaq DNA Polymerase (Thermo Fisher Scientific, Cat No./ID: EP0702, Massachusetts, USA). The amplification reactions were performed in a total volume of 20 µl, containing 0.1 µl DreamTaq DNA polymerase, 2 µl 10×DreamTaq buffer, 0.4 µl dNTP mixture (5 mM each), 1 µl forward and reverse primers (10 µM), 2 µl cDNA, and 14.5 µl ddH_2O. The semi-quantitative RT-PCR amplification program was as follows: 95℃ for 5 min; 95℃ for 30 s, 52℃ for 30 s, 72℃ for 30 s (30 cycles); 72℃ for 30 s.

Accession numbers

Sequence data from this article can be found under the following accession numbers. For genes from tobacco and *O. sativa*, sequences can be found in the NCBI database (https://www.ncbi.nlm.nih.gov/): *NtCBL5A* (XM_016642104.1), *NsylCBL5* (KM658159.1), *NtomCBL5* (XM_018767788.1), *OsCBL1* (DQ201195), *OsCBL2* (DQ201196), *OsCBL3* (DQ201197), *OsCBL4* (DQ201198), *OsCBL5* (DQ201199), *OsCBL6* (DQ201200), *OsCBL7* (DQ201201), *OsCBL8* (DQ201202), *OsCBL9* (DQ201203), *OsCBL10* (DQ201204). For genes from *S. lycopersicum*, sequences can be found in the SGN database (https://solgenomics.net/): *SlCBL1* (Solyc06g060980), *SlCBL2* (Solyc12g015870), *SlCBL4-1* (Solyc08g036590), *SlCBL4-2* (Solyc12g055920), *SlCBL8* (Solyc08g054570), *SlCBL10* (Solyc08g065330). For genes from *A. thaliana*, squences can be found in the TAIR

database (https://www.arabidopsis.org/): *AtCBL1* (AT4G17615), *AtCBL2* (AT5G55990), *AtCBL3* (AT4G26570), *AtCBL4* (AT5G24270), *AtCBL5* (AT4G01420), *AtCBL6* (AT4G16350), *AtCBL7* (AT4G26560), *AtCBL8* (AT1G64480), *AtCBL9* (AT5G47100), *AtCBL10* (At4G33000). The RNA-seq data from this article can be found in the National Center for Biotechnology Information Gene Expression Omnibus (GEO) data repository under accession number GSE181164 (https://www.ncbi.nlm.nih.gov/geo/subs/?view=samples&series=181164).

Statistical analysis

Statistical analysis was done using IBM SPSS Statistics 23 software. Significant differences were examined by one-way ANOVA using the LSD test at $P<0.05$ and <0.001. The figures were drawn by GraphPad Prism 6.0.

RESULTS

The cloning and expression analysis of *NtCBL5A*

N. tabacum is a natural allotetraploid derived from two diploid progenitors: *N. sylvestris* as the maternal genome donor and *Nicotiana tomentosiformis* as the paternal genome donor (Yukawa et al., 2006). We predicted and cloned 12 *NsylCBLs* based on the *N. sylvestris* genome data published in NCBI (https://www.ncbi.nlm.nih.gov/) (An et al., 2020). One of these 12 *NsylCBLs* (NCBI reference sequence: XM_009758979.1) had the closest phylogenetic relationship with *AtCBL5* (At4g01420) and therefore was named *NsylCBL5* (GenBank: KM658159.1). The ortholog of *NsylCBL5* in *N. tabacum* L. cv. Zhongyan 100 was subsequently cloned and named *NtCBL5A* (NCBI reference sequence number: XM_016642104.1). The coding sequence (CDS) of *NtCBL5A* is identical to the CDS of *NsylCBL5* and has 28 nucleotide differences with the CDS of *NtomCBL5* (NCBI reference sequence number: XM_018767788.1) (Figure S1A).

The CDS of *NtCBL5A* is 642 bp in length, encoding a 213-amino-acid protein. The NtCBL5A protein is predicted to have four potential elongation factor hands (EF-hands) by the SMART (http://smart.embl-heidelberg.de/) (Letunic and Bork, 2018)

and SWISS-MODEL (https://swissmodel.expasy.org/) (Waterhouse et al., 2018) (Figure 1A, B). The EF-hand motif is the conserved domain of CBL proteins with an α-helix-loop-α-helix structure that binds Ca^{2+} (Sánchez-Barrena et al., 2013). A phylogenetic tree of NtCBL5A with all identified CBL proteins in *A*. *thaliana*, *O*. *sativa*, and *S*. *lycopersicum* distributed the CBL members over 4 clusters, and NtCBL5A was included in Cluster Ⅰ with closest phylogenetic relationship to AtCBL5 (Figure 1C).

Semi-quantitative RT-PCR indicated that *NtCBL5A* is specifically expressed at a higher level in stems and a relatively lower level in main veins of young tobacco seedlings, and it is not detectable in roots and leaf blades (with main veins removed) at 30 days after germination (DAG) (Figure 2A). We examined tissue-specific expression in more detail using independent *ProNtCBL5A::GUS* transgenic tobacco lines with a 2780 bp upstream regulatory region of *NtCBL5A* including the promoter (Figure S1B) driving expression of a *GUS* reporter gene. Consistent with the semi-quantitative RT-PCR result, strong GUS activity was mainly detected in veins and stems of tobacco seedlings (Figure 2B-F). At 3 DAG and 20 DAG, GUS staining was only observed in the veins and the top of the stem (Figure 2B-D). At 40 DAG, GUS staining was still limited to the veins and the stem (Figure 2E, F).

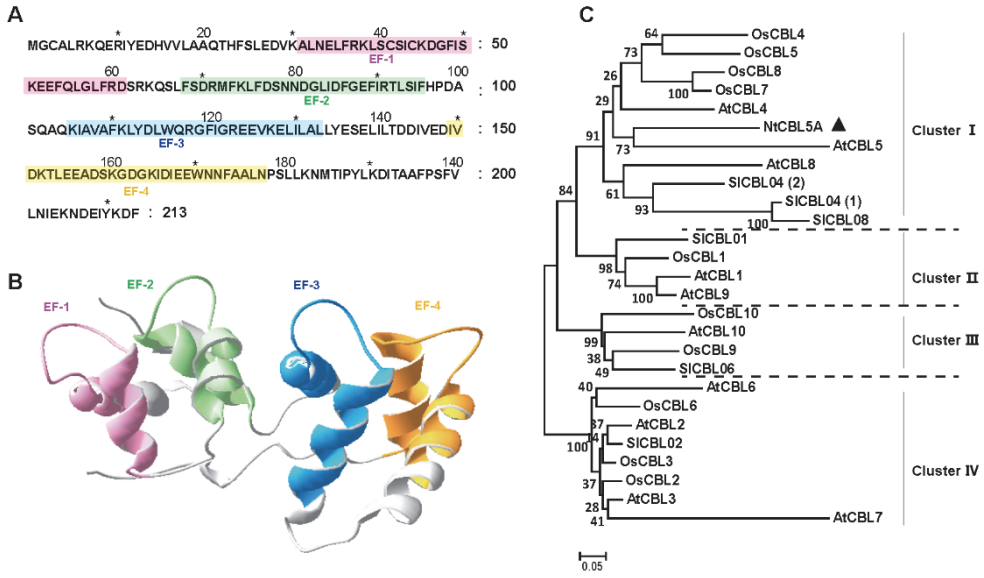

Figure 1 | Structure and phylogenetic relationship of NtCBL5A. (A) Amino acid sequence of NtCBL5A and the positions of four EF-hands predicted by SMART. **(B)** The 3D structure of NtCBL5A predicted by SWISS-MODEL. **(C)** Phylogenetic analysis of NtCBL5A and all known CBL members from *A. thaliana*, *O. sativa*, and *S. lycopersicum*. The amino acid sequences of AtCBLs, OsCBLs, and SlCBLs were downloaded from TAIR (https://www.arabidopsis.org/), NCBI (https://www.ncbi.nlm.nih.gov/), and Sol Genomics Network (https://solgenomics.net/), respectively. The phylogenetic tree was constructed by MEGA6 using the Neighbor-Joining method.

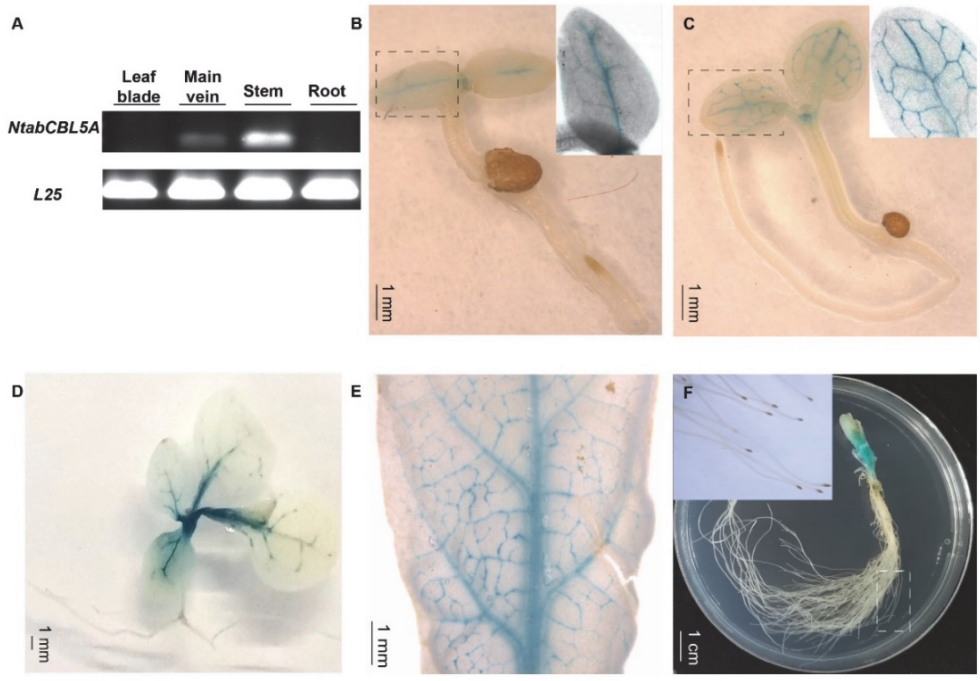

Figure 2 | The expression profile of *NtCBL5A* in tobacco plants. (A) The expression profile detection in different tissues by semi-quantitative RT-PCR at 30 days after germination (DAG), *L25* is the reference gene (Schmidt and Delaney, 2010). **(B-F)** The GUS staining of different tissues of *ProNtCBL5A::GUS* plants at different growth stages. They are seedlings at 3 DAG **(B)**, seedlings at 5 DAG **(C)**, seedlings at 20 DAG **(D)**, leaves of the seedlings at 40 DAG **(E)**, stem and root tissues of the seedlings at 40 DAG **(F)**, respectively.

Overexpression of *NtCBL5A* induces salt supersensitivity with necrotic lesions on leaves

Two independent homozygous *NtCBL5A*-OE lines (OE-2, OE-15) with different overexpression levels were selected for salt tolerance evaluation (Figure 3A, B). Wild-type (WT) and *NtCBL5A*-OE lines were treated under control conditions (1/2 Hoagland's nutrient solution) and saline conditions (1/2 Hoagland's nutrient solution with 100 mM NaCl) in a hydroponic growth system. Under control conditions, there were no phenotype differences between WT and *NtCBL5A*-OE lines. Under saline

conditions, constitutive overexpression of *NtCBL5A* led to salt supersensitivity (Figure 3C). There were leaf chlorosis spots on *NtCBL5A*-OE leaves at the early stage of salt stress that developed fast into severe necrotic lesions within two weeks (Figure 4A). In each *NtCBL5A*-OE plant, the 5th leaf that emerged just before the initiation of the salt treatment showed the most severe necrotic lesions (Figure 3C), and the occurrence of necrotic lesions started from leaf tip and leaf margin (Figure 4A). The overexpression level of *NtCBL5A* appeared to be related to the necrotic phenotype, for the OE-2 line with higher *NtCBL5A* expression level showed more severe necrotic lesions than OE-15 (Figure 4A).

Shoot dry weight and fresh weight of each tobacco line were reduced significantly under salt stress, and the reduction of *NtCBL5A*-OE lines was larger than that of WT at 9 DAT (Figure 3D, E). Under saline conditions, the length and width of the 5th *NtCBL5A*-OE leaves were more reduced with curly and narrow leaf shapes (Figure 4). In addition, ROS accumulation in the 5th *NtCBL5A*-OE leaves was higher than that in WT leaves under salt stress at 2 DAT and 6 DAT (Figure S2; Figure 4D). Root lengths of *NtCBL5A*-OE lines and WT were similarly affected by salinity, but root fresh weight was reduced more in the *NtCBL5A*-OE lines than in WT at 9 DAT (Figure S3).

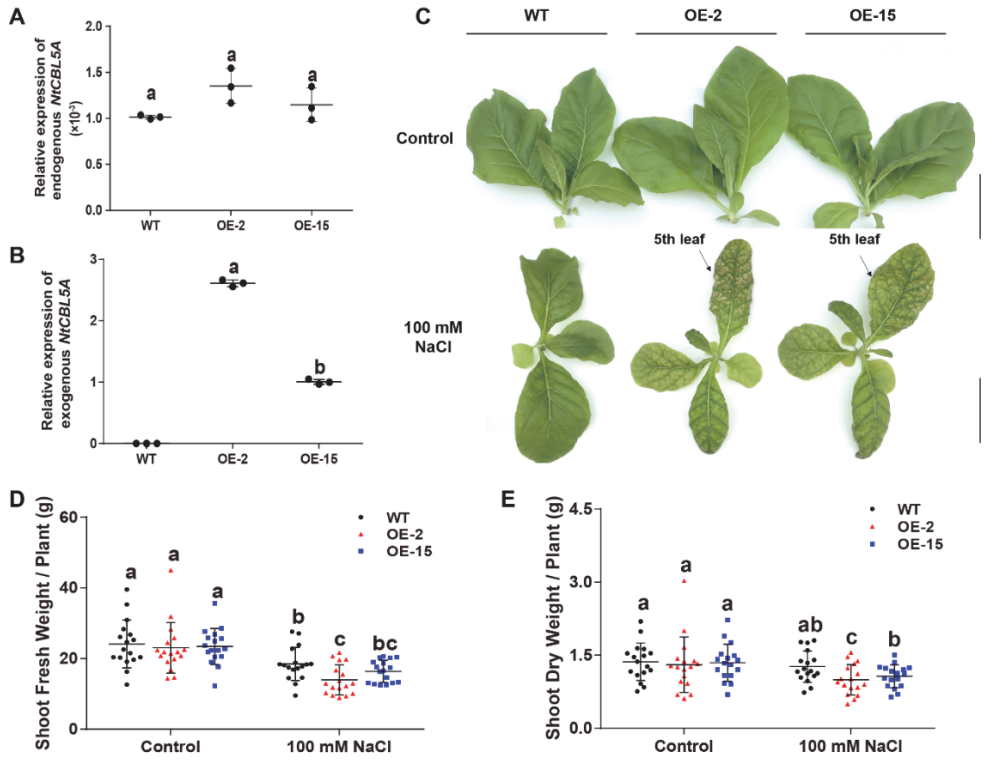

Figure 3 | The detection of *NtCBL5A* expression and above-ground phenotype of wild-type (WT) and *NtCBL5A*-overexpressing (OE) lines (OE-2 and OE-15) under control conditions and salt stress (100 mM NaCl). Scale bars=10 cm. **(A)** Relative expression analysis of endogenous *NtCBL5A* (the *NtCBL5A* driven by 35S promoter) determined by RT-qPCR in different tissues of tobacco seedlings at 4 days after the start of treatment (DAT). The expression of *NtCBL5A* is relative to the reference gene *L25* and the seedlings are 30-DAG (days after germination) old. **(B and C)** Relative expression analysis of endogenous *NtCBL5A* and exogenous *NtCBL5A* (the *NtCBL5A* driven by its own promoter in tobacco) determined by RT-qPCR in whole plants. The expression of *NtCBL5A* is relative to the reference gene *L25* and the seedlings are 12-DAG old. The reverse primer pCHF3-AIIcheck-1 used for amplifying exogenous *NtCBL5A* was designed according to the sequence of the overexpression vector pCHF3, referring to pCHF3-AIIcheck-2 (Shi et al., 2021). **(D)** The shoot phenotype of WT and *NtCBL5A*-OE lines at 9 DAT. **(E and F)** The shoot fresh weight and dry weight of WT and *NtCBL5A*-OE lines at 9 DAT. Error bars indicate ±SD (n=3 for gene expression detection, n=17 for shoot fresh/dry weight determination),

different letters above bars (a, b, and c) indicate significant statistical difference based on one-way ANOVA with LSD test (P<0.05).

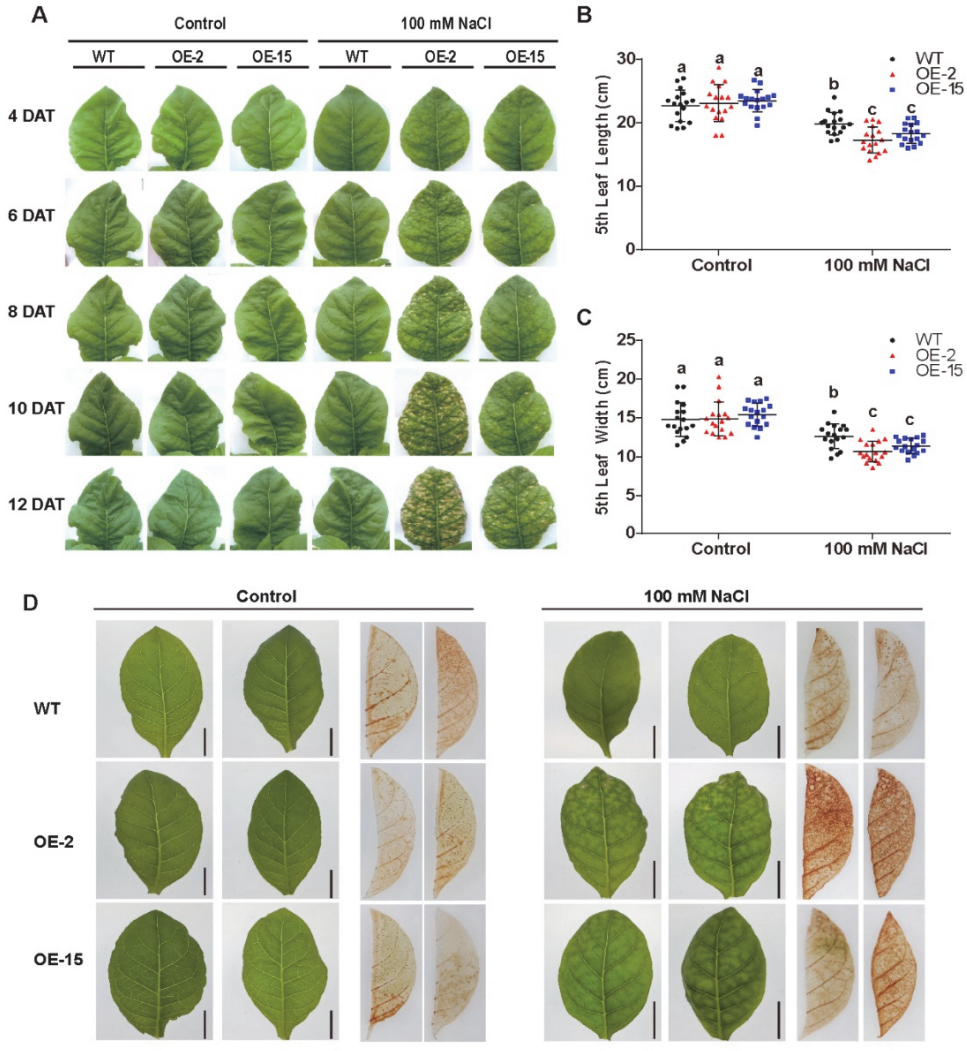

Figure 4 | The determination of physiological parameters in wild-type (WT) and *NtCBL5A*-overexpressing lines (OE-2 and OE-15). (A) The phenotype of the 5th leaf of WT and *NtCBL5A*-OE lines under control conditions and salt stress (100 mM NaCl) from 4 DAT to 13 DAT. **(B and C)** Leaf length and leaf width determination of the 5th leaf at 8 DAT. **(D)** DAB staining of tobacco under control conditions and salt stress (100 mM NaCl) at 6 DAT. Error bars indicate ±SD (n=17), different letters above bars (a,

b, and c) indicate significant statistical difference based on one-way ANOVA with LSD test ($P<0.05$). Scale bars=2 cm.

The necrotic lesions are specifically induced by high Na^+ in the nutrient solution

The response to the osmotic component of salt stress bears similarity to the response to drought (Bartels and Sunkar, 2005). Therefore, the effect of drought stress on *NtCBL5A*-OE plants was determined as well. WT and *NtCBL5A*-OE lines were exposed to drought stress in pots under greenhouse conditions. At 21 DAT, all the lines showed reduced growth compared to the control plants with no water limitation, but there were no significant phenotype differences between the WT and *NtCBL5A*-OE plants under drought stress (Figure 5A). Under drought stress, plant height, fresh and dry shoot weight of each line were decreased, while chlorophyll content of each line was significantly increased compared to control conditions (Figure 5B-E). There were no differences between WT and *NtCBL5A*-OE lines under drought stress (Figure 5B-E), suggesting that osmotic stress alone did not trigger necrotic lesions on *NtCBL5A*-OE leaves. A 15% PEG6000 treatment was conducted to confirm that the necrotic lesions on transgenic lines are not caused by osmotic stress. Indeed, the PEG6000-induced osmotic stress did not induce leaf necrosis in OE-2 and OE-15 lines (Figure 6B).

Under saline conditions, both Na^+ and Cl^- can be toxic to the plant (Munns et al., 2008). To identify the ion that is responsible for the necrotic phenotype of *NtCBL5A*-OE lines under salt stress, the plants were exposed not only to 100 mM NaCl, but also to 100 mM $NaNO_3$, 100 mM KNO_3, and 100 mM KCl (Quan et al., 2007). At 9 DAT, both WT and *NtCBL5A*-OE lines exhibited reduced growth under all treatments relative to control conditions (Figure 6). *NtCBL5A*-OE lines showed leaf necrosis only under NaCl and $NaNO_3$ treatments but not under KNO_3 and KCl treatments (Figure 6C-F), suggesting that the necrotic lesions on *NtCBL5A*-OE lines are specifically induced by high levels of Na^+ in the nutrient solution.

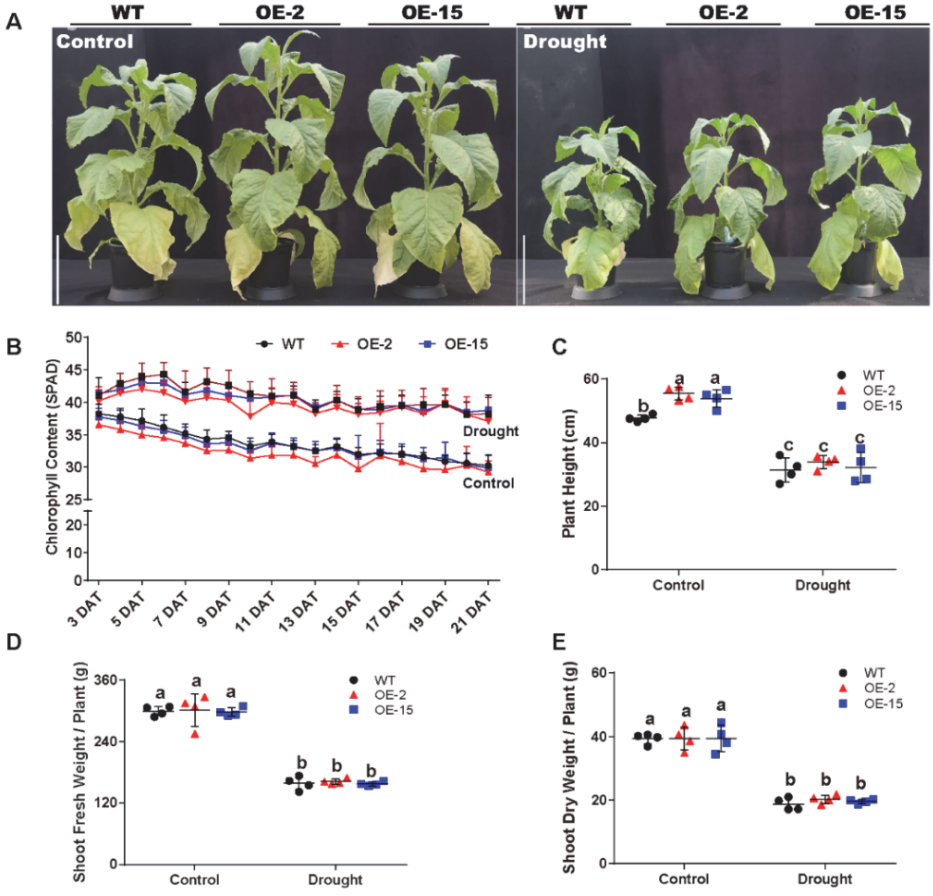

Figure 5 | Phenotypic analysis of wild-type (WT) and *NtCBL5A*-overexpressing (OE) lines (OE-2 and OE-15) under control conditions and drought stress. Scale bars=30 cm. **(A)** The phenotype of WT and *NtCBL5A*-OE lines under control conditions and drought stress at 21 days after the start of treatment (DAT) and 64 days after germination (DAG). **(B)** The chlorophyll content of the 8th leaf of WT and *NtCBL5A*-OE lines from 3 DAT to 21 DAT. **(C-E)** The plant height, fresh shoot biomass, and dry shoot biomass of WT and *NtCBL5A*-OE lines at 21 DAT. Error bars indicate ±SD (n=4), different letters above bars (a, b, and c) indicate significant statistical difference based on one-way ANOVA with LSD test ($P<0.05$).

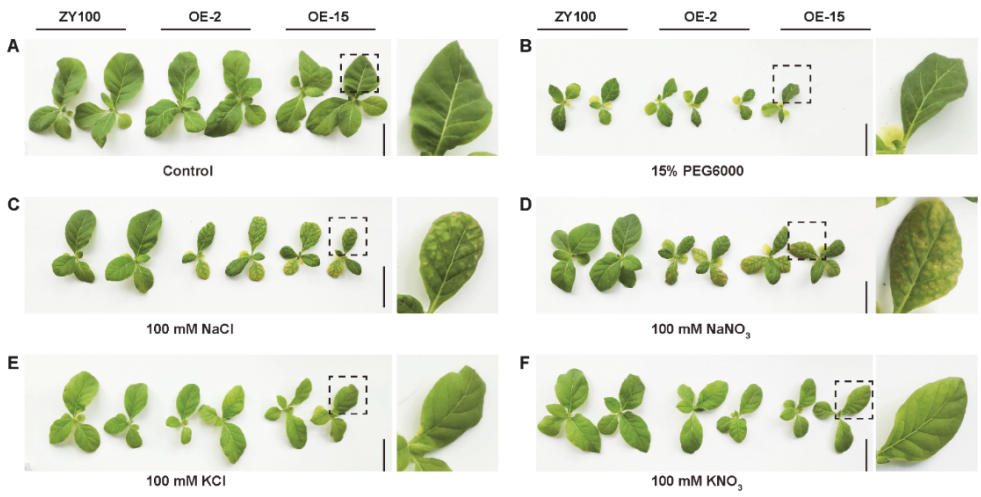

Figure 6 | Ion and osmotic stress evaluation on wild-type (WT) and *NtCBL5A*-overexpressing lines (OE-2 and OE-15) at 9 days after the start of treatment. (A) The phenotype of WT and *NtCBL5A*-OE lines under control condition (1/2 Hoagland's nutrient solution). **(B)** The phenotype of WT and *NtCBL5A*-OE lines under osmotic stress (1/2 Hoagland's nutrient solution added 15% PEG6000). **(C-F)** The phenotype of WT and *NtCBL5A*-OE lines under ion stresses (1/2 Hoagland's nutrient solutions added 100 mM NaCl, 100 mM $NaNO_3$, 100 mM KCl, and 100 mM KNO_3, respectively). Scale bars=10 cm. 4th leaves under light (Light), covered by aluminum-foil paper (Covered), and under dark (Dark), which were zoomed in at the right part of the panel.

Overexpression of *NtCBL5A* enhances the sensitivity of transgenic tobacco leaves to Na^+

To elucidate the cause of the salt-induced necrotic lesions in *NtCBL5A*-OE leaves, we measured the ion contents in the 5th leaf blades (with main veins removed) of all tobacco lines at three treatment time points (4, 6, 9 DAT). It needs to mention first that there was no significant difference between leaf water contents of WT and *NtCBL5A*-OE (Figure S4A). Na^+ contents in the 5th leaf blades of all lines were strongly increased under salt stress relative to control conditions and increased with treatment time. Compared to WT, Na^+ contents in the 5th leaf blades of *NtCBL5A*-OE lines were higher under salt stress but the difference was not large (Figure 7A).

More specifically, during the 4~9 DAT, the Na^+ contents in the 5th leaf blades of WT, OE-2, and OE-15 tobacco plants are in the range of 39.18~51.64 μg/mg, 44.95~69.71 μg/mg, and 47.36~64.31 μg/mg, respectively. In other words, the 5th leaf blades of WT lines could reach a similar Na^+ content level to that of OE lines with treatment time, but they did not exhibit any necrotic lesions at all during the treatment period (Figure 7A; Figure 4A). Cl^- contents in the 5th leaf blades of all lines were strongly increased under salt stress relative to control conditions and increased with time, but there was no significant difference between WT and *NtCBL5A*-OE lines under salt stress (Figure 7C). K^+, Ca^{2+}, and Mg^{2+} contents in all lines were significantly decreased under salt stress but also for these ions there was still no significant difference between WT and *NtCBL5A*-OE plants (Figure S4B-D).

We also measured the Na^+ and Cl^- contents in different tissues (leaf blades: all leaves with main veins removed; main veins: main veins from all leaves; stems; roots) of all lines under control conditions and 100 mM NaCl stress at 10 DAT. Under salt stress, Na^+ contents in all tissues of all lines were strongly increased relative to control conditions, and Na^+ contents in leaf blades of *NtCBL5A*-OE lines were significantly higher than those of WT (Figure 7B). In contrast, Na^+ contents in main veins, stems, and roots of OE-2 and OE-15 were significantly lower than those of WT under salt stress (Figure 7B). Cl^- contents in all tissues of all lines were strongly increased under salt stress relative to control conditions but there was no significant difference between different lines (Figure 7D). Taken together, ion content data suggested that the overexpression of *NtCBL5A* may promote Na^+ loading into leaf blades, but the necrotic lesions are caused by the increased Na^+ sensitivity of *NtCBL5A*-OE leaves.

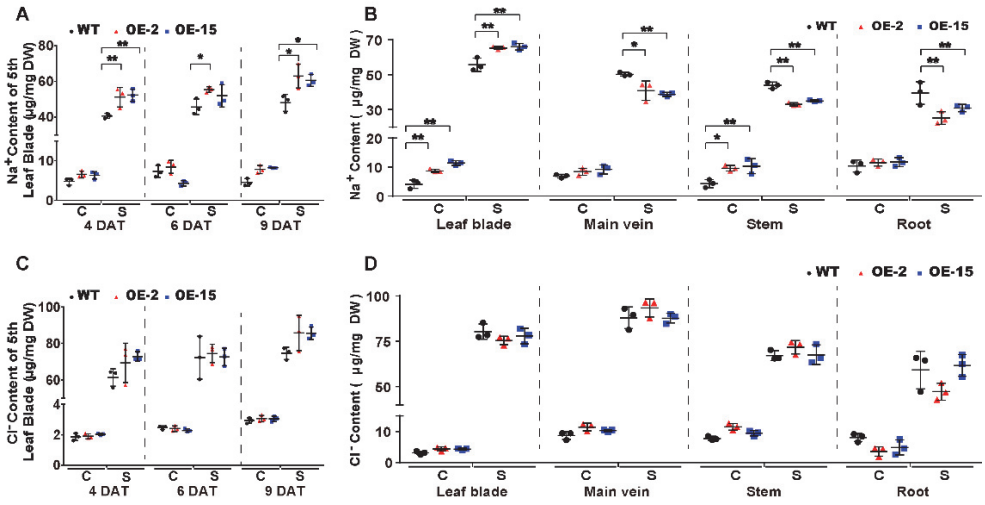

Figure 7 | Na^+ and Cl^- contents in wild-type (WT) and *NtCBL5A*-overexpressing lines (OE-2 and OE-15) under control conditions and salt stress (100 mM NaCl). (A and C), Na^+ and Cl^- contents in the 5th leaf blades (with main veins removed) at 4 DAT, 6 DAT, and 9 DAT. **(B and D)** Na^+ and Cl^- contents in different tissues (leaf blades: all leaves with main veins removed; main veins: main veins from all leaves; stems; roots) at 10 DAT. C means control conditions, while S means salt stress. Error bars indicate ±SD (n=3), every biological replication is a mixed pool of 3 plants. One-way ANOVA with LSD test (*P<0.05 and **P<0.01) was used to analyze statistical significance.

Differentially expressed genes (DEGs) in *NtCBL5A*-OE leaves under salt stress were analyzed

To further identify the genes and pathways involved in the necrotic phenotype of *NtCBL5A*-OE lines, the leaf transcriptome profiling of WT and OE-2 lines grown under control conditions and salt stress (100 mM NaCl) at 4 DAT were sequenced and compared. Two datasets of differentially expressed genes (DEGs) were made in which we identified the genes that were differentially expressed as a result of the overexpression of *NtCBL5A*: Control-WT vs Control-OE2 (C-WT/C-OE2), Salt-WT vs Salt-OE2 (S-WT/S-OE2). Another two datasets were also used to identify the transcripts that were responsive to the salt treatments: Control-WT vs Salt-WT (C-WT/S-WT) and Control-OE2 vs Salt-OE2 (C-OE2/S-OE2). DEGs from C-WT/C-OE2

and S-WT/S-OE2 were compared to select the transcripts affected by *NtCBL5A* overexpression only under salt stress (dotted lines in Figure 8A, D; Figure S5). We also compared DEGs from C-WT/S-WT and C-OE2/S-OE2 to identify the specific transcripts affected by salt stress and only in *NtCBL5A*-OE lines (dotted lines in Figure 8B, E; Figure S5). This procedure was done for two independent experiments, and only DEGs that were identified in both experiments were considered (highlighted part in Figure 8A, B, D, E). The OE-affected DEGs and salt-affected DEGs together resulted in 2079 up-regulated DEGs and 1154 down-regulated DEGs (Figure 8C, F), strongly affected by the combination of *NtCBL5A* overexpression and salt stress.

The up-regulated DEGs were enriched in 10 KEGG (Kyoto encyclopedia of genes and genomes) (Kanehisa et al., 2020) pathways (padj<0.05) (Figure 8G). Among them, “plant-pathogen interaction” (KEGG ID: sly04626) and “MAPK signaling pathway-plant” (KEGG ID: sly04016) attracted our attention because many DEGs identified as belonging to these two pathways are related to HR and cell death, including *PATHOGENESIS RELATED PROTEIN 1a* (*PR1a*), *PR1b*, *PR1c*, *PR-Q*, *PR-R* major form, *PR-R* minor form, *ETHYLENE RESPONSE FACTOR 1* (*ERF1*), *ENHANCED DISEASE SUSCEPTIBILITY 1* (*EDS1,* SA-related signal transducers), and *RPM1-INTERACTING PROTEIN 4* (*RIN4*). Besides, Ca^{2+} channels *CYCLIC NUCLEOTIDE-GATED ION CHANNEL* (*CNGC*) and other two types of Ca^{2+}-sensor genes *CML* and *CDPK* were also enriched in the MAPK signaling pathway-plant. Interestingly, these genes are highly up-regulated only under the combination of *NtCBL5A* overexpression and salt stress. The down-regulated DEGs were enriched in 4 KEGG pathways (padj<0.05) (Figure 8H). In “photosynthesis” (KEGG ID: sly00195) and “photosynthesis-antenna proteins” (KEGG ID: sly00196) pathways, many genes related to photosystem I (e.g., *PsaD*, *PsaH*, and *PsaE*), photosystem Ⅱ (e.g., *PsbD*, *PsbQ*, and *PsbW*), photosynthetic electron transport (*PetE*, *PetF*, and *PetH*), and light-harvesting chlorophyll protein complex (e.g. *Lhca1-5*, *Lhcb1*, and *Lhcb3-6*) were significantly down-regulated.

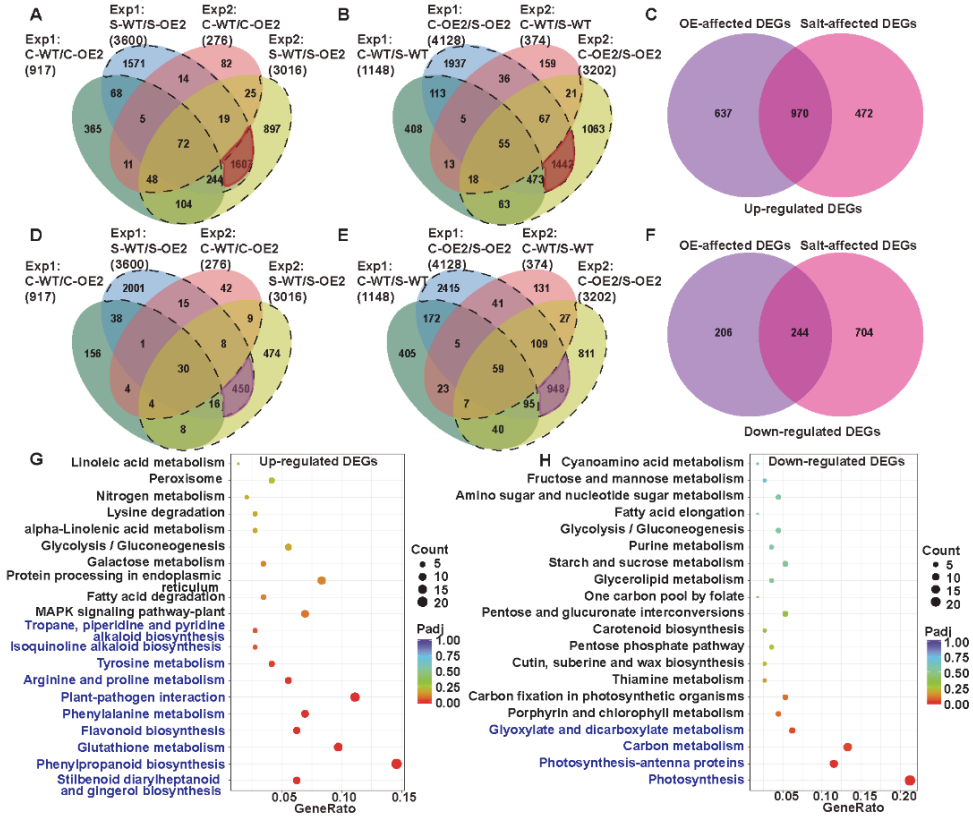

Figure 8 | The analysis of leaf transcriptome data of wild-type (WT) and the *NtCBL5A*-overexpressing line (OE-2) at 4 DAT. (A) Venn diagram with four up-regulated gene sets: Experiment 1 (Exp1)-C-WT/C-OE2, Exp 1-S-WT/S-OE2, Exp 2-C-WT/C-OE2, and Exp 2-S-WT/S-OE2. **(B)** Venn diagram with four up-regulated gene sets: Exp1-C-WT/S-WT, Exp 1-C-OE2/S-OE2, Exp 2-C-WT/S-WT, and Exp 2-C-OE2/S-OE2. **(C)** Venn diagram with two sets: OE-affected up-regulated DEGs and Salt-affected up-regulated DEGs. **(D)** Venn diagram with four down-regulated gene sets: Exp 1-C-WT/C-OE2, Exp 1-S-WT/S-OE2, Exp 2-C-WT/C-OE2, and Exp 2-S-WT/S-OE2. **(E)** Venn diagram with four down-regulated gene sets: Exp 1-C-WT/S-WT, Exp 1-C-OE2/S-OE2, Exp 2-C-WT/S-WT, and Exp 2-C-OE2/S-OE2. **(F)** Venn diagram with two sets: OE-affected down-regulated DEGs and Salt-affected down-regulated DEGs. **(G and H)** KEGG enrichment of up-regulated genes and down-regulated genes. The pathways labeled in blue were significantly enriched pathways. Count: the number of DEGs, bigger circle means more DEGs number; GeneRatio: the number of DEGs / the total number of genes in this pathway;

padj: P-value, padj<0.05 means significant difference, redder color means greater significance. The raw data of RNA-seq can be found in GEO data repository with the accession number GSE181164, in which samples were named as C-WT-1, S-WT-1, C-OE2-1, S-OE2-1, C-WT-2, S-WT-2, C-OE2-2, S-OE2-2. "C" refers to "Control", "S" refers to "Salt", "WT" refers to "wild-type", "OE2" refers to the OE2 line of *NtCBL5A*-overexpressing lines, "1" refers to "Experiment 1", and "2" refers to "Experiment 2".

Plant defense- and cation homeostasis-related genes are regulated in *NtCBL5A*-OE leaves under salt stress

Under salt stress, *NtCBL5A*-OE leaves exhibited necrotic lesions that bear resemblance to hypersensitive reaction (HR)-like cell death in plant response to pathogen infection. To understand the causes of the necrotic lesions, we specifically examined the expression of the HR marker genes *N-RICH PROTEIN* (*NRP*) (Ludwig and Tenhaken, 2001) and *HYPERSENSITIVE-RELATED 203J* (*hypersensitive-related 203J*) (Pontler et al., 1994), as well as the plant defense-related genes in the "Plant-pathogen interaction" pathway and "MAPK signaling pathway-plant" pathway (Figure 8G). *NPR* and *HSR203J* genes were strongly up-regulated in *NtCBL5A*-OE leaves under salt stress (Figure 9A, B). In addition, the expression levels of plant defense-related genes like *PR* genes (*PR1a*, *PR1b*, *PR1c*, *PR-Q*, and *PR-R*) (Sinha et al., 2014), *EDS1* (Lapin et al., 2020), *RIN4* (Ray et al., 2019), *ERF1* (Lorenzo et al., 2003), and *CATALASE 1* (*CAT1*) (Tran and Jung, 2020) were much higher in *NtCBL5A*-OE leaves than those in WT leaves under salt stress (Figure 9C-H; Figure S6A-D). Taken together, these data suggested that salinity stress activates an immunity-related response specifically in the *NtCBL5A*-OE lines.

Under saline conditions, Na^+ accumulation in *NtCBL5A*-OE leaves was slightly higher than that in WT leaves (Figure 7A). Therefore, we hypothesized that *NtCBL5A* overexpression may affect the expression of several cation homeostasis-related genes involved in salt stress response. Based on the transcriptome analysis, several genes required for K^+, Na^+, and Ca^{2+} homeostasis were significantly up- or down-regulated by combined condition of *NtCBL5A* overexpression and salt stress. The

expression profile of these genes was validated by RT-qPCR. *Cation/H*$^{+}$ *EXCHANGER 18* (*CHX18*) and *Na*$^{+}$*/Ca*$^{2+}$ *EXCHANGER 1* (*NCX1*) gene were strongly up-regulated (Figure 9 I, J), while *vacuolar CATION/PROTON 3* (*CAX3*) gene involved in ion vacuolar compartmentalization (Martinoia et al., 2007; Zhao et al., 2007) was down-regulated in WT and even more strongly inhibited in *NtCBL5A*-OE lines under saline conditions (Figure 9K). In addition, the expression of Ca^{2+} channels *CNGC1* was up-regulated in *NtCBL5A*-OE leaves under saline conditions (Figure 9L). The results of RT-qPCR were consistent with the transcriptome data and indicated that *NtCBL5A* overexpression greatly affects the expression of cation homeostasis-related genes under salt stress.

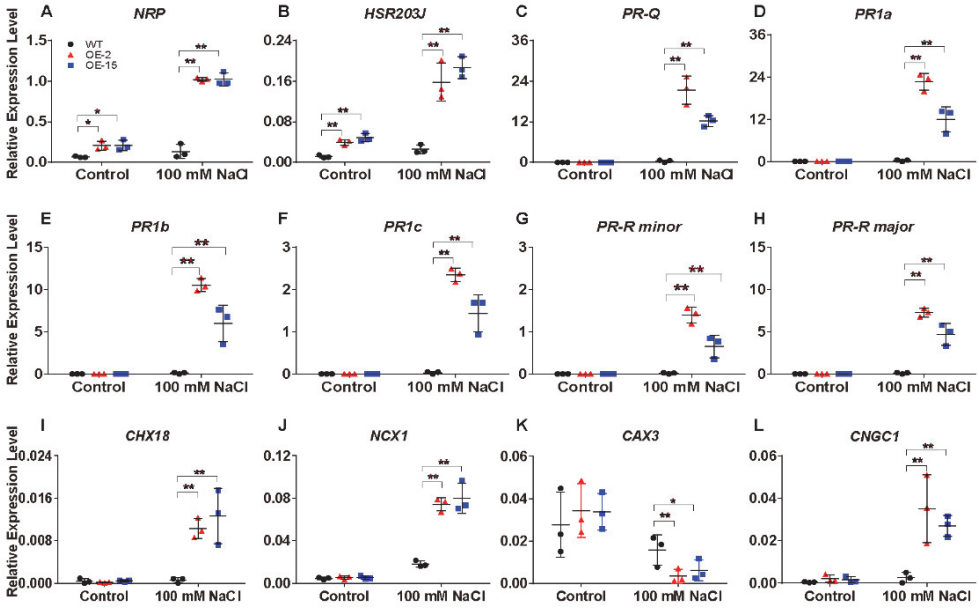

Figure 9 | Relative expression analysis of plant defense-related marker genes, Na^{+} homeostasis- and Ca^{2+} homeostasis-related genes determined by RT-qPCR in tobacco leaves. (A-L) The expression of these genes are relative to the reference gene *L25* under control conditions and salt stress (100 mM NaCl) at 4 days after the start of treatment. Their gene IDs in the reference tobacco genome database (ftp://ftp.solgenomics.net/genomes/Nicotiana_tabacum/edwards_et_al_2017/assembly/Nitab-

v4.5_genome_Chr_Edwards2017.fasta.gz) are *NRP* (Nitab4.5_0000798g0120), *HSR203J* (Nitab4.5_0002719g0120), *PR-Q* (Nitab4.5_0003207g0080), *PR1a* (Nitab4.5_0003771g0010), *PR1b* (Nitab4.5_0005400g0020), *PR1c* (Nitab4.5_0004861g0040), *PR-R* minor (Nitab4.5_0004097g0050), *PR-R* major (Nitab4.5_0000360g0100), *CHX18* (Nitab4.5_0006998g0030), *NCX1* (Nitab4.5_0005404g0030), *CAX3* (Nitab4.5_0000102g0080), *CNGC1* (Nitab4.5_0000258g0120). Error bars indicate ±SD (n=3). One-way ANOVA with LSD test (*P<0.05, **P<0.01) was used to analyze statistical significance.

Photosynthetic machinery-related genes are strongly inhibited in *NtCBL5A*-OE leaves under salt stress

Under salt stress, *NtCBL5A*-OE leaves exhibited chlorotic spots developing into necrotic lesions from 4 DAT (Figure 4A). To gain further insight into the causes of the chlorotic spots, we examined the expression levels of the photosynthesis essential genes in the “Photosynthesis” pathway and “Photosynthesis-antenna proteins” pathway (Figure 8H). *PsaH*, *PsaE*, and *PsaD* in photosystem Ⅰ; *PsbQ*, *PsbX*, and *OXYGEN EVOLVING ENHANCER PROTEIN 1* (*OEE1*) in photosystem Ⅱ; *LIGHT-HARVESTING CHLOROPHYLL PROTEIN COMPLEX* (*Lhca3*, *Lhcb3*, and *Lhcb4*); *FERREDOXIN* (*Fd*) in photosynthetic electron transport; *F-ATPase delta subunit*; and *GLYCERALDEHYDE-3-PHOSPHATE DEHYDROGENASE A* (*GAPA*) in Calvin cycle were examined, RT-qPCR results showed that their expression in both WT and *NtCBL5A*-OE leaves were significantly inhibited by salinity at 4 DAT (Figure 10). More importantly, their expression levels in *NtCBL5A*-OE leaves were significantly lower than that in WT leaves under salt stress (Figure 10). These data suggested that the photosynthetic machinery might be more severely affected in *NtCBL5A*-OE leaves than in WT leaves under salt stress at 4 DAT.

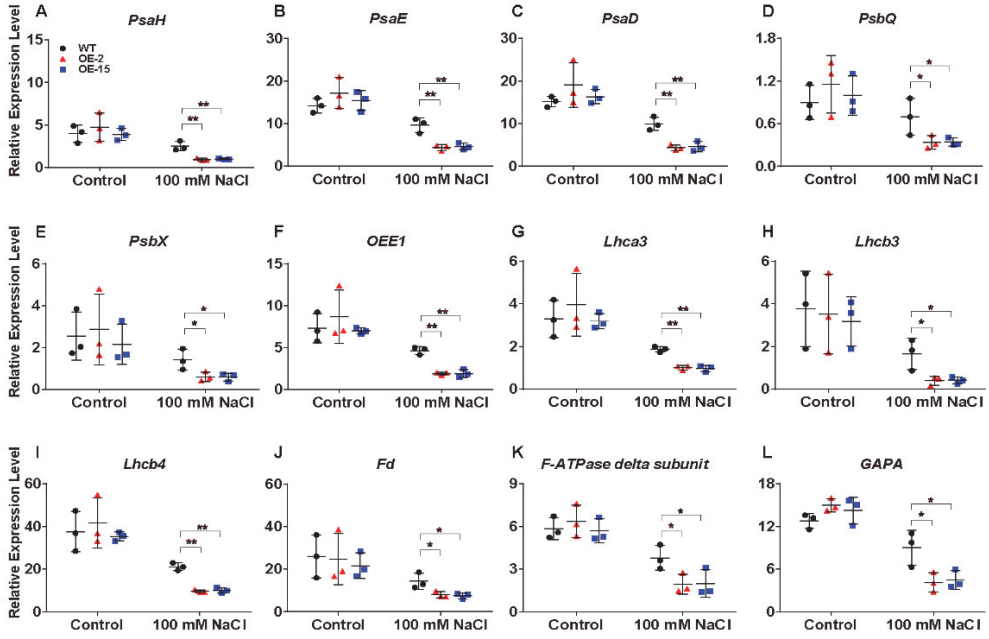

Figure 10 | Relative expression analysis of photosynthesis-related genes determined by RT-qPCR in tobacco leaves. (A-L) The expression of these genes are relative to the reference gene *L25* under control conditions and salt stress (100 mM NaCl) at 4 days after the start of treatment (DAT). Their gene IDs in the reference tobacco genome database (ftp://ftp.solgenomics.net/genomes/Nicotiana_tabacum/edwards_et_al_2017/assembly/Nitab-v4.5_genome_Chr_Edwards2017.fasta.gz) are *PsaH* (Nitab4.5_0000351g0060), *PsaE* (Nitab4.5_0000385g0230), *PsaD* (Nitab4.5_0014875g0010), *PsbQ* (Nitab4.5_0002345g0070), *PsbX* (Nitab4.5_0000073g0060), *OEE1* (Nitab4.5_0000108g0110), *Lhca3* (Nitab4.5_0000923g0200), *Lhcb3* (Nitab4.5_0012832g0010), *Lhcb4* (Nitab4.5_0011597g0020), *Fd* (Nitab4.5_0004129g0010), *F-ATPase delta subunit* (Nitab4.5_0006745g0030), *GAPA* (Nitab4.5_0010299g0040). Error bars indicate ±SD (n=3). One-way ANOVA with LSD test (*P<0.05, **P<0.01) was used to analyze statistical significance.

DISCUSSION

The mechanisms of salt stress response have been the subject of many research studies. A lot of candidate genes involved in salt stress response have been identified, including genes responsible for sensing and signaling in roots,

photosynthesis, Na^+ accumulation in shoots and vacuoles, and accumulation of organic solutes (Munns et al., 2008). However, actual improvements to salt tolerance in crops have been limited, partially because salt tolerance is a polygenic trait controlled by quantitative loci (Ismail and Horie, 2017). Therefore, more pathway components in the salt stress response need to be explored. The strategy of generating a phenotype by targeted overexpression can be used as a powerful tool to identify the potential response pathway components (Prelich, 2012). In this study, constitutive overexpression of *NtCBL5A* greatly interferes with the normal salt stress response of tobacco and induces Na^+-dependent salt supersensitivity with necrotic lesions on leaves. Analysis of this phenotype generated by *NtCBL5A* overexpression may provide insight into genes and relatively poorly explored pathways that are involved in the salt stress response of plants.

CBL-CIPK complexes act as important nodes in the plant signaling cascade, linking environmental stimuli with multiple biochemical and physiological responses. $[Ca^{2+}]_{cyt}$ triggered by salinity stress can be sensed by CBLs (Perochon et al., 2011). One CBL can interact with different CIPKs and each CIPK may phosphorylate diverse targets (Ma et al., 2020). Therefore, constitutive overexpression of a *CBL* gene may generate a cascade effect, overreacting to the $[Ca^{2+}]_{cyt}$ transients triggered by salinity stress and leading to unexpected phenotypes. To elucidate the mechanisms underlying the necrotic phenotype, the *NtCBL5A*-OE lines were evaluated at the physiological, biochemical, and molecular levels. We found that the necrotic phenotype was uniquely induced by high levels of Na^+ rather than Cl^- and osmotic stress in the nutrient solution. Many genes related to cation homeostasis, plant immunity, and the photosynthetic machinery were affected at the transcriptional level in *NtCBL5A*-OE leaves under salt stress. The constitutive overexpression of *NtCBL5A* may make more potential pathway components in salt stress response detectable.

Constitutive overexpression of *NtCBL5A* may interfere with the network responsible for tobacco tolerance

Under saline conditions, plants suffer from Na^+ toxicity due to Na^+ accumulation in the leaves (Munns et al., 2008). Generally, Na^+ can accumulate to toxic concentrations earlier in old leaves than in younger growing leaves because the old leaves no longer expand and so no longer dilute the salt (Munns et al., 2008). In addition, basal zones of leaf blades accumulate more ions than tip zones because the dehydration process starts at the leaf tip (de Lacerda et al., 2003). Inconsistent with the normal pattern of Na^+ accumulation in plants, however, the 5th leaf of *NtCBL5A*-OE tobacco developed the earliest and most severe necrotic lesions in this study (Figure 3C) and the occurrence of necrotic lesions started from leaf tip and leaf margin (Figure 4A). Ion content determination provides us with more information about the necrotic lesions. Although the severe necrotic lesions occurring on *NtCBL5A*-OE leaves were Na^+-dependent, their total Na^+ accumulation was only slightly higher than that of WT leaves. The difference in Na^+ concentrations is statistically significant but not large. Specifically, during 4~9 DAT, the Na^+ contents in the 5th leaves of WT, OE-2, and OE-15 are in the range of 39.18~51.64 μg/mg, 44.95~69.71 μg/mg, and 47.36~64.31 μg/mg, respectively (Figure 7A). The 5th leaves of WT plants remained green with Na^+ accumulating up to 51.64 μg/mg, while *NtCBL5A*-OE lines exhibited obvious chlorotic spots or necrotic lesions with a similar level of Na^+ accumulation in their leaves (Figure 4A; Figure 7A). Taken the phenotypic analysis and Na^+ determination together, it is possible that the distribution of Na^+ over different tissues and cell organelles was affected by *NtCBL5A* overexpression. We did find the expression of several cation homeostasis-related genes such as C*HX18*, *NCX1*, and vacuolar *CAX3* were regulated in salt-stressed *NtCBL5A*-OE leaves (Figure 9). To sum up, the compromised Na^+-handling ability and Na^+ homeostasis may contribute more to the formation of necrotic lesions on *NtCBL5A*-OE leaves.

Overexpression phenotypes often result from competition-based mechanisms

(Prelich, 2012). The necrotic phenotype may result from the interference of ectopically expressed *NtCBL5A* with other components of the CBL-CIPK network that are important in the salt stress response of tobacco. CBL members with close phylogenetic relationships were shown to be able to interact with the same CIPK. Both AtCBL1 and AtCBL9 interact with AtCIPK23 to regulate K^+ uptake under low-potassium conditions by activating K^+ transporters (Li et al., 2006; Aleman et al., 2011; Ragel et al., 2015). In addition, AtCBL2 and AtCBL3 both interact with AtCIPK12 as crucial regulators of vacuole dynamics (Steinhorst et al., 2015), and work with AtCIPK3/9/23/26 at the tonoplast to sequester Mg^{2+} into vacuole to avoid high Mg^{2+} toxicity (Tang et al., 2015). Some CBL family members are supposedly able to compete for the same CIPK member, but they are "spatially isolated" because of different subcellular localization or tissue-specific expression. For example, both AtCBL4 and AtCBL10 interact with AtCIPK24 to regulate Na^+ homeostasis under salt stress, but the AtCBL4-AtCIPK24 complex mainly works in roots for Na^+ exclusion, the AtCBL10-AtCIPK24 complex mainly works in shoots for Na^+ efflux or compartmentalization (Kim et al., 2007; Lin et al., 2009). This cooperation or competition of CBL family members suggests that ectopically expressed *NtCBL5A* might compete with other NtCBLs for the same NtCIPK and interfere with their functions, for instance with the NtCBL-NtCIPK complex that is regulating Na^+ vacuolar compartmentalization and thus affect Na^+ sequestration into the vacuole. As a result, Na^+ might be less efficiently compartmentalized in vacuole, increasing the toxicity of Na^+ in the cytoplasm. This would be in agreement with our hypothesis that the Na^+ sensitivity of the *NtCBL5A*-OE lines under saline conditions might be partly caused by compromised distribution of Na^+ within the leaves. This hypothesis can be verified by co-overexpression of *NtCBL5A* and its competing *NtCBL*, which may reverse the necrotic phenotype of *NtCBL5A*-OE leaves (Prelich, 2012).

The Na^+ sensitivity of *NtCBL5A*-OE leaves may be related to defective photosystems and ROS

Both transcriptome analyses and RT-qPCR results indicated that the expression of

photosynthesis-related genes in *NtCBL5A*-OE leaves were significantly inhibited by salinity at 4 DAT (Figures 8H and 10), which is consistent with the dotted chlorosis phenotype at this time point (Figure 4A). To understand whether photosynthesis dysfunction is related to the salt-induced necrotic phenotype of *NtCBL5A*-OE leaves, we examined the expression levels of photosynthesis-related genes at very early stages of salt treatment (1 DAT and 2 DAT) when there were no chlorotic spots or necrotic lesions in *NtCBL5A*-OE leaves. RT-qPCR results showed that their expression levels in *NtCBL5A*-OE leaves were lower than those in WT already at 1 DAT (Figure S6E-P), which suggests that the photosynthetic machinery of *NtCBL5A*-OE leaves may be affected shortly after the start of salt treatment.

It has been reported that some leaf lesion-mimic phenotypes are connected to defective photosystems (Zulfugarov et al., 2014; Bruggeman et al., 2015; Wang et al., 2015; Tang et al., 2020). Light energy input exceeds energy utilization when CO_2 assimilation and $NADP^+$ regeneration in the Calvin cycle are inhibited by salinity-induced stomatal limitation, leading to overreduction of the electron transport chain and the generation of ROS (Attia et al., 2009; Hajiboland, 2014). If the capacity of the ROS scavenging system is not sufficient, excessive ROS will accumulate and lead to damage. The ROS accumulation in *NtCBL5A*-OE leaves was higher than that in WT under salt stress already at 2 DAT and 6 DAT (Figure S2; Figure 4D). Possibly, the light energy input in *NtCBL5A*-OE leaves exceeds energy utilization when the Calvin cycle is more inhibited than light reaction in the photosynthesis of *NtCBL5A*-OE leaves under salt stress, and the resulting ROS generation in *NtCBL5A*-OE leaves might beyond the ROS scavenging ability and lead to the necrotic lesions.

The question then remains that how overexpression of *NtCBL5A* in combination with high Na^+ in the root environment triggers excess ROS production and affects the photosynthetic machinery. It is remarkable that the expression of photosynthetic machinery-related genes already changed at 1 DAT, ROS appeared to be already elevated at 2 DAT, and chlorotic symptoms developed quickly after the start of salt treatment. This might indicate that the salt supersensitivity is initiated already during

the early salinity response of the plant. Although it is generally accepted that the first response to salt stress in plants is triggered by the osmotic stress component of salinity, recent studies indicated that plants also specifically sense the presence of high Na^+ in the soil at the early stages of salt stress (Lamers et al., 2020; Van Zelm et al., 2020). This triggers Ca^{2+} waves in the roots that even reach the leaves (Choi et al., 2014). Additionally, ROS are rapidly activated (Miller et al., 2010). Members of the CBL-CIPK signaling network may play a role in the translation of the second messenger Ca^{2+} (Manishankar et al., 2018), and the AtCBL1/9-AtCIPK26 complex was shown to be able to interact with AtRbohF which is a member of the ROS burst-regulating Rboh gene family (Drerup et al., 2013). It is therefore conceivable that ectopic and constitutive overexpression of *NtCBL5A* may interfere with the Ca^{2+} and ROS-mediated response of plants following early sensing of high Na^+ levels in the root environment. Further exploration of the reason for necrotic lesions on *NtCBL5A*-OE leaves might help to gain insight into this early Na^+ response of plants as part of the response to salinity, and the crosstalk between the salt stress response and photosynthesis.

The Na^+ sensitivity of *NtCBL5A*-OE leaves may be related to plant immune response

Transcriptome analysis provided additional information on cause of the fast-developing necrotic symptoms of NtCBL5A-OE tobacco. The expression of cell death- and immune response-related genes were induced in NtCBL5A-OE leaves under salt stress. These included NRP and HSR203J, which are immunity-related cell death HR marker genes that are activated as part of the plant disease defense and execution of the cell death programme (Ludwig and Tenhaken, 2001). In addition, many plant defense-related genes like PR genes, ERF1, EDS1, and RIN4 were also specifically strongly up-regulated in NtCBL5A-OE lines under saline conditions (Figure 9A-H; Figure S6A-D), suggesting that PAMP- and effector-triggered responses are induced in NtCBL5A-OE leaves under salt stress. The CBL-CIPK network has been widely reported to be involved in HR-related plant immunity to

pathogens, such as SlCBL10-SlCIPK6 (Gutiérrez-Beltrán et al., 2017), AtCIPK6 (Sardar et al., 2017), OsCIPK15 (Kurusu et al., 2010), CaCIPK1 (Ma et al., 2019), TaCBL4-TaCIPK5 (Liu et al., 2018), TaCIPK10 (Liu et al., 2019), and MeCBL1/9-MeCIPK23 (Yan et al., 2018). Moreover, Cassava MeCBL1/9-MeCIPK23 positively regulates plant's defense against Xanthomonas axonopodis pv. manihotis via affecting the expression of defense-related genes including PR1, PR2, PR5, and NPR1 (nonexpresser of PR genes 1) (Yan et al., 2018). Crosstalk between the response to abiotic and biotic stress and the role of plant immune-related genes in this crosstalk has been shown by others (Nejat and Mantri, 2017; Saijo and Loo, 2020), and it is possible that some plant immune-related DEGs in NtCBL5A-OE leaves under salt stress might be involved in the combined salt stress and biotic stress response.

CONFLICT OF INTEREST STATEMENT

The authors declare that the research was conducted in the absence of any commercial or financial relationships that could be construed as a potential conflict of interest.

AUTHOR CONTRIBUTIONS

J.M. conceived the original research plans, performed the experiments, and analyzed the data; H.L., Q.W., and C.G.V.L. co-supervised the experiments; A.L. generated *ProNtCBL5A::GUS* transgenic tobacco lines; J.Y. and Z.M. provided technical assistance to J.M.; S.S. generated *NtCBL5A*-OE lines in T0 generation; J.M. conceived the project and wrote the article with contributions of all the authors; Y.S. and G.L. helped with manuscript revision; R.G.F.V., Y.B., H.L., Q.W., and C.G.V.L. supervised and completed the writing. H.L. and Q.W. agrees to serve as the authors responsible for contact and ensures communication. All authors contributed to the article and approved the submitted version.

FUNDING

This work was supported by the Fundamental Research Funds for China Agricultural

Academy of Sciences (1610232021002), the Agricultural Science and Technology Innovation Program (ASTIP-TRIC02, ASTIP-TRIC03), China Scholarships Council (CSC No. 201803250083), International Foundation of Tobacco Research Institute of CAAS (IFT202102), and International Exchange Scholarship of the GSCAAS.

ACKNOWLEDGMENTS

We would like to acknowledge the support of the PhD Education Programs between The GSCAAS and WUR. We would like to thank Dr. Pádraic Flood from Plant Breeding, WUR for critically reading the manuscript; Geurt Versteeg and Sean Geurts from Unifarm of WUR for helps on plant caring; Prof. Yi Shi, Prof. Yongfeng Guo, Prof. Aiguo Yang, Dr. Yiting Li, and Mengmeng Cui from Tobacco Research Institute of CAAS for technical support; Sri Sunarti from Plant Breeding of WUR and interns Chong Zhang from Jining Medical University for experimental assistance.

DATA AVAILABILITY STATEMENT

The original contributions presented in the study are publicly available. RNA-seq data can be found here: National Center for Biotechnology Information Gene Expression Omnibus (GEO) data repository under accession number GSE181164.

REFERENCES

Aleman, F., Nieves-Cordones, M., Martinez, V., and Rubio, F. (2011). Root K^+ acquisition in plants: the *Arabidopsis thaliana* model. *Plant Cell Physiol*. 52, 1603-1612.

An, L. L., Mao, J. J., Che, H. Y., Shi, S. J., Dong, L. H., Xu, D. Z., Song, Y. F., Xu, F. Z., Liu, G. S., Wang, Q., and Liu, H. B. (2020). Screening and identification of NsylCBL family members interacting with protein kinase NsylCIPK24a in *Nicotiana Sylvestris*. *Mol. Plant Breed*. 11, 1-10.

Attia, H., Karray, N., and Lachaâl, M. (2009). Light interacts with salt stress in regulating superoxide dismutase gene expression in Arabidopsis. *Plant Sci*. 177, 161-167.

Bartels, D., and Sunkar, R. (2005). Drought and salt tolerance in plants. *CRC Crit. Rev. Plant Sci*. 24, 23-58.

Bruggeman, Q., Raynaud, C., Benhamed, M., and Delarue, M. (2015). To die or not to die? Lessons from lesion mimic mutants. *Front. Plant Sci*. 6, 24.

Chakraborty, K., Sairam, R. K., and Bhattacharya, R. C. (2012). Differential expression of salt overly sensitive pathway genes determines salinity stress tolerance in *Brassica* genotypes. *Plant Physiol. Biochem*. 51, 90-101.

Chen, L., Ren, F., Zhou, L., Wang, Q. Q., Zhong, H., and Li, X. B. (2012). The *Brassica napus* Calcineurin B-like 1/CBL-interacting protein kinase 6 (CBL1/CIPK6) component is involved in the plant response to abiotic stress and ABA signalling. *J. Exp. Bot*. 63, 6211-6222.

Cheong, Y. H. (2003). CBL1, a calcium sensor that differentially regulates salt, drought, and cold responses in *Arabidopsis*. *Plant Cell*. 15, 1833-1845.

Cheong, Y. H., Sung, S. J., Kim, B. G., Pandey, G. K., Cho, J. S., Kim, K. N., and Luan, S. (2010). Constitutive overexpression of the calcium sensor CBL5 confers osmotic or drought stress tolerance in Arabidopsis. *Mol. Cell*. 29, 159-165.

Cho, J. H., Choi, M. N., Yoon, K. H., and Kim, K. N. (2018). Ectopic expression of *SjCBL1*, calcineurin B-like 1 gene from *Sedirea japonica*, rescues the salt and osmotic stress hypersensitivity in Arabidopsis *cbl1* mutant. *Front. Plant Sci*. 9, 1188.

Choi, W. G., Toyota, M., Kim, S. H., Hilleary, R., and Gilroy, S. (2014). Salt stress-induced Ca^{2+} waves are associated with rapid, long-distance root-to-shoot signaling in plants. *Proc. Nati. Acad. Sci. U.S.A*. 111, 6497-6502.

de Lacerda, C. F., Cambraia, J., Oliva, M. A., Ruiz, H. A., and Prisco, J. T. n. (2003). Solute accumulation and distribution during shoot and leaf development in two sorghum genotypes under salt stress. *Environ. Exp. Bot*. 49, 107-120.

Dong, L. H., Wang, Q., Manik, S. M. N., Song, Y. F., Shi, S. J., Su, Y. L., Liu, G. S., and Liu, H. B. (2015). *Nicotiana sylvestris* calcineurin B-like protein NsylCBL10 enhances salt tolerance in transgenic *Arabidopsis*. *Plant Cell Rep*. 34, 2053-2063.

Drerup, M. M., Schlucking, K., Hashimoto, K., Manishankar, P., Steinhorst, L., Kuchitsu, K., and Kudla, J. (2013). The calcineurin B-like calcium sensors CBL1 and CBL9 together with their interacting protein kinase CIPK26 regulate the *Arabidopsis* NADPH oxidase RBOHF. *Mol. Plant*. 6, 559-569.

Egea, I., Pineda, B., Ortiz-Atienza, A., Plasencia, F. A., Drevensek, S., Garcia-Sogo, B., Yuste-Lisbona, F. J., Barrero-Gil, J., Atares, A., Flores, F. B., Barneche, F., Angosto, T., Capel, C., Salinas, J., Vriezen, W., Esch, E., Bowler, C., Bolarin, M. C., Moreno, V., and Lozano, R. (2018). The SlCBL10 calcineurin B-like protein ensures plant growth under salt stress by regulating Na^+ and Ca^{2+} homeostasis. *Plant Physiol*. 176, 1676-1693.

Gong, Z. Z., Xiong, L. M., Shi, H. Z., Yang, S. H., Herrera-Estrella, L. R., Xu, G. H., Chao, D. Y., Li, J. R., Wang, P. Y., Qin, F., Li, J. G., Ding, Y. L., Shi, Y. T., Wang, Y., Yang, Y. Q., Guo, Y., and Zhu, J. K. (2020). Plant abiotic stress response and nutrient use efficiency. *Sci. China Life Sci*. 63, 635-674.

Gutiérrez-Beltrán, E., Personat, J. M., de la Torre, F., and Del Pozo, O. (2017). A universal stress protein involved in oxidative stress is a phosphorylation target for protein kinase CIPK6. *Plant Physiol*. 173, 836-852.

Hajiboland, R. 2014. Reactive oxygen species and photosynthesis. In: Ahmad P. Oxidative damage to plants. the United States of America: Elsevier, 1-63.

Horsch, R. B., Fry, J. E., Hoffmann, N. L., Eichholtz, D., Rogers, S. G., and Fraley, R. T. (1985). A simple and general method for transferring genes into plants. *Science*. 227, 1229-1231.

Hu, D. G., Li, M., Luo, H., Dong, Q. L., Yao, Y. X., You, C. X., and Hao, Y. J. (2012). Molecular cloning and functional characterization of *MdSOS2* reveals its involvement in salt tolerance in apple callus and *Arabidopsis*. *Plant Cell Rep*. 31, 713-722.

Ismail, A. M., and Horie, T. (2017). Genomics, physiology, and molecular breeding approaches for improving salt tolerance. *Annu. Rev. Plant Biol*. 68, 405-434.

Kanehisa, M., Furumichi, M., Sato, Y., Ishiguro-Watanabe, M., and Tanabe, M. (2020). KEGG: integrating viruses and cellular organisms. *Nucleic Acids Res*. 49, D545-D551.

Kim, B.-G., Waadt, R., Cheong, Y. H., Pandey, G. K., Dominguez-Solis, J. R., Schültke, S., Lee, S. C., Kudla, J., and Luan, S. (2007). The calcium sensor CBL10 mediates salt tolerance by regulating ion homeostasis in *Arabidopsis*. *Plant J*. 52, 473-484.

Kissoudis, C. 2016. Genetics and regulation of combined abiotic and biotic stress tolerance in tomato. PhD thesis, Wageningen University.

Knight, H., and Knight, M. R. (2001). Abiotic stress signalling pathways: specificity and cross-talk. *Trends Plant Sci*. 6, 262-267.

Kurusu, T., Hamada, J., Nokajima, H., Kitagawa, Y., Kiyoduka, M., Takahashi, A., Hanamata, S., Ohno, R., Hayashi, T., Okada, K., Koga, J., Hirochika, H., Yamane, H., and Kuchitsu, K. (2010). Regulation of microbe-associated molecular pattern-induced hypersensitive cell death, phytoalexin production, and defense gene expression by calcineurin B-like protein-interacting protein kinases, OsCIPK14/15, in rice cultured cells. *Plant Physiol*. 153, 678-692.

Lamers, J., van der Meer, T., and Testerink, C. (2020). How plants sense and respond to stressful environments. *Plant Physiol*. 182, 1624-1635.

Lapin, D., Bhandari, D. D., and Parker, J. E. (2020). Origins and immunity networking functions of EDS1 family proteins. *Annu. Rev. Phytopathol*. 58, 253-276.

Letunic, I., and Bork, P. (2018). 20 years of the SMART protein domain annotation resource. *Nucleic Acids Res*. 46, D493-D496.

Li, D. D., Xia, X. L., Yin, W. L., and Zhang, H. C. (2012). Two poplar calcineurin B-like proteins confer enhanced tolerance to abiotic stresses in transgenic *Arabidopsis thaliana*. *Bio. Plant*. 57, 70-78.

Li, L., Kim, B.-G., Cheong, Y. H., Pandey, G. K., and Luan, S. (2006). A Ca^{2+} signaling pathway regulates a K^+ channel for low-K response in *Arabidopsis*. *Proc. Nati. Acad. Sci. U.S.A*. 103, 12625-12630.

Li, Z. Y., Xu, Z. S., He, G. Y., Yang, G. X., Chen, M., Li, L. C., and Ma, Y. Z. (2012). Overexpression of soybean *GmCBL1* enhances abiotic stress tolerance and promotes hypocotyl elongation in *Arabidopsis*. *Biochem. Biophys. Res. Commun*. 427, 731-736.

Lin, H. X., Yang, Y. Q., Quan, R. D., Mendoza, I., Wu, Y. S., Du, W. M., Zhao, S. S., Schumaker, K. S., Pardo, J. M., and Guo, Y. (2009). Phosphorylation of SOS3-LIKE CALCIUM BINDING PROTEIN8 by

SOS2 protein kinase stabilizes their protein complex and regulates salt tolerance in Arabidopsis. *Plant Cell*. 21, 1607-1619.

Ling, Q. H., Huang, W. H., and Jarvis, P. (2011). Use of a SPAD-502 meter to measure leaf chlorophyll concentration in *Arabidopsis thaliana*. *Photosyn Res*. 107, 209-214.

Liu, P., Duan, Y. H., Liu, C., Xue, Q. H., Guo, J., Qi, T., Kang, Z. S., and Guo, J. (2018). The calcium sensor TaCBL4 and its interacting protein TaCIPK5 are required for wheat resistance to stripe rust fungus. *J. Exp. Bot*. 69, 4443-4457.

Liu, P., Guo, J., Zhang, R. M., Zhao, J. X., Liu, C., Qi, T., Duan, Y. H., Kang, Z. S., and Guo, J. (2019). TaCIPK10 interacts with and phosphorylates TaNH2 to activate wheat defense responses to stripe rust. *Plant Biotechnol. J.* 17, 956-968.

Livak, K. J., and Schmittgen, T. D. (2001). Analysis of relative gene expression data using real-time quantitative PCR and the $2^{-\Delta\Delta CT}$ method. *Methods*. 25, 402-408.

Lorenzo, O., Piqueras, R., Sanchez-Serrano, J. J., and Solano, R. (2003). ETHYLENE RESPONSE FACTOR1 integrates signals from ethylene and jasmonate pathways in plant defense. *Plant Cell*. 15, 165-178.

Luan, S. (2009). The CBL-CIPK network in plant calcium signaling. *Trends Plant Sci*. 14, 37-42.

Ludwig, A. A., and Tenhaken, R. (2001). A new cell wall located N-rich protein is strongly induced during the hypersensitive response in *Glycine max* L. *Eur. J. Plant Pathol*. 107, 323-336.

Lv, F. L., Zhang, H. C., Xia, X. L., and Yin, W. L. (2014). Expression profiling and functional characterization of a CBL-interacting protein kinase gene from *Populus euphratica*. *Plant Cell Rep*. 33, 807-818.

Ma, X., Gai, W. X., Qiao, Y. M., Ali, M., Wei, A. M., Luo, D. X., Li, Q. H., and Gong, Z. H. (2019). Identification of CBL and CIPK gene families and functional characterization of CaCIPK1 under Phytophthora capsici in pepper (*Capsicum annuum* L.). *BMC Genom*. 20, 1-18.

Ma, X., Li, Q. H., Yu, Y. N., Qiao, Y. M., Haq, S. U., and Gong, Z. H. (2020). The CBL-CIPK pathway in plant response to stress signals. *Int. J. Mol. Sci*. 21, 5668.

Manishankar, P., Wang, N., Koster, P., Alatar, A. A., and Kudla, J. (2018). Calcium signaling during salt stress and in the regulation of ion homeostasis. *J. Exp. Bot*. 69, 4215–4226.

Martinez-Atienza, J., Jiang, X., Garciadeblas, B., Mendoza, I., Zhu, J. K., Pardo, J. M., and Quintero, F. J. (2007). Conservation of the salt overly sensitive pathway in rice. *Plant Physiol*. 143, 1001-1012.

Martinoia, E., Maeshima, M., and Neuhaus, H. E. (2007). Vacuolar transporters and their essential role in plant metabolism. *J. Exp. Bot*. 58, 83-102.

Miller, G., Suzuki, N., Ciftci-Yilmaz, S., and Mittler, R. (2010). Reactive oxygen species homeostasis and signalling during drought and salinity stresses. *Plant Cell Environ*. 33, 453-467.

Munns, R. (2005). Genes and salt tolerance: bringing them together. *New Phytol*. 167, 645-663.

Munns, R., and Tester, M. (2008). Mechanisms of salinity tolerance. *Annu. Rev. Plant Biol*. 59, 651-681.

Nejat, N., and Mantri, N. (2017). Plant immune system: grosstalk between responses to biotic and abiotic stresses the missing link in understanding plant defence. *Curr. Issues Mol. Biol*. 23, 1-16.

Perochon, A., Aldon, D., Galaud, J. P., and Ranty, B. (2011). Calmodulin and calmodulin-like proteins in plant calcium signaling. *Biochimie*. 93, 2048-2053.

Pertea, M., Pertea, G. M., Antonescu, C. M., Chang, T. C., Mendell, J. T., and Salzberg, S. L. (2015). StringTie enables improved reconstruction of a transcriptome from RNA-seq reads. *Nat. Biotechnol*. 33, 290-295.

Pontler, D., Godiard, L., Marco, Y., and Roby, D. (1994). *hsr203J*, a tobacco gene whose activation is rapid, highly localized and specific for incompatible plant/pathogen interactions. *Plant J*. 5, 507-521.

Prelich, G. (2012). Gene overexpression: uses, mechanisms, and interpretation. *Genetics*. 190, 841-854.

Qiu, Q. S., Guo, Y., Dietrich, M. A., Schumaker, K. S., and Zhu, J. K. (2002). Regulation of SOS1, a plasma membrane Na^+/H^+ exchanger in *Arabidopsis thaliana*, by SOS2 and SOS3. *Proc. Nati. Acad. Sci. U.S.A*. 99, 8436-8441.

Qiu, Q. S., Guo, Y., Quintero, F. J., Pardo, J. M., Schumaker, K. S., and Zhu, J. K. (2004). Regulation of vacuolar Na^+/H^+ exchange in *Arabidopsis thaliana* by the salt-overly-sensitive (SOS) pathway. *J. Biol. Chem*. 279, 207-215.

Quan, R., Lin, H., Mendoza, I., Zhang, Y., Cao, W., Yang, Y., Shang, M., Chen, S., Pardo, J. M., and Guo, Y. (2007). SCABP8/CBL10, a putative calcium sensor, interacts with the protein kinase SOS2 to protect Arabidopsis shoots from salt stress. *Plant Cell*. 19, 1415-1431.

Ragel, P., Ródenas, R., García-Martín, E., Andrés, Z., Villalta, I., Nieves-Cordones, M., Rivero, R. M., Martínez, V., Pardo, J. M., and Quintero, F. J. (2015). CIPK23 regulates HAK5-mediated high-affinity K^+ uptake in *Arabidopsis* roots. *Plant Physiol*. 169, 2863-2873.

Ray, S. K., Macoy, D. M., Kim, W. Y., Lee, S. Y., and Kim, M. G. (2019). Role of RIN4 in regulating PAMP-

triggered immunity and effector-triggered immunity: current status and future perspectives. *Mol. Cells*. 42, 503-511.

Saijo, Y., and Loo, E. P. (2020). Plant immunity in signal integration between biotic and abiotic stress responses. *New Phytol*. 225, 87-104.

Sánchez-Barrena, M. J., Martínez-Ripoll, M., and Albert, A. (2013). Structural biology of a major signaling network that regulates plant abiotic stress: The CBL-CIPK mediated pathway. *Int. J. Mol. Sci*. 14, 5734-5749.

Sardar, A., Nandi, A. K., and Chattopadhyay, D. (2017). CBL-interacting protein kinase 6 negatively regulates immune response to *Pseudomonas syringae* in *Arabidopsis*. *J. Exp. Bot*. 68, 3573-3584.

Satir, O., and Berberoglu, S. (2016). Crop yield prediction under soil salinity using satellite derived vegetation indices. *Field Crops Res*. 192, 134-143.

Schmidt, G. W., and Delaney, S. K. (2010). Stable internal reference genes for normalization of real-time RT-PCR in tobacco (*Nicotiana tabacum*) during development and abiotic stress. *Mol. Genet. Genomics*. 283, 233-241.

Shi, H. Z., Quintero, F. J., Pardo, J. M., and Zhu, J. K. (2002). The putative plasma membrane Na^+/H^+ antiporter SOS1 controls long-distance Na^+ transport in plants. *Plant Cell*. 14, 465-477.

Shi, S.J., An, L.L., Mao, J.J., Aluko, O.O., Ullah, Z., Xu, F.Z., Liu, G.S., Liu, H.B., Wang, Q. (2021). The CBL-interacting protein kinase NtCIPK23 positively regulates seed germination and early seedling development in tobacco (*Nicotiana tabacum* L.). *Plants (Basel)*. 10, 323.

Sinha, M., Singh, R. P., Kushwaha, G. S., Iqbal, N., Singh, A., Kaushik, S., Kaur, P., Sharma, S., and Singh, T. P. (2014). Current overview of allergens of plant pathogenesis related protein families. *Sci World J*. 2014, 543195.

Snedden, W. A., and Fromm, H. (1998). Calmodulin, calmodulin-related proteins and plant responses to the environment. *Trends Plant Sci*. 3, 299-304.

Snedden, W. A., and Fromm, H. (2001). Calmodulin as a versatile calcium signal transducer in plants. *New Phytol*. 151, 35-66.

Steinhorst, L., Mähs, A., Ischebeck, T., Zhang, C., Zhang, X., Arendt, S., Schültke, S., Heilmann, I., and Kudla, J. (2015). Vacuolar CBL-CIPK12 Ca^{2+}-sensor-kinase complexes are required for polarized pollen tube growth. *Curr. Biol*. 25, 1475-1482.

Sun, H., Sun, X., Wang, H., and Ma, X. (2020). Advances in salt tolerance molecular mechanism in tobacco plants. *Hereditas*. 157, 5.

Tang, R.-J., Zhao, F.-G., Garcia, V. J., Kleist, T. J., Yang, L., Zhang, H.-X., and Luan, S. (2015). Tonoplast CBL-CIPK calcium signaling network regulates magnesium homeostasis in *Arabidopsis*. *Proc. Nati. Acad. Sci. U.S.A*. 112, 3134-3139.

Tang, R. J., Liu, H., Bao, Y., Lv, Q. D., Yang, L., and Zhang, H. X. (2010). The woody plant poplar has a functionally conserved salt overly sensitive pathway in response to salinity stress. *Plant Mol. Biol*. 74, 367-380.

Tang, R. J., Yang, Y., Yang, L., Liu, H., Wang, C. T., Yu, M. M., Gao, X. S., and Zhang, H. X. (2014). Poplar calcineurin B-like proteins PtCBL10A and PtCBL10B regulate shoot salt tolerance through interaction with PtSOS2 in the vacuolar membrane. *Plant Cell Environ*. 37, 573-588.

Tang, Y., Gao, C. C., Gao, Y., Yang, Y., Shi, B., Yu, J. L., Lyu, C., Sun, B. F., Wang, H. L., Xu, Y., Yang, Y. G., and Chong, K. (2020). OsNSUN2-mediated 5-methylcytosine mRNA modification enhances rice adaptation to high temperature. *Dev. Cell*. 53, 272-286.

Tran, B. Q., and Jung, S. (2020). Modulation of chloroplast components and defense responses during programmed cell death in tobacco infected with Pseudomonas syringae. *Biochem. Biophys. Res. Commun*. 528, 753-759.

Trewavas, A. J., and Malhó, R. (1998). Ca^{2+} signalling in plant cells: the big network! *Curr. Opin. Plant Biol*. 1, 428-433.

Van Zelm, E., Zhang, Y. X., and Testerink, C. (2020). Salt tolerance mechanisms of plants. *Annu. Rev. Plant Biol*. 71, 403-433.

Wang, C. T., Yin, X. L., Kong, X. X., Li, W. S., Ma, L., Sun, X. D., Guan, Y. L., Todd, C. D., Yang, Y. P., and Hu, X. Y. (2013). A series of TA-based and zero-background vectors for plant functional genomics. *PLoS ONE*. 8, e59576.

Wang, J., Ye, B. Q., Yin, J. J., Yuan, C., Zhou, X. G., Li, W. T., He, M., Wang, J. C., Chen, W. L., Qin, P., Ma, B. T., Wang, Y. P., Li, S. G., and Chen, X. W. (2015). Characterization and fine mapping of a light-dependent *leaf lesion mimic mutant 1* in rice. *Plant Physiol. Biochem*. 97, 44-51.

Waterhouse, A., Bertoni, M., Bienert, S., Studer, G., Tauriello, G., Gumienny, R., Heer, F. T., de Beer, T. A. P., Rempfer, C., Bordoli, L., Lepore, R., and Schwede, T. (2018). SWISS-MODEL: homology

modelling of protein structures and complexes. *Nucleic Acids Res*. 46, W296-W303.

Yan, Y., He, X. Y., Hu, W., Liu, G. Y., Wang, P., He, C. Z., and Shi, H. T. (2018). Functional analysis of MeCIPK23 and MeCBL1/9 in cassava defense response against *Xanthomonas axonopodis* pv. *manihotis*. *Plant Cell Rep*. 37, 887-900.

Yin, X. C., Xia, Y. Q., Xie, Q., Cao, Y. X., Wang, Z. Y., Hao, G. P., Song, J., Zhou, Y., and Jiang, X. Y. (2019). CBL10-CIPK8-SOS1, A novel SOS pathway, functions in Arabidopsis to regulate salt tolerance. *J. Exp. Bot*. 1-14.

Yukawa, M., Tsudzuki, T., and Sugiura, M. (2006). The chloroplast genome of *Nicotiana sylvestris* and *Nicotiana tomentosiformis*: complete sequencing confirms that the *Nicotiana sylvestris* progenitor is the maternal genome donor of *Nicotiana tabacum*. *Mol. Genet. Genomics*. 275, 367-373.

Zaman, M., and Heng, S. A. S. L. 2018. Guideline for salinity assessment, mitigation and adaptation using nuclear and related techniques. Switzerland: Springer Nature Switzerland AG.

Zhang, H. C., Lv, F. L., Han, X., Xia, X. L., and Yin, W. L. (2013). The calcium sensor PeCBL1, interacting with PeCIPK24/25 and PeCIPK26, regulates Na^+/K^+ homeostasis in *Populus euphratica*. *Plant Cell Rep*. 32, 611-621.

Zhao, J., Barkla, B. J., Marshall, J., Pittman, J. K., and Hirschi, K. D. (2007). The *Arabidopsis cax3* mutants display altered salt tolerance, pH sensitivity and reduced plasma membrane H^+-ATPase activity. *Planta*. 227, 659-669.

Zulfugarov, I. S., Tovuu, A., Eu, Y.-J., Dogsom, B., Poudyal, R. S., Nath, K., Hall, M., Banerjee, M., Yoon, U. C., Moon, Y.-H., An, G., Jansson, S., and Lee, C.-H. (2014). Production of superoxide from Photosystem II in a rice (*Oryza sativa* L.) mutant lacking PsbS. *BMC Plant Biol*. 14, 1-15.

Supplementary Material

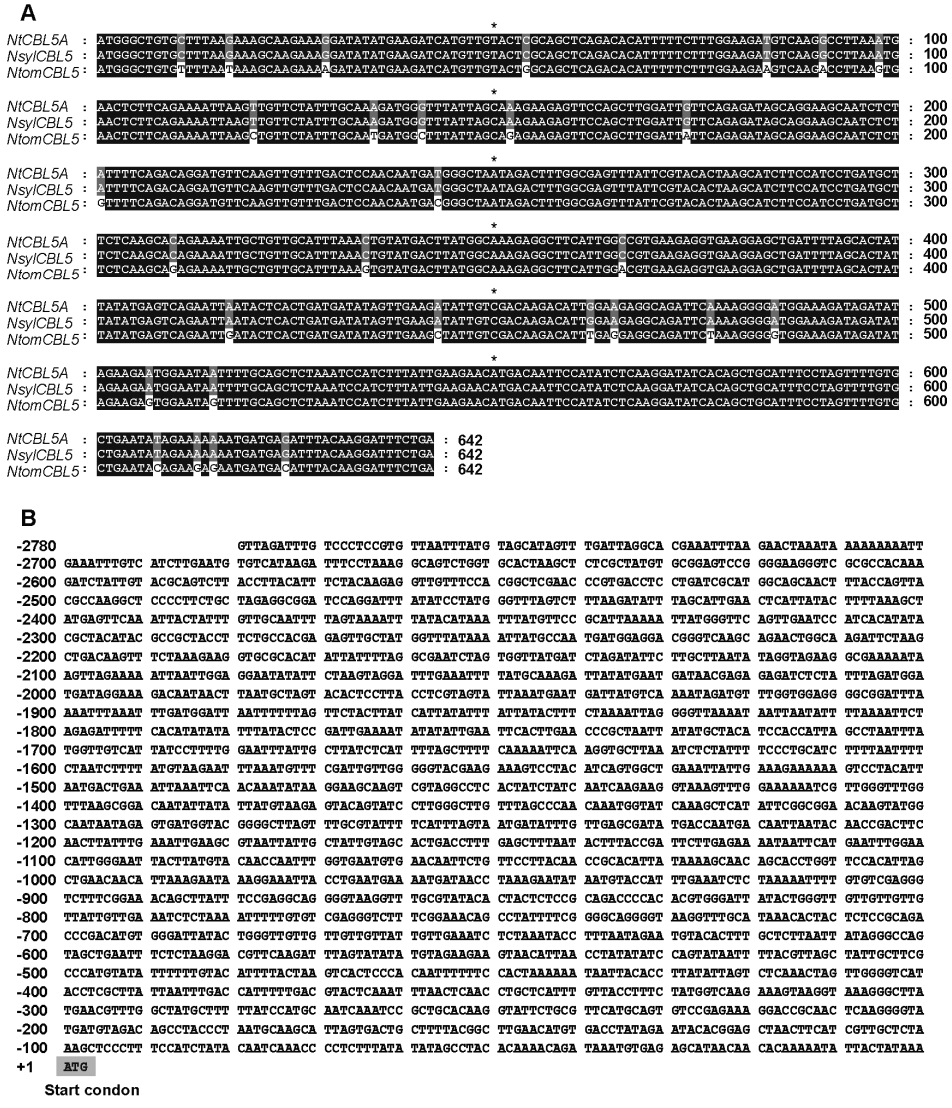

Figure S1 | The coding sequence alignment of *NtCBL5A*, *N. sylvestris CBL5* (*NsylCBL5*), and *N. tomentosiformis CBL5* (*NtomCBL5*) (A) and the cloned upstream regulatory region of *NtCBL5A* (B).

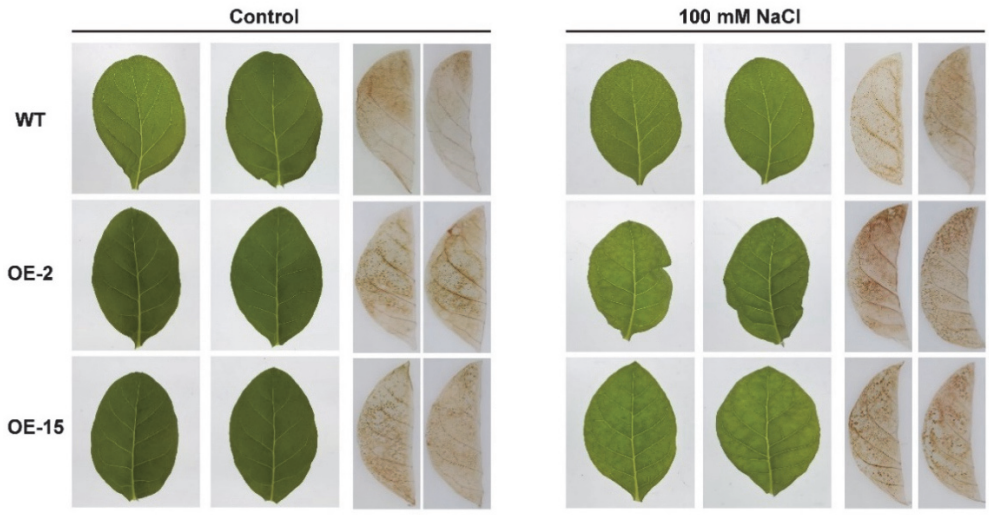

Figure S2 | DAB staining of tobacco under control conditions and salt stress (100 mM NaCl) at 2 DAT.

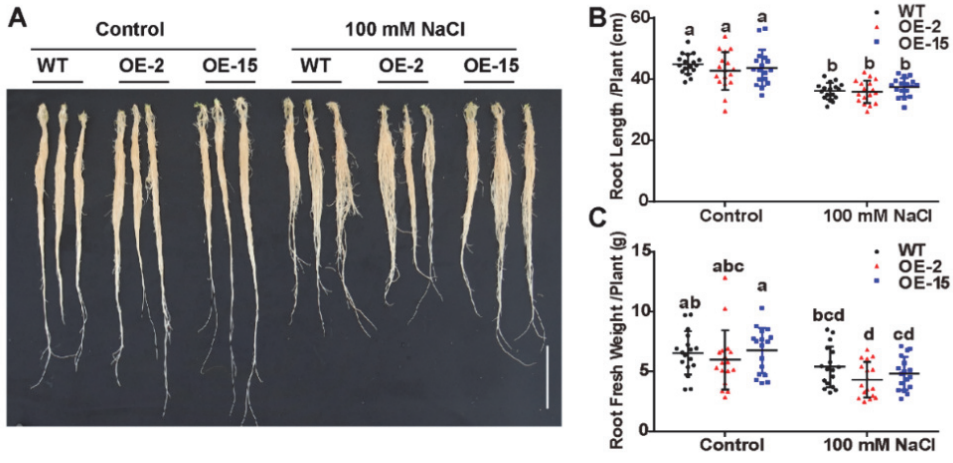

Figure S3 | Root phenotype (A), root length (B), and root fresh weight (C) of wild-type (WT) and *NtCBL5A*-overexpressing lines (OE-2 and OE-15) under control conditions and salt stress (100 mM NaCl) at 9 DAT. Scale bar=10 cm. Error bars indicate ±SD (n=17), different letters above bars (a, b, and c) indicate significant statistical difference based on one-way ANOVA with LSD test (P<0.05).

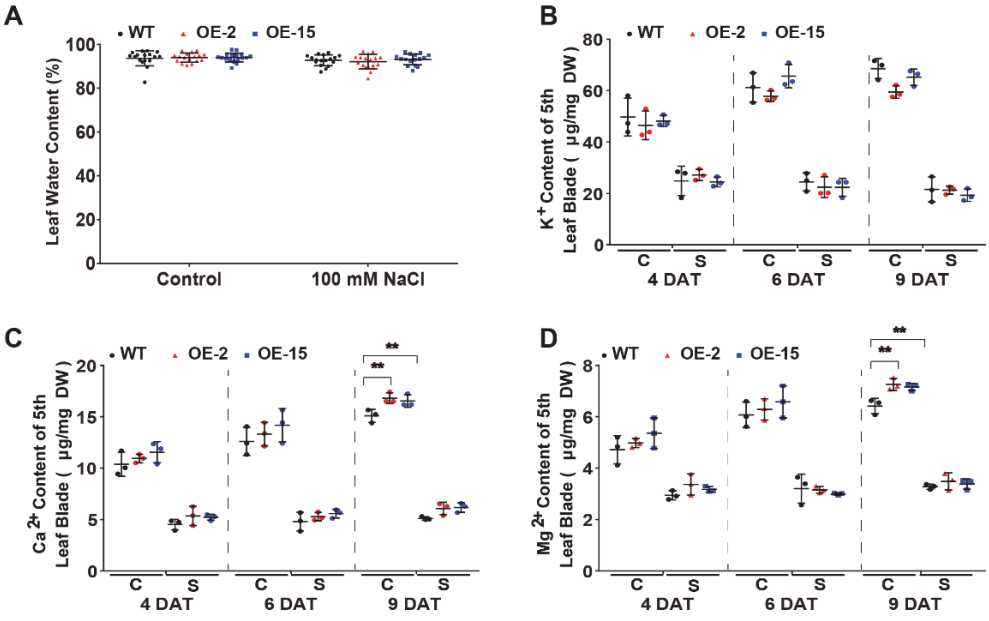

Figure S4 | Leaf water content and K^+, Ca^{2+}, Mg^{2+} determination. (A) Leaf water content of wild-type (WT) and *NtCBL5A*-overexpressing lines (OE-2 and OE-15) under control conditions and salt stress (100 mM NaCl) at 9 DAT. Leaf water content (%) =(W_{fresh}-W_{dry})/W_{fresh}*100% (W_{fresh} is the leaf fresh weight and W_{dry} is the leaf dry weight). Error bars indicate ±SD (n=17). **(C-D)** K^+, Ca^{2+}, and Mg^{2+} contents in the 5th leaf (without main vein) of WT and *NtCBL5A*-OE lines under control conditions and salt stress (100 mM NaCl) at 4 DAT, 6 DAT, and 9 DAT. C means control conditions, while S means salt stress. Error bars indicate ±SD (n=3), every biological replication is a mixed pool of 3 plants. One-way ANOVA with LSD test (*P<0.05 and **P<0.01) was used to analyze statistical significance.

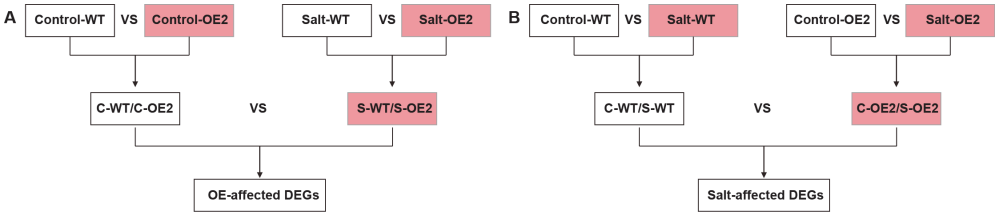

Figure S5 | The flow of OE-affected DEGs (A) and Salt-affected DEGs analysis (B). The read color indicates the “Treatment Group” relative to “Control Group” for transcriptome analysis.

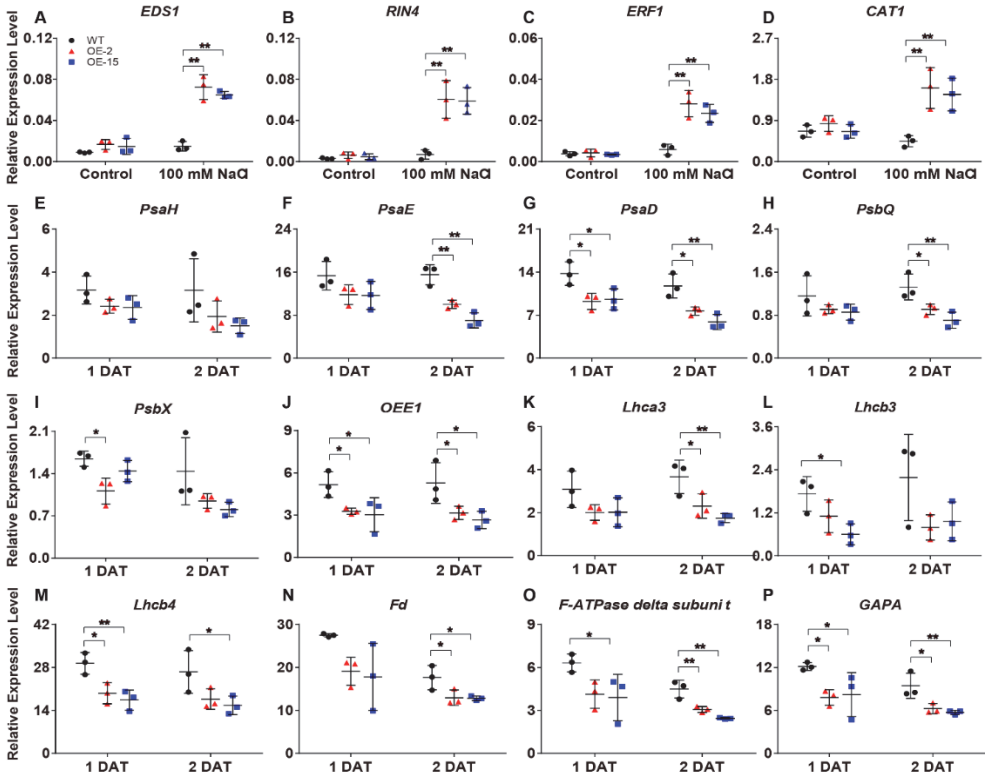

Figure S6 | Relative expression analysis of immunity-related genes and photosynthesis-related genes to reference gene *L25* by RT-qPCR. (A-D) Gene expression analysis of immunity-related genes at 4 DAT under control conditions and salt stress (100 mM NaCl). **(E-P)** Gene expression analysis of photosynthesis-related genes at 1 DAT and 2 DAT under salt stress (100 mM NaCl). Their gene IDs in the reference tobacco genome database (ftp://ftp.solgenomics.net/genomes/Nicotiana_tabacum/edwards_et_al_2017/assembly/Nitab-v4.5_genome_Chr_Edwards2017.fasta.gz) are *EDS1* (Nitab4.5_0002101g0050), *RIN4* (Nitab4.5_0003020g0010), *ERF1* (Nitab4.5_0010541g0010), *CAT1* (Nitab4.5_0009821g0010), *PsaH* (Nitab4.5_0000351g0060), *PsaE* (Nitab4.5_0000385g0230), *PsaD* (Nitab4.5_0014875g0010), *PsbQ* (Nitab4.5_0002345g0070), *PsbX* (Nitab4.5_0000073g0060), *OEE1* (Nitab4.5_0000108g0110), *Lhca3* (Nitab4.5_0000923g0200), *Lhcb3* (Nitab4.5_0012832g0010), *Lhcb4* (Nitab4.5_0011597g0020), *Fd* (Nitab4.5_0004129g0010), *F-ATPase delta subunit* (Nitab4.5_0006745g0030), *GAPA* (Nitab4.5_0010299g0040). Error bars indicate ±SD (n=3). One-way ANOVA with LSD test (*P<0.05, **P<0.01) was used to analyze statistical significance.

Table S1 | Primers used for gene expression analysis and plasmid construction

Primer name	Sequence (5' to 3')	Description
NtCBL5A-1F	ATGGGCTGTGCTTTAAGAAAGCAAGA	Used for the clone of *NtCBL5A* CDS
NtCBL5A-1R	TCAGAAATCCTTGTAAATCTCATC	
NtCBL5A-3F-*Sac* I	CGAGCTCATGGGCTGTGCTTTAAGAAAGCAAGA	Used for the construction of plasmid pCHF3- NtCBL5A
NtCBL5A-3R-*Kpn* I	GGGGTACCTCAGAAATCCTTGTAAATCTCATC	
NtCBL5Apro-1F-*Sal* I	ACGCGTCGACGTTAGATTTGTCCCTCCGTG	Used for the construction of plasmid pBI101- NtCBL5Apro::GUS
NtCBL5Apro-1R-*Sma* I	TCCCCCGGGTTTATAGTAATATTTTTGTGTTGTTATG	
pCHF3-R	ATTCTGGTGTGTGCGCAATG	For the indentification of *NtCBL5A*-OE transgenic tobacco.
pBI101-F	CCGATTCATTAATGCAGCTG	For the indentification of *NtCBL5Apro::GUS* transgenic tobacco.
NtCBL5A-UTR-31F	TTTGCTAATAAACCCATCTTTG	For the identification of endogenous *NtCBL5A*, NtCBL5A-UTR-31F was designed based on the 5'-UTR sequence of *NtCBL5A*
NtCBL5A-81R	TCCAAAGAAAAATGTGTCTGAG	
NtCBL5A-564F	CTCAAGGATATCACAGCTGCATT	For the identification of exogenous *NtCBL5A*, pCHF3-Allcheck-1 was designed based on the sequence of 3'-UTR of exogenous *NtCBL5A*, referring to pCHF3-Allcheck-2 (Shi et al., 2021).
pCHF3-Allcheck-1	TGCAGGTCGACTCTAGAGGAT	
NRP-qF	ACTATGTTTCCAAAAGGCCTGA	RT-qPCR primers for *NRP*

Primer name	Sequence (5' to 3')	Description
NRP-qR	CCATTTAAGCCAAAATCAAGAACC	(Nitab4.5_0000798g0120)
HSR203J-qF	CTTGCGATGCCGGTTTTTCC	RT-qPCR primers for *HSR203J*
HSR203J-qR	GGCGAGTCGCATTGGAGATA	(Nitab4.5_0002719g0120)
PR1a-qF	GTAATATCCCACTCTTGCCGTG	RT-qPCR primers for *PR1a*
PR1a-qR	CCTCAGCTAGGTTTTCGCCG	(Nitab4.5_0003771g0010)
PR1b-qF	ACCATTAACTTGGGACAACGG	RT-qPCR primers for *PR1b*
PR1b-qR	TACGCCAAACCACCTGAGTA	(Nitab4.5_0005400g0020)
PR1c-qF	ATCCCACTCTTGTCATGCTC	RT-qPCR primers for *PR1c*
PR1c-qR	GAAATCGCCACTTCCCCAAG	(Nitab4.5_0004861g0040)
PR-Q-qF	GTGGATCCCTGAGTGCAGAA	RT-qPCR primers for *PR-Q*
PR-Q-qR	CGTGGGAAGATGGCTTGTTG	(Nitab4.5_0003207g0080)
PR-R minor-qF	AACTAATGGCGGTTGCCGTA	RT-qPCR primers for *PR-R minor*
PR-R minor-qR	CCACATGATCCAGGCCCATT	(Nitab4.5_0004097g0050)
PR-R major-qF	GTGAACCCAGGAACAGTCCA	RT-qPCR primers for *PR-R major*
PR-R major-qR	ACGACATCCTCCATTGGTCG	(Nitab4.5_0000360g0100)
EDS1-qF	AGGCCGAAGCGTTATAGGTT	RT-qPCR primers for *EDS1*
EDS1-qR	GGGACCAATCCCATGCCTTT	(Nitab4.5_0002101g0050)
RIN4-qF	GGGATGAACCAATGGGGCTA	RT-qPCR primers for *RIN4*
RIN4-qR	TTCCCTTCCAAAACAGGCGA	(Nitab4.5_0003020g0010)
ERF1-qF	GCTTCCTCAAGTACTCCACACA	RT-qPCR primers for *ERF1*
ERF1-qR	TGTAACGGTGATTGATCTTGGA	(Nitab4.5_0010541g0010), ERF1-qF was designed from 5'-UTR
CAT1-qF	TGTTCAAGTACTGTGGTCATCTTCT	RT-qPCR primers for *CAT1*
CAT1-qR	AACGGAAGACAGAGTAGCAGC	(Nitab4.5_0009821g0010), CAT1-qF and CAT1-qR were designed from 3'-UTR
CHX18-qF	CAGCACCCCTGAAATGTCCA	RT-qPCR primers for *NHX18*
CHX18-qR	ACAACACGTGGCTGTCTCAA	(Nitab4.5_0006998g0030)

Primer name	Sequence (5' to 3')	Description
NCX1-qF	CCGAGAAGAGAAGTGCTTGGA	RT-qPCR primers for *NCX1*
NCX1-qR	TCTTGGCAAGTCAAGTGGCA	(Nitab4.5_0005404g0030)
CAX3-qF	TGTCTGTGGAACCAGTACTTAACA	RT-qPCR primers for *CAX3*
CAX3-qR	ATAACCGCCTCATCTTCCGC	(Nitab4.5_0000102g0080)
CNGC1-qF	TCCTGATAATCTGAGAGCACGA	RT-qPCR primers for *CNGC1*
CNGC1-qR	AGTCGACCACACATTGCATCT	(Nitab4.5_0000258g0120)
PsaH-qF	CCATTGCCGGAACAAAACTCA	RT-qPCR primers for *PsaH*
PsaH-qR	GAACTTGCTCTGAAGGGGGT	(Nitab4.5_0000351g0060)
PsaE-qF	AGCAGAGACAAAGACATGGCAA	RT-qPCR primers for *PsaE*
PsaE-qR	AACGAGCCTCGGGAAGTTG	(Nitab4.5_0000385g0230), PsaE-qF was designed from 5'-UTR
PsaD-qF	TGGCAACTCAAGCTTCTCTCTT	RT-qPCR primers for *PsaD*
PsaD-qR	CTTCTTTTGTGGCGGCTTCTT	(Nitab4.5_0014875g0010)
PsbQ-qF	TCCCCCACCCTACTTCTATCA	RT-qPCR primers for *PsbQ*
PsbQ-qR	TAACAGTGCTCAAACGGGCT	(Nitab4.5_0002345g0070), PsbQ-qF was designed from 5'-UTR
PsbX-qF	TGCCAATAAGGCCATCAAAACAAA	RT-qPCR primers for *PsbX*
PsbX-qR	CAGCAGCTTGTGCTACATCAG	(Nitab4.5_0000073g0060)
OEE1-qF	GGAGCTCCAGAAGGAGAACG	RT-qPCR primers for *OEE1*
OEE1-qR	ACCCCAAGGTCTTAAAAATCTCTCT	(Nitab4.5_0000108g0110), OEE1-qR was designed from 3'-UTR
Lhca3-qF	TGATCATTTGGCTGATCCCGT	RT-qPCR primers for *Lhca3*
Lhca3-qR	CCCCTTTTTAGCATTACAGATGACA	(Nitab4.5_0000923g0200), Lhca3-qR was designed from 3'-UTR
Lhcb3-qF	TGTCACTGGCAAAGGTCCTC	RT-qPCR primers for *Lhcb3*
Lhcb3-qR	GCTAGTGGTATTTATCACATGGCA	(Nitab4.5_0012832g0010), Lhcb3-qR was designed from 3'-UTR

Primer name	Sequence (5' to 3')	Description
Lhcb4-qF	CCCAACGCACCTTGTTTTTCA	RT-qPCR primers for *Lhcb4* (Nitab4.5_0011597g0020), both Lhcb4-qF and Lhcb4-qR were designed from 3'-UTR
Lhcb4-qR	TAGCGTTTGATATTTCCTTCTCCT	
Fd-qF	TCCTTACTCATGCAGAGCTGG	RT-qPCR primers for *Fd* (Nitab4.5_0004129g0010)
Fd-qR	ATTGAGGGGTTTAGGCAGTGA	
F-ATPase delta subunit-qF	CAGTCCAGATCACCCCCGA	RT-qPCR primers for *F-ATPase delta subunit* (Nitab4.5_0006745g0030)
F-ATPase delta subunit -qR	TAGGGTTCCGTTCGACTTGG	
GAPA-qF	ACACTGGTGGTGTCAAGCAA	RT-qPCR primers for *GAPDH* (Nitab4.5_0010299g0040)
GAPA-qR	TCTTGGCTCCAGCCTGAATG	

Chapter 5

NtCBL10A and *NtCBL10B* are essential for the salt tolerance of tobacco

Jingjing Mao, Kaiyan Han, Guang Yuan, Richard G.F. Visser, Yuling Bai, Haobao Liu, Qian Wang, C. Gerard van der Linden

To be submitted

ABSTRACT

Overexpression of *Nicotiana tabacum NtCBL5A* was shown to induce severe necrotic lesions on leaves under salt stress. We hypothesized that overexpression of *NtCBL5A* may interfere with the function of other NtCBLs, possibly through competition of binding to similar NtCIPK partners. In this study, we examined possible *NtCBL*/*NtCIPK* candidates that overexpressed *NtCBL5A* may interfere with and their role in the salt stress response of tobacco. We assessed the salt tolerance of *NtCBL5A::NtCBL10A* co-overexpressing lines and found that *NtCBL10A* overexpression relieved the necrotic phenotype of *NtCBL5A*-OE lines, indicating *NtCBL10A* may play a role in salt tolerance of tobacco. Further studies showed that *Nt-cbl10a* and *Nt-cbl10b* single mutants exhibited salt sensitivity with reduced chlorophyll content and chlorotic spots on leaves. In addition, *Nt-cbl10acbl10b* double mutants showed salt hypersensitivity with fast-developing chlorosis and severe necrotic lesions on leaves under salt stress. Interestingly, the necrosis phenotype of *Nt-cbl10acbl10b* double mutants is light-dependent, while the chlorosis phenotype of *Nt-cbl10acbl10b* double mutants is light-independent. The stomatal conductance and photochemical efficiency of photosystem 2 (PhiPS2) of the *Nt-cbl10acbl10b* double mutant were significantly inhibited at the very early salt stress response stage. NtCIPK24A is a common interactor of NtCBL5A and NtCBL10A, and *Nt-cipk24a* and *Nt-cipk24b* single mutants showed slight salt sensitivity. Results in this study indicate that *NtCBL10* is a key component in the salt tolerance of tobacco, and NtCIPK24A could be one of the partners of NtCBL10 in the salt stress response of tobacco.

Keywords: CBL10, CBL5, CBL4, CIPK24, salt tolerance, tobacco, Na^+; Cl^-

INTRODUCTION

The Calcineurin B-like Protein (CBL) - CBL-interacting Protein Kinase (CIPK) network is involved in plant development and stress adaptation as well as in the crosstalk between development and stress adaptation (Mao et al., 2022). In *Arabidopsis thaliana*, several CBL and CIPK components have been reported to be involved in the salt stress response of plants. The most well-known CBL-CIPK pathway that is responsible for salt tolerance is the SOS (salt overly sensitive) pathway: AtCBL4 (AtSOS3) works with AtCIPK24 (AtSOS2) to phosphorylate and activate the PM-localized Na^+/H^+ antiporter AtSOS1, leading to Na^+ extrusion from the plant cells (Qiu et al., 2002; Shi et al., 2002; Nunez-Ramirez et al., 2012).

The SOS pathway was reported to be conserved in many other plant species, including *Brassica napus*, *Malus domestica*, *Oryza sativa*, *Populus trichocarpa*, *Setaria italica*, and *Solanum lycopersicum* (Martinez-Atienza et al., 2007; Tang et al., 2010; Hu et al., 2012; Liu et al., 2015; Zhang et al., 2017; Cho et al., 2021). Recently, the SOS pathway was shown to include additional CBL-CIPK components. AtCBL8 was reported to be a Ca^{2+}-sensor switch for enhanced SOS pathway efficiency (Steinhorst et al., 2022). The AtCBL8-AtCIPK24-AtSOS1 pathway is activated by a higher Ca^{2+}-signal amplitude: the structural conformation, interaction with AtCIPK24, and AtCIPK24-mediated phosphorylation of AtCBL8 are largely Ca^{2+}-dependent. This indicates that the AtCBL8-AtCIPK24 pathway activates SOS1 when enough cytosolic Ca^{2+} is induced by high salt stress. Furthermore, different from *At-cbl4* mutants that are sensitive to a very low degree of salt stress (25 mM NaCl), the *At-cbl8* mutant only exhibits salt sensitivity under a high degree of salt stress (75 mM or 100 mM NaCl) (Mehra and Bennett, 2022; Steinhorst et al., 2022). AtCBL10 is regarded as another addition to the SOS pathway because AtCBL10-AtCIPK8 positively regulates the SOS1 activity of extruding excess Na^+ from shoots of plants subjected to salinity (Yin et al., 2019). In addition, AtCBL10-AtCIPK24 was predicted to activate a tonoplast-localized Na^+/H^+ exchanger AtNHX for Na^+ sequestration into vacuoles in leaves but this has not been evidenced (Kim et al., 2007).

Tobacco (*Nicotiana tabacum*) is considered to be a relatively salt-tolerant crop but the underlying tolerance mechanisms are unknown. A recent report showed that the isolated leaves from *N. benthamiana* plants were able to detoxify Na^+ rapidly even under massive salt loads by compartmentation of cytosolic Na^+ into vacuoles (Graus et al., 2023). Whether *CBL* genes play a regulatory role in salt tolerance of tobacco, for instance in regulating Na^+ transport over the vacuolar membrane similar to *Arabidopsis*, remains to be established. We showed in a previous report that there are 24 *NtCBL* genes in *N. tabacum*, and that overexpression of *NtCBL5A* and *NtCBL4A-1* enhanced the salt sensitivity of transgenic tobacco, leading to similar necrotic lesions on leaves (Chapter 3, Chapter 4) (Mao et al., 2021). Whether these genes indeed play roles in the salt stress response and salt tolerance in wild-type tobacco remains to be established. The ectopic overexpression of a gene, especially for the gene whose expression is normally limited to specific conditions or specific cell types, can interfere with other proteins, complexes, or pathways, for instance by competitive interaction (Prelich, 2012). We hypothesized that the ectopic (over)expression of *NtCBL5A* or *NtCBL4A-1* might compete with other components of the CBL-CIPK network (for instance the CBL10-CIPK pathway) (Mao et al., 2021).

To identify potential CBL-CIPK pathways that overexpressed *NtCBL5A* and *NtCBL4A-1* may interfere with, we conducted a yeast-two hybrid assay first to screen the NtCBL proteins that share the same NtCIPK interactors with NtCBL5A and NtCBL4A-1. Then we co-overexpressed *NtCBL5A* and the candidate gene *NtCBL10A* and evaluated the salt tolerance of *NtCBL10A::NtCBL5A* co-overexpressing lines as well as loss-of-function mutants of *NtCBL10*. In addition, we also constructed the loss-of-function mutants of *NtCIPK24* and evaluated their salt tolerance because NtCIPK24A is the common interactor of NtCBL4A-1, NtCBL5A, and NtCBL10A. In summary, our results demonstrate that *NtCBL10* is a key component in the salt tolerance of tobacco, with likely diverse functions in ion homeostasis that are essential for maintaining photosynthetic capacity. Furthermore, we hypothesize that NtCIPK24A could be one of the partners of NtCBL10 in the salt

stress response of tobacco.

MATERIALS AN D METHODS

Plant materials, growth conditions, and application of salt treatment

N. tabacum L. cv. Zhongyan 100 cultivar was used as plant material in this study. For determining the expression profiles of *NtCBL* genes in different tobacco tissues at a young stage, tobacco plants were grown in 2022 at Unifarm, Wageningen University & Research in the Netherlands. The conditions of the greenhouse were 16 h light / 8 h dark at 25/23^{o}C and 70% relative humidity. The shortwave radiation level was maintained in the greenhouse compartment using artificial PAR (photosynthetically active radiation) when the incoming shortwave radiation was below 200 Wm^{-2} (Mao et al., 2021). Tobacco seeds were first sown in the soil. At 20 days after germination (DAG), the young tobacco plants were transplanted in rock-wool plugs within float trays for hydroponic cultivation (1/2 Hoagland's nutrient solution). After 6 days of acclimatization (at ~26 DAG), plants were transplanted to a circular flow hydroponic system filled with 1/2 Hoagland's nutrient solution (500 L). The water used to prepare 1/2 Hoagland's nutrient solution contained trace amounts of Na^{+} and Cl^{-} (5.51 µg/ml and 7.88 µg/ml, respectively). After 6 days of acclimatization (at ~ 32 DAG), NaCl was added to the nutrient solution to a concentration of 50 mM on the first day to avoid salt shock, and 100 mM NaCl concentration was reached the next day, and 200 mM NaCl concentration was reached the next day after 100 mM NaCl treatment. From the day of 100 mM NaCl treatment, photographs of the plants were taken and different tissues (leaf blades: all leaves with main veins removed; main veins: main veins from all leaves; stems; roots) of young tobacco plants were sampled every day for ion content measurement until harvest. For assessing salt tolerance, chlorophyll content was measured with the Apogee MC-100 Chlorophyll Meter (Masaló and Oca, 2020), and stomatal conductance and chlorophyll fluorescence were measured with the LI-600 Porometer/Fluorometer (Price, 2021).

Cultivation of grafted and excised plants

For grafting, strong tobacco plants were selected. The stems of the scion and stock plants were cut with grafting scissors and joined by wrapping the wound with preservative film. After one month the wound was healed and the grafted plants were subjected to salt stress. For excised plants, the roots of plants were cut and their stems were planted in rock-wool plugs for 1 week of acclimatization, then salt stress was applied.

Application of dark treatment

For the covering treatment, the 4th leaves of the used plants were covered with aluminum foil at the same time as the initiation of the salt treatment. For the dark treatment, whole plants were covered with light-tight black trays at the same time as the initiation of the salt treatment.

Generation of NtCBL10A-OE plants and NtCIPK24A-OE plants

To generate the gene overexpressing lines, *Agrobacterium* carrying pCHF3-NtCBL10A plasmid and pCHF3-NtCIPK24A plasmid were introduced into cultivar Zhongyan 100 by the *Agrobacterium*-mediated leaf disc transformation method (Horsch et al., 1985). The screening of homozygous transgenic plants was done as previously described (Mao et al., 2021). Primers for cloning genes, identifying positive transgenic plants, and quantifying overexpression levels are listed in Table S2.

Generation of gene-editing mutants

The sgRNAs (Table S2) were designed on the online website CRISPR MultiTargeter http://www.multicrispr.net/index.html. The sgRNA fragments were synthesized and inserted at the *Bsa* I site of the pDC45 vector (Li et al., 2022) using T4 ligase (Accurate Biotechnology (Hunan) Co., Ltd, Cat No./ID: AG11801, Changsha, China). To generate the gene-editing lines, pDC45-NtCBL10A, pDC45-NtCBL10B, pDC45-NtCBL10, pDC45-NtCIPK24A, pDC45-NtCIPK24B, and pDC45-NtCIPK24 plasmids were transformed into *Agrobacterium tumefaciens* EHA105 and then were introduced into Zhongyan 100 by the *Agrobacterium*-mediated leaf disc transformation method (Horsch et al., 1985). The edited sequences of *NtCBL10A*

and *NtCBL10B* were identified by PCR with the primer pairs pDC45-NtCBL10A-JCF/pDC45-NtCBL10A-JCR and pDC45-NtCBL10B-JCF/pDC45-NtCBL10B-JCR (Table S2), respectively. The editing of *NtCIPK24A* and *NtCIPK24B* were identified by PCR with the primer pairs pDC45-NtCIPK24A-JCF/pDC45-NtCIPK24A-JCR and pDC45-NtCIPK24B-JCF/pDC45-NtCIPK24B-JCR (Table S2), respectively.

Yeast two-hybrid assay

The coding sequences of *NtCBL1A-1/1A-2/2A/3A/4A-1/5A/6A/9A/10A* were cloned into the pGADT7 vector, then the plasmids were transformed into yeast strain AH109 (Mehla et al., 2015). The coding sequences of *NtCIPK1A-1/2A/4A/6A/7A-2/11A-2/16A/17A/24A/25A/27A/28A* were cloned into the pGBKT7 vector, and then the plasmids were transformed into another yeast strain Y187 (Mehla et al., 2015). AH109 yeast colony containing a pGADT7-NtCBL plasmid and Y187 yeast colony containing a pGBKT7-NtCIPK plasmid were raised in 0.5 mL 2×YPDA medium for mating 24 hrs (30 ^{0}C, 50 rpm shaking bed). Then the 2×YPDA medium with mated AH109 and Y187 yeast strains was centrifuged at 6000 rpm for 1 min, the supernatant was discarded and the yeast was washed three times with 1 mL 0.9% NaCl. 100 µL suspension was distributed onto SD/-Leu-Trp and SD/-Leu-Trp-Ade-His medium, then the Petri dishes were incubated at 30 ^{0}C for 3-5 days. The yeast colony grew on the SD/-Leu-Trp-Ade-His medium was transferred to new SD/-Leu-Trp-Ade-His medium for further screening (repeat three times).

Statistical analysis

Statistical analysis was done using IBM SPSS Statistics 23 software. Significant differences were examined by Student's *t* test or one-way ANOVA with LSD test at $p<0.05$ and $p<0.01$. The figures were drawn by GraphPad Prism 6.0.

RESULTS

The identification of NtCIPK family members and their interactions with NtCBLs

A genome-wide search for NtCIPKs was conducted in the *N. tabacum* genome using

the protein sequences of 26 *A. thaliana* AtCIPKs as queries. Fifty-seven *NtCIPK* genes were identified and numbered according to the names of the most similar *AtCIPK* genes (Figure S1, Table S1). Twenty-nine NtCIPKs had the highest sequence similarity with CIPKs of the maternal progenitor *N. sylvestris* and were labeled “A”, while 28 NtCIPKs were more similar to CIPKs of the paternal progenitor *N. tomentosiformis* and were labeled “B”. *NtCIPK*s with the highest similarity to the same *AtCIPK* protein were numerically ordered. For example, the three *NtCIPK* genes that were found to be the most similar to *AtCIPK1* were named *NtCIPK1A-1*, *NtCIPK1A-2*, and *NtCIPK1A-3*. For brevity, we refer to all the paralogous genes of one specific NtCIPK when “A” or “B” is not specifically pointed out in this paper. The number of amino acids (AA), theoretical isoelectric point (p*I*), and molecular weight (MW) of the NtCIPKs are listed in Table S1. Some *NtCIPK* genes encode splicing variants that are translated into proteins of different lengths. For these, the one encoded longest protein was selected as a representative.

Twelve *NtCIPK* genes (*NtCIPK1A-1/2A/4A/6A/7A-2/11A-2/16A/17A/24A/25A/27A/28A*) were successfully cloned in our lab. To identify NtCBL proteins that are able to interact with the NtCIPK proteins encoded by these genes, a yeast-two hybrid assay was conducted. The results showed that NtCBL4A-1 and NtCBL5A were able to bind to the same NtCIPKs, and so were NtCBL1A-1 and NtCBL1A-2, as well as NtCBL2A and NtCBL3A (Figure 1). These pairs of NtCBL proteins also have similar amino acid sequences (Chapter 3). NtCBL4A-1 and NtCBL5A share putative NtCIPK partners with NtCBL2A/3A/9A/10A (Figure 1), indicating overexpressed NtCBL4A-1 and NtCBL5A may be able to compete with these proteins for their NtCIPK partners when expressed in the same tissues.

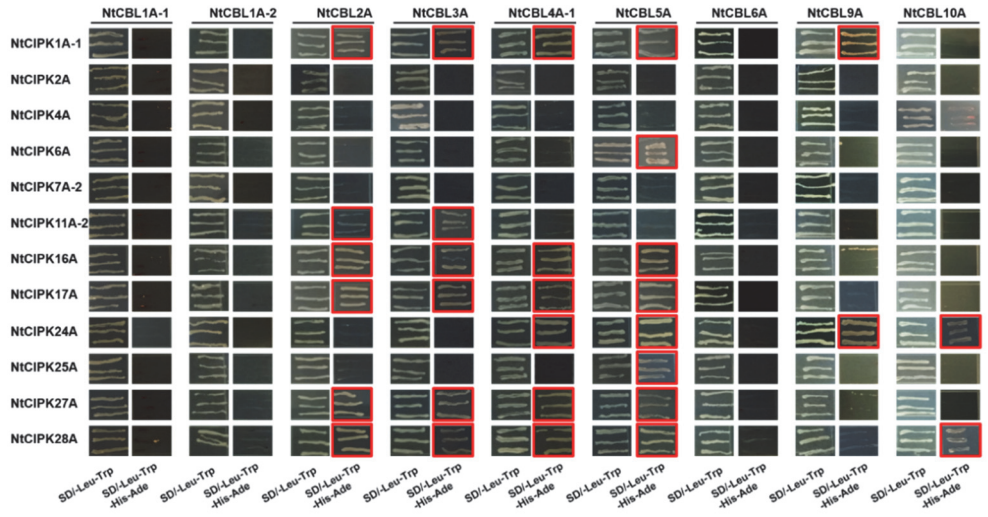

Figure 1. The interaction between NtCBL proteins and NtCIPK proteins. SD/-Leu-Trp indicates the synthetic defined (SD) media lacking tryptophan (Trp) and leucine (Leu). SD/-Ade/-His/-Leu/-Trp indicates SD media lacking tryptophan (Trp), leucine (Leu), histidine (His), and adenine (Ade). Red squares indicate the positive interaction between proteins in the yeast-hybrid system.

The salt sensitivity of *NtCBL5A*-OE is dependent on the shoot genotype

Most *NtCBL* members have expression preference for either shoots or roots: *NtCBL2*, *3*, and *10* are mainly expressed in shoots while *NtCBL9* is mainly expressed in roots (Chapter 3). The phenotype of *NtCBL4A-1*-OE and *NtCBL5A*-OE transgenic tobacco plants is mainly manifested in the leaves. To see whether the phenotype is established by interference with NtCBL-involving salt stress response mechanisms that originate in the roots or the shoots, we conducted a grafting experiment with WT as root stock and NtCBL5A-OE line (OE-2) as the scion, and vice versa. Results showed that the necrotic phenotype was visible in the plants with *NtCBL5A*-OE as the scion, but not with *NtCBL5A*-OE as the stock (Figure 2A and 2B). In addition, we conducted salt stress on excised (rootless) shoots (Figure 2C). The rootless shoots of *NtCBL5A*-OE lines (OE-2 and OE-15) also exhibited the necrosis phenotype under salt stress. These results demonstrate that the salt-induced necrosis of *NtCBL5A*-OE under salt stress is triggered in the shoot. Therefore, *NtCBL5A*

overexpression is more likely to interfere with the function of other *NtCBL* genes such as *NtCBL2*, *NtCBL3*, *and NtCBL10* which are mainly expressed in shoots. (Chapter 3).

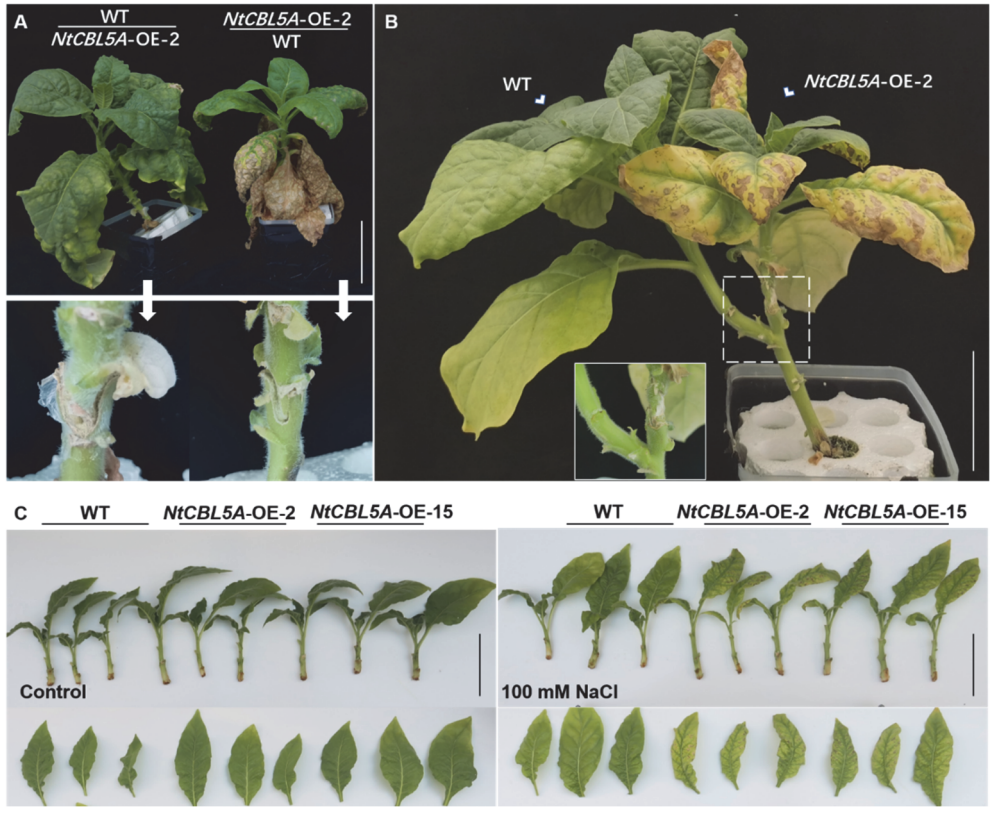

Figure 2. Salt treatments on grafted or excised WT and *NtCBL5A*-OE lines under salt stress (100 mM NaCl). Scale bars=10 cm. **(A)** The phenotype of grafted plants under salt stress at 30 DAT (days after reaching 100 mM NaCl treatment). The left grafted plant is *NtCBL5A*-OE-2 as the stock and WT as the scion, and the right grafted plant is WT as the stock and *NtCBL5A*-OE-2 as the scion. **(B)** The phenotype of the grafted plant with *NtCBL5A*-OE-2 as the scion of a lateral branch of WT at 30 DAT. **(C)** The phenotype of excised shoot of WT and *NtCBL5A*-OE lines under salt stress at 7 DAT.

NtCBL10A overexpression relieves the salt sensitivity of *NtCBL5A*-OE lines

Of the three possible candidates involved in the salt-sensitive necrotic phenotype of *NtCBL4A-1*-OE and *NtCBL5A*-OE lines, *NtCBL10* is the most likely candidate.

Arabidopsis AtCBL10 is a well-known component in the salt stress signaling and response pathway that is linked to the SOS pathway (AtCBL4-AtCIPK24 pathway) and it was suggested to regulate Na^+ sequestration into vacuoles (Kim et al., 2007).

To establish a possible role for *NtCBL10* in the salt stress response of tobacco and the necrotic phenotype of *NtCBL4A-1* and *NtCBL5A*, we crossed the homozygous *NtCBL5A*-OE-2 line with homozygous *NtCBL10A*-OE lines (OE-1, OE-16) and assessed the phenotype of the hybrid lines co-overexpressing *NtCBL5A* and *NtCBL10A* under salt stress. Lines co-overexpressing *NtCBL4A* and *NtCBL5A* were included as well. Co-overexpression of *NtCBL4A-1* and *NtCBL5A* had an additive effect on the salt sensitivity of transgenic tobacco with fast-developing necrosis (Figure 3A), while *NtCBL10A* overexpression greatly relieved the necrotic symptoms of *NtCBL5A*-OE lines (Figure 3A) and improved growth vigor under saline conditions (Figure 3C and 3D). These results are in line with the hypothesis that ectopic (over)expression of *NtCBL5A* interferes with the function of *NtCBL10A* in salt tolerance.

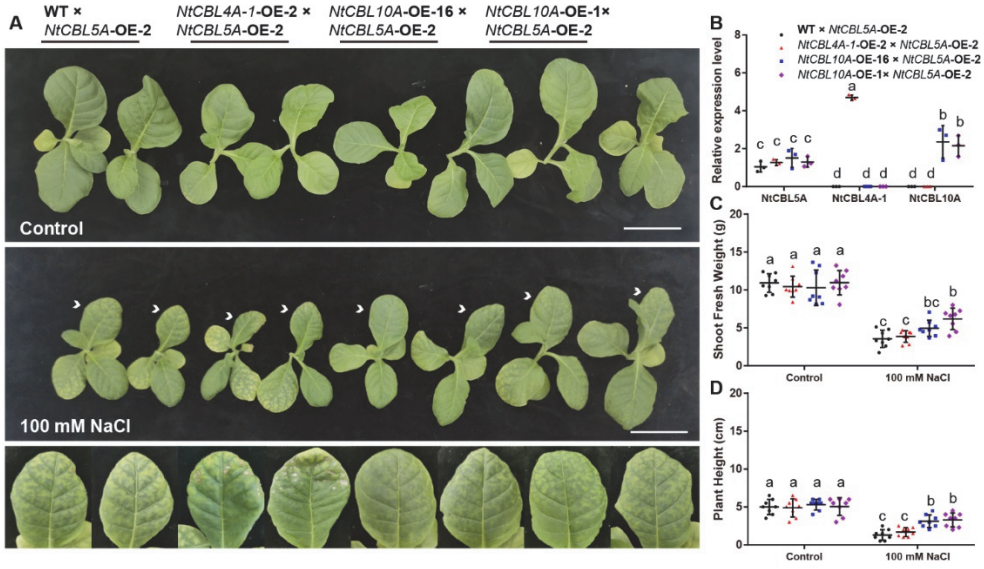

Figure 3. The shoot phenotype of hybrid lines (WT×*NtCBL5A*-OE, *NtCBL4A-1*-OE×*NtCBL5A*-OE, *NtCBL10A*-OE-16×*NtCBL5A*-OE, *NtCBL10A*-OE-1×*NtCBL5A*-OE) under control conditions and salt stress (100 mM NaCl). Scale bars=10 cm. **(A)** The shoot phenotype of hybrid lines at 9 DAT (days after reaching 100 mM NaCl treatment). White arrowheads indicate the leaves which were zoomed in at the bottom part of the panel. **(B)** Relative expression analysis of exogenous *NtCBL5A*, *NtCBL4A-1*, and *NtCBL10A* in leaves of different hybrid lines determined by RT-qPCR. Error bars indicate ±SD (n=3). The expression levels are relative to the reference gene *NtL25* (Schmidt and Delaney, 2010). **(C** and **D)** The shoot fresh weight and plant height of hybrid lines at 9 DAT. Error bars indicate ±SD (n=8). Different letters above bars (a, b, and c) indicate significant statistical differences based on one-way ANOVA with LSD test (P<0.05).

Growth response to salt stress of *NtCBL10* loss-of-function mutants

Being an allotetraploid, tobacco has two copies of *AtCBL10* orthologs: *NtCBL10A* and *NtCBL10B* originating from the maternal diploid tobacco species *N. sylvestris* and paternal diploid tobacco species *N. tomentosiformis*, respectively (Chapter 3). *NtCBL10A* has a higher overall expression level (about 3 fold) than *NtCBL10B* in all detected tissues (Chapter 3) and both their expression levels were upregulated in the leaf blade by 100 mM NaCl stress. Their protein sequences differ only at three amino acids (Figure S2), indicating they may have functional redundancy. To gain further insight into the role of *NtCBL10* in salt tolerance of tobacco and the interference of *NtCBL4A-1* and *NtCBL5A* overexpression with this role, we constructed the single mutants *Nt-cbl10a* (Figure S3A) and *Nt-cbl10b* (Figure S3B) as well as the double mutant *Nt-cbl10acbl10b* (Figure S3C) using the CRISPR/Cas9 technique. All of the gene editing-induced mutations cause premature termination of protein translation (Figure S3).

The salt tolerance of the knock-out mutants was assessed under 100 mM NaCl treatment. At 7 DAT (days after reaching 100 mM NaCl treatment), the phenotype and growth characteristics of the mutants were similar to WT plants under control conditions (Figure 4). Under salt stress, however, the *Nt-cbl10a* and *Nt-cbl10b* single mutants exhibited chlorotic spots on their leaves, and the *Nt-cbl10acbl10b* double

mutant even showed extremely fast-developing severe chlorosis with necrotic lesions (Figure 4A, Figure S4). In addition, the growth vigor of *Nt-cbl10acbl10b* double mutant was significantly reduced under salt stress compared to WT plants (Figure 4B-E). These results clearly indicate that *NtCBL10A* and *NtCBL10B* play a key role in the salt tolerance of tobacco and they may be functionally redundant. The *Nt-cbl10a* single mutants exhibited earlier and more severe salt-sensitive phenotype than *Nt-cbl10b* single mutant (Figure S4), which is consistent with the higher expression level of *NtCBL10A* compared to *NtCBL10B* (Chapter 3).

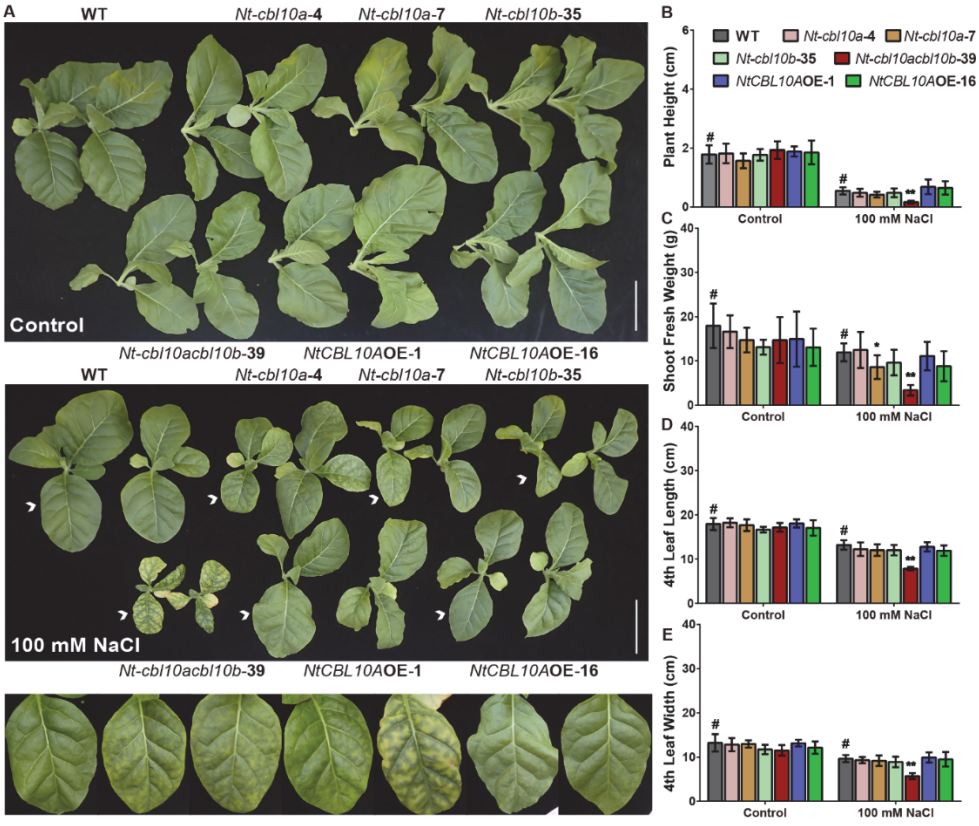

Figure 4. The shoot phenotype of WT, *Nt-cbl10a* single mutant, *Nt-cbl10b* single mutant, *Nt-cbl10acbl10b* double mutant, and *NtCBL10A*-OE lines under control conditions and salt stress (100 mM NaCl). Scale bars=10 cm. **(A)** The shoot phenotype of plants at 8 DAT. White arrowheads indicate the 4th leaves which were zoomed in at the bottom part of the panel. **(B-E)** The plant height,

shoot fresh weight, 4th leaf width, and 4th leaf length of all lines at 8 DAT (days after reaching 100 mM NaCl treatment). Error bars indicate ±SD (n=6). Asterisks indicate statistically significant differences compared with WT (#) under control or saline conditions (Student's *t* test, **p*<0.05 and ***p*<0.01).

Physiological response to salt stress of *NtCBL10* loss-of-function mutants

For the physiological characterization of the salt response of the *NtCBL10* loss-of-function mutants, we measured the chlorophyll content, stomatal conductance, and photochemical efficiency of photosystem 2 (PhiPS2) at 3 DAT and 7 DAT. The chlorophyll content of the *Nt-cbl10acbl10b* double mutant was already greatly reduced under salt stress at 3 DAT (Figure 5A). At 7 DAT, the chlorophyll contents of *Nt-cbl10a* and *Nt-cbl10b* single mutants were also significantly reduced by salt stress but much less than that of *Nt-cbl10acbl10b* double mutant (Figure 5D). Similarly, stomatal conductance and chlorophyll fluorescence of *Nt-cbl10acbl10b* double mutant were also decreased already at 3 DAT (Figure 5B and 5C). The PhiPS2 of *Nt-cbl10a* and *Nt-cbl10b* single mutants was not significantly reduced at both 3 DAT and 7 DAT compared to WT (Figure 5C and 5F), indicating that the loss of single *NtCBL10A* or *NtCBL10B* did not severely affect the photosynthesis of tobacco.

The leaf ion contents of all lines were measured to assess whether changed ion homeostasis would underly the extreme salt sensitivity of the *NtCBL10* loss-of-function mutants. Results showed that Na^+, Ca^{2+}, and Mg^{2+} contents were not significantly different between WT, mutants, and *NtCBL10A*-OE lines under both control and saline conditions (Figure 5G, S5A, and S5B). Interestingly, the Cl^- content of the *Nt-cbl10acbl10b* double mutant was significantly lower than that of WT and other mutants under salt stress (Figure 5H), while the K^+ content was increased in the double mutant (Figure 5I).

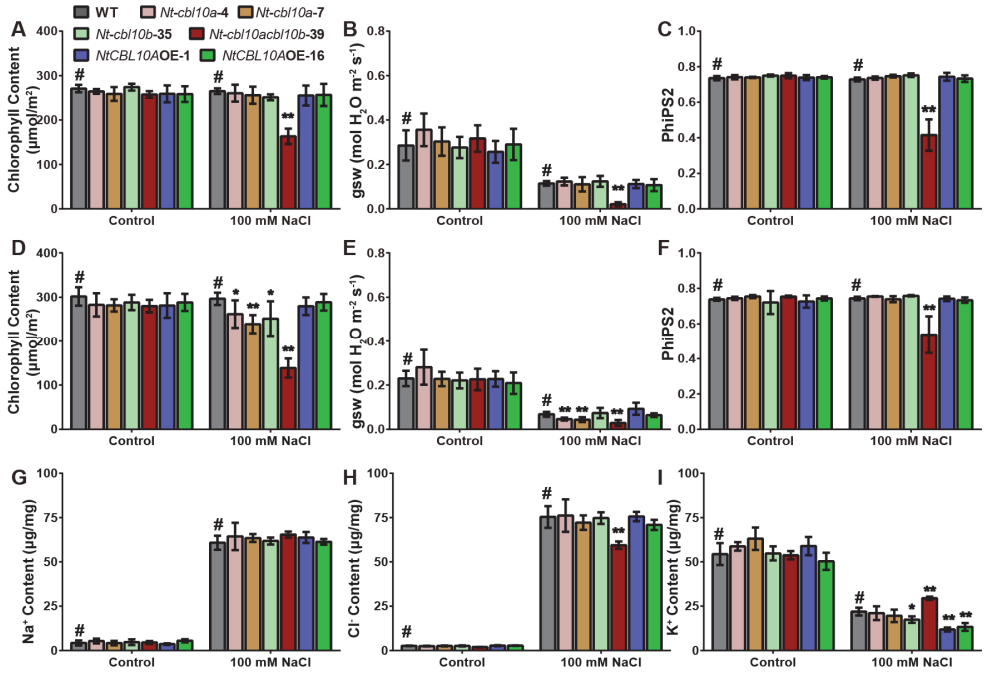

Figure 5. The determination of physiological parameters of WT, *Nt-cbl10a*, *Nt-cbl10b* single mutants, *Nt-cbl10acbl10b* double mutant, and *NtCBL10A*-OE lines under control conditions and salt stress (100 mM NaCl). (A-F) The chlorophyll content, stomatal conductance, and chlorophyll fluorescence of all lines at 3 DAT (days after reaching 100 mM NaCl treatment) (A-C) and 7 DAT (D-F). Error bars indicate ±SD (n=6). **(G-I)** Ion contents (Na^+, Cl^-, and K^+) in leaf blades of all lines under control and saline conditions at 7 DAT. Error bars indicate ±SD (n=4). Asterisks indicate statistically significant differences compared with WT (#) under control or saline conditions (Student's *t* test, **p*<0.05 and ***p*<0.01).

Our results showed that in the *Nt-cbl10acbl10b* double mutant, photosynthetic activity is inhibited and chlorophyll breakdown is initiated very shortly after imposing salt stress. We examined this fast-developing phenotypic response of the double mutant in more detail, monitoring changes in photosynthetic parameters and ion contents in the *Nt-cbl10acbl10b* double mutant and WT tobacco plants every day after imposing 100 mM NaCl stress (0-5 DAT). The chlorophyll content, stomata conductance, and photochemical efficiency of photosystem 2 (PhiPS2) of *Nt-cbl10acbl10b* double mutant were affected already at 1 DAT (48 hrs after the first 50

mM NaCl addition at 0 DAT, 24 hrs after reaching 100 mM NaCl) (Figure 6B-D) with chlorotic symptoms visible already at 1 DAT and necrotic spots visible at 2 DAT (Figure 6A), and further developing chlorosis and necrosis over the next few days. At these very early stages of salt treatment, Na^+ contents were only slightly increased in all plants, and Na^+ content of the *Nt-cbl10acbl10b* double mutant accumulated at a similar rate as WT from 0 to 5 DAT (Figure 6E). These results do not support a role for leaf Na^+ accumulation and toxicity in the severe salt sensitivity phenotype of the *Nt-cbl10acbl10b* double mutant. Ca^{2+} and Mg^{2+} contents were not significantly different between WT and mutants under both control and saline conditions (Figure S5C and S5D). In addition, the Na^+/K^+ ratios of WT and *Nt-cbl10acbl10b* double mutant under salt stress were also quite similar (Figure S5E), indicating the salt-sensitive phenotype of the double mutant is not likely because of the imbalanced Na^+/K^+ ratio. Interestingly, Cl^- accumulated at a significantly lower rate in the *Nt-cbl10acbl10b* double mutant compared to WT (Figure 6F), and the Na^+/Cl^- accumulation ratio in the double mutant was much higher than that in the WT (Figure S5F).

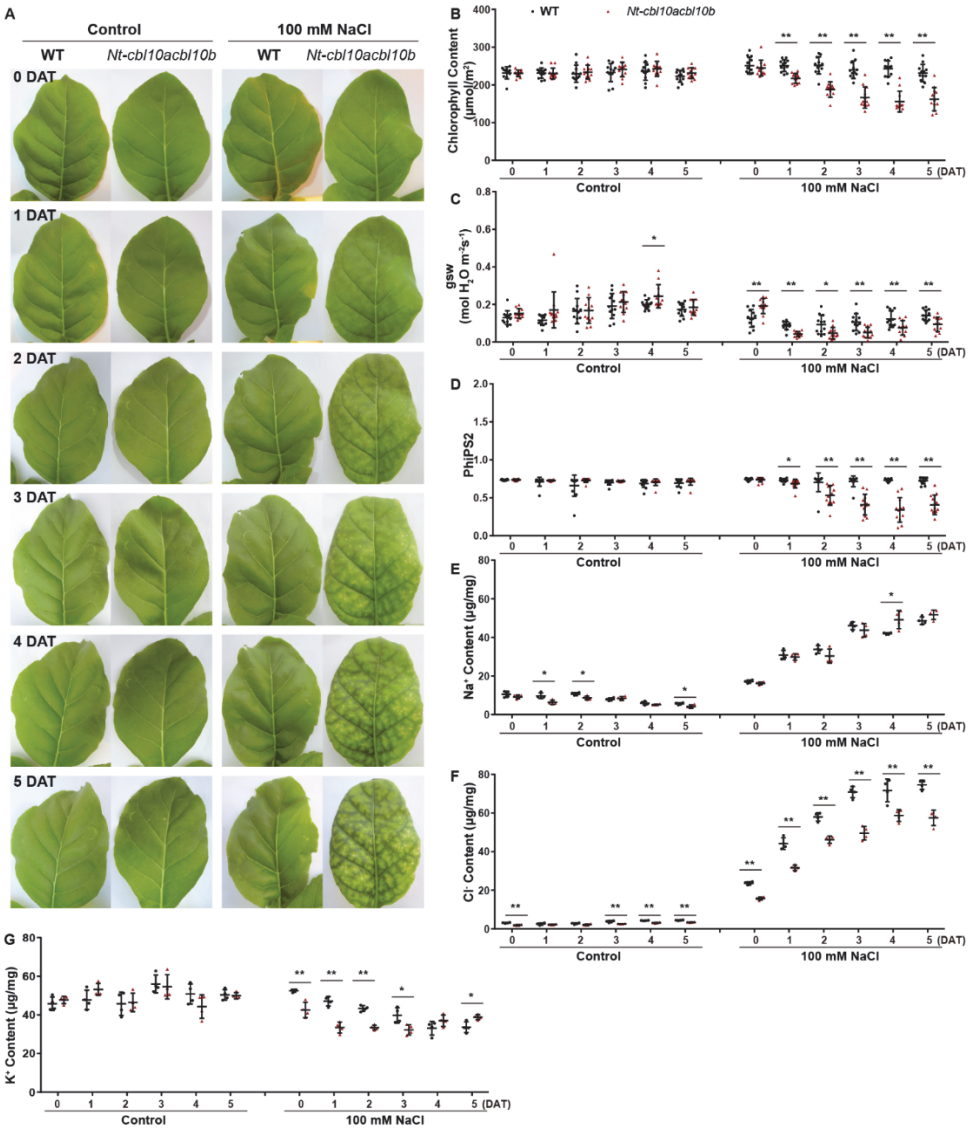

Figure 6. The phenotype and physiological parameters of WT and *Nt-cbl10acbl10b* double mutant on different time points after salt treatment (100 mM NaCl). (A) The shoot phenotype of plants at 0-5 DAT (days after reaching 100 mM NaCl treatment). **(B-D)** The chlorophyll content, stomatal conductance, and chlorophyll fluorescence of all lines at 0-5 DAT. Error bars indicate ±SD (n=12). **(E-G)** Ion contents (Na^+, Cl^-, and K^+) in leaf blades of all lines under control and saline conditions at 0-5 DAT. Error bars indicate ±SD (n=4). Asterisks indicate statistically significant differences of *Nt-cbl10acbl10b* double

mutant compared with WT under control or saline conditions at different time points (Student's *t* test, **p*<0.05 and ***p*<0.01).

The chlorosis and necrosis phenotypes of *Nt-cbl10acbl10b* double mutant under salt stress are independent

Previous reports have shown that some lesion-mimic phenotype is connected to light or defective photosystems (Zulfugarov et al., 2014; Bruggeman et al., 2015; Wang et al., 2015; Tang et al., 2020). In the *Nt-cbl10acbl10b* double mutant, photosynthesis was affected already at a very early stage of salt treatment (Figure 5C and 6D). We explored whether the salt-sensitive phenotype of the *Nt-cbl10acbl10b* double mutant leaves was light-dependent in a dark treatment (whole plants in the dark at the same time with salt treatment). Results showed that the *Nt-cbl10acbl10b* double mutant leaves still suffered possibly even more from early chlorophyll breakdown and chlorosis of the leaf blades in the dark, but necrotic lesions were no longer visible (Figure 7B). These results suggest that the salt stress-induced necrosis of the *Nt-cbl10acbl10b* double mutant leaves is dependent on light but the breakdown of chlorophyll is light-independent.

Ion content results showed that Na^+ accumulation of both WT and *Nt-cbl10acbl10b* double mutants was very low from 1 DAT to 6 DAT (Figure 7D), which may argue against a role for Na^+ accumulation in the chlorophyll breakdown of the *Nt-cbl10acbl10b* double mutant. Interestingly, the reduced rate of Cl^- accumulation in the *Nt-cbl10acbl10b* double mutant compared to WT under salt stress was reversed in the leaves grown in the dark (Figure 6F and 7E). Ca^{2+} and Mg^{2+} contents were still not significantly different between WT and mutants under both control and saline conditions in the dark (Figure S5G and S5H).

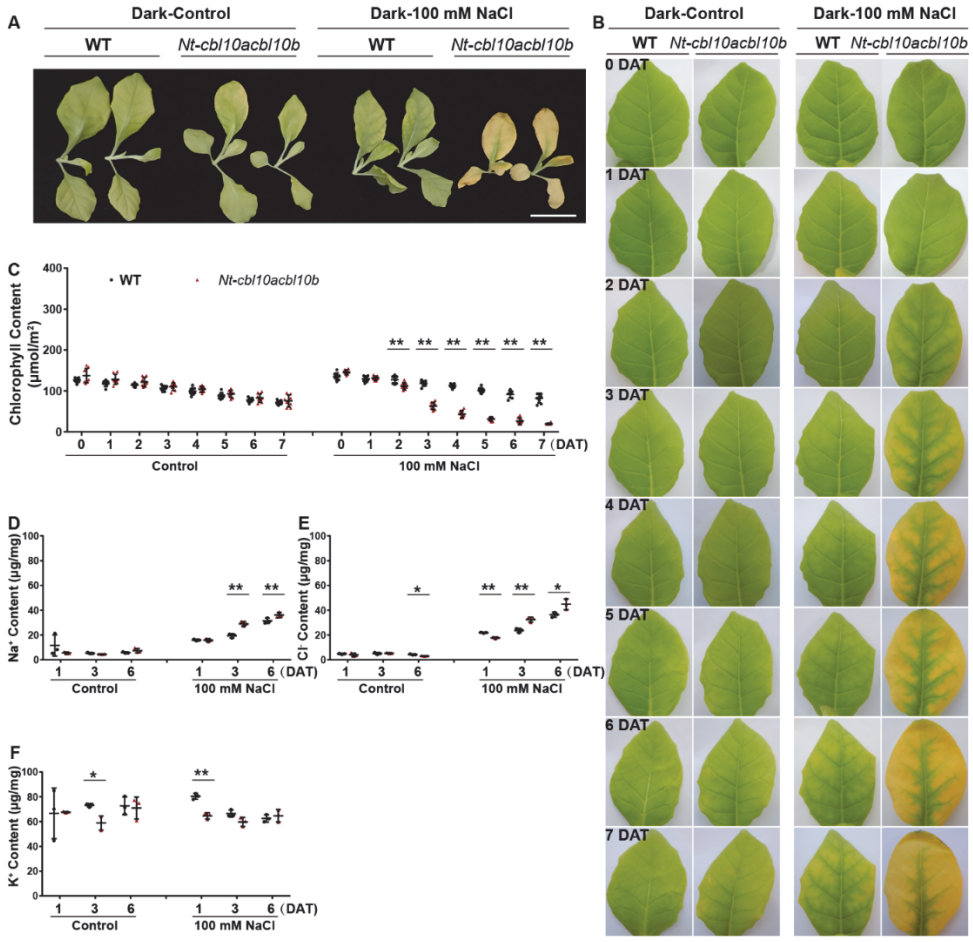

Figure 7. The phenotype and physiological parameters of WT and *Nt-cbl10acbl10b* double mutant on different time points after salt treatment (100 mM NaCl) in the dark. (A) The shoot phenotype of plants at 7 DAT (days after reaching 100 mM NaCl treatment). **(B)** The shoot phenotype of plants at 0-7 DAT. Scale bar=10 cm. **(C)** The chlorophyll content of all lines at 0-7 DAT. Error bars indicate ±SD (n=8). **(D-F)** Ion contents (Na^+, Cl^-, and K^+) in leaf blades of all lines under control and saline conditions at 1, 3, and 6 DAT. Error bars indicate ±SD (n=3). Asterisks indicate statistically significant differences of *Nt-cbl10acbl10b* double mutant compared with WT under control or saline conditions at different time points (Student's *t* test, **p*<0.05 and ***p*<0.01).

NtCIPK24 loss-of-function mutants exhibited slight salt sensitivity under high salt stress

A suggested CBL10-interacting partner in the vacuole-targeted salt stress response is CIPK24 (Kim et al., 2007). To study the role of NtCIPK in the salt stress response of tobacco, we constructed the single mutants *Nt-cipk24a* and *Nt-cipk24b* (Figure S6A and S6B), and also tried to construct the double mutant *Nt-cipk24acipk24b* (Figure S6C). However, the double knockout of both *NtCIPK24A* and *NtCIPK24B* failed because of defective callus development (Figure S6D), indicating that *NtCIPK24* may have a key function in plant development.

The salt tolerance of *Nt-cipk24a* and *Nt-cipk24b* single mutants was assessed under 100 mM NaCl and 200 mM NaCl treatments. Under control conditions, the *Nt-cipk24b-7* mutant had an inferior growth vigor compared to WT, all of the other lines showed similar growth vigor as the WT under control. Under 100 mM NaCl treatment, the growth vigor of *Nt-cipk24a* and *Nt-cipk24b* single mutants was slightly inhibited (Figure 8). The growth vigor inhibition of *Nt-cipk24a* and *Nt-cipk24b* single mutants was more obvious under 200 mM NaCl treatment (Figure 8). In addition, the *Nt-cipk24a* and *Nt-cipk24b* single mutants had a minor salt-sensitive phenotype with chlorosis spots on the leaves under 200 mM NaCl (Figure 8A and 8E). The *Nt-cipk24b* single mutant was a bit more sensitive to salt stress than the *Nt-cipk24a* single mutant (Figure 8), which is consistent with *NtCIPK24B* having a slightly higher expression level than that of *NtCIPK24A* (analysis from published RNA-seq data, Figure S7). However, we did not find a significant difference in stomatal conductance, chlorophyll fluorescence, and ion contents between WT and *Nt-cipk24* single mutants under 200 mM NaCl (Figure S8). This may be because of functional redundancy between *NtCIPK24A* and *NtCIPK24B* in the salt stress response of tobacco.

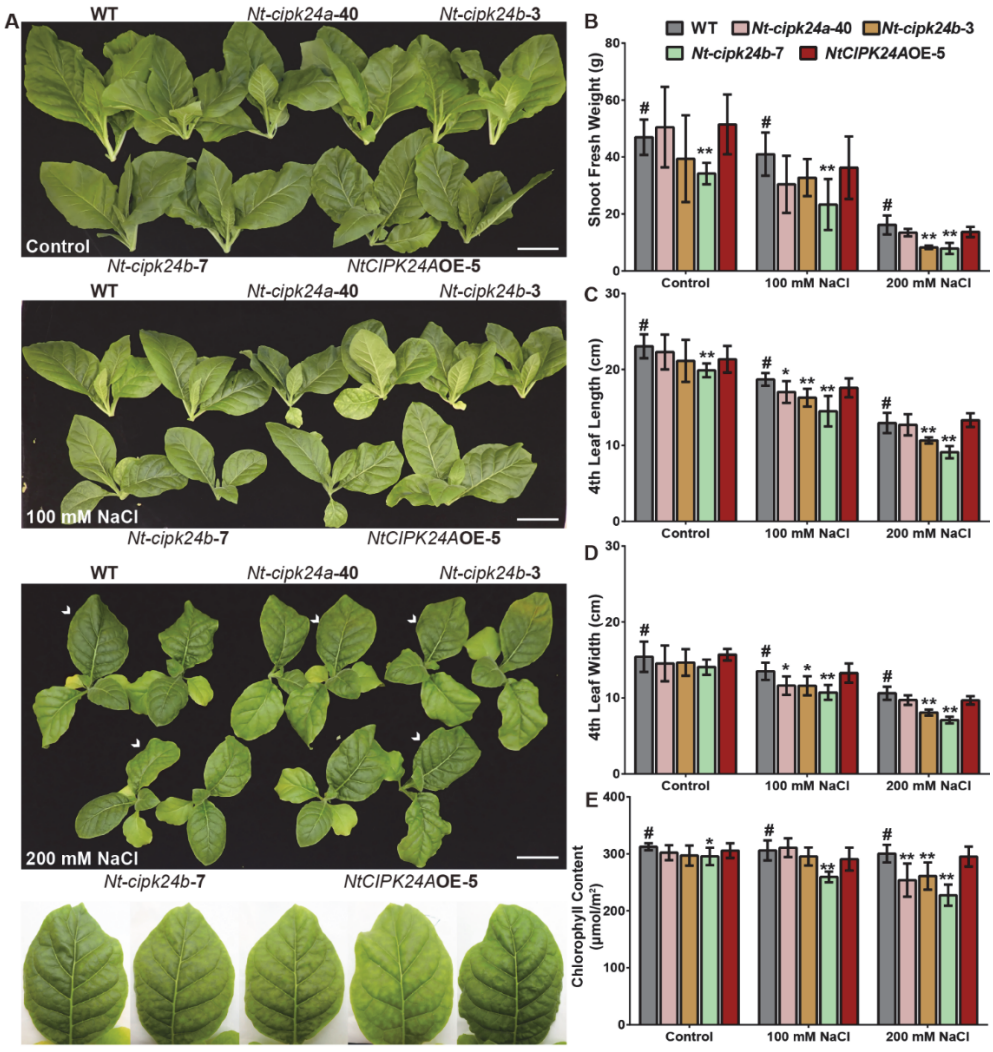

Figure 8. The shoot phenotype and physiological parameters of wild-type (WT), *Nt-cipk24a* single mutant, *Nt-cipk24b* single mutant, and *NtCIPK24A*-overexpressing (OE) line (OE-5) under control conditions and salt stress (100 mM and 200 mM NaCl). Scale bars=10 cm. **(A)** The shoot phenotype of WT, *Nt-cipk24a* single mutant, *Nt-cipk24b* single mutant, and *NtCIPK24A*-OE line at 13 DAT (days after reaching 100 mM NaCl treatment). White arrowheads indicate the 4th leaves which were zoomed in at the bottom part of the panel. **(B-E)** The shoot fresh weight, 4th leaf length, 4th leaf width, and **c**hlorophyll content of all lines. Error bars indicate ±SD (n=6). Asterisks indicate statistically significant differences compared with WT (#) under control or saline conditions (Student's *t* test, **p*<0.05 and ***p*<0.01).

DISCUSSION

Members of the *CBL* gene family play important roles in stress response of plants, and very often are involved in the regulation of ion homeostasis (Mao et al., 2022). The severe salt stress-sensitive necrotic phenotype of tobacco plants ectopically overexpressing *NtCBL4A-1* and *NtCBL5A* led us to propose that *NtCBL4A-1* and *NtCBL5A* might affect essential salt stress signaling pathways and the salt stress response, possibly by interfering with the function of other CBL family members (Chapter 3 and 4). In this study, we demonstrate that NtCBL10 is a potential candidate that can bind the same CIPK partner (NtCIPK24A) as NtCBL4A-1 and NtCBL5A. Knocking out *NtCBL10* in tobacco results in an even more severe salt-sensitive phenotype that includes very fast-developing chlorosis in addition to necrotic symptoms. The early breakdown of chlorophyll along with fast-reduced PhiPS2 suggests a direct devastating effect on photosynthetic components in the *Nt-cbl10acbl10b* double mutant. Our results show that *NtCBL10* is of pivotal importance to the salt tolerance of tobacco, and that *NtCBL10* may be involved in the regulation of several essential salt stress response pathways.

In this study, the *Nt-cbl10acbl10b* double mutant exhibited a phenotype with both chlorosis and necrosis under salt stress in the light, while it only exhibited the chlorosis symptom under salt stress in the dark. These results indicate that the chlorosis phenotype is light-independent and the necrosis phenotype is light-dependent, and these two kinds of phenotype may be caused by different disturbed pathways because of the loss of *NtCBL10*. A possible explanation for this may be linked to the wide range of regulatory functions that *CBL10* appears to have in response to salt stress. In *Arabidopsis*, AtCBL10 was found to regulate not only Na^+ transport, but also H^+, K^+, and Ca^{2+} transport through both CIPK-dependent and CIPK-independent pathways (Plasencia et al., 2020).

The light-dependent necrotic phenotype of *Nt-cbl10acbl10b* and Na^+ homeostasis as well as Cl^- homeostasis

A dark treatment was conducted on *NtCBL5A*-OE lines as well, and the results

showed that their necrotic phenotype is also light-dependent (Figure 9), which is similar to the necrosis observed in the *Nt-cbl10acbl10b* double mutant. However, the light-independent fast-developing chlorosis phenotype appears to be unique to the *Nt-cbl10acbl10b* double mutant. These results indicate that the ectopic overexpression of *NtCBL5A* may only interfere with the *NtCBL10* activities that protect against necrosis under saline conditions.

A role for CBL10 together with CIPK24 in regulating Na^+ transport over the tonoplast was proposed in *Arabidopsis* (Kim et al., 2007). It was suggested that the tonoplast-localized CBL10-CIPK24 complex regulates Na^+ sequestration into the vacuole through the vacuolar NHX transporter, which was initially thought to be a Na^+/H^+ antiporter (Kim et al., 2007). However, there is some controversy regarding the function of the vacuolar NHX transport activity, and other Na^+ transporters may be involved (Plasencia et al., 2020).

The fact that tonoplast-targeted regulation of Na^+ transport by CBL10 under saline conditions requires association with CIPK24 may explain why overexpression of *NtCBL4A-1* and *NtCBL5A* resulted in necrosis but not extensive chlorosis as observed in the *Nt-cbl10acbl10* double mutant: when ectopically expressed, NtCBL4A-1 and NtCBL5A may compete with NtCBL10 for NtCIPK24 binding, thus negatively affecting the CBL10-CIPK24-regulated Na^+ sequestration in the vacuole specifically. This hypothesis is supported by two observations: (1) the *NtCBL4A-1*-OE::*NtCBL5A*-OE hybrid plants had more severe salt sensitivity than WT:: *NtCBL5A*-OE hybrid plants, indicating *NtCBL4A-1* overexpression may interfere with the same component as *NtCBL5A* overexpression. (2) *NtCBL10A* overexpression was able to partly reverse the salt-sensitive phenotype caused by overexpression of *NtCBL5A* in a *NtCBL10A*-OE::*NtCBL5A*-OE hybrid plant with more moderate salt sensitivity than WT:: *NtCBL5A*-OE hybrid plants.

The initial increase in whole leaf Na^+ content of the *Nt-cbl10acbl10b* double mutant was shown to be quite similar to that of WT plants (Figure 6E). However, WT plants can store excess Na^+ in the vacuole. If Na^+ is not transported to the vacuole in the

Nt-cbl10acbl10b double mutant, Na^+ will accumulate to toxic levels in the cytosol much faster, and this can cause necrotic symptoms. In recent years, it has become evident that CBL10 also affectes Na^+ transport over the plasma membrane as part of the SOS pathway (Plasencia et al, 2021). AtCBL10-AtCIPK8 and AtCBL10-AtCIPK24 modules appear to be able to interact with SOS1 activity of extruding Na^+ into the apoplast (Quan et al., 2007; Lin et al., 2009; Yin et al., 2019). In the *Nt-cbl10acbl10b* double mutant, the loss of this Na^+ extruding activity would also contribute to a higher relative Na^+ concentration in the cytosol. The lack of necrotic symptoms under a dark treatment may then be explained by the significantly lower leaf Na^+ accumulation rate of leaves in the dark (Figure 7D).

The *Nt-cbl10acbl10b* double mutant also accumulated significantly less Cl^- under salt stress compared to WT (Figure 5H and 6F), indicating that *NtCBL10* is also involved in Cl^- homeostasis. To our knowledge, there is no report about the role of *CBL10* in Cl^- homeostasis regulation. Geilfus (2018) suggested that the disturbance of chloroplastidial Cl^- homeostasis might affect the generation of the pH gradient between the lumen and stroma under Cl^- salinity via an unbalancing of the proton-counterbalancing fluxes of Cl^-, which would lead to the reduction of PSⅡ, but this has not been experimentally confirmed. In the dark treatment, the reduced rate of Cl^- accumulation in the *Nt-cbl10acbl10b* double mutant compared to WT under salt stress was reversed (Figure 7E), which is also consistent with the disappearance of the necrotic phenotype in the dark. But whether the difference in Cl^- handling is functionally related to the necrotic symptoms remains to be established.

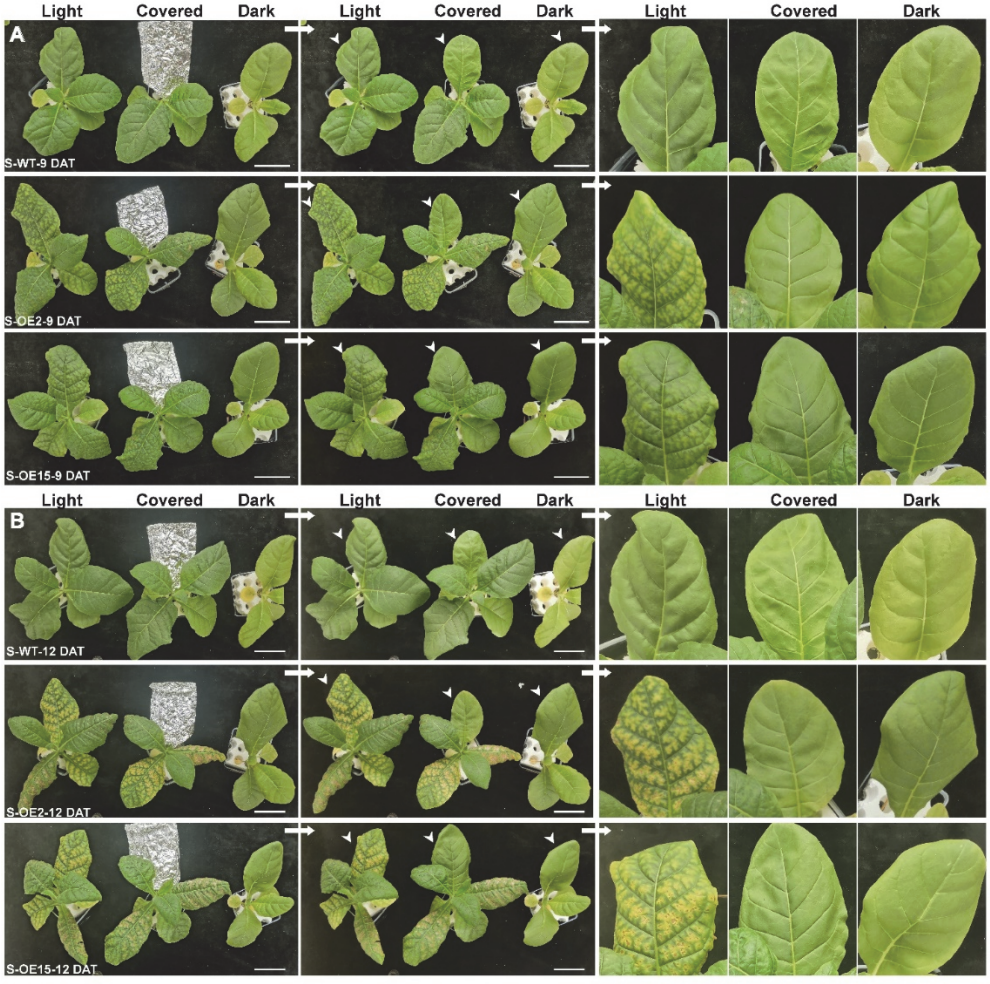

Figure 9. Shoot phenotype of wild-type (WT) and *NtCBL5A*-overexpressing lines (OE-2 and OE-15) under salt stress (100 mM NaCl) in the dark treatment. Scale bars=10 cm. **(A)** The phenotype of WT and *NtCBL5A*-OE lines under salt stress (S) at 9 DAT (days after reaching 100 mM NaCl treatment). **(B)** The phenotype of WT and *NtCBL5A*-OE lines under salt stress at 12 DAT. White arrowheads indicate the 4th leaves under light (Light), covered by aluminum-foil paper (Covered), and under dark (Dark), which were zoomed in at the right part of the panel.

The light-independent chlorotic phenotype of *Nt-cbl10acbl10b* double mutant and other regulatory functions of *CBL10*

The chlorotic symptoms in the *Nt-cbl10acbl10b* double mutant developed much

faster than in the *NtCBL4A-1* and *NtCBL5A*-overexpressing lines. Moreover, the chlorotic symptoms of the *Nt-cbl10acbl10b* double mutant were observed both under light and dark conditions, while the necrosis was no longer visible under dark conditions. This indicates that the fast-developing chlorosis of the *Nt-cbl10acbl10b* double mutant under salt stress may be linked to another impaired function of *NtCBL10* than the one linked to necrosis.

The chlorotic symptoms in the *Nt-cbl10acbl10b* double mutant were already detected within 24 hrs of reaching the final NaCl concentration of 100mM NaCl (Figure 6A and 7A). Both chlorophyll content and photochemical efficiency of photosystem 2 (PhiPS2) were also decreased by this time, and decreased further in the next few days (Figure 6B and 6D). This suggests that chlorophyll and possibly other components of the photosynthetic machinery were directly affected by the saline conditions in the *Nt-cbl10acbl10b* double mutant, and that *NtCBL10* may play an essential role in protecting chlorophyll and photosynthetic capacity already at very early stages of salt stress.

Although we cannot rule out a role for cytosolic Na^+ accumulation in the development of the chlorotic symptoms, the low rate of leaf Na^+ concentration increase in the *Nt-cbl10acbl10b* double mutant grown in the dark while chlorotic symptoms still developed very fast suggests that Na^+ accumulation itself is not causal to the chlorosis and fast breakdown of chlorophyll. As mentioned before, *CBL10* was shown to be involved in the regulation of the transport and distribution of several ions under salt stress, including not only Na^+ but also H^+, K^+, and Ca^{2+} (Plasencia et al., 2020). This leads to the possibility that the effect of the *Nt-cbl10acbl10b* double mutant on photosynthetic components and parameters is linked to other regulatory functions of *CBL10*.

Other targets for CBL10 regulation of the salt stress response may be the H^+ transporters in the tonoplast. In a tomato *Sl-cbl10* mutant, the gene expression of the vacuolar H^+ pumps *SlAVP1* and *SlVHA-A1* was downregulated under saline conditions (Egea et al., 2018). These are thought to provide the proton gradient over

the tonoplast that drives the Na^+ transport into the vacuole. In addition, AtCBL10 was suggested to regulate plasma membrane H^+-ATpase activity in *Arabidopsis thaliana* in a CIPK-independent manner, directly interacting with plasma membrane H^+-ATPases AtAHA4 and AtAHA11 (Xie et al., 2022). Proton pumps in the tonoplast and plasma membrane need to be tuned and are under strict regulation to ensure a balanced pH in the cytosol, which may also involve the NHX family of antiporters (Cosse and Seidel, 2021). Impaired regulation of the H^+ pumps may result in impaired H^+ homeostasis and pH regulation, which can be highly damaging to the leaf cell functioning, and induce chlorophyll breakdown (Long et al., 2017). Whether impaired pH regulation is causal to the fast-developing chlorosis in the *Nt-cbl10acbl10b* double mutant under salt stress remains to be established.

CBL10 also functions as a repressor by directly interacting with targets in a CIPK-independent way. AtCBL10 was reported to competitively interact with AKT1 against the AtCBL1/9-AtCIPK23 complex, repressing the potassium uptake regulated by AtCBL1/9-AtCIPK23 (Ren et al., 2013). Our results also showed the K^+ accumulation in *Nt-cbl10acbl10b* double mutant was affected under salt stress compared to WT (Figure 5I and 6G). At the very early stage of salt treatment (0-3 DAT), the K^+ accumulation in the double mutant is significantly lower than that in WT but the difference is decreasing with time (Figure 6G). At 5 DAT and 7 DAT, our data showed a higher K^+ accumulation in *Nt-cbl10acbl10b* double mutant than that in WT (Figure 5I and 6G). The Na^+/K^+ ratios in WT and *Nt-cbl10acbl10b* are always similar during 0-5 DAT (Figure S5E). These results showed that the K^+ homeostasis affected by the loss of *NtCBL10* is changing with time and is complicated, which may rather be a consequence than a cause of salt sensitivity.

Interestingly, CBL10 was also found to directly interact with and repress TOC34 protein, a member of the TOC (translocon of the outer membrane of the chloroplasts) complex with GTPase activity to regulate protein importation into chloroplasts (Cho et al., 2016). The interaction between CBL10 and chloroplast-localized protein seems also linked to the chlorophyll breakdown and PS Ⅱ defect in *NtCBL10* loss-of-function mutants but needs more research to provide the evidence.

REFERENCES

Bruggeman, Q., Raynaud, C., Benhamed, M., and Delarue, M. To die or not to die? Lessons from lesion mimic mutants. *Front Plant Sci*. **2015**, *6*, 24.

Cho, J. H., Lee, J. H., Park, Y. K., Choi, M. N., and Kim, K. N. Calcineurin B-like protein CBL10 directly interacts with TOC34 (translocon of the outer membrane of the chloroplasts) and decreases its GTPase activity in Arabidopsis. *Front Plant Sci*. **2016**, *7*, 1911.

Cho, J. H., Sim, S. C., and Kim, K. N. Calcium sensor SlCBL4 associates with SlCIPK24 protein kinase and mediates salt tolerance in *Solanum lycopersicum*. *Plants (Basel)*. **2021**, *10*, 2173.

Cosse, M., and Seidel, T. Plant proton pumps and cytosolic pH-homeostasis. *Front Plant Sci*. **2021**, *12*, 672873.

Egea, I., Pineda, B., Ortiz-Atienza, A., Plasencia, F. A., Drevensek, S., Garcia-Sogo, B., Yuste-Lisbona, F. J., Barrero-Gil, J., Atares, A., Flores, F. B., Barneche, F., Angosto, T., Capel, C., Salinas, J., Vriezen, W., Esch, E., Bowler, C., Bolarin, M. C., Moreno, V., and Lozano, R. The SlCBL10 calcineurin B-like protein ensures plant growth under salt stress by regulating Na^+ and Ca^{2+} homeostasis. *Plant Physiol*. **2018**, *176*, 1676-1693.

Geilfus, C. M. Chloride: from nutrient to toxicant. *Plant Cell Physiol*. **2018**, *59*, 877-886.

Graus, D., Li, K., Rathje, J. M., Ding, M., Krischke, M., Muller, M. J., Cuin, T. A., Al-Rasheid, K. A. S., Scherzer, S., Marten, I., Konrad, K. R., and Hedrich, R. Tobacco leaf tissue rapidly detoxifies direct salt loads without activation of calcium and SOS signaling. *New Phytol*. **2023**, *237*, 217-231.

Horsch, R. B., Fry, J. E., Hoffmann, N. L., Eichholtz, D., Rogers, S. G., and Fraley, R. T. A simple and general method for transferring genes into plants. *Science*. **1985**, *227*, 1229-1231.

Hu, D. G., Li, M., Luo, H., Dong, Q. L., Yao, Y. X., You, C. X., and Hao, Y. J. Molecular cloning and functional characterization of MdSOS2 reveals its involvement in salt tolerance in apple callus and *Arabidopsis*. *Plant Cell Rep*. **2012**, *31*, 713-722.

Kim, B.-G., Waadt, R., Cheong, Y. H., Pandey, G. K., Dominguez-Solis, J. R., Schültke, S., Lee, S. C., Kudla, J., and Luan, S. The calcium sensor CBL10 mediates salt tolerance by regulating ion homeostasis in *Arabidopsis*. *Plant J*. **2007**, *52*, 473-484.

Li, B., shang, Y., Wang, L., Lv, J., Wang, F., Chao, J., Mao, J., Ding, A., Wu, X., Cui, M., Sun, Y., and Dai, C. Highly efficient multiplex genome editing in dicots using improved CRISPR/Cas systems. *bioRxiv* **2022**.

Li, W., Zhang, H., Li, X., Zhang, F., Liu, C., Du, Y., Gao, X., Zhang, Z., Zhang, X., Hou, Z., Zhou, H., Sheng, X., Wang, G., and Guo, Y. Intergrative metabolomic and transcriptomic analyses unveil nutrient remobilization events in leaf senescence of tobacco. *Sci Rep*. **2017**, *7*, 12126.

Lin, H. X., Yang, Y. Q., Quan, R. D., Mendoza, I., Wu, Y. S., Du, W. M., Zhao, S. S., Schumaker, K. S., Pardo, J. M., and Guo, Y. Phosphorylation of SOS3-LIKE CALCIUM BINDING PROTEIN8 by SOS2

protein kinase stabilizes their protein complex and regulates salt tolerance in *Arabidopsis*. *Plant Cell*. **2009**, *21*, 1607-1619.

Liu, W. Z., Deng, M., Li, L., Yang, B., Li, H., Deng, H., and Jiang, Y. Q. Rapeseed calcineurin B-like protein CBL4, interacting with CBL-interacting protein kinase CIPK24, modulates salt tolerance in plants. *Biochem Biophys Res Commun*. **2015**, *467*, 467-471.

Long, A., Zhang, J., Yang, L. T., Ye, X., Lai, N. W., Tan, L. L., Lin, D., and Chen, L. S. Effects of low pH on photosynthesis, related physiological parameters, and nutrient profiles of citrus. *Front Plant Sci*. **2017**, *8*, 185.

Mao, J., Mo, Z., Yuan, G., Xiang, H., Visser, R. G. F., Bai, Y., Liu, H., Wang, Q., and Linden, C. G. v. d. The CBL-CIPK network is involved in the physiological crosstalk between plant growth and stress adaptation. *Plant Cell Environ*. **2022**.

Mao, J., Yuan, J., Mo, Z., An, L., Shi, S., Visser, R. G. F., Bai, Y., Sun, Y., Liu, G., Liu, H., Wang, Q., and van der Linden, C. G. Overexpression of *NtCBL5A* leads to necrotic lesions by enhancing Na^+ sensitivity of tobacco leaves under salt stress. *Front Plant Sci*. **2021**, *12*, 740976.

Martinez-Atienza, J., Jiang, X., Garciadeblas, B., Mendoza, I., Zhu, J. K., Pardo, J. M., and Quintero, F. J. Conservation of the salt overly sensitive pathway in rice. *Plant Physiol*. **2007**, *143*, 1001-1012.

Masaló, I., and Oca, J. Evaluation of a portable chlorophyll optical meter to estimate chlorophyll concentration in the green seaweed Ulva ohnoi. *J Appl Phycol*. **2020**, *32*, 4171-4174.

Mehla, J., Caufield, J. H., and Uetz, P. Mapping protein-protein interactions using yeast two-hybrid assays. *Cold Spring Harb Protoc*. **2015**, *2015*, 442-452.

Mehra, P., and Bennett, M. J. A novel Ca^{2+} sensor switch for elevated salt tolerance in plants. *Dev Cell*. **2022**, *57*, 2045-2047.

Nunez-Ramirez, R., Sanchez-Barrena, M. J., Villalta, I., Vega, J. F., Pardo, J. M., Quintero, F. J., Martinez-Salazar, J., and Albert, A. Structural insights on the plant salt-overly-sensitive 1 (SOS1) Na^+/H^+ antiporter. *J Mol Biol*. **2012**, *424*, 283-294.

Plasencia, F. A., Estrada, Y., Flores, F. B., Ortiz-Atienza, A., Lozano, R., and Egea, I. The Ca^{2+} sensor calcineurin B-Like protein 10 in plants: emerging new crucial roles for plant abiotic stress tolerance. *Front Plant Sci*. **2020**, *11*, 599944.

Prelich, G. Gene overexpression: uses, mechanisms, and interpretation. *Genetics*. **2012**, *190*, 841-854.

Price, E. Measuring stomatal conductance and chlorophyll fluorescence with the new LI-600 porometer/fluorometer. ASHS Annual Conference, ASHS. **2021**.

Qin, Y., Bai, S., Li, W., Sun, T., Galbraith, D. W., Yang, Z., Zhou, Y., Sun, G., and Wang, B. Transcriptome analysis reveals key genes involved in the regulation of nicotine biosynthesis at early time points after topping in tobacco (*Nicotiana tabacum* L.). *BMC Plant Biol*. **2020**, *20*, 1-15.

Qiu, Q.-S., Guo, Y., Dietrich, M. A., Schumaker, K. S., and Zhu, J.-K. Regulation of SOS1, a plasma membrane Na^+/H^+ exchanger in *Arabidopsis thaliana*, by SOS2 and SOS3. *Proc Natl Acad Sci U S*

A. **2002**, *99*, 8436-8441.

Quan, R., Lin, H., Mendoza, I., Zhang, Y., Cao, W., Yang, Y., Shang, M., Chen, S., Pardo, J. M., and Guo, Y. SCABP8/CBL10, a putative calcium sensor, interacts with the protein kinase SOS2 to protect *Arabidopsis* shoots from salt stress. *Plant Cell*. **2007**, *19*, 1415-1431.

Ren, X. L., Qi, G. N., Feng, H. Q., Zhao, S., Zhao, S. S., Wang, Y., and Wu, W. H. Calcineurin B-like protein CBL10 directly interacts with AKT1 and modulates K^+ homeostasis in Arabidopsis. *Plant J*. **2013**, *74*, 258-266.

Schmidt, G. W., and Delaney, S. K. Stable internal reference genes for normalization of real-time RT-PCR in tobacco (*Nicotiana tabacum*) during development and abiotic stress. *Mol Genet Genomics*. **2010**, *283*, 233-241.

Shi, H., Quintero, F. J., Pardo, J. M., and Zhu, J.-K. The putative plasma membrane Na^+/H^+ antiporter SOS1 controls long-distance Na^+ transport in plants. *Plant Cell*. **2002**, *14*, 465-477.

Shi, S. J., An, L. L., Mao, J. J., Aluko, O. O., Ullah, Z., Xu, F. Z., Liu, G. S., Liu, H. B., and Wang, Q. The CBL-interacting protein kinase NtCIPK23 positively regulates seed germination and early seedling development in tobacco (*Nicotiana tabacum* L.). *Plants (Basel)*. **2021**, *10*, 323.

Steinhorst, L., He, G., Moore, L. K., Schultke, S., Schmitz-Thom, I., Cao, Y., Hashimoto, K., Andres, Z., Piepenburg, K., Ragel, P., Behera, S., Almutairi, B. O., Batistic, O., Wyganowski, T., Koster, P., Edel, K. H., Zhang, C., Krebs, M., Jiang, C., Guo, Y., Quintero, F. J., Bock, R., and Kudla, J. A Ca^{2+}-sensor switch for tolerance to elevated salt stress in Arabidopsis. *Dev Cell*. **2022**, *57*, 2081-2094 e2087.

Tang, R. J., Liu, H., Bao, Y., Lv, Q. D., Yang, L., and Zhang, H. X. The woody plant poplar has a functionally conserved salt overly sensitive pathway in response to salinity stress. *Plant Mol Biol*. **2010**, *74*, 367-380.

Tang, Y., Gao, C. C., Gao, Y., Yang, Y., Shi, B., Yu, J. L., Lyu, C., Sun, B. F., Wang, H. L., Xu, Y., Yang, Y. G., and Chong, K. OsNSUN2-mediated 5-methylcytosine mRNA modification enhances rice adaptation to high temperature. *Dev Cell*. **2020**, *53*, 272-286.

Wang, J., Ye, B. Q., Yin, J. J., Yuan, C., Zhou, X. G., Li, W. T., He, M., Wang, J. C., Chen, W. L., Qin, P., Ma, B. T., Wang, Y. P., Li, S. G., and Chen, X. W. Characterization and fine mapping of a light-dependent *leaf lesion mimic mutant 1* in rice. *Plant Physiol Biochem*. **2015**, *97*, 44-51.

Xie, Q., Yang, Y., Wang, Y., Pan, C., Hong, S., Wu, Z., Song, J., Zhou, Y., and Jiang, X. The calcium sensor CBL10 negatively regulates plasma membrane H^+-ATPase activity and alkaline stress response in *Arabidopsis*. *Environ Exp Bot*. **2022**, *194*, 104752.

Yin, X., Xia, Y., Xie, Q., Cao, Y., Wang, Z., Hao, G., Song, J., Zhou, Y., and Jiang, X. The protein kinase complex CBL10-CIPK8-SOS1 functions in *Arabidopsis* to regulate salt tolerance. *J Exp Bot*. **2019**, 1801-1814.

Zhang, Y., Linghu, J., Wang, D., Liu, X., Yu, A., Li, F., Zhao, J., and Zhao, T. *Foxtail Millet* CBL4 (SiCBL4) interacts with SiCIPK24, modulates plant salt stress tolerance. *Plant Mol Biol Rep*. **2017**, *35*, 634-

646.

Zulfugarov, I. S., Tovuu, A., Eu, Y.-J., Dogsom, B., Poudyal, R. S., Nath, K., Hall, M., Banerjee, M., Yoon, U. C., Moon, Y.-H., An, G., Jansson, S., and Lee, C.-H. Production of superoxide from Photosystem II in a rice (*Oryza sativa* L.) mutant lacking PsbS. *BMC Plant Biol*. **2014**, *14*, 1-15.

Supplementary Material

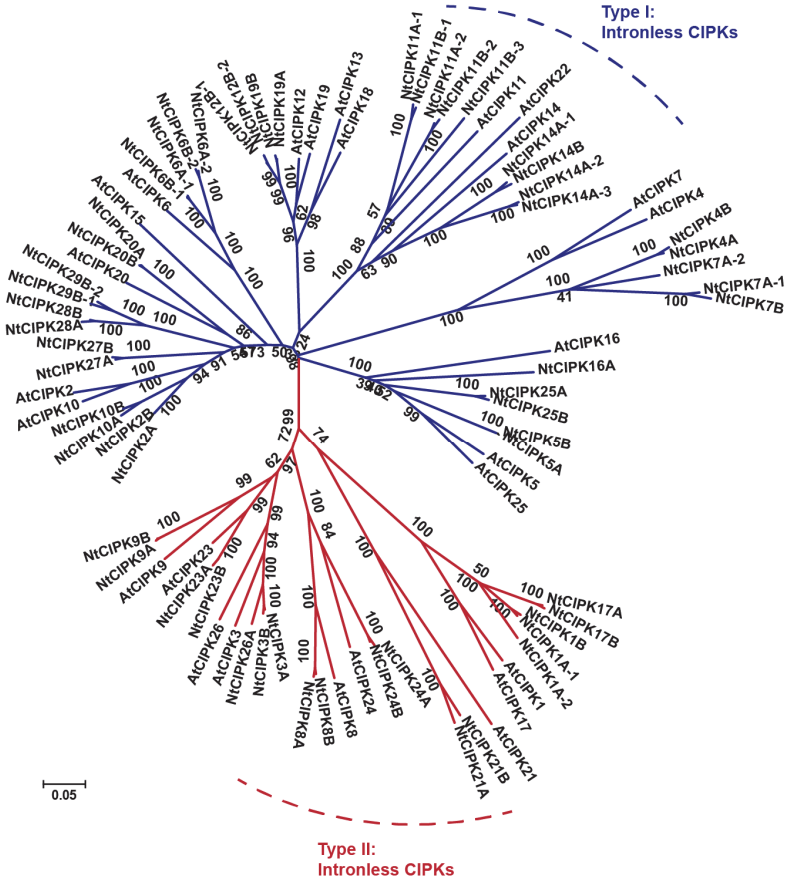

Figure S1. Phylogenetic tree of the NtCIPKs and AtCIPKs. The amino acid sequences of AtCIPKs were downloaded from TAIR (https://www.arabidopsis.org/). The phylogenetic tree was constructed by MEGA6 using the Neighbor-Joining method.

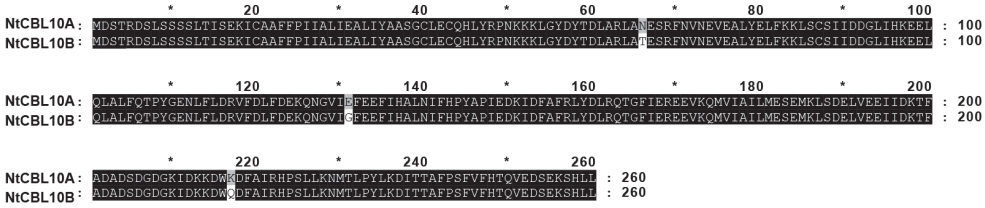

Figure S2. The protein sequence alignment of NtCBL10A and NtCBL10B.

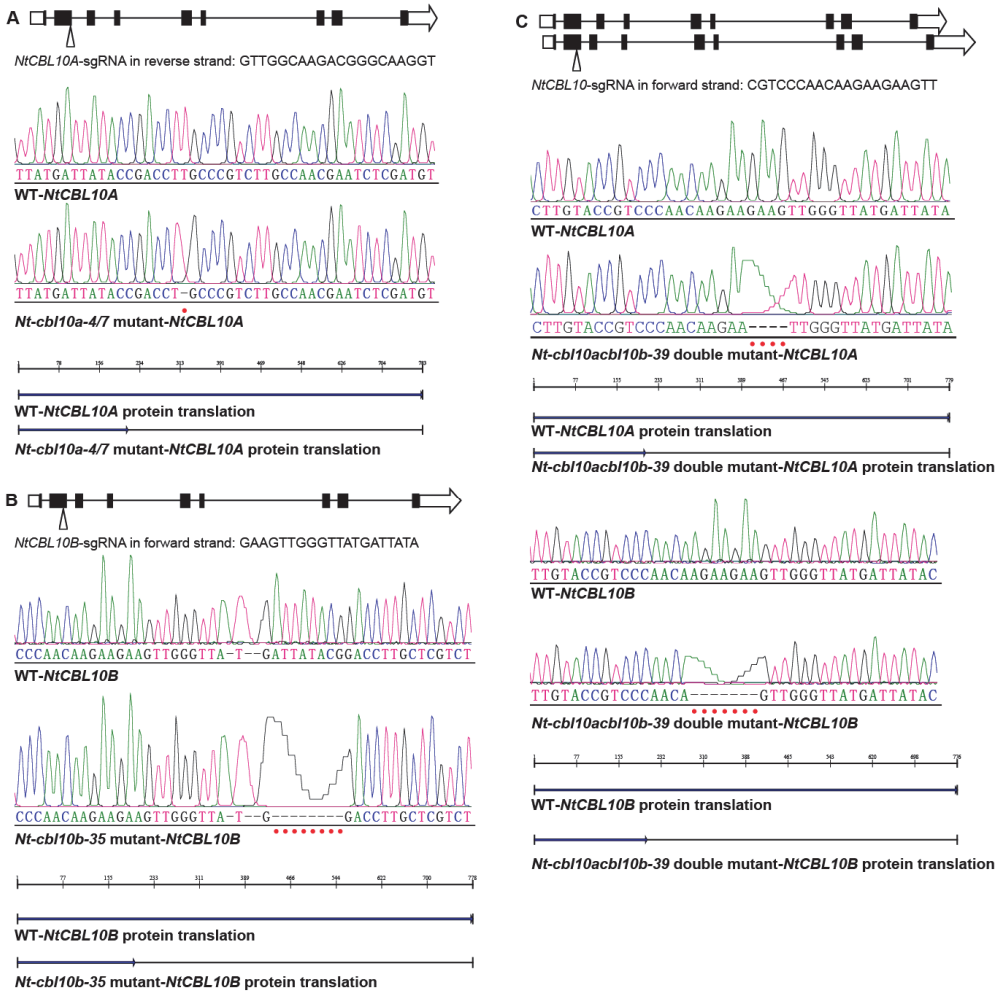

Figure S3. The position of gRNA, edited sequence, and protein translation of the edited sequence of *Nt-cbl10a* single mutant (A), *Nt-cbl10b* single mutant (B), and *Nt-cbl10acbl10b* double mutant (C).

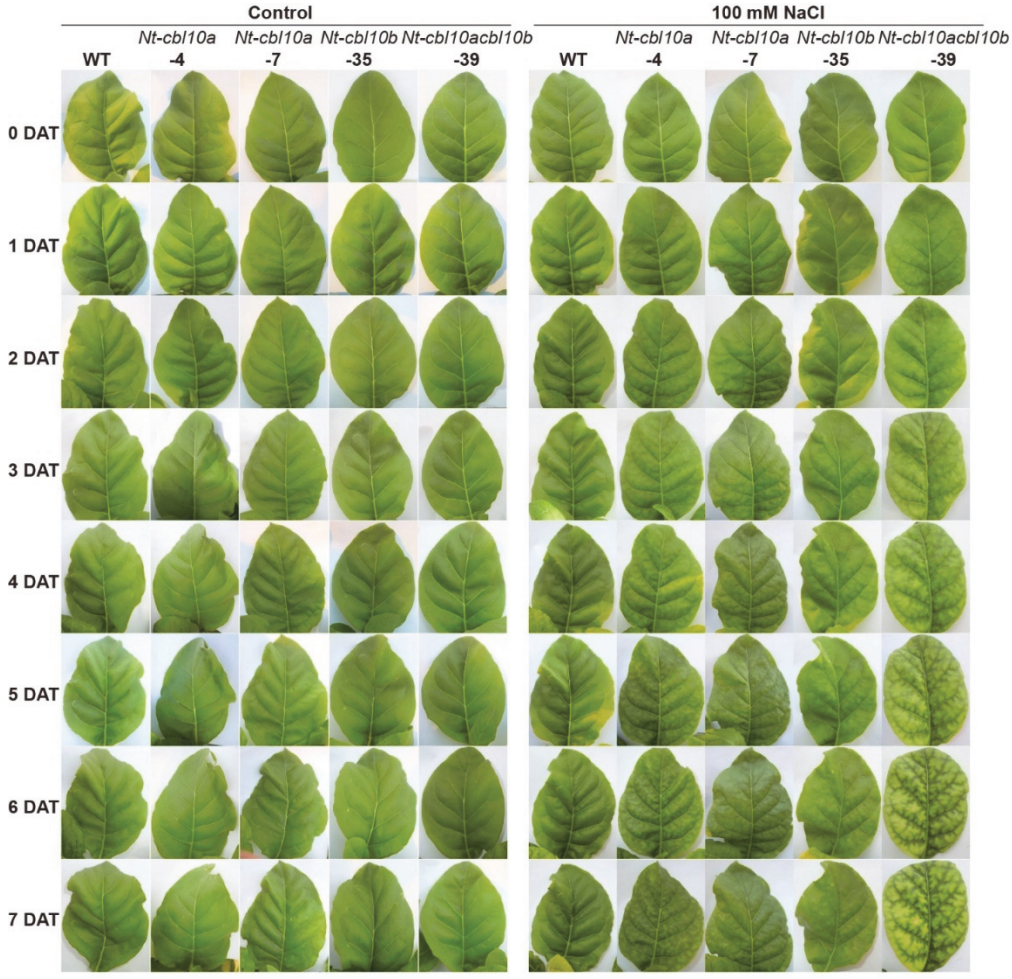

Figure S4. The phenotype of WT and *Nt-cbl10acbl10b* double mutants under salt stress on different days after treatment (DAT).

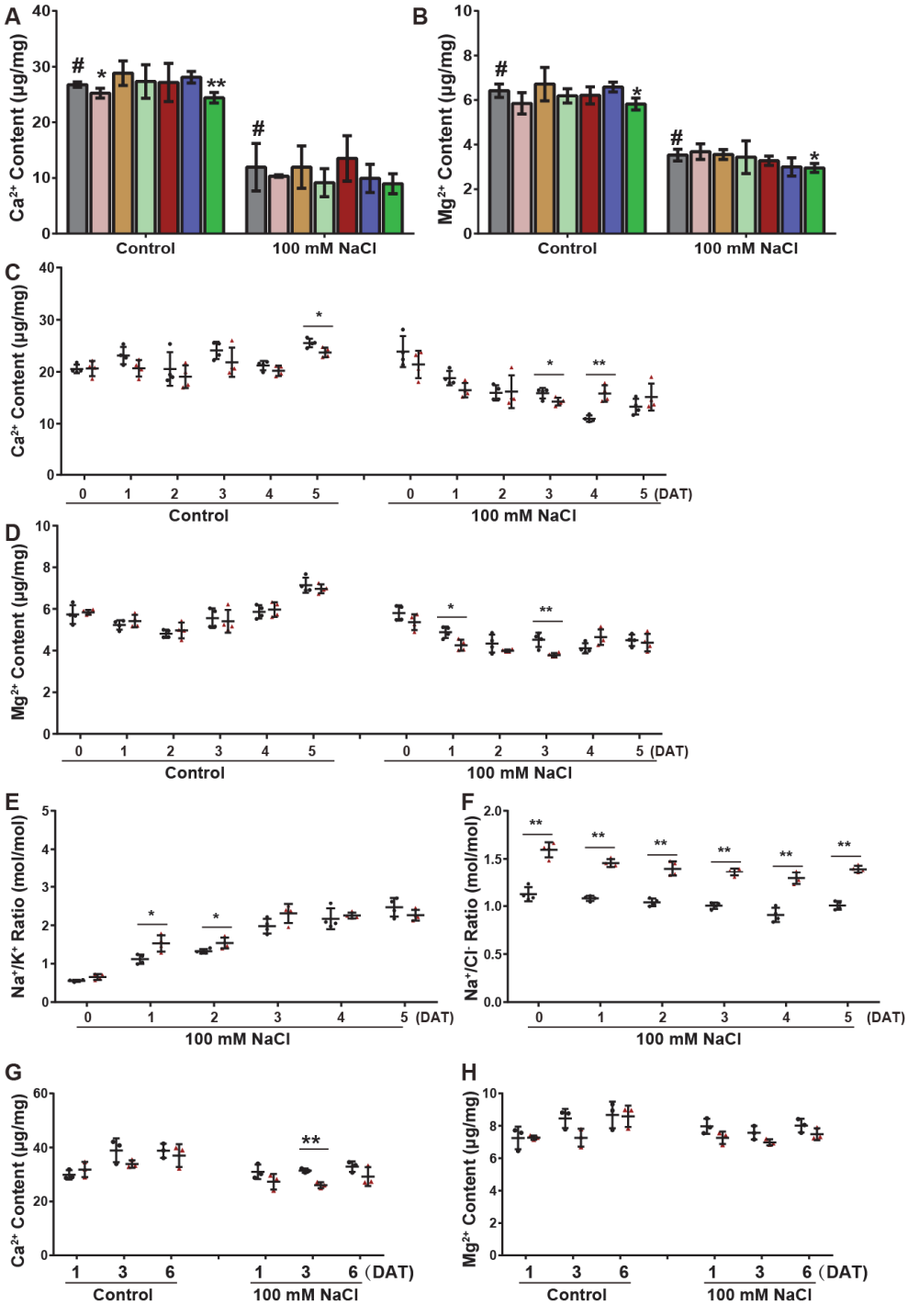
A
Ca2+ Content (μg/mg)
Control
100 mM NaCl
B
Mg2+ Content (μg/mg)
Control
100 mM NaCl
C
Ca2+ Content (μg/mg)
Control
100 mM NaCl
(DAT)
D
Mg2+ Content (μg/mg)
Control
100 mM NaCl
(DAT)
E
Na+/K+ Ratio (mol/mol)
100 mM NaCl
(DAT)
F
Na+/Cl- Ratio (mol/mol)
100 mM NaCl
(DAT)
G
Ca2+ Content (μg/mg)
Control
100 mM NaCl
(DAT)
H
Mg2+ Content (μg/mg)
Control
100 mM NaCl
(DAT)

Figure S5. Ca^{2+} and Mg^{2+} contents in leaf blades of plants under control conditions and salt stress (100 mM NaCl). (A and B) Ca^{2+} and Mg^{2+} contents of WT, *Nt-cbl10a*, *Nt-cbl10b* single mutants, *Nt-cbl10acbl10b* double mutant, and *NtCBL10A*-OE lines under control conditions and salt stress (100 mM NaCl) at 7 DAT (days after reaching 100 mM NaCl treatment). Error bars indicate ±SD (n=4). **(C and D)** Ca^{2+} and Mg^{2+} contents in leaf blades of WT and *Nt-cbl10acbl10b* double mutant under control and saline conditions at 0-5 DAT. Error bars indicate ±SD (n=4). **(E and F)** Na^+/K^+ ratio (mol/mol) and Na^+/Cl^- ratio (mol/mol) in WT and *Nt-cbl10acbl10b* double mutant under salt stress at 0-5 DAT. **(G and H)** Ca^{2+} and Mg^{2+} contents in leaf blades of WT and *Nt-cbl10acbl10b* double mutant under control and saline conditions at 1, 3, and 6 DAT in the dark. Error bars indicate ±SD (n=3). Asterisks indicate statistically significant differences compared with WT (#) under control or saline conditions (Student's *t* test, **p*<0.05 and ***p*<0.01).

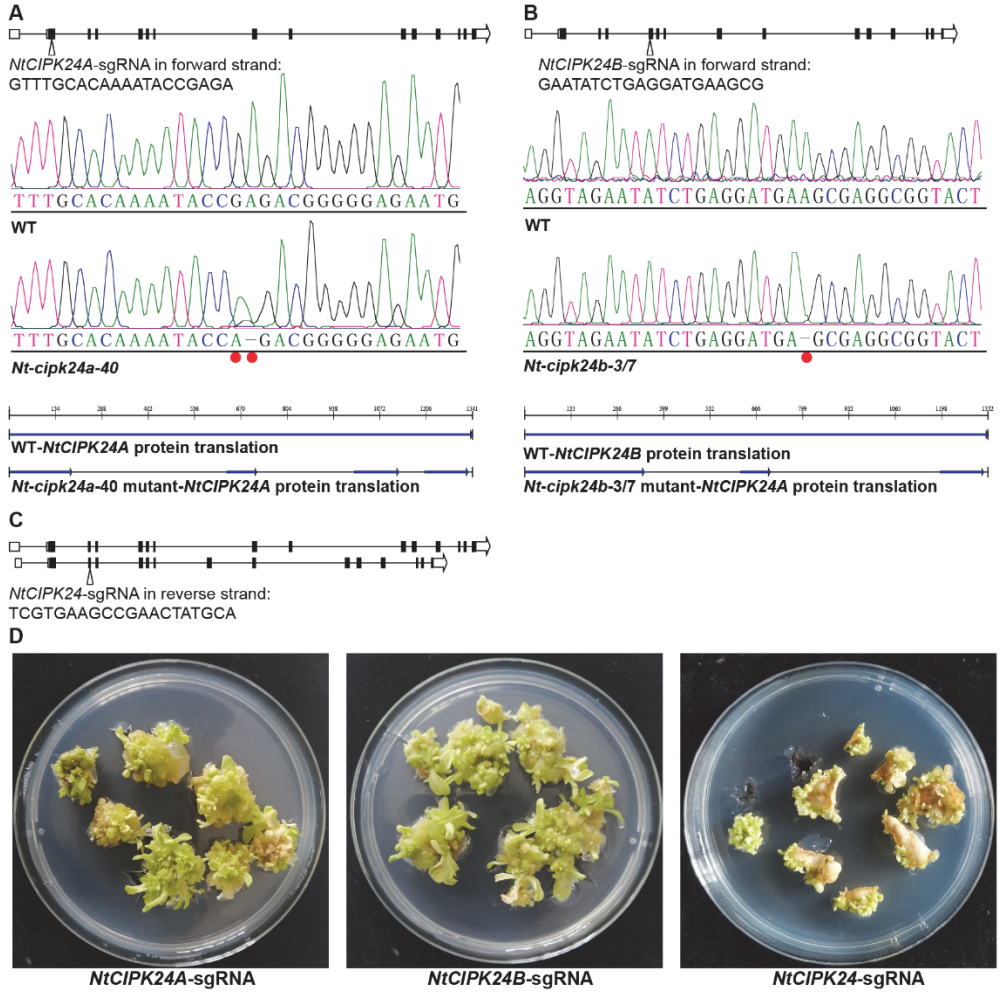

Figure S6. The editing way and tissue culture of *Nt-cipk24* mutants. The sgRNA position, edited sequence, and protein translation of the edited sequence of *Nt-cipk24a*-40 mutant **(A)**, *Nt-cipk24b*-3/7 mutants **(B)**, and *Nt-cipk24acipk24b* double mutant **(C). (D)** The callus vigor with different sgRNA in tissue culture.

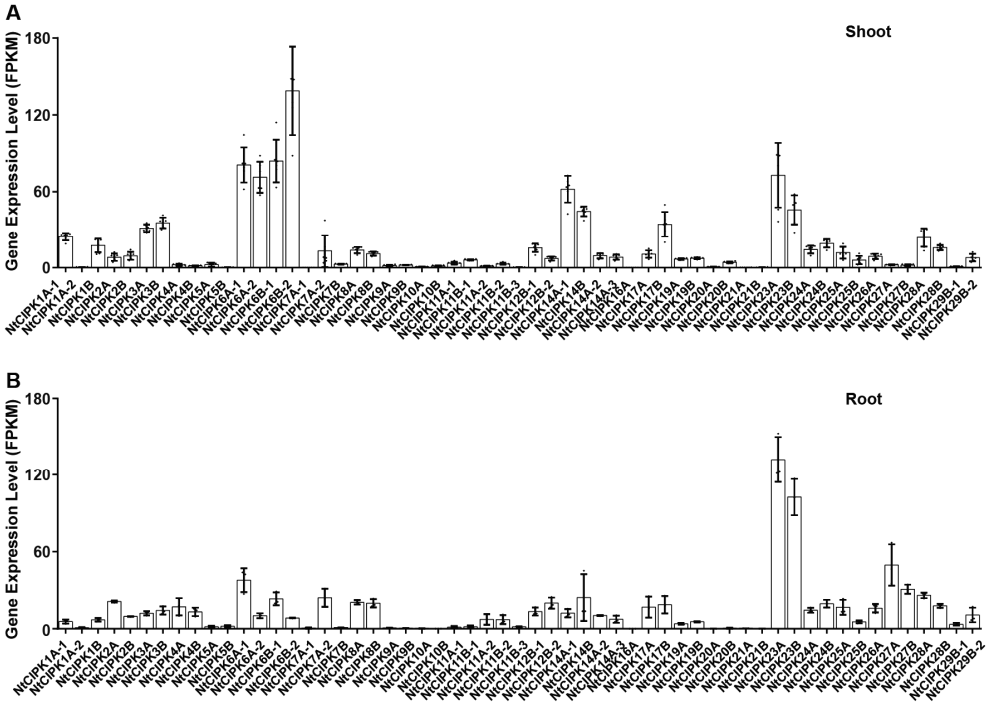

Figure S7. Expression profiles of *NtCIPK* genes in different tissues of tobacco plants at the adult stage. Gene expression level of *NtCIPK* genes in leaves **(A)** (SRA accession ID: SRX2655430, SRX2655478, SRX2655480, SRX2655632, SRX2655633, SRX2655634) and roots **(B)** (SRA accession ID: SRX4407884, SRX4407877, SRX4407878) of tobacco at the adult stage that determined by published RNA-seq data (Li et al., 2017; Qin et al., 2020). The six biological replicates (every two replicates for upper, middle, and lower leaves) of leaves are sampled at 15 days after topping (75 days after transplanting) (Li et al., 2017), while the three biological replicates of roots are sampled at 0 h after topping (56 days after transplanting) (Qin et al., 2020).

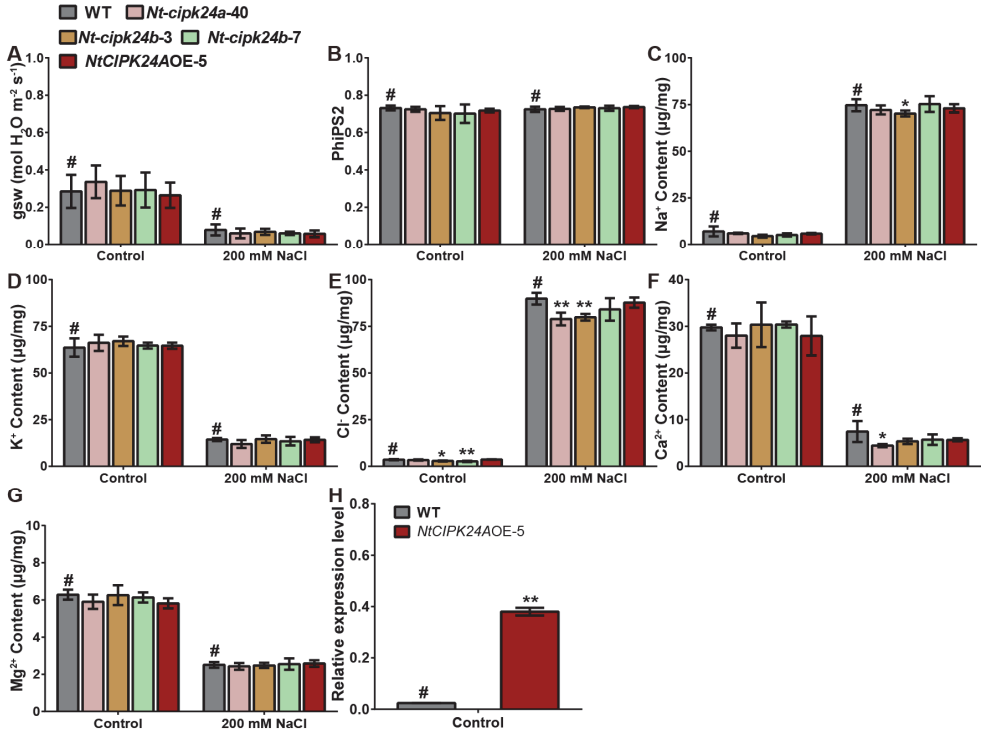

Figure S8. Physiological parameters of wild-type (WT), *Nt-cipk24a* single mutant, *Nt-cipk24b* single mutant, and *NtCIPK24A*-overexpressing (OE) line (OE-5) under control conditions and salt stress (200 mM NaCl) at 8 DAT and the detection of *NtCIPK24A* expression level in WT and *NtCIPK24AOE*-5 leaves. (A and B) The stomatal conductance and chlorophyll fluorescence of all lines at 13 DAT (days after reaching 100 mM NaCl treatment). Error bars indicate ±SD (n=6). **(C-G)** The ion contents **(**Na^+, Cl^-, K^+, Ca^{2+}, and Mg^{2+}) in leaves of all lines at 13 DAT. Error bars indicate ±SD (n=4). (H) The expression level of *NtCIPK24A* (endogenous and exogenous) in WT and *NtCIPK24A*OE-5 plant leaves determined by RT-qPCR. Error bars indicate ±SD (n=3). The expression levels are relative to the reference gene *NtL25* (Schmidt and Delaney, 2010). Asterisks indicate statistically significant differences compared with WT (#) under control or saline conditions (Student's *t* test, **p*<0.05 and ***p*<0.01).

Table S1 Properties of NtCIPKs

Name	Diploid Progenitors	Gene Symbol in NCBI	Representative Protein Accession	AA	NW	p*I*
NtCIPK1A-1	*N. sylvestris*	LOC107821370	XP_016503297.1	454	51226.57	6.45
NtCIPK1A-2	*N. sylvestris*	LOC107827270	XP_016509849.1	450	51004.78	8.78
NtCIPK1B	*N. tomentosiformis*	LOC107802461	XP_016481456.1	454	51260.58	6.40
NtCIPK2A	*N. sylvestris*	LOC107810567	XP_016490846.1	483	54811.93	8.97
NtCIPK2B	*N. tomentosiformis*	LOC107824126	XP_016506349.1	483	55020.19	9.01
NtCIPK3A	*N. sylvestris*	LOC107776926	XP_016452366.1	438	50019.45	8.06
NtCIPK3B	*N. tomentosiformis*	LOC107807209	XP_016487035.1	438	50066.42	7.15
NtCIPK4A	*N. sylvestris*	LOC107803544	XP_016482770.1	450	50397.05	9.17
NtCIPK4B	*N. tomentosiformis*	LOC107782505	XP_016458873.1	439	49161.75	9.15
NtCIPK5A	*N. sylvestris*	LOC107808490	XP_016488508.1	455	52179.35	8.75
NtCIPK5B	*N. tomentosiformis*	LOC107797269	XP_016475627.1	455	52168.33	8.85
NtCIPK6A-1	*N. sylvestris*	LOC107807183	XP_016487006.1	432	48477.30	9.03
NtCIPK6A-2	*N. sylvestris*	LOC107796784	XP_016475078.1	425	47667.16	9.16
NtCIPK6B-1	*N. tomentosiformis*	LOC107769442	XP_016444144.1	432	48523.34	9.03
NtCIPK6B-2	*N. tomentosiformis*	LOC107782385	XP_016458754.1	425	47452.09	9.27
NtCIPK7A-1	*N. sylvestris*	LOC107764765	XP_016438856.1	437	48601.01	9.18
NtCIPK7A-2	*N. sylvestris*	LOC107760209	XP_016433711.1	443	49909.52	9.13
NtCIPK7B	*N. tomentosiformis*	LOC107815522	XP_016496610.1	437	48516.88	9.14
NtCIPK8A	*N. sylvestris*	LOC107780181	XP_016456199.1	454	51223.00	7.61

Name	Diploid Progenitors	Gene Symbol in NCBI	Representative Protein Accession	AA	NW	p*I*
NtCIPK8B	*N. tomentosiformis*	LOC107771583	XP_016446477.1	447	50690.28	6.66
NtCIPK9A	*N. sylvestris*	LOC107783805	XP_016460311.1	446	50760.95	8.92
NtCIPK9B	*N. tomentosiformis*	LOC107826251	XP_016508704.1	446	50689.87	8.70
NtCIPK10A	*N. sylvestris*	LOC107824640	XP_016506926.1	466	53428.65	8.87
NtCIPK10B	*N. tomentosiformis*	LOC107829924	XP_016512882.1	463	52980.05	8.54
NtCIPK11A-1	*N. sylvestris*	LOC107762191	XP_016436014.1	433	49625.59	9.16
NtCIPK11B-1	*N. tomentosiformis*	LOC107831457	XP_016514707.1	430	49200.03	8.74
NtCIPK11A-2	*N. sylvestris*	LOC107824639	XP_016506925.1	441	50349.43	8.54
NtCIPK11B-2	*N. tomentosiformis*	LOC107829925	XP_016512883.1	441	50309.43	8.66
NtCIPK11B-3	*N. tomentosiformis*	LOC107762565	XP_016436426.1	413	47348.67	8.47
NtCIPK12B-1	*N. tomentosiformis*	LOC107781785	XP_016458041.1	479	53995.97	8.71
NtCIPK12B-2	*N. tomentosiformis*	LOC107802445	XP_016481439.1	479	54064.09	8.71
NtCIPK14A-1	*N. sylvestris*	LOC107782101	XP_016458427.1	449	50474.71	7.12
NtCIPK14B	*N. tomentosiformis*	LOC107796817	XP_016475123.1	449	50653.05	6.74
NtCIPK14A-2	*N. sylvestris*	LOC107777345	XP_016452834.1	447	50445.10	9.47

Name	Diploid Progenitors	Gene Symbol in NCBI	Representative Protein Accession	AA	NW	p*I*
NtCIPK14A-3	*N. sylvestris*	LOC107792810	XP_016470533.1	441	49886.45	9.43
NtCIPK16A	*N. sylvestris*	LOC107804789	XP_016484207.1	475	53478.46	9.13
NtCIPK17A	*N. sylvestris*	LOC107779145	XP_016454982.1	454	51480.67	5.97
NtCIPK17B	*N. tomentosiformis*	LOC107830418	XP_016513448.1	454	51453.60	5.78
NtCIPK19A	*N. sylvestris*	LOC107788099	XP_016465245.1	467	52676.70	8.57
NtCIPK19B	*N. tomentosiformis*	LOC107786980	XP_016463980.1	466	52572.63	8.58
NtCIPK20A	*N. sylvestris*	LOC107802446	XP_016481441.1	462	52494.39	9.11
NtCIPK20B	*N. tomentosiformis*	LOC107781784	XP_016458040.1	462	52510.39	9.10
NtCIPK21A	*N. sylvestris*	LOC107822258	XP_016504268.1	442	50666.48	7.95
NtCIPK21B	*N. tomentosiformis*	LOC107765371	XP_016439495.1	427	48904.96	9.25
NtCIPK23A	*N. sylvestris*	LOC107774785	XP_016449915.1	454	51045.65	9.05
NtCIPK23B	*N. tomentosiformis*	LOC107761884	XP_016435661.1	454	51058.73	9.05
NtCIPK24A	*N. sylvestris*	LOC107806313	XP_016485936.1	446	50347.24	9.14
NtCIPK24B	*N. tomentosiformis*	LOC107795862	XP_016474051.1	443	50078.82	9.02
NtCIPK25A	*N. sylvestris*	LOC107806709	XP_016486416.1	449	50969.73	8.98
NtCIPK25B	*N. tomentosiformis*	LOC107831360	XP_016514613.1	449	51011.88	8.91
NtCIPK26A	*N. sylvestris*	LOC107817023	XP_016498273.1	438	50235.79	7.22
NtCIPK27A	*N. sylvestris*	LOC107784517	XP_016461145.1	457	51966.36	9.14
NtCIPK27B	*N. tomentosiformis*	LOC107821353	XP_016503277.1	473	53967.46	9.08
NtCIPK28A	*N. sylvestris*	LOC107813683	XP_016494457.1	441	49825.50	9.00

Name	Diploid Progenitors	Gene Symbol in NCBI	Representative Protein Accession	AA	NW	p*I*
NtCIPK28B	*N. tomentosiformis*	LOC107829119	XP_016512043.1	441	49860.66	9.18
NtCIPK29B-1	*N. tomentosiformis*	LOC107803568	XP_016482796.1	446	50435.56	9.17
NtCIPK29B-2	*N. tomentosiformis*	LOC107810628	XP_016490908.1	446	50339.30	8.90

AA, the number of amino acids; p*I*, theoretical isoelectric point; MW, molecular weights. The AA, p*I*, and MW were calculated with the ExPASy tool (https://web.expasy.org/protparam/).

Table S2 | Primer and sgRNA sequences

Primer name	Sequence (5' to 3')	Description
NtCBL10A-1F	ATGGATTCAACCCGAGATTCTC	For the amplification of *NtCBL10A*
NtCBL10A-1R	TCACAACAAATGGCTTTTCTCCG	
NtCIPK24A-1F	ATGAAGAAAGTGAAGAGGAAG	For the amplification of *NtCIPK24A*
NtCIPK24A-1R	TCAGCGAGTCATTGTTCTAAG	
pCHF3-R	ATTCTGGTGTGTGCGCAATG	For the identification of *NtCBL10A*-OE and NtCIPK24A-OE transgenic tobacco together with NtCBL10A-1F and NtCIPK24A-1F, respectively.
pCHF3-Allcheck-2	GATGATACGAACGAAAGCTCTGC	pCHF3-Allcheck-2 (Shi et al., 2021) was designed based on the sequence of 3'-UTR of exogenously overexpressed genes
NtCBL5A-564F	CTCAAGGATATCACAGCTGCATT	For detecting the expression level of exogenous *NtCBL5A* together with pCHF3-Allcheck-2
NtCBL4A-1-qF	AGTTCTTTCAGATGATGTTGTCG	For detecting the expression level of exogenous *NtCBL4A-1* together with pCHF3-Allcheck-2

Primer name	Sequence (5' to 3')	Description
NtCBL10A-qF	ACTGGGTTCATTGAGCGAGA	For detecting the expression level of exogenous *NtCBL10A* together with pCHF3-Allcheck-2
NtCIPK24A-qF	ACAAAATACCGAGACGGGGG	For the detection of *NtCIPK24A* expression (both endogenous and exogenous) level in the *NtCIPK24A*-OE plants
NtCIPK24A-qR	AAAACCTCGTGAAGCCGAAC	
NtL25-qF	CAAAAGTTACATTCCACCG	Primers of reference gene *NtL25* (Schmidt and Delaney, 2010) for RT-qPCR
NtL25-qR	TTTCTTCGTCCCATCAGGC	
NtCBL10A-sgRNA	GTTGGCAAGACGGGCAAGGT	The gRNA sequence for knocking out of *NtCBL10A*
NtCBL10B-sgRNA	GAAGTTGGGTTATGATTATA	The gRNA sequence for knocking out of *NtCBL10B*
NtCBL10-sgRNA	CGTCCCAACAAGAAGAAGTT	The gRNA sequence for knocking out of *NtCBL10*
NtCIPK24A-sgRNA	GTTTGCACAAAATACCGAGA	The gRNA sequence for knocking out of *NtCIPK24A*
NtCIPK24B-sgRNA	GAATATCTGAGGATGAAGCG	The gRNA sequence for knocking out of *NtCIPK24B*
NtCIPK24-sgRNA	TCGTGAAGCCGAACTATGCA	The gRNA sequence for knocking out of *NtCIPK24*
pDC45-NtCBL10A-JCF	CCTTTCTCTCTCTCTCTCTGAATTAT	For the identification of edited gene sequence of *NtCBL10A* in *Nt-cbl10a* mutants and *Nt-cbl10acbl10b* mutants
pDC45-NtCBL10A-JCR	GATTTCTTCAGAGTTCGAGTTC	
pDC45-NtCBL10B-JCF	ACCACATAAAAACACACACCTT	For the identification of edited gene sequence of *NtCBL10B* in *Nt-cbl10b* mutants and *Nt-cbl10acbl10b* mutants
pDC45-NtCBL10B-JCR	AACAAAAGCAAAGGAAAAAAGG	

Primer name	Sequence (5' to 3')	Description
pDC45-NtCIPK24A-JCF	AATTTTGCCAGCTGTAATGTC	For the identification of edited gene sequence of *NtCIPK24A* in *Nt-cipk24a* mutants
pDC45-NtCIPK24A-JCR	CGAAAGGAAGTATATTTTAGTACCTG	
pDC45-NtCIPK24B-JCF	CCTTCTAGTAAGTAAAAAATTCCATC	For the identification of edited gene sequence of *NtCIPK24B* in *Nt-cipk24b* mutants
pDC45-NtCIPK24B-JCR	CAGTTAAATGCTTAGGATAGATAATTC	

Chapter 6

General Discussion

CBL and CIPK family genes form a complex CBL-CIPK regulatory network that plays vital roles in both plant development and stress responses (Mao et al., 2022). The CBL-CIPK regulatory network is involved in two levels of crosstalk between plant development and stress adaptation: direct crosstalk through interaction with regulatory proteins, and indirect crosstalk through adaptation of correlated physiological processes that affect both plant development and stress responses (Chapter 2) (Mao et al., 2022). The roles of the CBL-CIPK regulatory network are best identified in the model plant *Arabidopsis thaliana* but much less is known in solanaceous crops.

The aim of this thesis was to identify key *CBL* genes in the salt stress response of tobacco. We first conducted a genome-wide analysis of the *NtCBL* gene family (Chapter 3). Twenty-four *NtCBL* genes were identified from *N*. *tabacum*, from which 14 *NtCBL* genes were derived from the maternal genome donor *N*. *sylvestris* and 10 were derived from the paternal genome donor *N*. *tomentosiformis*. These NtCBLs were clustered into three different groups based on phylogenetic analysis, and these groups have distinct N-terminal characteristics. The EF-hand motifs of NtCBLs contain amino acid substitutions and configuration changes that may be responsible for the variation in Ca^{2+}-binding abilities. Most *NtCBL* genes have splicing variants. The 5'-UTRs of homoeologous *NtCBL* genes from the parental genomes of allotetraploid tobacco differ in length and intron presence, which may contribute to variations in gene translation efficiency or preferences of protein interaction. The expression profile of *NtCBL* genes in different tissues and under salt/drought stress was also determined. The presented information lays a good foundation for the following gene functional analysis of *NtCBL* genes.

CBL4 (also known as *SOS3*) is a well-known gene that was reported to play an important positive role in salt tolerance in many plant species. Therefore tobacco *NtCBL4A-1* was expected to play a role in the salt tolerance of tobacco. However, the expression of *NtCBL4A-1* was greatly inhibited by salt stress (Chapter 3), which does not seem consistent with the conserved role of *CBL4* in the salt tolerance of

other plant species. This may point to a different function of tobacco *NtCBL4A-1*. In order to understand the role of *NtCBL4A-1* in the salt stress response of tobacco, the *NtCBL4A-1*-overexpressing (*NtCBL4A-1*-OE) lines were evaluated for salt tolerance. In Chapter 3, results showed that the overexpression of *NtCBL4A-1* lead to a salt-supersensitive phenotype. There are three *NtCBL4* homoeologous genes (*NtCBL4A-1*, *NtCBL4A-2*, and *NtCBL4B*) in *N*. *tabacum*, and they may have functional redundancy given the high sequence similarity. Experiments involving loss-of-function mutants of *NtCBL4* may provide additional insight into the role of *NtCBL4* homoeologs in salt tolerance but I did not have enough time within the context of my PhD thesis to construct the single mutant of *NtCBL4A-1* nor the triple mutant of *NtCBL4*.

We also observed a salt-supersensitive phenotype in *NtCBL5A*-overexpressing (*NtCBL5A*-OE) lines (Chapter 4) (Mao et al., 2022), which is very similar to the phenotype we observed in *NtCBL4A-1*-OE lines (Chapter 3). Considering endogenous *NtCBL4A-1* is mainly expressed in roots (Chapter 3) and *NtCBL5A* is mainly expressed in veins and stems (Chapter 4) (Mao et al., 2022), we hypothesized that the salt-supersensitive phenotype of *NtCBL4A-1*-OE leaves and *NtCBL5A*-OE leaves may be caused by the ectopic overexpression of these genes, thus interrupting other CBL-CIPK pathways rather than the CBL-CIPK modules that *NtCBL4A-1* and *NtCBL5A* are endogenously involved in during the tobacco salt response. The phenotype of the loss-of-function mutant of *NtCBL5* (we evaluated the salt tolerance of *Nt-cbl5a*, *Nt-cbl5b*, and *Nt-cbl5acbl5b* double mutant) is similar to the WT phenotype under salt stress, which confirms that *NtCBL5A* is not likely to be a key component in the salt tolerance of tobacco (Figure 1).

In the yeast-two hybrid experiment, we evidenced that NtCBL4A-1, NtCBL5A, and NtCBL10A can bind the same NtCIPK (Chapter 5). In addition, *NtCBL10A* overexpression was shown to relieve the salt-sensitive phenotype of *NtCBL5A*-OE lines, supporting our hypothesis that *NtCBL5A* overexpression may interfere with another CBL-CIPK (i.e. CBL10-CIPK) pathway. *NtCBL4A-1* overexpression was

shown to enhance the salt-sensitive phenotype of *NtCBL5A*-OE lines, indicating that overexpression of *NtCBL4A-1* and *NtCBL5A* may interfere with the same CBL-CIPK pathway. Therefore, we concluded that *NtCBL10* plays a key role in the salt tolerance of tobacco. Further stress tolerance assessment of the loss-of-function mutants of *NtCBL10* confirmed that *NtCBL10A* and *NtCBL10B* are key components in salt stress response (Chapter 5). Based on the two possibly independent salt-sensitive phenotypes (chlorosis and necrosis) of the *Nt-cbl10acbl10b* double mutant under salt stress, we concluded that the knockout of *NtCBL10* may interfere with several physiological pathways, in line with the recent reports in the literature reviewed by Plasencia et al (2021). Because NtCIPK24 is a candidate partner of NtCBL10 in salt tolerance mechanisms of tobacco, we also evaluated the salt tolerance of *Nt-cipk24a* single and *Nt-cipk24b* single mutants (double mutant failed to be constructed because of a lethal callus). We detected slight salt sensitivity of the *Nt-cipk24a* and *Nt-cipk24b* single mutants and suggest that NtCIPK24 may indeed be one of the partners of NtCBL10 in salt stress response.

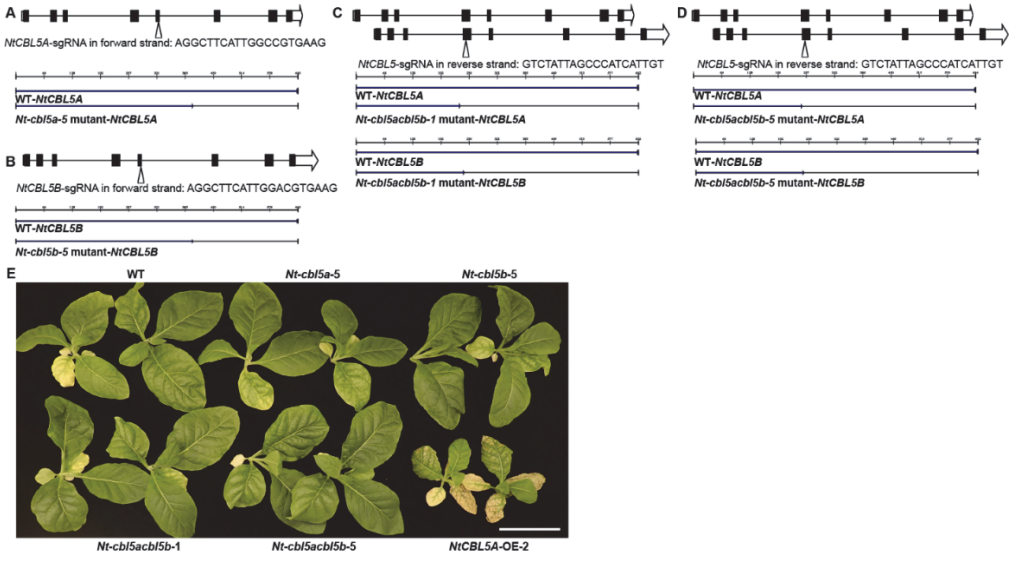

Figure 1. The editing ways of loss-of-function mutants of *NtCBL5* and the phenotype of plants under salt stress (100 mM NaCl) at 13 DAT (days after salt treatment). (A-D) The position of gRNA and protein translation of the edited sequence of *Nt-cbl5a* single mutant (A), *Nt-cbl5b* single mutant (B),

Nt-cbl5acbl5b-1 double mutant (C), and *Nt-cbl5acbl5b*-5 double mutant (D). (E) The shoot phenotype of wild-type (WT), *Nt-cbl5a* single mutant, *Nt-cbl5b* single mutant, *Nt-cbl5acbl5b* double mutant, and *NtCBL5A*-OE-2 plants under salt treatment.

The versatile roles of *CBL10* and the salt-sensitive phenotypes of *Nt-cbl10acbl10b* double mutant

CBL10 is considered to be a key master regulator of stress signaling and response under salinity, drought, flooding, and K^+ deficiency stresses, by activating (in a CIPK-dependent manner) or repressing (by direct interaction) downstream targets in different subcellular locations (Plasencia et al., 2021). *CBL10* was shown to be involved in the regulation of the transport and distribution of several ions under salt stress, including not only Na^+ but also H^+, K^+, and Ca^{2+} (Plasencia et al., 2021). This means that the homeostasis of not only Na^+ but also other ions may be affected in a loss-of-function mutant of *CBL10*. In Chapter 5, we observed two possibly independent salt-sensitive symptoms (chlorosis and necrosis) of the *Nt-cbl10acbl10b* double mutant under salt stress. The question that still needs to be answered is which *NtCBL10*-dependent adaptations to stress are underlying the different aspects of the salt-hypersensitive phenotype of the *Nt-cbl10acbl10b* double mutant. Although we did not have time within the thesis project to target all the regulatory functions of *NtCBL10* in response to salt stress experimentally, the results give rise to highly interesting insights and hypotheses on *NtCBL10* functions under salt stress that are further discussed below.

The role of *CBL10* and the necrotic phenotype of *Nt-cbl10acbl10b* double mutant

Na^+ homeostasis

We found similar necrotic lesions in the *NtCBL5A*-OE and *Nt-cbl10acbl10b* double mutant under salt stress (Chapter 4, Chapter 5). Even though we found that Na^+ accumulation in both *NtCBL5A*-OE leaves and *Nt-cbl10acbl10b* double mutant leaves were comparable to that of WT, Na^+ accumulation may still play a role in the development of the necrotic lesions when the distribution of Na^+ within the leaf and

leaf cells is considered. This hypothesis is based on the report that the tonoplast-localized CBL10-CIPK24 pathway positively regulates the Na^+ sequestration into the vacuole (Kim et al., 2007). If Na^+ transport to the vacuole is affected in the *Nt-cbl10acbl10b* double mutant, Na^+ will accumulate to toxic levels in the cytosol much faster, and this may cause necrotic symptoms (Figure 2). In addition, AtCBL10 was also reported to interact with AtCIPK24 and AtCIPK8 (which has high sequence similarity with AtCIPK24, 60.9% AA pairwise identity), regulating Na^+ transport over the plasma membrane out of the cell (Quan et al., 2007; Lin et al., 2009; Kleist et al., 2014; Yin et al., 2019). If *NtCBL10* has the same function as *AtCBL10*, the loss-of-function of *NtCBL10* may also lead to impaired Na^+ extrusion, thus contributing to a higher relative Na^+ concentration in the cytosol (Figure 2).

The hypothesis of disturbed Na^+ homeostasis in the cytosol seems in line with the fact that the necrotic symptoms of *NtCBL5A*-OE lines and the *Nt-cbl10acbl10b* double mutant under salt stress are light-dependent (Chapter 5). Plants grown under dark conditions transpire much less than plants grown under light, which will influence the transpiration flow. This is likely to affect the accumulation rate of Na^+ in the leaves: Na^+ is transported to the leaf blades with the transpiration stream and is deposited there under continuous salt stress, and only a small proportion of the Na^+ is recirculated to roots through phloem for most plants (Tester, 2003). Therefore, it is likely that the Na^+ accumulates faster in plant leaves under light conditions (with high transpiration flow) than under dark conditions, which is evidenced by the leaf Na^+ measurements in light and dark-treated leaves (Chapter 5, Figure 6E and 7D). In this case, the appearance of necrotic symptoms of *NtCBL5A*-OE lines and *Nt-cbl10acbl10b* double mutant may be possibly delayed in dark conditions.

Cl^- homeostasis

In Chapter 5, it was shown that the *Nt-cbl10acbl10b* double mutant accumulated significantly less Cl^- under salt stress compared to WT. This does not seem to be caused by less xylem flow/transpiration even though the stomatal conductance of *Nt-cbl10acbl10b* double mutant is lower than that of WT (Chapter 5, Figure 5B and

5E), because the Na^+ accumulation between WT and mutant was not significantly different. Therefore, it may be related to Cl^- uptake in the roots or the efficiency of Cl^- root-to-shoot translocation. Although there is no report of CBL10 playing a role in Cl^- homeostasis, the CBL-CIPK network has been reported to regulate the Cl^- root-to-shoot translocation. AtCBL1/9-AtCIPK23 can activate the anion channel SLOW-TYPE ANION CHANNEL (SLAC1) in *Xenopus oocytes*, which is a PM-localized protein that is highly permeable to malate and chloride in guard cells (Maierhofer et al., 2014). SLAC1 has four homologues, which are the SLAC1-associated homologues 1 to 4 (SLAH1 to SLAH4). SLAH3 can also be activated by AtCBL1/9-AtCIPK23 in *Xenopus oocytes*, and it can form chloride-conducting heteromeric channels with SLAH1 in xylem-pole pericycle cells to regulate chloride root-to-shoot translocation (Maierhofer et al., 2014; Cubero-Font et al., 2016). AtCBL10 is reported to be able to interfere with AtCBL1/9-AtCIPK23 complexes by directly and competitively interacting with downstream targets. For instance, AtCBL10 competes with AtCBL1/9-AtCIPK23 in the interaction with AKT1 and repress the potassium uptake induced by AtCBL1/9-AtCIPK23 (Ren et al., 2013). Whether CBL1/9-CIPK23 also activates SLAC1 as well as its homologues (SLAH), and whether the reduced Cl^- accumulation in the leaves of the *Nt-cbl10acbl10b* double mutant under saline conditions is linked to the lack of *CBL10* regulation of this mechanism is still speculative (Figure 2).

For most plant species, Na^+ tends to reach a toxic concentration before Cl^- does, so Cl^- has received much less attention in salt tolerance research than Na^+ (Munns and Tester, 2008). For some species with woody stems and roots including soybean, grapevines, and citrus, Cl^- becomes the more toxic component under salt stress because the plant can manage the Na^+ transport better than Cl^- transport by effectively withholding Na^+ root-to-shoot translocation (Munns and Tester, 2008). Excessive Cl^- is considered toxic mainly because it is widely thought of as an antagonistic molecule of NO_3^-, an important source of nitrogen (Colmenero-Flores et al., 2019). Cl^- is a micronutrient for plant growth, working as an essential cofactor for

the oxygen evolution of the photosystem Ⅱ and regulating cell osmolarity and the electrical charge balance of cations (Colmenero-Flores et al., 2019). Cl^- is a non-assimilating highly mobile anion and is preferred by plants to balance the electric charges of important cations to stabilize the electric potential of cell membranes and regulate pH gradients (Geilfus, 2018b; Colmenero-Flores et al., 2019). The chloroplast envelops and the thylakoid membrane exhibit a high permeability for Cl^- (U and W, 1981; Bose et al., 2017) and Cl^- is the most abundant anion in the chloroplast stroma (50-90 mM) (Neuhaus and Wagner, 2000). Cl^- influx from the stroma to the lumen is essential for thylakoid swelling after the onset of illumination, and Cl^- re-export to the stroma would cause the thylakoid to shrink during the transition to darkness (Colmenero-Flores et al., 2019). In addition, the accumulated protons in the thylakoid lumen can be electrically counterbalanced by Cl^- influx, thus possibly regulating the pH gradient between the lumen and the stroma. Therefore, the disturbance of chloroplastidial Cl^- homeostasis might lead to the reduction of PS Ⅱ (Geilfus, 2018a). In our study, the reduced rate of Cl^- accumulation in the *Nt-cbl10acbl10b* double mutant compared to WT under salt stress was reversed in the leaves grown in the dark (Chapter 5, Figure 6F and 7E), and the necrotic lesions disappeared. Whether there is any connection between Cl^- accumulation in *Nt-cbl10acbl10b* and the necrotic phenotype remains to be established, but it is interesting to explore.

Reactive oxygen species (ROS)

In Chapter 4, we found that ROS accumulation in *NtCBL5A*-OE leaves was higher than that in WT under salt stress already at 2 DAT (days after reaching 100 mM NaCl treatment) and 6 DAT (Chapter 4, Figure S2 and 4D) (Mao et al., 2021). Under salt stress, the Calvin cycle is inhibited by salinity-induced stomatal limitation, leading to the over-reduction of the electron transport chain and the generation of ROS (Attia et al., 2009; Hajiboland, 2014). Possibly, the light energy input in *NtCBL5A*-OE leaves may exceed energy utilization when the Calvin cycle is more inhibited than the light reaction in the photosynthesis of *NtCBL5A*-OE leaves under salt stress.

Therefore, the resulting ROS generation in *NtCBL5A*-OE leaves might exceed the ROS scavenging ability, leading to necrotic lesions. Even though we do not have ROS accumulation data of the *Nt-cbl10acbl10b* mutant under salt stress, it is not unlikely that ROS species also accumulated in *Nt-cbl10acbl10b* double mutant. Our results showed that the stomata conductance of *Nt-cbl10acbl10b* double mutant was more severely inhibited by salt stress since 1 DAT (Chapter 5, Figure 6). This stomatal limitation may cause an enhanced imbalance between ROS production and scavenging at the very early stage of salt treatment, thus leading to the necrotic symptom of the *Nt-cbl10acbl10b* double mutant.

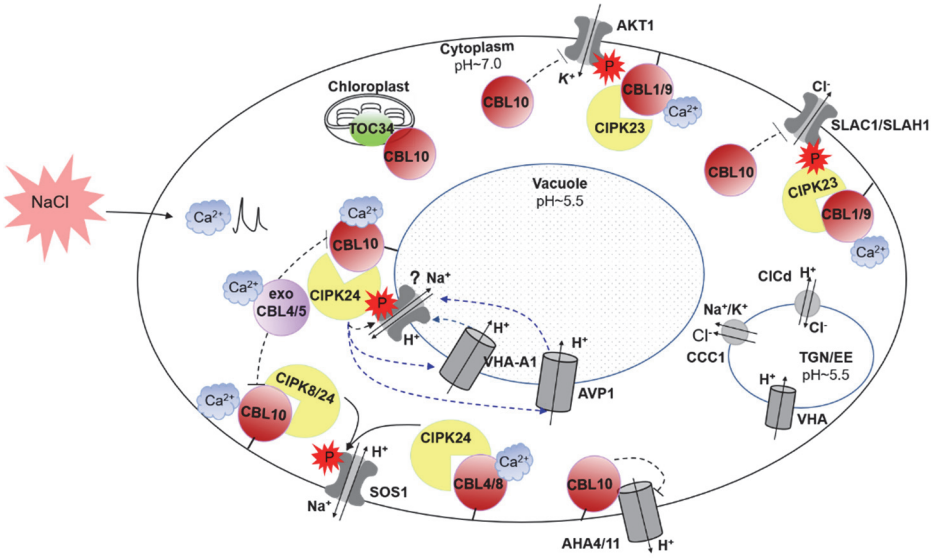

Figure 2. Schematic picture to show the pathways that NtCBL10 may be involved in by activating (in a CIPK-dependent manner) or repressing (by direct interaction) downstream targets in different subcellular locations. Exo CBL4/5 means overexpressed exogenous *NtCBL4/5*. Pointed and blunt arrowheads indicate activating and inhibitory processes, respectively. The dotted lines indicate proposed connections that still require validation. The question mark (?) means the Na^+/H^+ antiporter has not been identified yet. The red lighting sign with a "P" inside means phosphorylation.

The role of *CBL10* and the chlorotic symptom of *Nt-cbl10acbl10b* double mutant

The chlorosis symptom of *Nt-cbl10acbl10b* double mutant is light-independent, in contrast to the light-dependent chlorotic spots on *NtCBL5A*-OE leaves. Although we cannot rule out a role for cytosolic Na^+ accumulation in the development of the chlorotic symptoms, the low rate of leaf Na^+ concentration increase in the *Nt-cbl10acbl10b* double mutant grown in the dark while chlorotic symptoms still developed very fast suggests that Na^+ accumulation itself is not causal to the chlorosis and fast breakdown of chlorophyll. So then the question remains: what causes the extreme and fast-developing chlorosis in the *Nt-cbl10acbl10b* double mutant?

CBL10 also appears to be involved in the regulation of H^+ homeostasis by amongst others affecting the activity of the vacuolar H^+-ATPase (V-ATPase, VHA) and the vacuolar H^+-pyrophosphatase (V-PPase, AVP1), which are two vital proton pumps in the tonoplast for energizing ion transport (Figure 2) (Hedrich et al., 1989). VHA consists of two subcomplexes which are the peripheral V_1 complex (eight subunits VHA-A to -H) for ATP hydrolysis and the membrane-integral V_0 complex (VHA-a, -c, -c', -c'', -d, and -e) for proton translocation (Cipriano et al., 2008). AtCIPK24 was reported to interact with the peripheral VHA-B subunits and stimulate H^+ transport activity (Batelli et al., 2007). In addition, in a tomato *Sl-cbl10* mutant, the gene expression of the vacuolar H^+ pumps *SlAVP1* and *SlVHA-A1* was downregulated under saline conditions compared to WT (Egea et al., 2018), suggesting *SlCBL10* affects H^+ homeostasis, possibly as a driver for Na^+ compartmentation into the vacuole. Therefore, CBL10-CIPK24 may contribute to Na^+ compartmentation by stimulating the tonoplast-localized proton pumps (regulating the H^+ homeostasis) (Figure 2). Furthermore, AtCBL10 was also suggested to negatively regulate the activity of AtAHA4 and AtAHA11 in an AtCIPK-independent manner by direct interaction (Figure 2) (Xie et al., 2022). Impaired regulation of the H^+ pumps under saline conditions may result in impaired H^+ homeostasis and pH regulation, which

can be highly damaging to the leaf cell functioning, and even induce chlorophyll breakdown (Long et al., 2017). Whether impaired pH regulation is causal to the fast-developing chlorosis in the *Nt-cbl10acbl10b* double mutant under salt stress remains to be established.

Interestingly, a VHA-deficient *det3* mutant showed severe salt sensitivity (Batelli et al., 2007), but this salt sensitivity was evidenced later to be caused by reduced VHA activity in the trans-Golgi network/early endosome (TGN/EE) but not at the tonoplast. A loss-of-function mutant of *VHA-a2* and *VHA-a3* (two VHA-a isoforms localized in the tonoplast) did not show salt sensitivity and still accumulated Na^+, while the loss-of-function of *VHA-a1* (an isoform localized in the TGN/EE) was salt-supersensitive (Krebs et al., 2010). The TGN/EE is an organelle with complex cellular roles, one of which is sorting and delivering proteins to the apoplast, PM, and vacuole. Plant cells always maintain a low luminal pH and the impaired TGN/EE pH regulation may lead to severe plant growth defects (McKay et al., 2022). These reports proposed a key role for H^+ homeostasis in the endosomal system that also greatly affects the salt tolerance of plants.

The VHA is often found to be co-localized with a specific member of the Cl^- channel (ClC) family of anion transporters (Scholl et al., 2021). ClCd and ClCf are two H^+/Cl^- antiporters that are colocalized with VHA-a1 in the TGN/EE and regulate the pH in the Golgi stack (Scholl et al., 2021). In addition, plant TGN/EE pH regulation requires the cation chloride cotransporter (CCC) that electroneutrally transports Cl^- across membranes with the cations Na^+/K^+ (McKay et al., 2022). These results showed that Cl^- homeostasis directly relates to and contributes to H^+ homeostasis and Na^+ homeostasis of the TGN/EE. The imbalanced accumulation of Na^+ and Cl^- in *Nt-cbl10acbl10b* may also lead to interfered H^+ homeostasis in the TGN/EE system of tobacco and thus to severe plant defects.

Interestingly, CBL10 was also found to directly interact with and repress the TOC34 protein (Figure 2), a member of the TOC (translocon of the outer membrane of the chloroplasts) complex with GTPase activity to regulate protein import into

chloroplasts (Cho et al., 2016). This study evidenced the subcellular localization of CBL10 in the chloroplast and indicated that *CBL10* may play a role in chloroplast functions, which seems in line with our result that the knockout of *NtCBL10* leads to chlorophyll breakdown and PS Ⅱ defects under salt stress. The importance of maintaining ion homeostasis in the different cellular organelles under salt stress conditions may be underestimated, and the putative role of CBL-CIPK network components in the correct functioning of these organelles under stress conditions is certainly worth exploring.

Considerations when using gene overexpression and gene knockout lines for gene characterization

Overexpressing a gene in the same species or another (model) species is a widely used strategy to explore gene function as a parallel approach to gene loss-of-function mutants (by silencing or knocking out genes). The expectation often is that overexpression and knockout/silencing of a gene will cause opposite phenotypes. However, that does not have to be the case. In practical experiments, overexpression may even cause the same phenotype with loss-of-function or no phenotype (Prelich, 2012), especially when the gene is expressed under a constitutive promoter that drives expression in all tissues, developmental stages, and conditions. The overexpression of a gene, in particular for the gene whose expression is normally limited to specific conditions or specific cell types, can cause inhibition or activation of a protein complex or pathway that it normally would not interact with (Prelich, 2012). Most examples of the inhibitory effect of gene overexpression involve protein-protein competitive interactions, inhibiting the original complex or pathway by competing with their interacting member (Prelich, 2012). The overexpression phenotype induced by competition-based mechanisms can be reversed by co-overexpression of the target protein (Prelich, 2012). In this thesis, we found that overexpression of *NtCBL5A* led to a supersensitivity phenotype under salt stress. However, the gene expression profile of *NtCBL5A* and the salt tolerance assessment results of *Nt-cbl5acbl5b* double mutant seem to confirm that the *NtCBL5* is not a key

component in salt stress tolerance of tobacco, and that the salt-sensitive phenotype of the *NtCBL5A*-OE lines is likely not related to its endogenous function. This shows that caution is required in deducing gene functions from overexpression phenotypes. At the same time, however, overexpression phenotypes can be highly insightful when interpreted correctly, as is also exemplified in this thesis. The proposed interference of *NtCBL5A* overexpression based on the salt-sensitive phenotype enabled us to hypothesize on the different activities of *NtCBL10* and the physiological processes underlying the salt hypersensitivity with fast-developing chlorosis and necrosis of the loss-of-function mutant of *NtCBL10*.

Gene loss-of-function mutants have been widely accepted as a convincing material to explore real gene functions. It is important to keep in mind that the mutant phenotype could be a combined result that attributes to several interfered signaling pathways, especially when this gene has versatile functions such as *NtCBL10* in this thesis.

Na^+-imaging technique for detecting Na^+ distribution in the cell is needed for our further studies

Whether Na^+ accumulation can be directly responsible for the salt sensitivity of *NtCBL4A-1*-OE lines, *NtCBL5A*-OE lines, and the *Nt-cbl10acbl10b* double mutant remains to be established. I only measured ion contents in the whole leaf blades. Disturbed distribution of Na^+ at the cellular level may result in highly elevated Na^+ concentrations in the cytosol and the chloroplast, even when the total Na^+ content of the leaf is not much different from that in WT. It would be highly insightful to be able to quantify ion contents in the different cellular compartments, and understand how the cellular distribution of the ions is affected in the *NtCBL* transgenic lines.

Future experiments therefore may be considered that use a Na^+ indicator with a high-resolution confocal imaging technique. A commonly used Na^+ indicator is CoroNA Green dye. Na^+ measurement by CoroNa Green fluorescent dye imaging was first conducted in animals (Meier et al., 2006). In 2015, Wu (Wu et al., 2015) published a protocol for quantifying Na^+ distribution between cytosol and vacuole of root cells by

CoroNa Green fluorescent dye imaging (Wu et al., 2015). By co-staining the plant cells with CoroNa Green-AM and FM4-64, another dye that stains both plasma and vacuolar membranes, a better resolution of Na^+-imaging can be obtained to observe the intracellular compartments (Wu et al., 2015). Then the cytosolic and vacuolar Na^+ fluorescent intensities are used to represent Na^+ concentration (Wu et al., 2015; Wu et al., 2018). This type of experiment will allow us to see whether *NtCBL10* is essential for the correct distribution of Na^+ in the (intra)cellular compartments, and whether the *NtCBL4A-1* and *NtCBL5A* overexpression interferes with this specific *NtCBL10* activity.

Low Na^+ might be used as nutrition for the tobacco growth

In our studies of salt treatment on tobacco, we found that WT tobacco growth was significantly inhibited under 100 mM NaCl. However, we also found in our experiments that tobacco had a significantly better growth vigor under very mild NaCl treatments (10 mM, 25 mM) than under control conditions at 9 DAT (Figure 3). There is substantial evidence that lower levels of Na^+ supply is of potential benefit to the normal growth and development of some species with moderate to high salt resistance (Slama et al., 2007; Subbarao et al., 2010; Gattward et al., 2012). Na^+ may be capable of replacing K^+ as internal osmoticum, stomatal function, photosynthesis, counter-ion in long-distance transport, and enzyme activation, the extent of which varies between plant species (Subbarao et al., 2010). The vacuolar K^+ is replaceable to a large extent by Na^+ because this osmotic function is nonspecific, and this replacement within the vacuole makes K^+ available for specific functions within the cell or for translocation (Marschner, 1971). This is thought to be the reason why Na^+ contributes to the osmotic relations and the mineral nutrition in moderate to high salt-tolerant plants (having the ability to accumulate large amounts of Na^+ in vacuoles), especially if K^+ is present at suboptimal levels (Wakeel et al., 2010). Growth stimulation by low levels of Na^+ attracts both practical and scientific interest because of the potential to utilize Na as inexpensive fertilizer. The underlying mechanism of growth stimulation by Na^+ in the relatively salt tolerance crop tobacco

has never been reported, but it would be interesting to investigate this.

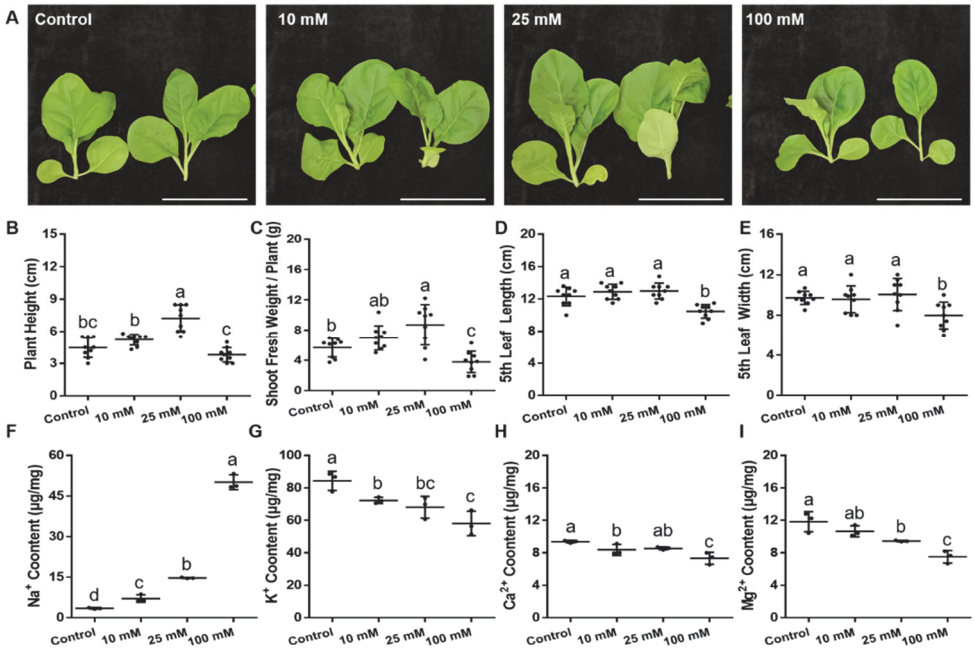

Figure 3. The shoot phenotype and physiological indicators of wild-type (WT) under control conditions and different salt stresses. Scale bars=10 cm. (A) The shoot phenotype of WT under control conditions and different salt stresses at 9 DAT. (B-E) The plant height, shoot fresh weight, 5th leaf length, and 5th leaf width of WT. Error bars indicate ±SD (n=9). (F-I) The Na^+, K^+, Ca^{2+}, and Mg^{2+} contents of the 5th leaves of WT tobacco. Error bars indicate ±SD (n=3). Different letters above bars (a, b, and c) indicate significant statistical differences based on one-way ANOVA with LSD test ($P<0.05$).

"Tolerant" or "Sensitive" is a relative term and should be restricted to specific evaluation criteria or situation

Plant tolerance is often defined as the degree to which the plant can withstand moderate or severe stress without significant adverse effects. However, plant tolerance is a relative term in practice. Researchers often assess and describe "tolerant" or "sensitive" based on the plant performance that is specific to their particular studies. But several points need to be considered to evaluate plant tolerance.

First, stress tolerance or sensitivity is affected by developmental stages. For instance, rice is salt-sensitive at two growth stages: the seedling stage and the reproductive stage. The salt sensitivity of rice at these two stages is controlled mostly by different sets of genes (Singh et al., 2010). The salt tolerance of rice at the reproductive stage is directly associated with rice yield (Palao et al., 2013). Therefore, a genotype with salinity tolerance at the seedling stage does not mean it is tolerant at the reproductive stage as well nor makes sure of a good rice yield, and vice versa (Ahmadizadeh et al., 2016). Second, "tolerant" or "sensitive" are determined based on agronomic traits. However, different agronomic traits may be needed with different breeding objectives. For example, the tolerance screening based on plant vigor may only identify the cultivars or breeding lines with non-dwarf plant types (Zeng et al., 2002). In addition, some traits which are disliked by breeders may contribute to survival and reproduction, which could be considered tolerant from a plant's perspective. For instance, plants may allocate Na^+ to old leaves, thus reducing Na^+ accumulation when old leaves die and be shed to protect the young leaves (Tester and Davenport, 2003). Therefore, the necrosis of old leaves is not necessarily a clue of salt sensitivity. Moreover, traits associated with tolerance may have a dual effect. For example, most traits associated with drought tolerance are positive in very severe scenarios and negative in milder scenarios, or the opposite trend (Tardieu, 2012). Therefore, spectacular results obtained in one drought scenario may have limited interest in improving food security in other geographical areas with water scarcity. Therefore, the description of "tolerant" or "sensitive" should be restricted to specific criteria or situations.

From an agronomical point of view, stress tolerance should mean (relatively) high yield and quality under stress conditions. For *Solanaceae*, that could mean leaves (tobacco), fruits (tomato), or tubers (for potato). In other words, breeding for different crops has different criteria for "tolerance". As researchers, we often define a stress-tolerant plant as a plant with the least reduction in biomass/yield when grown under stress conditions compared to the biomass/yield under normal ideal conditions. Any

genotype that is able to maintain growth may have very interesting stress tolerance traits that can contribute to higher yield, no matter whether it is the one with the highest yield under stress. For breeders, however, stress-tolerant varieties often should have high yields under stress as well as under normal conditions. Many genes that are responsible for stress tolerance and are proposed as targets for improving stress tolerance of crops may also be involved in plant development via direct involvement or indirect physiological connection, thus leading to a trade-off between stress tolerance and yield (higher tolerance under stress conditions but lower yield under normal conditions). This may be the main reason why only very few salt-tolerant genes identified in the lab have been successfully used for improving stress tolerance without yield penalties in the field trials, even though numerous stress-tolerant genes were reported based on lab experiments. Aligning and/or managing expectations with respect to stress tolerance between scientists, breeders, and growers is therefore important. Scientists may need to carefully select traits with a minimal trade-off, or investigate the effects of a combination of traits in the same variety to minimize growth trade-offs and fulfill the requirement of breeders and growers.

Possible breeding strategies targeting *CBL* genes

Genome-editing based on the CRISPR-Cas technique is regarded as a highly efficient plant breeding technology, especially with the development of non-transgenic genome editing techniques. Yang et al (2023) designed fusions of Cas9 and guide RNA transcripts to tRNA-like sequence motifs that can move RNAs from transgenic rootstocks (*Arabidopsis)* to grafted WT scions (*Arabidopsis* or *Brassica rapa*) and achieve heritable gene editing. In addition, an engineered biocontainable RNA virus (TSWV) was also developed to deliver CRISPR/Cas nucleases to achieve non-transgenic heritable mutations without tissue culture (Liu et al., 2023). With these state-of-the-art genome editing techniques, different combinations of favorable alleles and flexible regulation of the combinations may be helpful to make considerable progress in stress tolerance breeding (transgene-free).

Could *CBL* genes be eligible as targets for improving the stress tolerance of crops? *AtCBL10* was reported to have a contrasting function in drought stress tolerance versus salt stress tolerance in *Arabidopsis*. The *At-cbl10* mutant exhibited a higher drought tolerance than WT with an unknown mechanism until now (Kang and Nam, 2016), so knocking out of *AtCBL10* may result in a line for improved drought tolerance but decreased salt tolerance. In this case, the best strategy might be to modify gene expression or protein function rather than knocking out the gene. Possibly, the native promoter of *CBL10* can be replaced by a salt stress-inducible promoter to make sure that *CBL10* still exerts its essential role during salt stress, while having low or no expression under normal and/or drought conditions. For allopolyploid plants like tobacco, knocking out only one of *NtCBL10* homoeologs (*NtCBL10A* or *NtCBL10B*) may be a possible alternative to enhance drought tolerance while hardly affecting the salt stress response. As described, AtCBL10 has diverse functions, at least partly attributed to its different subcellular localizations (PM, tonoplast, chloroplast, and membrane vesicles) (Quan et al., 2007; Batistic et al., 2010). The tonoplast association of AtCBL10 requires *S*-acylation of the C residue at position 38 and contributes to salt tolerance (Chai et al., 2020). The substitution of this C residue to Ser (S) in AtCBL10 leads to cytoplasmic and nuclear localization and dysfunction under salt stress (Chai et al., 2020). This demonstrates that inducing targeted mutations to modify the subcellular location of proteins can be a strategy to modify the protein functions. The precondition for this is we have a detailed understanding of how the protein works in different subcellular locations. With respect to fine-tuning different activities, the multiple splicing variants for *CBL* genes may provide an additional tool (Mao et al., 2022). Overexpressing or knocking out specific splice variants could result in functional moderation of CBL functions. However, a more detailed functional characterization of these splicing variants would be required first.

Concluding remarks

In this thesis, I conducted the genome-wide analysis of *CBL* family gene in

allotetraploid tobacco, obtaining a comprehensive understanding of the sequence, protein characteristics, and gene expression profiles of *NtCBL* family genes. Overexpression of *NtCBL4A-1* and *NtCBL5A* led to salt supersensitivity of transgenic tobacco, which may be because the ectopic overexpression of them interfered with the function of other *NtCBL*s. In the end, *NtCBL10* was evidenced to play a vital role in salt tolerance. In addition, NtCBL10-interacting NtCIPK24 also contributes to salt tolerance. This study provides data for the functional identification of *CBL* genes and the selection of candidate stress-tolerant genes in *N. tabacum*, which will likely be useful for the genetic improvement of *Solanaceae* crops in general. In addition, this thesis provides insight into the physiological roles of the CBL-CIPK network in the crosstalk between plant growth and stress adaptation, and the crosstalk between homeostasis regulation of different ions, enhancing the knowledge of the mechanisms underlying salt stress response of plants.

REFERENCES

Ahmadizadeh, M., Vispo, N. A., Calapit-Palao, C. D. O., Pangaan, I. D., Viña, C. D., and Singh, R. K. Reproductive stage salinity tolerance in rice: a complex trait to phenotype. *Indian J Plant Physiol*. **2016**, *21*, 528-536.

Batelli, G., Verslues, P. E., Agius, F., Qiu, Q., Fujii, H., Pan, S., Schumaker, K. S., Grillo, S., and Zhu, J. K. SOS2 promotes salt tolerance in part by interacting with the vacuolar H^+-ATPase and upregulating its transport activity. *Mol Cell Biol*. **2007**, *27*, 7781-7790.

Batistic, O., Waadt, R., Steinhorst, L., Held, K., and Kudla, J. CBL-mediated targeting of CIPKs facilitates the decoding of calcium signals emanating from distinct cellular stores. *Plant J*. **2010**, *61*, 211-222.

Bose, J., Munns, R., Shabala, S., Gilliham, M., Pogson, B., and Tyerman, S. D. Chloroplast function and ion regulation in plants growing on saline soils: lessons from halophytes. *J Exp Bot*. **2017**, *68*, 3129-3143.

Chai, S., Ge, F. R., Zhang, Y., and Li, S. S‐acylation of CBL10/SCaBP8 by PAT10 is crucial for its tonoplast association and function in salt tolerance. *J Integr Plant Biol*. **2020**, *62*, 718-722.

Cho, J. H., Lee, J. H., Park, Y. K., Choi, M. N., and Kim, K. N. Calcineurin B-like protein CBL10 directly interacts with TOC34 (translocon of the outer membrane of the chloroplasts) and decreases its GTPase activity in Arabidopsis. *Front Plant Sci*. **2016**, *7*, 1911.

Cipriano, D. J., Wang, Y., Bond, S., Hinton, A., Jefferies, K. C., Qi, J., and Forgac, M. Structure and

regulation of the vacuolar ATPases. *Biochim Biophys Acta*. **2008**, *1777*, 599-604.

Colmenero-Flores, J. M., Franco-Navarro, J. D., Cubero-Font, P., Peinado-Torrubia, P., and Rosales, M. A. Chloride as a beneficial macronutrient in higher plants: new roles and regulation. *Int J Mol Sci*. **2019**, *20*, 4686.

Cubero-Font, P., Maierhofer, T., Jaslan, J., Rosales, M. A., Espartero, J., Diaz-Rueda, P., Muller, H. M., Hurter, A. L., Al-Rasheid, K. A., Marten, I., Hedrich, R., Colmenero-Flores, J. M., and Geiger, D. Silent S-type anion channel subunit SLAH1 gates SLAH3 open for chloride root-to-shoot translocation. *Curr Biol*. **2016**, *26*, 2213-2220.

Egea, I., Pineda, B., Ortiz-Atienza, A., Plasencia, F. A., Drevensek, S., Garcia-Sogo, B., Yuste-Lisbona, F. J., Barrero-Gil, J., Atares, A., Flores, F. B., Barneche, F., Angosto, T., Capel, C., Salinas, J., Vriezen, W., Esch, E., Bowler, C., Bolarin, M. C., Moreno, V., and Lozano, R. The SlCBL10 calcineurin B-like protein ensures plant growth under salt stress by regulating Na^+ and Ca^{2+} homeostasis. *Plant Physiol*. **2018**, *176*, 1676-1693.

Gattward, J. N., Almeida, A. A., Souza, J. O., Jr., Gomes, F. P., and Kronzucker, H. J. Sodium-potassium synergism in *Theobroma* cacao: stimulation of photosynthesis, water-use efficiency and mineral nutrition. *Physiol Plant*. **2012**, *146*, 350-362.

Geilfus, C. M. Chloride: from nutrient to toxicant. *Plant Cell Physiol*. **2018a**, *59*, 877-886.

Geilfus, C. M. Review on the significance of chlorine for crop yield and quality. *Plant Sci*. **2018b**, *270*, 114-122.

Hedrich, R., Kurkdjian, A., Guern, J., and Flugge, U. I. Comparative studies on the electrical properties of the H^+ translocating ATPase and pyrophosphatase of the vacuolar-lysosomal compartment. *EMBO J*. **1989**, *8*, 2835-2841.

Kang, H. K., and Nam, K. H. Reverse function of ROS-induced CBL10 during salt and drought stress responses. *Plant Sci*. **2016**, *243*, 49-55.

Kim, B. G., Waadt, R., Cheong, Y. H., Pandey, G. K., Dominguez-Solis, J. R., Schultke, S., Lee, S. C., Kudla, J., and Luan, S. The calcium sensor CBL10 mediates salt tolerance by regulating ion homeostasis in Arabidopsis. *Plant J*. **2007**, *52*, 473-484.

Kleist, T. J., Spencley, A. L., and Luan, S. Comparative phylogenomics of the CBL-CIPK calcium-decoding network in the moss *Physcomitrella*, *Arabidopsis*, and other green lineages. *Front Plant Sci*. **2014**, *5*, 187.

Krebs, M., Beyhl, D., Gorlich, E., Al-Rasheid, K. A., Marten, I., Stierhof, Y. D., Hedrich, R., and Schumacher, K. Arabidopsis V-ATPase activity at the tonoplast is required for efficient nutrient storage but not for sodium accumulation. *Proc Natl Acad Sci U S A*. **2010**, *107*, 3251-3256.

Lin, H. X., Yang, Y. Q., Quan, R. D., Mendoza, I., Wu, Y. S., Du, W. M., Zhao, S. S., Schumaker, K. S., Pardo, J. M., and Guo, Y. Phosphorylation of SOS3-LIKE CALCIUM BINDING PROTEIN8 by SOS2 protein kinase stabilizes their protein complex and regulates salt tolerance in Arabidopsis. *Plant Cell*.

2009, *21*, 1607-1619.

Liu, Q., Zhao, C., Sun, K., Deng, Y., and Li, Z. Engineered biocontainable RNA virus vectors for non-transgenic genome editing across crop species and genotypes. *Mol Plant*. **2023**.

Maierhofer, T., Diekmann, M., Offenborn, J. N., Lind, C., Bauer, H., Hashimoto, K., Al-Rasheid, K. A. S., Luan, S., Kudla, J., Geiger, D., and Hedrich, R. Site- and kinase-specific phosphorylation-mediated activation of SLAC1, a guard cell anion channel stimulated by abscisic acid. *Sci Signal*. **2014**, *7*, ra86-ra86.

Mao, J., Mo, Z., Yuan, G., Xiang, H., Visser, R. G. F., Bai, Y., Liu, H., Wang, Q., and Linden, C. G. v. d. The CBL-CIPK network is involved in the physiological crosstalk between plant growth and stress adaptation. *Plant Cell Environ*. **2022**.

Mao, J., Yuan, J., Mo, Z., An, L., Shi, S., Visser, R. G. F., Bai, Y., Sun, Y., Liu, G., Liu, H., Wang, Q., and van der Linden, C. G. Overexpression of *NtCBL5A* leads to necrotic lesions by enhancing Na^+ sensitivity of tobacco leaves under salt stress. *Front Plant Sci*. **2021**, *12*, 740976.

Marschner, H. Why can sodium replace potassium in plants? In. Potassium in biochemistry and physiology, 50-63. **1971**.

McKay, D. W., McFarlane, H. E., Qu, Y., Situmorang, A., Gilliham, M., and Wege, S. Plant trans-Golgi network/early endosome pH regulation requires Cation Chloride Cotransporter (CCC1). *Elife*. **2022**, *11*, e70701.

Meier, S. D., Kovalchuk, Y., and Rose, C. R. Properties of the new fluorescent Na^+ indicator CoroNa Green: comparison with SBFI and confocal Na^+ imaging. *J Neurosci Methods*. **2006**, *155*, 251-259.

Munns, R., and Tester, M. Mechanisms of salinity tolerance. *Annu Rev Plant Biol*. **2008**, *59*, 651-681.

Neuhaus, H. E., and Wagner, R. Solute pores, ion channels, and metabolite transporters in the outer and inner envelope membranes of higher plant plastids. *Biochimica et Biophysica Acta*. **2000**, *1465*, 307-323.

Palao, C. D. C., Viña, C. B. D., Gregorio, G. B., and Singh, R. K. A new phenotyping technique for salinity tolerance at the reproductive stage in rice. *Oryza*. **2013**, *50*, 199-207.

Plasencia, F. A., Estrada, Y., Flores, F. B., Ortiz-Atienza, A., Lozano, R., and Egea, I. The Ca^{2+} sensor calcineurin B-Like protein 10 in plants: emerging new crucial roles for plant abiotic stress tolerance. *Front Plant Sci*. **2021**, *11*, 599944.

Prelich, G. Gene overexpression: uses, mechanisms, and interpretation. *Genetics*. **2012**, *190*, 841-854.

Quan, R., Lin, H., Mendoza, I., Zhang, Y., Cao, W., Yang, Y., Shang, M., Chen, S., Pardo, J. M., and Guo, Y. SCABP8/CBL10, a putative calcium sensor, interacts with the protein kinase SOS2 to protect Arabidopsis shoots from salt stress. *Plant Cell*. **2007**, *19*, 1415-1431.

Ren, X. L., Qi, G. N., Feng, H. Q., Zhao, S., Zhao, S. S., Wang, Y., and Wu, W. H. Calcineurin B-like protein CBL10 directly interacts with AKT1 and modulates K^+ homeostasis in Arabidopsis. *Plant J*. **2013**, *74*, 258-266.

Scholl, S., Hillmer, S., Krebs, M., and Schumacher, K. ClCd and ClCf act redundantly at the trans-Golgi network/early endosome and prevent acidification of the Golgi stack. *J Cell Sci*. **2021**, *134*, jcs258807.

Singh, R. K., Redonã, E. D., and Refuerzo, L. Varietal improvement for abiotic stress tolerance in crop plants: Special reference to salinity in rice. In: Pareek A, Sopory SK and Bohnert HJ. Abiotic stress adaptation in plants: Physiological, molecular and genomic foundation. Netherland: Springer. **2010**.

Slama, I., Ghnaya, T., Messedi, D., Hessini, K., Labidi, N., Savoure, A., and Abdelly, C. Effect of sodium chloride on the response of the halophyte species *Sesuvium portulacastrum* grown in mannitol-induced water stress. *J Plant Res*. **2007**, *120*, 291-299.

Subbarao, G. V., Ito, O., Berry, W. L., and Wheeler, R. M. Sodium—a functional plant nutrient. *CRC Crit Rev Plant Sci*. **2010**, *22*, 391-416.

Tardieu, F. Any trait or trait-related allele can confer drought tolerance: just design the right drought scenario. *J Exp Bot*. **2012**, *63*, 25-31.

Tester, M. Na^+ tolerance and Na^+ transport in higher plants. *Ann Bot*. **2003**, *91*, 503-527.

Tester, M., and Davenport, R. Na^+ tolerance and Na^+ transport in higher plants. *Ann. Bot.* **2003**, *91*, 503-527.

U, H., and W, H. H. The chloroplast envelope: structure, function, and role in leaf metabolism. *Annu Rev Plant Physiol*. **1981**, *32*, 139-168.

Wakeel, A., Steffens, D., and Schubert, S. Potassium substitution by sodium in sugar beet (*Beta vulgaris*) nutrition on K-fixing soils. *J Soil Sci Plant Nutr*. **2010**, *173*, 127-134.

Wu, H., Shabala, L., Azzarello, E., Huang, Y., Pandolfi, C., Su, N., Wu, Q., Cai, S., Bazihizina, N., Wang, L., Zhou, M., Mancuso, S., Chen, Z., and Shabala, S. Na^+ extrusion from the cytosol and tissue-specific Na^+ sequestration in roots confer differential salt stress tolerance between durum and bread wheat. *J Exp Bot*. **2018**, *69*, 3987-4001.

Wu, H., Shabala, L., Liu, X., Azzarello, E., Zhou, M., Pandolfi, C., Chen, Z. H., Bose, J., Mancuso, S., and Shabala, S. Linking salinity stress tolerance with tissue-specific Na^+ sequestration in wheat roots. *Front Plant Sci*. **2015**, *6*, 71.

Xie, Q., Yang, Y., Wang, Y., Pan, C., Hong, S., Wu, Z., Song, J., Zhou, Y., and Jiang, X. The calcium sensor CBL10 negatively regulates plasma membrane H^+-ATPase activity and alkaline stress response in *Arabidopsis*. *Environ Exp Bot*. **2022**, *194*, 104752.

Yang, L., Machin, F., Wang, S., Saplaoura, E., and Kragler, F. Heritable transgene-free genome editing in plants by grafting of wild-type shoots to transgenic donor rootstocks. *Nat Biotechnol*. **2023**, 1-10.

Yin, X., Xia, Y., Xie, Q., Cao, Y., Wang, Z., Hao, G., Song, J., Zhou, Y., and Jiang, X. The protein kinase complex CBL10-CIPK8-SOS1 functions in *Arabidopsis* to regulate salt tolerance. *J Exp Bot*. **2019**, *71*, 1801-1814.

Zeng, L., Shannon, M. C., and Grieve, C. M. Evaluation of salt tolerance in rice genotypes by multiple agronomic parameters. *Euphytica*. **2002**, *127*, 235-245.

Summary

Summary

Ca^{2+} transients in the cytosol ($[Ca^{2+}]_{cyt}$) act as major physiological signals to initiate appropriate responses. The CBL-CIPK network decodes $[Ca^{2+}]_{cyt}$ transients that are initiated during plant development and in response to environmental changes. Several functions of the CBL-CIPK regulatory network have been identified in more detail in the model plant *A. thaliana*, but much less is known about their functions in solanaceous crops.

Chapter 1 introduced the CBL-CIPK network and current knowledge on how it decodes Ca^{2+} transients triggered by stress stimuli. It summarized current knowledge on salt stress response mechanisms and the role of CBL-CIPK modules in the regulation of these mechanisms.

Chapter 2 is a review that describes how the CBL-CIPK regulatory network is involved in two levels of crosstalk between plant development and stress adaptation: direct crosstalk through interaction with regulatory proteins, and indirect crosstalk through adaptation of correlated physiological processes that affect both plant development and stress responses. This chapter thus provides novel insights into the physiological roles of the CBL-CIPK network in plant growth and stress adaptation and the trade-off between plant growth and stress response.

In **Chapter 3**, a genome-wide analysis of the *NtCBL* gene family in tobacco was performed. Twenty-four *NtCBL* genes were identified in *N. tabacum*, of which 14 *NtCBL* genes were derived from the maternal genome donor *N. sylvestris* and 10 from the paternal genome donor *N. tomentosiformis*. Based on their sequences we predicted the subcellular localization and Ca^{2+}-binding ability of NtCBL proteins, as well as gene structure and splicing variants of *NtCBL* genes at the level of individual homoeologs. In addition, the expression profiles of *NtCBL* genes were determined in different tissues and at different developmental stages, as well as under salt and drought stress. The *NtCBL4A-1* gene from the ancestral *N. sylvestris* genome was characterized in more detail because of its reported role in the salt stress response of other plant species but its deviating expression response in tobacco from that of other species. Results showed that the overexpression of *NtCBL4A-1* led to a salt-

supersensitive phenotype. There are three *NtCBL4* homoeologous genes (*NtCBL4A-1*, *NtCBL4A-2*, and *NtCBL4B*) in *N. tabacum*, and they may have functional redundancy because of their high sequence similarity. Experiments involving loss-of-function mutants of *NtCBL4* may provide additional insights into the role of *NtCBL4* homoeologs in salt tolerance but I did not have enough time within the context of my PhD thesis to construct the single mutant of *NtCBL4A-1* nor the triple mutant of *NtCBL4*.

In **Chapter 4,** we focused on another member of the CBL family that was suggested to play a role in salt tolerance: CBL5. Tobacco plants overexpressing *NtCBL5A* were evaluated under saline conditions and exhibited hypersensitivity to salt stress (expressed as highly necrotic leaves). This hypersensitive phenotype was shown to be potentially linked to abnormal Na^+ compartmentalization, plant photosynthesis, and plant immune response triggered by the constitutive overexpression of *NtCBL5A*. The salt-supersensitive phenotype of *NtCBL5A*-overexpressing (OE) lines was very similar to the phenotype we observed in *NtCBL4A-1*-OE lines under salt stress. Considering that both *NtCBL4A-1* and *NtCBL5A* were ectopically overexpressed in the leaf blades of these transgenic plants, we hypothesized that the salt-supersensitive phenotype of *NtCBL4A-1*-OE leaves and *NtCBL5A*-OE leaves may be caused by interference with other CBL-CIPK pathways rather than their native functions in salt stress response. The response to salt stress of the loss-of-function mutant of *NtCBL5* (*Nt-cbl5a*, *Nt-cbl5b*, and *Nt-cbl5acbl5b* double mutant) was later shown to be similar to WT plants (Chapter 6), confirming that *NtCBL5A* does not appear to be a key component in the salt tolerance of tobacco

In **Chapter 5**, we further investigated the salt-supersensitive response of *NtCBL4A-1*-OE and *NtCBL5A*-OE lines and the possible interference with other CBL-CIPK pathways. We evaluated the salt tolerance of *NtCBL4A-1::NtCBL5A* co-overexpressing lines and *NtCBL10A::NtCBL5A* co-overexpressing lines. Results showed that co-overexpression of *NtCBL4A-1* and *NtCBL5A* had an additive effect on the salt sensitivity of transgenic tobacco, while *NtCBL10A* overexpression greatly

relieved the salt sensitivity of *NtCBL5A*-OE lines. This indicated that the salt sensitivity caused by *NtCBL4A-1* overexpression and *NtCBL5A* overexpression may be linked to the function of *NtCBL10A*. This was corroborated by the fact that NtCBL4A-1, NtCBL5A, and NtCBL10A interacted with the same NtCIPK24A in the yeast two-hybrid system. Increased salt sensitivity of *Nt-cbl10a* single mutants and *Nt-cbl10b* single mutants, and the hypersensitivity of the *Nt-cbl10acbl10b* double mutants further demonstrated that *NtCBL10A* and *NtCBL10B* are essential for the salt tolerance of tobacco. The *Nt-cipk24a* and *Nt-cipk24b* single mutants also showed increased salt sensitivity compared to WT. We were however not able to obtain the *Nt-cipk24acipk24b* double mutant because of defective callus development.

In **Chapter 6**, I summarized all findings and discussed our hypothesis on the salt-sensitive phenotypes induced by the overexpression of *NtCBL4A-1*, *NtCBL5A*, and the knock-out of *NtCBL10*. Our results indicated that two possibly independent salt-sensitive phenotypes (chlorosis and necrosis) of the *Nt-cbl10acbl10b* double mutant are exhibited under salt stress, and the salt sensitivity of *NtCBL4A-1*-OE and *NtCBL5A*-OE lines may link to the necrotic symptoms of *Nt-cbl10acbl10b* under salt stress. The question that still needs to be answered is which *NtCBL10*-dependent adaptations to stress are underlying the different aspects of the salt-hypersensitive phenotype of the *Nt-cbl10acbl10b* double mutant. I did not have time within this thesis project to add data targeting all the regulatory functions of *NtCBL10* in response to salt stress, but I discussed the results based on the available literature. The necrotic symptoms of *Nt-cbl10acbl10b* double mutant may be linked to disturbed Na^+ homeostasis, Cl^- homeostasis, and ROS production. I hypothesized that the fast-developing chlorotic symptoms of *Nt-cbl10acbl10b* double mutant may be caused by abnormal regulation of H^+ homeostasis in the plasma membrane, tonoplast, and trans-Golgi network/early endosome. Further experiments are needed to test these intriguing hypotheses. Finally, I discussed the results of this thesis in the context of breeding for abiotic stress tolerance and the improvement of crops.

Acknowledgments

Acknowledgments

Time flies! As I sit here reflecting on my PhD experience, I am filled with complex emotions—both excitement for the intriguing discoveries and frustration with the intricate results. Life is full of ups and downs that can make you laugh or cry. Throughout this journey, I have come to realize that the people who have supported me, loved me, and worked alongside me are the most important part of my life. Therefore, I would like to express my heartfelt gratitude to those who have cheered for my achievements and encouraged me during difficult times.

I am fortunate to have encountered many kind and knowledgeable supervisors, and I would like to express my sincere gratitude towards them first in the order of our acquaintance.

Prof. Dr. Haobao Liu, thank you for your guidance and encouragement during the critical junctures of my studies. Our journey together began almost a decade ago in September 2013, and since then, your selfless dedication to learning and commitment to elevating your students to greater heights has had a profound impact on me. You supported me to apply for the PhD Education Programs jointly offered by the Graduate School of Chinese Academy of Agricultural Science and Wageningen University & Research. This decision has proven to be one of the most pivotal in my life, as it opened up numerous opportunities to interact with exceptional researchers, forge lasting friendships, and acquire invaluable techniques that have become a treasure trove in my personal and professional development. You are not just a supervisor to me, but a true mentor who has played an instrumental role in shaping my trajectory. I have always admired your leadership style and your unwavering commitment to excellence. Your wife, doctor **Zhaomei Yang**, has also been incredibly supportive and caring towards me in my daily life - preparing delicious meals for us, organizing team-building activities, and even sending medicine when I fell ill. I am truly grateful for everything you and your wife have done for me.

Prof. Dr. Qian Wang, I would like to express my sincere gratitude for your meticulous guidance and assistance in experimental operations and design. Your rigorous and

serious academic style, as well as your passion for scientific research, have deeply influenced me. As the saying goes, “Sneaking into the night with the wind, silently moistening things”. Your dedication to your work has left a lasting impression on me. I will always remember your earnest teachings and strive to continuously improve myself in my future pursuit of scientific research.

Prof. Dr. Richard G.F. Visser, thanks for your invaluable help and guidance throughout my PhD project, as well as for providing me with the opportunity to pursue my studies at WUR. I still recall the day when I sent a brief email via the contact box on Plant Breeding’s website, inquiring about potential admission to the PhD Education programs between GSCAAS and WUR. My email read, “Dear Richard, I am currently working on functional gene identification in response to salt stress, would you be interested in knowing more about me?” At that time, I was uncertain whether my message would reach you among the deluge of correspondence you receive on a daily basis. Furthermore, I was not sure if you would entertain the idea of contacting someone without prior knowledge of their background. However, your discerning consideration was evident through the prompt response from Prof. Dr. Yuling Bai shortly after I dispatched my initial message. Yuling conveyed that she was acting on your behalf in requesting a copy of my curriculum vitae for evaluation purposes.

Prof. Dr. Yuling Bai, I am immensely grateful for your unwavering encouragement and support since our first contact. Your positive feedback after reviewing my CV and subsequent arrangements to meet me in Beijing, China, and treat me and Xiaoxiao to a lovely dinner near CAAS was a defining moment for me. During the meeting, I had the privilege of discussing my research topic for my master’s thesis with you, which turned out to be a stimulating discussion. You played an instrumental role in assisting me with my CSC scholarship and visa application process. I still remember the moment when you picked me and Menghe up from the reception on the first day of my arrival at WUR. Your elegance, warmth, and rigorous academic spirit, combined with an unwavering fighting spirit, have been an inspiration to me. I am truly grateful for your invaluable assistance and insightful suggestions on my PhD

project, especially for introducing me to Gerard – my exceptional research partner and daily supervisor.

Dr. C. G. Gerard van der Linden, I am deeply grateful for the extensive guidance and support you have provided me throughout my PhD study. I remember vividly the day we first met, with you fully absorbed in your writing as Yuling led me into your office. At that moment, I felt a bit nervous and uncertain, as we had never met or interacted before. However, your kindness, understanding, and unwavering support quickly helped me feel at ease, and we established a weekly meeting routine to discuss my research progress. Prior to working with you, I had always struggled with making detailed plans and preferred to conduct experiments as quickly as possible. During our early meetings, you patiently guided me in the process of creating detailed experimental plans and perfecting them step by step, resulting in significant time savings and improved efficiency. Even when I returned to China, we maintained regular online meetings to continue the progress. I will never forget your support during a difficult period when you were suffering from a serious health problem, yet you still helped me with my first paper. Despite the challenges, we persevered and completed a successful paper, and subsequent papers became easier to write as we worked together. Your talent for concise and innovative storytelling proved invaluable in reviewing papers, as we reorganized my review and produced exceptional work. As the deadline for my thesis approached, we worked together more efficiently than ever before, and we completed the work to an excellent standard. You taught me to read literature critically and carefully analyze conclusions, and your passion for science and love of puzzles have been truly inspiring throughout my research journey. Thank you for being an outstanding supervisor and mentor.

My dear paranymphs, **Alejandro** and **Yingjie**, I would like to express my sincere gratitude for accepting my invitation to be my paranymphs. Despite our relatively short acquaintance, I found talking to both of you very comforting as you both have been kind, friendly, and helpful to me. **Alejandro**, I am impressed by your expertise in bioinformatics, and I appreciate your remarkable efficiency in your work. It is no wonder that you are popular in Plant Breeding and have many friends around you.

Yingjie, your cheerful and enthusiastic personality always warms my heart, and I enjoy talking to you very much. I am confident that we can develop a strong and lasting friendship.

Dr. Susan Urbanus, you have been an incredibly supportive PhD advisor. Your warm and patient nature, coupled with your willingness to always listen and provide the best problem-solving strategies, has been invaluable to me throughout my program. I am also grateful to **Sean** and **Martijn**, who were instrumental in helping me with my hydroponic experiments. Without your assistance, the experiments would not have been completed so seamlessly. And last but not least, **Annemarie**, thank you for your help with the ion content measurement. Although I encountered obstacles in the beginning, your guidance and support were instrumental in enabling me to complete all the measurements successfully.

I would like to express my heartfelt gratitude to all my colleagues at CAAS, particularly **Lianhong Dong**, **Sujuan Shi**, **Yulong Su**, **Ge Zhang**, **Shugui Li**, **Chuanzong Li**, **Guang Yuan**, **Shuaijun Deng**, **Zhijie Mo**, **Jiaping Yuan**, **Kaiyan Han**, and the entire team at Tobacco Research Institute of CAAS. Working alongside you has been a pleasure and an honor. From sharing meals and conducting experiments together, to playing and laughing together, you have made me feel like part of a warm and supportive family. I am grateful for the camaraderie and friendship that we have shared, and I will always cherish the memories of our time together.

I would also like to thank all my colleagues at WUR, particularly **Robert**, **Elly**, **Lucia**, **Clemens**, **Johan**, and the entire group of Breeding for Abiotic Stress Tolerance. It was a pleasure to attend the weekly group meetings, where we discussed scientific topics and caught up on each other's recent activities. Your expertise and knowledge have been invaluable to me, and I am grateful for the opportunity to learn from each of you.

My dear friend **Sri (Artik)**, I am grateful for your guidance and support during my early days at WUR. You patiently introduced me to the lab and greenhouse rules, and even accompanied me on grocery shopping trips, familiarizing me with the

various stores and their unique features. Our shared cooking experiences and enjoyable meals were a highlight of my time abroad, and your sisterly advice and care have been invaluable.

To my dear Chinese friends in Wageningen, including but not limited to **He Meng**, **Xiaoxiao Xie**, **Qian Li**, **Lina Hu**, **Yusi Liu**, **Lei Deng**, **Dazhi Liu**, **Panpan Fan**, **Qingbo Qu**, **Dong Zhang**, **Xulan Wang** (in no particular order ☺), I am grateful for your support and assistance during my time in Wageningen. Our shared cooking and chatting moments were filled with joy and warmth, and I am grateful for the treasured memories we have created together.

To my beloved boyfriend, I am grateful for your companionship and the serendipitous encounter that brought us together. Your admirable qualities of gentleness and erudition have drawn me to you, and our relationship continues to be filled with sweetness. We did have disagreements at times, but each time we were able to understand each other better. I sincerely hope that we can continue to share our love for many more years to come.

I want to thank my parents for their boundless love and guidance, which have been a source of strength and inspiration for me. I am also thankful for giving birth to my younger brother, who has brought joy and companionship into my life, and our shared similarities and interests have made our conversations lively and fulfilling. I know that we will continue to support and love each other throughout our lives.

In the end, I want to acknowledge myself for the strength and determination that I have cultivated throughout this journey. I have learned to trust and believe in myself, and to strive for personal growth and excellence. As I look forward, I am committed to embracing life with enthusiasm and dedication, and to pursue my happiness to the fullest.

Jingjing Mao

April 2023 in Wageningen

About the Author

Jingjing Mao was born on February 12, 1992 in Anyang, Henan Province. In 2014, she obtained her bachelor degree at the Henan Agricultural University, Zhengzhou, China. After that, she was recommended by her university to be a master at Tobacco Research Institute of Chinese Academy of Agricultural Science without examination. In 2017, she was admitted as a PhD candidate to the joint PhD Program of the Graduate School of Chinese Academy of Agricultural Science and that of Experimental Plant Sciences of Wagenigen University & Research. Her research is mainly focused on the functional identification of key *CBL* and *CIPK* genes in salt stress response of tobacco. This thesis presents the outcomes of her PhD research on “The role of *CBL* genes in the salt stress response of *Nicotiana tabacum*”.

Publications by the author

Mao J, Yuan G, Han K, et al., Genome-wide identification of *CBL* family genes in *Nicotiana tabacum* and the functional analysis of *NtCBL4A-1* under salt stress. **Environmental and Experimental Botany**. 2023. 105311.

Mao J, Mo Z, Yuan G, et al., The CBL-CIPK network is involved in the physiological crosstalk between plant growth and stress adaptation. **Plant, Cell & Environment**, 2022.

Mao J, Yuan J, Mo Z, et al., Overexpression of *NtCBL5A* leads to necrotic lesions by enhancing Na^+ sensitivity of tobacco leaves under salt stress. **Frontiers in Plant Science**, 2021, 12: 18-36.

Education Statement of the Graduate School

Experimental Plant Sciences

Issued to: Jingjing Mao
Date: 13 June 2023
Group: Plant Breeding
University: Wageningen University & Research

1) Start-Up Phase	date	cp
▶ **First presentation of your project**		
Mechanisms and physiological roles of the CBL-CIPK networking system	05 Nov 2018	1.5
▶ **Writing or rewriting a project proposal**		
CBL-CIPK pathways in the drought and salt stress response of *Solanaceae* : The role of *CBL5*	13 Jan 2020	6.0
▶ **Writing a review or book chapter**		
Mao J. *et al.* The CBL-CIPK network is involved in the physiological crosstalk between plant growth and stress adaptation.	13 Jul 2022	6.0
▶ **MSc courses**		
Plant Breeding (PBR-22303)	Sep 2018	3.0
Subtotal Start-Up Phase		16.5

2) Scientific Exposure	date	cp
▶ **EPS PhD days**		
Annual EPS PhD Days 'Get2Gether 2019', Soest (NL)	11-12 Feb 2019	0.6
Annual EPS PhD Days 'Get2Gether 2023', Soest (NL)	1-2 May 2023	0.6
▶ **EPS theme symposia**		
EPS Theme 3 Symposium 'Metabolism and Adaptation', Online	30 Oct 2020	0.2
EPS Theme 4 Symposium 'Genome Biology', Online	11 Dec 2020	0.2
EPS Theme 2 Symposium 'Interactions between Plants and Biotic Agents', Online	9 Feb 2021	0.2
EPS Theme 4 Symposium 'Genome Biology', Online	17 Jan 2022	0.3
EPS Theme 4 Symposium 'Genome Biology and Gene Regulation', Amsterdam (NL)	6 Dec 2022	0.3
▶ **Lunteren Days and other national platforms**		
Annual Meeting Experimental Plant Sciences 2019, Lunteren (NL)	8-9 Apr 2019	0.6
Annual Meeting Experimental Plant Sciences 2021, Online	12-13 Apr 2021	0.5
Fourth National Symposium on Plant Stress Biology, Shanghai (CN)	31 May-3 Jun 2021	0.9
▶ **Seminars (series), workshops and symposia**		
Seminar: Prof. Wolf Frommer, Logistics: Allocation of carbon and energy for yield and pathogen resistance	17 Jan 2019	0.1
Seminar: Dr. Luis Lopez-Molina, The role of the endosperm in Arabidopsis early post-embryonic development	25 Jan 2019	0.1
Seminar: Dr José Miguel Mulet, Drought tolerance in plants as well as his work in science communication and GMO public	17 May 2019	0.1
Seminar: Prof. Ralph Panstruga, Phenotypic and molecular characterization of partially mlo-virulent isolates of the barley	20 May 2019	0.1
Seminar: Dr. Jaime Prohens, Introgression breeding from wild species for crops adaptation to climate change	23 May 2019	0.1
Seminar: Prof Sergey Shabala, Crop halophytism: environmentally sustainable solution for global food security, Online	2 Dec 2021	0.1
Seminar: Dr. Zhegnqing Fu, Transcriptional regulations of plant growth and defense: old school but with new tricks, Online	30 Jun 2022	0.1
Seminar: Prof. Bikram S Gill, Cytogenetic basis of acquired herbicide resistance and relevance to crop breeding, Online	30 Jun 2022	0.1
Seminar: Prof. Chunpeng Song, Decoding the development of the maize stomata, Online	30 Jun 2022	0.1
Seminar: Carlos L. Ballare, Growth-defense tradeoffs in plants: concepts and mechanisms involving phytochrome and	28 Jul 2022	0.1
Seminar: James Schnable, Genes controlling phenotype variation across environment and time, Online	28 Jul 2022	0.1
Seminar: Jian-Kang Zhu, CRISPR/Cas technologies for breeding, diagnostics and therapeutics, Online	29 Jul 2022	0.1
Seminar: Yusaku Uga, Root design: Towards the development of climate-resilient crops, Online	29 Jul 2022	0.1
Seminar: Mary Lou Guerinot, Shining light on iron deficiency signaling in Arabidopsis, Online	30 Jul 2022	0.1
Seminar: Dae-Jin Yun, Inverse regulation of SOS1 and HKT1 protein localization and stability by SOS3/CBL4 in *Arabidopsis*	30 Jul 2022	0.1
Seminar: Ralph Hückelhoven, Mechanisms of barley susceptibility to powdery mildew	18 Nov 2022	0.1
Workshop: Breeding for sustainability - Perspectives from a company and academic plant breeder, Wageningen (NL)	20 Nov 2018	0.3
Workshop: Sino-Dutch Seed Sector Innovation Workshop, Online	19 May 2022	0.2
Symposium: Breeding Data - Statistical Adavances in Modern Plant Breeding, Wageningen (NL)	16 Oct 2018	0.3
▶ **Seminar plus**		
▶ **International symposia and congresses**		
Keystone Conference Climate Change-Linked Stress Tolerance in Plants, Hannover (DE)	13-16 May 2019	0.9
SOL International Meeting 2020, Online	9-11 Nov 2020	0.6
The 2022 International Symposium on Horticulture and Plant Biology (ISHPB2022), Online	8-10 Aug 2022	0.9
▶ **Presentations**		
CBL-CIPK pathways in the abiotic stress response of *Solanaceae* : The role of CBL5, Annual Meeting Experimental Plant	8-9 Apr 2019	1.0
CBL-CIPK pathway and salt stress, EPS Theme 4 Symposium "Genome Biology and Gene Regulation", oral presentation	6 Dec 2022	1.0
▶ **IAB interview**		
▶ **Excursions**		
Subtotal Scientific Exposure		11.2

3) In-Depth Studies	date	cp
▶ **Advanced scientific courses & workshops**		
CAAS course 'Progress in Agricultural Science and Technology', Beijing (CN)	Dec 2017	1.1
EPS course 'Transcription Factors and Transcriptional Regulation', Wageningen (NL)	10-12 Dec 2018	1.0
CAAS course 'Progress in Crop Cultivation and Farming System', Beijing (CN)	Jun 2020	0.6
G2P-SOL Advanced Training School II, Online	11-13 Oct 2021	0.6
EPS-ELIXIR course 'PLAZA-functional plant bioinformatics', Online	25-26 Oct 2021	0.6
▶ **Journal club**		
Literature Discussion Club at Tobacco Research Institute, Qiangdao (CN)	Sep 2020-Sep 2022	1.5
▶ **Individual research training**		
Subtotal In-Depth Studies		5.4

Education Statement

4) Personal Development	date	cp
► **General skill training courses**		
WGS-CAAS course 'Effective Academic Development', Beijing (CN)	11-22 Sep 2017	3.0
WUR Introduction to the Netherlands, Wageningen (NL)	9 Oct 2018	0.2
WGS workshop 'Reviewing a Scientific Paper', Wageningen (NL)	28 Nov 2018	0.1
CAAS course 'Classic Literature Reading', Qingdao (CN)	Jun 2020	0.6
CAAS course 'Academic Writing & Presenting in English', Qingdao (CN)	Jun 2020	1.4
EPS Introduction Course, Online	20 Apr 2021	0.3
► **Organisation of meetings, PhD courses or outreach activities**		
► **Membership of EPS PhD Council**		
Subtotal Personal Development		5.6

TOTAL NUMBER OF CREDIT POINTS*	38.7
Herewith the Graduate School declares that the PhD candidate has complied with the educational requirements set by the Educational Committee of EPS with a minimum	

** A credit represents a normative study load of 28 hours of study.*

Acknowledgments of Financial Support

The author is from the PhD Education Programs between the Graduate School of CAAS and WUR. The research described in this thesis was financially supported by the National Natural Science Foundation of China, the Fundamental Research Funds for China Agricultural Academy of Sciences, the International Foundation of Tobacco Research Institute of CAAS, the Agricultural Science and Technology Innovation Program, the Key Funding of CNTC and YNTI, the China Scholarships Council, and the International Exchange Scholarship of the GSCAAS.

Financial support from Wageningen University & Research for printing this thesis is gratefully acknowledged.

Cover design by Zhaixihuan Culture Communication Co., LTD.